

Institute of Engineering, Surveying
and Space Geodesy

Precise Positioning in Urban Canyons: Applied to the Localisation of Buried Assets

By
Jean-Philippe Montillet BEng MSc.E.E.

Thesis submitted to the University of Nottingham for
the degree of Doctor of Philosophy
March 2008

ABSTRACT

The last decades have seen the applications related to Global Positioning Systems (GPS) flourishing in various and unrelated ways such as car navigation, electronic advertisement, military defense (e.g. missile tracking) ... etc. The increasing consumers interest in positioning market is also due to the recent coupling of mobile phone and GPS technologies which is deemed to kick-off the location based services market (LBS). The LBS market are electronic services for providing information that has been created, compiled, selected or filtered taking into consideration the current locations of the users or those of other persons or mobile objects. Analysts foresee that these services will open a new era of mass consumption market where all positioning technologies will play a key role. The level of positioning accuracy (e.g. 1 cm or 1 m) will be a service that the user may order from his mobile phone, laptop or other devices.

In this background, the aim of the conducted research is to locate accurately buried pipes in built up areas using GPS and other positioning technologies. This work should be considered as an attempt to solve the general problem: positioning accurately everywhere and every time. Thus, the research work undertaken at the University of Nottingham Institute of Engineering Surveying and Space Geodesy (IESSG) focused on the integration of GPS with other existing technologies (e.g. signal from cellular networks). Algorithms are developed and then tested through simulations. The results showed that the integration of the GPS and GSM technologies may provide a position accuracy of an user no better than 20 m. The main issue is the lack of synchronisation between the two technologies.

In a second part, a network of ground-based transceivers called LOCATA is introduced and studied in detail with statistics on the residual of the signal (e.g. multipath, fading) and the time series of the rover's position. Results were averaged on various environments (e.g. downs, urban canyons). The overall results showed that it is possible to locate the LOCATA rover better than 5 cm in 3D and better than 2 cm in 2D in both urban and open field scenarios.

However some unwanted phenomena (interferences) were found which degraded the performances of this new technology (from a few centimetres to tens of centimetres). Finally, the LOCATA prototype was studied beyond its actual capabilities (at the time of writing this thesis) via simulations of the coupling with GPS technology. Results were extracted from a simulator and the statistics calculated from the data collected in the previous chapters. It gave a proof that the LOCATA-GPS technology may achieve the centimetre level in the urban canyons (in 3D).

Acknowledgements

This PhD project has been undertaken at the Institute of Engineering Surveying and Space Geodesy, University of Nottingham. Funding for the project has been supplied by the VISTA (Visualising integrated information on buried assets to reduce streetworks) project which gathers a group of industries and academics to solve together the challenges of positioning buried assets in urban canyons. I am thankful for the opportunity that the IESSG gave me to study brend new positioning technologies through this research work.

I would like to extend my thanks to all those who have aided me as I conducted the research for the project with particular thanks to my academic supervisors Dr. Gethin W. Roberts and Dr. Xiaolin Meng; Mr. Huib De Light, Dr. Samantha Waugh, Dr. Oluropo Ogundipe and Mr. Craig Hancock for the help in planning and carrying out the experiments. *LOCATA Corp.* and Dr. Joel Barnes have also given valuable inputs during the experiments and the explanations of some of the results when using the LOCATA technology. Special mention should also be given to my family and especially my father and my mother who have always supported me since the beginning of my studies and in my choice for doing this PhD.

I also would like to conclude on the value of doing this thesis. It is often mistaken that a PhD is an extended Master research work. However, there is a fundamental difference: a PhD work contains more blue sky research. The research student needs to plan and have a bit of intuition on the results he may end up to avoid any waste of time. Three years seem to be a long time for most of the students, but it goes very fast and only a tight planned work may keep you on track to finish the thesis within the scholarship duration. Finally, this thesis is a fantastic adventure where for the first time after all those years at the University you can see what you are able to do alone. What a great accomplishment to see your own thesis finished.

Contents

1 Introduction **5**

1.1 Precise Positioning and Surveying in Urban Canyons 6

1.2 Research Aims and Novelty of the Work 7

1.3 Thesis Outline 9

2 Research Background **11**

2.1 General Overview of the Project 12

2.1.1 Project Background 12

2.1.2 Buried Assets 12

2.1.2.1 Mapping the Assets: a Costly Process 12

2.1.2.2 Digging Holes in the Street 14

2.1.3 Project Funding 15

2.1.3.1 EPSRC and Industry's Sponsorship 15

2.1.3.2 The VISTA Project 15

2.1.4 Precise Positioning of the Assets 17

2.2 Technologies Already Available on the Market to Locate Precisely Buried Assets 20

2.3 Summary 21

3 GPS Technology and Challenges in Urban Canyons **23**

3.1 Introduction 24

3.2 GPS Architecture 25

3.2.1 Signal Characteristics 25

3.2.2 Space Segment 27

3.2.3 Control Segment . . . 27
3.2.4 User Segment . . . 27
3.3 Positioning with GPS . . . 29
3.3.1 Pseudorange and Carrier-Phase Observables . . . 29
3.3.1.1 Pseudoranges Ranging . . . 30
3.3.1.2 Carrier-Phase Ranging . . . 31
3.3.2 Receiver's Position . . . 33
3.3.3 Different Positioning Solutions in GPS Technology . . . 35
3.4 Challenges in Urban Canyons . . . 37
3.4.1 Satellite Geometry . . . 37
3.4.2 Signal Multipath . . . 38
3.5 Summary . . . 39

4 Ubiquitous Positioning 41
4.1 Introduction . . . 42
4.2 UMTS and GSM Network Architecture . . . 43
4.2.1 General Definition of a Cellular Network . . . 43
4.2.2 GSM to UMTS Architecture . . . 44
4.3 Synchronisation and Location Algorithms . . . 46
4.3.1 GSM Network . . . 46
4.3.2 UMTS Network . . . 49
4.4 Hybrid Systems . . . 52
4.4.1 Wireless Assisted GPS . . . 52
4.4.2 Precise Positioning in Urban Canyons using GPS and GSM . . . 55
4.4.2.1 Mixing GPS and GSM Measurements . . . 55
4.4.2.2 Kalman Filter Smoothing . . . 57
4.4.2.3 Results . . . 58
4.4.3 Validation of the Results . . . 64
4.5 Summary . . . 65

5 LOCATA Technology 67
5.1 Background and Definition of the LOCATA Technology . . . 68

5.1.1 Introduction . . . 68
5.1.2 A Definition of the LOCATA Technology . . . 69
5.2 Characteristics of the LOCATA Signal . . . 71
5.2.1 The IEEE 802.11 Standard and the ISM Frequency Band . . . 71
5.2.2 Antennas . . . 73
5.2.3 Multiple Access Schemes and Near-Far Effect . . . 75
5.2.4 Network Synchronisation . . . 77
5.2.5 L1/C1 Characteristics . . . 81
5.3 The LOCATA Setup Files . . . 82
5.4 A Dedicated LocataNet . . . 86
5.4.1 The Different Steps to Set Up the Network . . . 86
5.4.2 Check and Run of the LocataNet . . . 89
5.5 Range Tests . . . 92
5.5.1 The LOCATA Radio Channel . . . 92
5.5.2 SNR and Multipath Fading Model . . . 96
5.6 Summary . . . 100

6 Achieving Centimetre Level Positioning Accuracy with LOCATA 101
6.1 Introduction to the Experiments . . . 102
6.1.1 General Comments . . . 102
6.1.2 Extraction of the Data . . . 103
6.2 Position Analysis with the LINE Software . . . 103
6.2.1 Block Diagram of LINE . . . 103
6.2.2 Static Positioning . . . 108
6.2.3 Kinematic Positioning . . . 114
6.3 Error Analysis . . . 119
6.3.1 Statistical Distribution . . . 119
6.3.2 Confidence Ellipse . . . 124
6.4 Summary . . . 128

7 LOCATA Technology: Issues and Solutions 131
7.1 Preamble . . . 132

7.2 Wi-Fi Interference . . . 132
7.2.1 Overview of the Problem . . . 133
7.2.2 A Dedicated LocataNet at the University of Nottingham . . . 134
7.2.3 Degradation of the LOCATA Accuracy . . . 136
7.2.3.1 General Observations . . . 136
7.2.3.2 Influence of the Data Throughput of the Wi-Fi APs . 146
7.3 Statistics from the SNR and Carrier-Phase Measurements . . . 147
7.3.1 Statistics of a Signal Blocked by Foliage . . . 148
7.3.1.1 General Results . . . 148
7.3.1.2 Statistics of the Carrier-Phase Signal . . . 152
7.3.2 Another Approach to the Wi-Fi Interference . . . 154
7.3.3 Comments on the SNR . . . 158
7.4 Real Time Kinematic GPS and LOCATA Technology . . . 163
7.4.1 Absolute and Relative Positioning . . . 163
7.4.2 Results . . . 165
7.5 Summary . . . 166

8 LOCATA Technology: Further Tests 169
8.1 Preamble . . . 170
8.2 The In-House Software . . . 170
8.2.1 Block Diagram . . . 170
8.2.2 Results . . . 175
8.3 Test Trial of the LOCATA Technology for the VISTA Project . . . 178
8.4 LOCATA Technology Performances Indoors . . . 184
8.5 Simulations on the Future Integration of GNSS and LOCATA Technologies . . . 186
8.5.1 Simulator: Integration of the LOCATA and the GNSS Signals 186
8.5.2 Analysis of the Results . . . 189
8.6 Summary . . . 194

9 Conclusion and Recommendations 195
9.1 Conclusions . . . 197

9.2 Recommendations for Future Work 200

A LOCATA: Additional Data 216

B Matlab Scripts to Extract Data 223

B.0.1 Master File 223

B.1 Processing Data File 224

B.2 Error Function 226

C Example of a LOCATA Rover Setup File 230

D Additional Information for the Chapter 7 247

E Additional Information for the Chapter 8 254

F Paper Accepted to the IeCCS Conference 256

F.0.1 Abstract 256

F.0.2 Introduction 257

F.0.3 CVB 258

F.0.4 MUSIC Algorithm 259

F.0.5 Simulations and Results 259

F.0.6 Conclusions 262

F.0.7 Acknowledgments 262

List of Figures

2.1 Map of the assets (right) and an excavation on site (left). 14

2.2 Trench showing buried assets (left) and a bundle of telecommunication wires (right). 18

3.1 Overview of the GPS segments [US.Army (1996)]. 28

4.1 Overview of the GSM and UMTS architecture [Kupper (2005)]. 45

4.2 Schemes of three algorithms for precise positioning in cellular networks. 49

4.3 Overview of the A-GPS technology. 54

4.4 Block diagram. 59

4.5 Position of the MS estimated using only GPS pseudoranges and then smoothed by carrier-phase measurements. 60

4.6 True track and track estimated by Hybrid GPS/GSM measurements. 61

4.7 Track estimated hybrid GPS/GSM measurements and smoothed with Kalman filter. 63

5.1 Typical setup of a LocataLite on a tripod (left) or on a roof (right). 70

5.2 LocataLites' antennas mounted on a temporary pole (left) and its specifications (right) [Inc (2004)]. 74

5.3 Rover's antenna (left) and gain pattern (right) in two planes (vertical and horizontal) [HyperLink (2005)]. 74

5.4 TDMA frame used in the LOCATA technology [Barnes (2006)]. 77

5.5 Different steps in the TimeLoc process. 78

5.6 Rover (left) and LocataLite (right) with a flash memory card. 82

5.7 Example of LocataLites setup file. 83

5.8 Example of LocataLites setup file. 84

5.9 Example of LocataLites setup file. 85

5.10 Orthophoto of a locataLites network with $LL1$ the master node (left), LocataLites setup (right). 87
5.11 A LocataNet (left), LocatLites mounted with GPS antennas on top (right). . . . 88
5.12 The different LED colours after powering up the LocataLites. 89
5.13 Hyperterminal parameters. 91
5.14 LOG file. 91
5.15 Signal propagated in urban areas. 93
5.16 Receiver physical layer. 94
5.17 Signal-to-Noise Ratio(SNR) and slow fading. 95
5.18 Snapshots of the scenarios for the open field (left) and urban canyon (right) scenarios. 98

6.1 Overview of the LINE software. 104
6.2 Pseudoranges and rollover for a dedicated LocataLite. 105
6.3 Phase error in meters and a cycle slip. 105
6.4 Parking of the IESSG (left) and yard close to the George Green library (right). . 108
6.5 Downs scenario. 109
6.6 Absolute value of the accuracy of the rover's position using carrier-phase measurements $[05-04-07]$. 113
6.7 Accuracy of the kinematic test at the UNSW. 117
6.8 RMSE and double difference of the carrier-phase measurements for the LocataLites $LL1$ and $LL6$ during the kinematic test. 118
6.9 Rician and Normal distribution fitting the data ($\mu = 2.7$, $StD = 0.5$). 121
6.10 Confidence ellipse for various values of σ_E. 125
6.11 Rotation of the confidence ellipse following the HDOP values. 127
6.12 Confidence ellipse applied to the data from the experiment $[28-03-07]$. 128

7.1 Test area to analyse the Wi-Fi interference on the LocataLites. 134
7.2 Test area showing the coverage of each antenna on the ground (left) and on the roof (right). 135
7.3 Rover's position error measured at midfield test point ($VDOP = 2.99$-$HDOP = 0.69$) $[30-08-07]$. 137

7.4 Absolute value of the rover's position error measured at midfield test point ($VDOP =$ 2.82-$HDOP = 0.65$) $[15-08-07]$. 138
7.5 Absolute value of the rover's position error measured at midfield test point($VDOP =$ 2.94-$HDOP = 0.66$) $[10-08-07]$. 139
7.6 Double difference of the carrier-phase signal (in cycles) for $LL2$ and $LL7$ $[15-08-07]$. 143
7.7 Interference when the Wi-Fi card is turned on the laptop. 145
7.8 Data throughput for each Wi-Fi access point surrounding the test area. 146
7.9 Data throughput for 3 Wi-Fi access points (cmb, $t2-d2$ and $t2-b2$) over August 2007. 146
7.10 Distribution of the carrier-phase measurements (left)and the LOCATA signal (right) for the experiments $[05-04-07]$ (transmitter 1). 152
7.11 Distribution of the carrier-phase measurements (left)and the LOCATA signal (right) for the experiments $[15-08-07]$ (transmitter 8). 152
7.12 LOCATA signal from LocataLite number 4 $(22-08-07)$. 156
7.13 Signal-to-Noise-Ratio for different LocataLites at $[5-04-07]$ (left) and $[15-08-07-Mid]$ (right). 159
7.14 Signal-to-Noise-Ratio for different LocataLites at $[30-08-07]$ during a kinematic experiment. 161
7.15 Delta carrier-phase measurements for the LocataLites 1 (left) and 6 (right) during the kinematic test $[30-08-07]$. 161
7.16 A comparison between the RMSE of the LOCATA and RTK GPS technologies. . 164

8.1 Block diagram of the in-house software. 171
8.2 Rover's position error output by the in-house software using carrier-phase measurements $[05-04-07]$. 178
8.3 The buried asset in the construction site (left) and the scheme of the LocataNet. 179
8.4 Time series of the rover's position error during thes trial $[14-02-08]$. 179
8.5 Time series of the rover's position error at different points $[P1]$ and $[P2]$ during the trial $[14-02-08]$. 182
8.6 LocataNet scheme $[20-11-2007]$. 184
8.7 Time series of the rover's accuracy $[20-11-2007]$. 185

8.8 3D model of the trajectory followed by the rover (bold green line) and the urban canyon scenario. 187

8.9 Time series of the rover position's error in absolute value using 4 satellites and 4 LocataLites. 190

8.10 RMSE and errors in absolute value in the East, North and Height coordinates - (standard deviations are the vertical bold lines). 191

8.11 RMSE and errors in absolute value in the East, North and Height coordinates while increasing the synchronisation error. 192

A.1 Accuracy of the rover's position with and without applying a Hatch filter [05 − 04 − 07]. 216

A.2 Accuracy of the rover's position with a Hatch filter (50 epochs). 217

A.3 Height error of the rover's position using carrier-phase measurements [28 − 03 − 07]. 218

A.4 Time series of the rover accuracy at another test point [28 − 03 − 07]. 218

A.5 Kinematic test at the UNSW. 219

A.6 Accuracy of the kinematic test at the University of Nottingham: the rover moves from *Tree* to *Hole*. 219

A.7 LocataLites mounted on a metal pole (left), and mounted on the roof (right). . . 220

A.8 Overview of the University of Nottingham main campus. 221

A.9 Histogram of the height error ([05 − 04 − 07]) using either the Normal or the Exponential distributions to fit the data. 222

A.10 Another view of the diagram of ellipse angle values shown in Section 6.11. 222

D.1 Wi-Fi interference recorded at Hole [10 − 08 − 07]. 248

D.2 Comparaison between the accuracy of the rover position and the rollover on the carrier-phase measurements [15 − 08 − 07]. 249

D.3 Wi-Fi interference during kinematic measurements [Australia]. 249

D.4 Wi-Fi interference during kinematics measurements [05 − 04 − 07]. 250

D.5 Network of points measured using the CUPT technique. 250

D.6 Comparison of RTK GPS and LOCATA accuracy done the [01 − 11 − 07]. 251

D.7 The track followed by the rover during the experiments [30 − 0807] starting at *Tree*. 251

E.1 Double difference of the carrier-phase signal from the LocataLite 6 during the test trial $[14-02-08]$. 254
E.2 LocataLites during the measurements in the construction site $[14-02-08]$. . . 255

F.1 Localisation Scenario in Cellular Networks 258
F.2 Bias (in chips) on the time delay estimation Vs the length of the subvector (m) . 260
F.3 Bias (in chips) on the time delay estimation Vs the SNR 261

List of Tables

4.1 GPS simulator parameters. 59

4.2 Mean and variance of hybrid GPS/GSM. 61

4.3 Validation of the simulations. 64

5.1 Physical layer characteristics of Bluetooth, IEEE802.11 and LOCATA [Crow et al. (1997)]. 72

5.2 Mean and standard deviation of the measurements recorded during the urban canyon trial. 99

5.3 Mean and standard deviation of the measurements recorded during the downs trial. 99

6.1 Position and coordinates accuracy in metres of the rover using pseudoranges. . . 110

6.2 Position and coordinates accuracy in metres of the rover using pseudoranges smoothed with carrier-phase measurements using 50 epochs. 111

6.3 Position and coordinates accuracy in metres of the rover using carrier-phase measurements. 112

6.4 RMSE in metres of the rover's coordinates using carrier-phase measurements averaged on 60 epochs for the GGL1 scenario. 115

6.5 RMSE in metres of the rover's coordinates using carrier-phase measurements (results averaged on 60 epochs) for the UNSW scenario. 116

6.6 Statistical model of the error using pseudoranges on the East, North, Height (Up) coordinates. [Ri]= Rician distribution, [N]= Normal distribution. 120

6.7 Statistical model of the error using carrier-phase measurements on the East, North and Height. [R]= Rayleigh/Rician distribution, [N]= Normal distribution and [Exp]= Exponential distribution. 123

7.1 Number of antennas in LoS or Non LoS with the rover for each test point. 141
7.2 Position error in metres of the rover in Wi-Fi area (R =total Error). 141
7.3 Position error in metres of the rover in a Wi-Fi area. 142
7.4 Characteristics of the LOCATA signal [$t = 2200$]. 149
7.5 Characteristics of the LOCATA signal [$t = 1952$]. 150
7.6 Characteristics of the LOCATA signal [$t = 1952$]. 155
7.7 Characteristics of the LOCATA signal [$t = 4400$]. 157
7.8 Signal-to-Noise-Ratio values for various experiments. 160
7.9 Accuracy of LOCATA and RTK GPS technologies averaged on the three coordinates. 165

8.1 Position and coordinates accuracy in metres of the rover using pseudoranges without Hatch filter / with Hatch filter [50 *epochs*] / and only carrier-phase measurements. 176
8.2 Error (in metres) on each coordinate averaged on 150 epochs using LOCATA technology. 181
8.3 Error (in metres) on each coordinate averaged on 100 epochs using RTK GPS. . 182
8.4 Standard deviation for each value of the synchronisation error averaged on a 1000 simulations. 193

A.1 Position and coordinates accuracy in metres of the rover using pseudoranges code smoothed with carrier-phase measurements using 10 epochs. 217

D.1 Position error in metres of the Rover in Wi-Fi area 247
D.2 Channel number of the WiFi access points. 248
D.3 Characteristics of the LOCATA signal [$t = 1355$]. 252
D.4 Characteristics of the LOCATA signal [$t = 910$]. 253

List of Acronyms

3D: 3 Dimensions

3G: third Generation

AoA: Angle-of-Arrival

AP: Access Point

AGC: Adaptive Gain Control

A-GPS: Assisted-GPS

BSC: Base Station Center

BSS: Base Station Subsystem

BTS: Base Transceiver Station

C/A: Coarse/Acquisition

CDMA: Code Division Multiple Access

C-P: Carrier-Phase

CPICH: Common Pilot Channel

CPP: Carrier Point Positioning

CS: Circuit Switched

CTIA: Cellular Telecommunications Industry Association

CVB: Cumulative Virtual Blanking

DDS: Direct Digital Synthesis

DGPS: Differential GPS

DSSS: Direct Sequences Spread Spectrum

DOP: Dilution Of Precision

EDGE: Enhanced Data for GSM Evolution

EGNOS: European Geo-stationary Navigation Overlay System

ENU: East North Up referential

E-OTD: Enhanced-Observation Time Difference

ETSI: European Telecommunications Standards Institute

FDD: Frequency Division Duplex

FDMA: Frequency Division Multiple Access

FHSS: Frequency Hopping Spread Spectrum

FPGA: Field-Programmable Gate Array

GGL: George Green Library

GLONASS: GLObal'naya NAvigatsionnaya Sputnikovaya Sistema

GMSC: Gateway MSC

GNSS: Global Navigation Satellite System

GPRS: General Packet Radio Service

GPS: Global Positioning System

GSM: Groupe Spcial Mobile

HDOP: Horizontal DOP

HLR: Home Location Register

IESSG: Institute of Engineering for Surveying and Space Geodesy

IPDL: Idle Period Down Link

IR: Infra Red

ISDN: Integrated Services Digital Network

ISM: Industrial Scientific Medical

L1: GPS L1 signal

L2: GPS L2 signal

LAMBDA: Least-squares AMBiguity Decorrelation Adjustment

LAAS: Local Area Augmentation System

LED: Light Emitting Diode

LINE: LOCATA Inline Navigation Engine

LLA: Latitude Longitude and Altitude reference system

LMU: Location Measurement Unit

LNA: Linear Gain Amplifier

LoS/NLoS: Line-Of-Sight /Non Line-Of-Sight

LocataLite: LOCATA transceiver

LocataNet: LOCATA Network

MIMO: Multiple-Inputs-Multiple-Outputs

MS: Mobile Station

MSC: Mobile Switching Center

MTU: Mapping The Underworld

MUSIC: MUltiple SIgnals Classification

NAVSTAR: NAVigation System with Timing and And Ranging Global Positioning System

NMEA: National Marine Electronics Association

OTDoA: Observation Time Difference Of Arrival

pdf: probability density function

PHY: Physical Layer

PRN: Pseudo Random Noise

Pseudolites: Pseudo-Satellites

RMSE: Root Mean Square Error

RTK: Real Time Kinematic

RV(rv): Random Variable

RX: Receiver

SDMA: Space Division Multiple Access

SMLC: Serving Mobile Location Center

SMSS: Mobile Switching and Management Subsystem

SNR: Signal-to-Noise-Ratio

StD: Standard Deviation

TDD: Time Division Duplex

TDMA: Time Division Multiple Access

TDOA: Time Difference Of Arrival

TDOP: Time DOP

ToA: Time of Arrival

TTFF: Time To First Fix

TX: Transmitter

UE: User Equipment

UMTS: Universal Mobile Telecommunications System

UNII: Unlicensed National Information Infrastructure band

UNSW: the University of New South Wales in Australia

UoN: the University of Nottingham

US: Uncorrelated Scattering

U-TDoA: Up link -TDoA

UTRAN: UMTS Terrestrial Access Network

VDOP: Vertical DOP

VISTA: Visualising integrated information on buried assets to reduce streetworks

VLR: Visitor Location Register

WADGPS: Wide Area DGPS

WGS84: World Geodetic System 1984

WLAN: Wirless Local Area Network

WLS: Weighted Least-Squares

WSS: Wide Sense Stationary

XPS: X-band Positioning System

Chapter 1

Introduction

1.1 Precise Positioning and Surveying in Urban Canyons

The increasing need of location information has opened a global positioning market: trucking companies want to know where their vehicles are, shippers want to know where their shipments are, utility companies want to know where their buried assets are.

Beneath the streets lie thousands of kilometres of cables and pipes, often buried decades ago. Disturbances such as accidents, weather conditions, traffic volume, and road work can be detrimental to these buried assets, many of which are not shown accurately on maps. Pipes and cables must be located precisely to increase the efficiency of streetwork projects. In this context, the UK's Department for Trade and Industry, along with a group of industries, funded a project called visualizing integrated information on buried assets to reduce streetworks (VISTA) to meet the need to precisely map buried assets in urban areas. This project brings together utility industries (e.g. Thames Water, UKWIR, Yorkshire Water), surveying companies (e.g. Adien) and academia (The University of Nottingham and Leeds University).

To perform this task, GPS is the most reliable and most efficient technology to provide a location anywhere at any time. Thanks to a constellation of over 24 satellites operating continuously and orbiting the earth, GPS receivers can calculate their location within a few metres if they can detect the signals from 4 well distributed satellites. The GPS accuracy may be improved to the centimetre level when using Real Time Kinematic GPS (RTK GPS). RTK GPS is a network of GPS receivers continuously transmitting corrections via radio communications when a GPS user requires them. Unfortunately, GPS has limitations. Satellites broadcast a 500 watts signal at $20,000$ km, but this signal is often obstructed by buildings and/or foliage before receiving it. This occurs often in urban canyon environments.

1.2 Research Aims and Novelty of the Work

This work focuses on alternative technologies to solve the challenges of mapping precisely any buried assets in urban canyons.

The first proposed solution is to augment the GPS signal with terrestrial based technologies. With a market of many millions of handsets worldwide, the cellular network is a promising candidate for locating and tracking users, especially in urban areas. This motivates the continuous investments by the operators to modify their network architecture in order to provide/improve the services and the coverage. Here, algorithms to mix Global Positioning System (GPS) and Groupe Spcial Mobile (GSM) signals are developed. Then, the testbed is a simulator mixing an existing GPS software at the Institute of Engineering, Surveying and Space Geodesy (IESSG) with a GSM one coded by the author of this work. The ideas behind this research are motivated by the outputs of the research on going for the location of a mobile user for emergency calls or location based services applications. In other words, many scientific papers were processed to extract the algorithms shown in this part. The objectives of this thesis were:

- The development of GSM simulations and their integration within an existing advanced GPS software.
- Research on the techniques to locate mobile phones in cellular networks, and development of an algorithm using both GPS and GSM signals to triangulate the receiver's position. It also includes some other post-processing algorithms (e.g. Kalman filter) for a final position of the receiver.
- Finally an assessment of this technology is carried out to compare the accuracy with the requirements of the VISTA project, and for future developments. For example, this work may be also of interest in research focused on the location based services applications such as the advertisements via SMS in shopping malls.

The second proposed solution is based on a prototype recently bought by the IESSG at the University of Nottingham. This prototype is viewed as an advanced network

of pseudolites. Back to the 1970s, research started on the development of ground based transmitters of GPS like signal, also called pseudolites. Because a GPS signal is too weak to be received in some dense wooded areas or in indoor environments, researchers and engineers focused on solutions to augment locally the GPS coverage with those transceivers. Recently *LOCATA Corp.* from Australia has developed a network of time-synchronised pseudolite transceivers. In their early publications, the company claimed that they could achieve the centimetre level of accuracy [Barnes et al. (2003d)] with this new prototype technology. However, the experiments were carried out in the Australian desert at their test site (Numerella) with no results in urban environments, or the comparison of the LOCATA accuracy with existing technologies (e.g. GPS). Research on this technology needed to be brought to the next level with the study of the prototype's features, the check of the truthworthiness of the preliminary results and some more experiments. That is why a large part of this thesis is dedicated to analyse the LOCATA technology from the signal basis (e.g. multipath, signal propagation) to the applications (e.g. urban canyons). As the technology is very new and not available on the market yet, the IESSG is one of the few institutions in the world having this technology after the United States Army, the University of New South Wales and LEICA Geosystems. The objectives of using this thesis work were:

- To develop a comprehensive documentation on how to use this technology and to set up a network.
- To perform many experiments in various environments (e.g. narrow streets, open fields) and to study the time series of the positioning error through comparison with the RTK GPS.
- To set up a permanent LOCATA network for the study of the accuracy in urban canyons and the possible unexpected effects (e.g. interferences).
- A statistical study of the LOCATA signal in order to see the effects of blocking the Line-of-Sight between the receiver and the transmitters. Furthermore, this milestone is interesting to explain why the accuracy degrades during an experiment.

- Software development: as there is no agreement between the IESSG and *LOCATA Corp.* to transfer any type of data such as software, the author needed to develop his own navigation software to triangulate the LOCATA receiver's position. This helps to explain how the one embedded inside the prototype outputs the receiver's location.

1.3 Thesis Outline

Chapter 2 provides the project background and the challenges to map buried assets in towns. It also reviews the technologies on the market to perform this job.
Chapter 3 is an overview of the fundamentals of Global Positioning System. The error sources which degrade the navigation accuracy are focused upon. The challenge of using GPS in urban canyons is also discussed.
Chapter 4 starts with the basic definitions in cellular networks technology. Some algorithms and techniques to locate a mobile phone are explained and discussed. The second part focuses on the algorithms developed by the author of this thesis to mix the GPS and GSM signals. To check the validity of the algorithms, a simulator is developed as testbed. Results and simulations are finally discussed.
Chapter 5 deals with the LOCATA technology. This section explains the advantages of triangulating the receiver's position with this technology. This chapter is also a kind of manual to set up the network of LOCATA transceivers. Some preliminary work is done through distance tests. The multipath is extracted from the LOCATA observables.
Chapter 6 is focused on how to achieve the centimetre level with the LOCATA technology. Various experiments are realised and exposed in detail, in different environments (mainly on the campus of the University of Nottingham). Results are analysed through the time series of the root mean square error. Both pseudoranges and carrier-phase observables are used separately to triangulate the receivers' positions. Thus, the accuracy of this position is intrinsic of the type of observables used. The navigation software embedded inside the prototype's firmware is also presented (LINE) and analysed. Some features of the LOCATA signal are also extracted from

the data. The end of the chapter deals with statistics on the time series of the root mean square error in various environments. The error ellipse is also calculated and ends with some theoretical conclusions. Note that the error (e.g. mean value, standard deviation, time series) is studied in absolute value in this chapter and in the following ones.

Chapter 7 starts with the set up of a permanent network on the roofs of the University of Nottingham's buildings to study the accuracy of this technology in urban canyons. Results are explained. During the test an unexpected phenomenon happened. The interference between the LOCATA signal and the Wi-Fi is comprehensively analysed. Some conclusions are given on what is missing in the LOCATA hardware/firmware design in order to end up with this interference. It follows an important analysis through statistics of the LOCATA signal and Signal-to-Noise-Ratio when blocked by foliage. This section ends with the comparison between the Real Time Kinematic Global Positioning System and the LOCATA accuracy.

The beginning of the Chapter 8 focuses on a navigation software developed by the author. LINE is the software embedded inside the prototype's firmware. It is useful to develop once an in-house software from an academic point of view and for a deeper understanding of the algorithms coded inside the LOCATA Inline Navigation Engine (LINE). Some experiments are then reprocessed and the errors are compared with the results given by LINE in the previous chapters. The chapter also includes a test in indoor warehouse in order to test this new equipment inside a so-called extreme multipath environment. This experiment may open a new way to survey indoors. Finally, the last section is dedicated to the simulation of the future integration of the LOCATA technology with the Global Navigation Satellite System. A simulations are carried out (re)using the architecture of the simulators developed in Chapter 4. The model of the errors in the carrier-phase measurements (from the satellites and the LOCATA transceivers) are explained in detail. It ends with the analysis of the results.

Chapter 9 concludes this dissertation. The major conclusions written through this work are gathered and reviewed. Some ideas for a future work on the LOCATA technology are discussed.

Chapter 2

Research Background

2.1 General Overview of the Project

2.1.1 Project Background

In the UK, there are currently approximately 4 million kilometres of buried pipes and cables providing utility service. These are a combination of telecommunications, water, gas, sewerage, electricity and drainage. It is estimated that there are 1.5 million holes dug each year in the UK on highways and footpaths by utility companies so that they can install new services and maintain existing ones. This is in addition to road building and repair work carried out by the Highway agency [Roberts et al. (2006)]. Over the past 25 years, the UK has seen an increase in traffic of 72%, with an increase in the number of cars on the road of 14 million from 10 million in 1972. In addition, the amount of freight carried on the roads has increased by 69% since 1980. Latest government figures forecast that road traffic will increase by about 40% over the next 20 years [Parker and Overton (2005)].

Congestion is an everyday part of our lives, and has many causes. Busy roads are very sensitive to small disturbances, such as accidents, weather conditions, traffic volume and road works.

One answer to enable these pipes and cables to be located is to map them in absolute terms (e.g. using GNSS). This is simple enough for new pipes and cables being laid, but difficult to do for those already underground. The combination of location devices such as GPS with detection devices such as Ground Penetrating Radar, Acoustics, and quasi-static fields is a way forward. In addition to this, the use of knowledge integration and pipeline-ground interaction can all add up to a combined system allowing the location of such utilities to become reality. However, this will be a mammoth task considering the number of utilities in existence [Research (2005)].

2.1.2 Buried Assets

2.1.2.1 Mapping the Assets: a Costly Process

Many utilities in the UK were laid in Victorian times when demands due to the economic boom were large, with pipes in older cities being greater than 150 years

old. Poor mapping techniques, and recording the pipe's location relative to a physical feature that no longer exists means that the exact location of many of today's networks are unknown, especially their position relative to other pipes and cables [Research (2005)].

In addition to this, many records do exist, but in a number of formats such as paper based, microfiche, and digital. Furthermore, the records that do exist are sometimes incompatible between various companies, hence being able to position one company's pipes relative to another's cables is difficult.

Today, there is another boom in cable laying. The Government is actively promoting the use of broadband within the general population. The fibre optic cables required for this are vast. Today there are well over 3 million km of fibre optic cables laid under the streets of the UK [Montillet et al. (2007b)].

In 2001, the UK Government announced the target to have the most competitive and extensive broadband market in the $G7$ group of countries (Canada, France, Germany, Italy, Japan and the USA) by the end of 2005. The DTI has commissioned research to benchmark the progress of the UK against the other $G7$ countries, including also Sweden, Ireland and Australia.

The UK has the most extensive broadband infrastructure in the $G7$ group of countries, with over 97% of households and businesses now able to receive broadband. British Telecoms announced in summer 2004 that it expected availability of broadband to rise to over 99% by the end of summer 2005. There are over 6 million subscribers in the UK and there are around $60,000$ new connections each week [Research (2005)].

Many utilities are reaching the end of their design lives. National Grid Transco, for example, has a programme to replace all their iron mains within 30 metres of properties over the next 30 years. Thames Water will replace more than $1,600$ km of iron mains in London over the next 5 years [Roberts et al. (2006)].

The utilities companies are being pushed by the customers' demands. It is now difficult to place more utilities into the tight space under the streets of some of the oldest cities without the risk of damaging those already in place.

However, the increasing use of plastic pipes is making detecting the utilities through geophysical techniques even more difficult [Roberts et al. (2006)].

2.1.2.2 Digging Holes in the Street

It is common practice to dig a series of trial holes in order to locate the utility required, then to come back some days later to excavate the actual trench. To do so, it is then required to know precisely beforehand the position of the assets and the various utilities that may lie in the layer above the target pipe. Although recently installed assets may have been well mapped (the level of accuracy of these existing maps is defined in the following sections), location and attribute data on older services can be very poor, in some cases even non existent (except perhaps knowing the location of the terminating points). This poor data quality can lead to unnecessary holes dug in the wrong place and third party damage to other underground services. Figure 2.1 shows a map of the utilities drawing by hand and an excavation in the street.

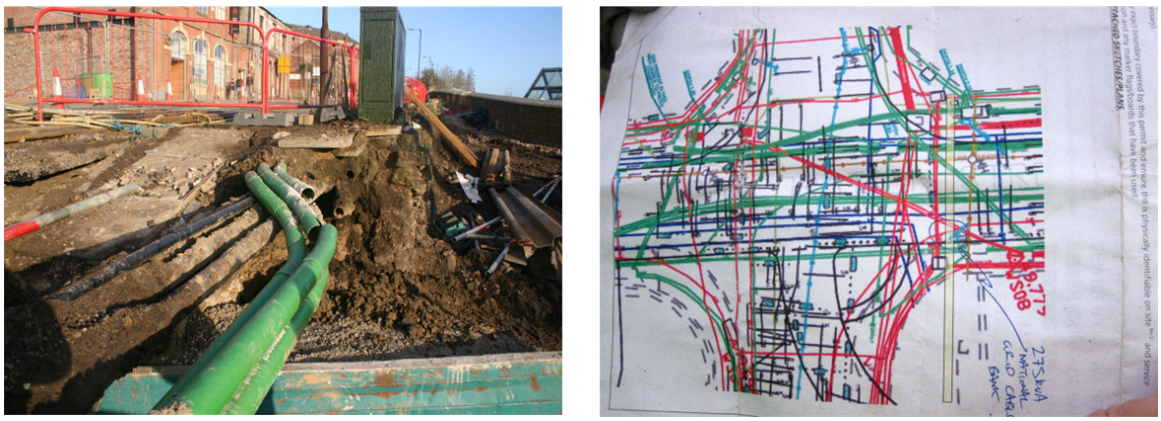


Figure 2.1: Map of the assets (right) and an excavation on site (left).

Equally important, there are also considerable indirect costs owing to disruption on the roads caused by works, waste and pollution. The core of the problem is that there is at present insufficient and inadequate knowledge about what is where. This causes extra disruption as well as excavation costs and defines the notion of time-efficient process. In other words, the research outcome should also limit the time of streetwork processes to avoid large traffic congestions or any other disruption of the community life.

Behind the economical cost of the work, there is a potential cost of human life. If the map of the utilities is not precise or not up-to-date enough, it may happen that

a pipe (e.g. gas pipe) breaks during the excavation process, and in the worse case scenario a contractor strikes a high power electricity wire. Furthermore, sometimes the whole pipe has to be replaced and the whole road has to be shut down, because of the health and safety issues.

2.1.3 Project Funding

2.1.3.1 EPSRC and Industry's Sponsorship

The UK's Engineering and Physical Sciences Research Council (EPSRC) announced in 2004 that it was establishing a programme as an initial attempt to start tackling the above issues. It organised a sandpit exercise, whereby invited academics, industrialists and EPSRC all got together in the Autumn of 2004 to think of ideas that could be put forward as research projects. The EPSRC put £1 million into the programme, and as a result four projects were funded, focusing on:

- Buried asset location, identification and condition assessment - a multi-sensor approach.
- Mapping and Positioning.
- Knowledge and Data Integration.
- Enhanced Methods of Detection of Buried Assets.

Following these projects, a network programme was also separately funded called: Mapping the Underworld. This network brings together academics from Universities in Bath, Birmingham, Leeds, Nottingham, Oxford, Sheffield and Southampton. In addition, industrial companies, such as UK Water Industry Research (UKWIR) are also heavily involved with the projects [Research (2005)].

2.1.3.2 The VISTA Project

A second project called Visualising Integrated Information on Buried Assets to Reduce Streetworks (VISTA) was funded by the UK's Department for Trade and Industry (DTI) in the middle of 2005. This project brings together the University of

Nottingham and Leeds University, as well as UKWIR and 18 other organisations, including various utility companies (e.g. United Utilities, Anglian Water, Thames Water, Yorkshire Water, BT, Severn Trent Water, Three Valleys Water, South East Water), professional organisations, excavation companies and survey companies (e.g. Adien Ltd). The full list of partners and shareholders of this project can be found at the following web link: www.vistadtiproject.org. The research carried out by the author of this work was completely funded by this project.

The research goal of this project shares the same framework as the Mapping The Underworld project. The overall aim is to investigate the feasibility of several novel approaches, alongside greatly enhanced existing techniques, to be combined in a single multi-modal approach to the location, identification and condition assessment of buried assets. Furthermore, it focuses especially on enhancement and integration of existing legacy asset information, together with dynamically acquired accurately geo-referenced data in the street and development of novel techniques to display the resulting knowledge to digging teams and network planners. Thus, the integration of the various positioning technologies together with the improvements of actual technologies is carried out by researchers at the IESSG, the University of Nottingham, whereas the creation of a database for all assets gathering paper based maps and modern electronic maps is the work investigated by the Leeds University.

⊘ **Research at the University of Nottingham**

It is well known that the accuracy, availability and reliability of satellite based positioning are very dependent on the number of tracked satellites and their spatial geometry. One of the limiting factors in using GPS is the requirement of having direct line of sight between the satellites themselves and the GPS receiver. Most of the work is carried out in built up areas where line of sight to a sufficient number of satellites is not always possible, or when it is available the geometry may be too poor to allow a precise position of any assets. In addition, the presence of trees and buildings can cause masking issues, as well as introducing multipath errors [Roberts et al. (2006)].

The objective of this sub-project is to research or to develop further existing posi-

tioning systems/techniques (e.g. ground-based positioning systema, GPS) to conduct precise three dimensional positioning at the centimetre level, by the integration of various technologies, such as GSM signal or LOCATA transmitters and GPS.
LOCATA technology is a ground-based positioning network of time synchronised transceivers (LocataLites). This technology is the next step in the evolution of pseudolite technology. The main positioning applications are work in open pit mining, bridge deformation and street work enhancement [Barnes et al. (2007)]. Researchers are working on the development of software to extract and analyse the accuracy of this novel technology. Then, algorithms to compare and integrate with GNSS technology will be developed. Finally, system validation and algorithms development are conducted at the Institute Engineering for Surveying and Space Geodesy through simulations and field trials. Finally, a comprehensive details of the work done at the University of Leeds may be found in [Boukhelifa and Duke (2007)] and [Hickinbotham and Cohn (2007)].

2.1.4 Precise Positioning of the Assets

This thesis focuses on the challenges of mapping precisely buried assets in difficult environments (e.g. urban canyon). From the VISTA definition, the GPS technology is not available or reliable enough in those kind of environments. Chapter 3 reviews the GPS technology and its limitations. Then, the solutions presented in the next chapters are based on the augmentation of GPS with other alternative technologies (i.e. GSM signal, LOCATA) to tackle the actual satellite based location system limitations. However, some definitions have to be given before starting the explanations of the various solutions.

Let us define the accuracy required by the industrial sponsors of this project. As a reminder, the ultimate goal is to map any kind of assets common in the streets. It starts from a large sewer pipe, to a couple of centimetres for the envelop containing a bundle of electrical wires. Figure 2.2 shows a trench with some assets and a bundle of wires.



Figure 2.2: Trench showing buried assets (left) and a bundle of telecommunication wires (right).

In the terminology used in the project reports, the industry sponsors and the academics are using the word centimetre level. In scientific words, this accuracy may lead to two perceived levels of error: the centimetre unit or tens of centimetres (decimetre). In this thesis, we keep the terminology centimetre level as used in the reports for the VISTA members, although this level has been recently redefined and all members are now agreed with a maximum error of 15 cm, which is closer to the decimetre than the centimetre. Will it influence the process of mapping the assets and later on visualising the results on a general map (e.g. Ordnance Survey map)? The answer is negative, because from [Parker and Overton (2005)] the centimetre accuracy was defined as the root mean square error in 2D (East and North coordinates in the ENU National Grid referential). In other words, the utility companies may solve most of their problems (e.g. hitting unknown pipe when digging a hole) with an accurate 2D map.
Nevertheless, there are advantages and drawbacks of an accurate 3D map. Future equipment of employees surveying in the street may include the virtual reality technology to ease their work, and a 3D model of the environment will then be required

[Roberts et al. (2002a)]. At the opposite, the assets are buried and the depth may change of few centimetres depending on some external factors such as how many tar layers are added to protect the road and the movements of the soil (human activity makes vibrations in the soil and that may moves little by little the buried assets) [Parker and Overton (2005)]. In addition, the excavation to repair an asset may need sometimes to open a large section of the road, and the road will be reshaped totally afterward. Thus, the depth calculated with any technologies suffers of additional errors intrinsic of the road pavement.

The precision of the location technologies is also an important parameter. In [Leick (2004)], precision refers to closeness of repeated observations to the sample mean, whereas accuracy refers to the closeness of the observations to the true value. In other words, the precision is related to the spread of the observations around the mean value and the accuracy is related to the difference between the mean value and the true value. Thus, the smaller is the standard deviation of a set of measurements, the more precise are the observations. Those definitions need to be emphasised especially when we need to study the time series of the error from the estimated coordinates. Some sections of this thesis are not focused only on the basic statistics of the error (mean and standard deviation), but also the error is modelled using common probability density functions (e.g. Gaussian distribution) and curve fitting tests (e.g. correlation coefficient). It was chosen to do the curve fitting test manually by testing different probability density functions and see through the correlation coefficient which one best fits the data. Another way would have been to test directly the set of data with a Chi-Square or Kolmogorov-Smirnov (see[Lynch and Willett (1998)]) test and evaluate their precision in terms of 1 Sigma, 2 Sigma ...etc. Here, the probability density function and the correlation coefficient value are given for each set of data modelled.

2.2 Technologies Already Available on the Market to Locate Precisely Buried Assets

The managements of the assets requires accurate information such as position, internal corrosion and state-of-the-art of the whole pipeline. All this information is taken into account by the utility companies when any decisions have to be made (e.g. replacement, excavation). Many companies are available on the market using various technologies to perform these tasks (e.g. Adien Ltd, Future Amtec Ltd, Sahara pipeline inspection). This section opens the door to these various techniques and may not be comprehensive. Before going further, it is difficult to describe technically all the technological solutions to locate, identify and check the assets, because some of these technologies were developed by companies and due to industrial secrecy not much information are released.

The first tool is the Ground Penetrating Radar (GPR). It is generally used in applications related to civil engineering such as voids beneath concrete, geological stratigraphy, water table mapping, road bed mapping and of course for utilities detection. This technology employs radio waves, typically in the 1 to 1000 MHz frequency band, to map structures or features buried in the ground [Daniels (2004)]. The exploration depth varies with the type of soil the GPR is used through. Equation (2.1) is a simple rule of thumb to give an approximately depth of exploration.

$$D = \frac{35}{\sigma} \tag{2.1}$$

where σ is the conductivity of the soil (unity: mS/m) and D the depth in metres. For example, the maximum depth is around 100 m if the soil is made of sand, whereas the GPR technology does not explore more than 10 m in concrete ground [Geomatrix (2004)]. Typically, this tool is used prior to any excavation work, in order to check if any utilities are buried in the ground not reported on the utilities map. Their costs start around $£10,000$ but reach $£100,000$ for the more advanced ones. A great deal of research on this technology is focused on the challenge of detecting non-metallic objects [Research (2005)].

Other tools used by utility companies include cable advoidance tools, cable and pipe

locators, and metal detectors. These offer cheaper solutions, but they are limited in terms of accuracy and their abilities to detect non-metallic object.

When it comes to monitoring the state of assets such as sewer pipes, a range of technologies may be used. These technologies are called invasive and they are used to accurately pin-point areas of external pipe damage, leakage, other services and key anomalies such as voids and solid masses.
Among them CCTV/Light Line is common. It operates to inspect boreholes, pipelines, chimneys and other inaccessible locations. The engineers monitor the inside of a pipe by watching the (colour) images sent from the camera generally at the end of a line. Some other technologies using acoustic waves are an alternative for the in pipe monitoring. Here are two approaches. The first one is the same as the CCTV technology: a sensor at the end of an umbilical cable radiates acoustic waves and records the incoming signal. As the umbilical cable is linked to a powerful server, generally inside a van, the signal is then processed to determine and locate any crack inside a pipe [Bond (2007)]. In the second approach, the sensor is not moving inside the pipe, but it just sends and receives the signal. Then, thanks to lots of signal processing algorithms, cracks, leakage and deteriorations may be recorded and localised [Horoshenkov et al. (2007)].

2.3 Summary

This chapter is an overview of the industrial motivations behind this research work. It introduces the VISTA project funded by the UK Department for Trade and Industry (DTI) during 2005 and also part of a bigger project called Mapping The Underworld. Two research centres (University of Nottingham and the Leeds University) together with 18 industrial partners are working towards the challenges of mapping buried assets everywhere. This research involves actively industries and academics by frequent meetings and workshops which allows a continuous knowledge exchange and it generates new ideas to investigate for the researchers.
Furthermore, this chapter has defined the level of accuracy aimed for as a positioning error of maximum 15 centimetres in three dimensions and a centimetre in two dimen-

sions (exclude depth) [Research (2005)].

Finally, this chapter already underlines some limits on existing positioning technologies such as GPS. The aim of this work is to look at other technologies to improve and augment this technology as we will see in the next chapters.

Chapter 3

GPS Technology and Challenges in Urban Canyons

3.1 Introduction

GPS is a shortening of Global Positioning System. Satellite-based positioning was an idea emerging back in the 1960s. GPS was designed as a dual-use system, with the primary purpose of meeting the military's needs for positioning and timing. The network is owned and operated by the U.S. government. The first generation of satellite (Block I) was designed with a 8 to 9 years life-time expectancy. The Block I generation of satellites were launched between 1978 and 1985 into three 63 degrees inclined orbital planes. With the evolution of this technology, more satellites (e.g. Block IIA, IIR (R means replenishment), IIF (F denotes follow on) and III (future generation of GPS satellites expected to be launched around 2030)) have been launched to orbit around the earth to cope with the needs of the market and new features have been added as the technology evolves constantly (e.g. more reliable and more precise navigation solution) [Hoffmann-Wellenhof et al. (2001)]. After the first generation, GPS satellites orbit at a 55 degrees with the equator line [US.Army (1996)].

The next section is an overview of the GPS architecture and some important definitions are given to understand the following chapters in this thesis. This part ends with an overview of Real Time Kinematic GPS. In Section 3.3, the pseudoranges and carrier-phase observables measured by a GPS receiver are discussed and the errors that degrade the satellites navigation technology are presented. Those sources of error are mainly the result of the propagation of the signal from the transmitting satellite to a GPS receiver on earth. Furthermore, the mathematics behind the triangulation of the GPS receiver's position are explained. Section 3.4 emphasises the so called difficult environments where GPS accuracy is degraded to such a level the position is useless for a precise positioning (e.g. less than 20 centimetre accuracy as defined in the VISTA project proposal [Research (2005)]). At the end, the problem of locating precisely buried assets in difficult environments is reviewed.

3.2 GPS Architecture

3.2.1 Signal Characteristics

Two kinds of signal are transmitted by GPS satellites: P (Precise) and C/A (Coarse/Acquisition) codes. The first one is only usable by precise positioning services (e.g. U.S. military), whereas the second one is used by anybody or also called Standard Positioning Services (SPS) (e.g. civilian). The details of the second signal are well documented [US.Army (1996)] and are available on line. However, the P code is encrypted to the Y code to deny its access to civilian users. Also, the SPS positioning capability was initially degraded by SA measures, including a dither in the satellite clocks and the falsification of the navigation messages. But this was permanently discontinued in May 2000 by the direction of the U.S. president [Leick (2004)].
The C/A code is only modulated on the L1 carrier wave at 1.57542 GHz. The P code is modulated on both L1 and L2 carrier waves. L2 carrier wave has a center frequency of 1.2276 GHz. The chipping rate of the C/A code is 1.023 MHz with a period of 1 ms, whereas P(Y) code is 10.23 MHz with a period of 38 weeks. It is implied that the length of the C/A and P codes are respectively 293 m and 29.3 m. The accuracy of the GPS technology comes from the atomic clocks embedded in the satellites and transmitting continuously the codes on L1 and L2 frequencies. The clocks may be considered as perfect in terms of clock drift, but on the surface of the earth the GPS receiver is much cheaper technology than the one embedded in a satellite for navigation. Thus the clock drift will depend on the grade/price of the product. For example, it is known that the accuracy of the position calculated using a GPS hand-held receiver is less than 10 m in open area, whereas with a GPS used for Geodesy applications the accuracy may be better than 5 cm depending on the measurement scenario [Schwieger (2003)], [Leick (2004)].

In the future of GPS modernisation, additional signals will be transmitted by satellites to improve the anti-jamming capability, the protection against anti-spoofing, to shorten the Time-To-First-Fix, and provide a civilian safety signal (L5) in the protected Aeronautical Radio Navigation Service (ARNS) frequency band. The new

L2C signal will increase robustness of the signal, improve resistance to interference, allow for longer integration times in the receiver, thereby reducing tracking noise and increasing accuracy for a more precise positioning in indoor environments and wooded areas [Liu (2002)]. The carrier frequency on L5 is 1.17645 GHz. The length of this code is 1 ms with a chipping rate of 10.23 MHz.

The GPS network consists mainly of three segments: the satellites constellation and a network of maintenance stations (control segment) to check the functioning of the GPS network. Finally, the collection of all GPS receivers is called the user segment [Hoffmann-Wellenhof et al. (2001)].

3.2.2 Space Segment

The space segment is a constellation of satellites operating in almost 12 hour orbits at an altitude of $20,183$ km. The constellation is nominally composed of 24 satellites in six orbital planes, each plane equally spaced about the equator and inclined at 55 degrees for the satellites built after the first generation (starts with the Block II).

3.2.3 Control Segment

The ground control segment consists of a master control centre, some monitor stations and ground control stations. The main tasks of this network tracks the satellites, precisely determines their orbits and clock determination and prediction, and periodically uploads almanac ephemeris for retransmission to the user segment. This segment was also responsible for imposing SA on the broadcast signals. There is one master station (Shriver AFB in Colorado Springs), five monitor stations (Hawaii, Colorado Springs, Ascension Island, Diego Garcia, Kwajalein). The ground control stations collocate with the monitor stations at Ascension, Diego Garcia and Kwajalein. They are the communication link between the monitor stations and the satellites and mainly consist of the ground antennas. Note that the monitor stations network is augmented of 14 additional sites operated by the National Imagery and Mapping Agency to compute the precise ephemerides [Hoffmann-Wellenhof et al. (2001)].

3.2.4 User Segment

The user segment is the collection of all GPS user receivers available on the market including military ones and their support equipments. Navigation with the receiver is accomplished by passive triangulation. More simply, the GPS receiver position is determined by the geometric intersection of several simultaneously observed ranges (satellite to receiver distances) from satellites with known coordinates in space. The receiver measures the transmission time required for a satellite signal to reach the receiver. Transit time is determined using code correlation techniques. The actual measurement is a unique time shift for which the code sequence transmitted by the satellite correlates with an identical code generated in the tracking receiver. The

receiver code is shifted until maximum correlation between the two codes is achieved. This time shift multiplied by the speed of light is the receivers measure of the range to the satellite [Parkinson and Spilker (1996)]. Figure 3.1 is the overview of the GPS constellation with the different corresponding segments.

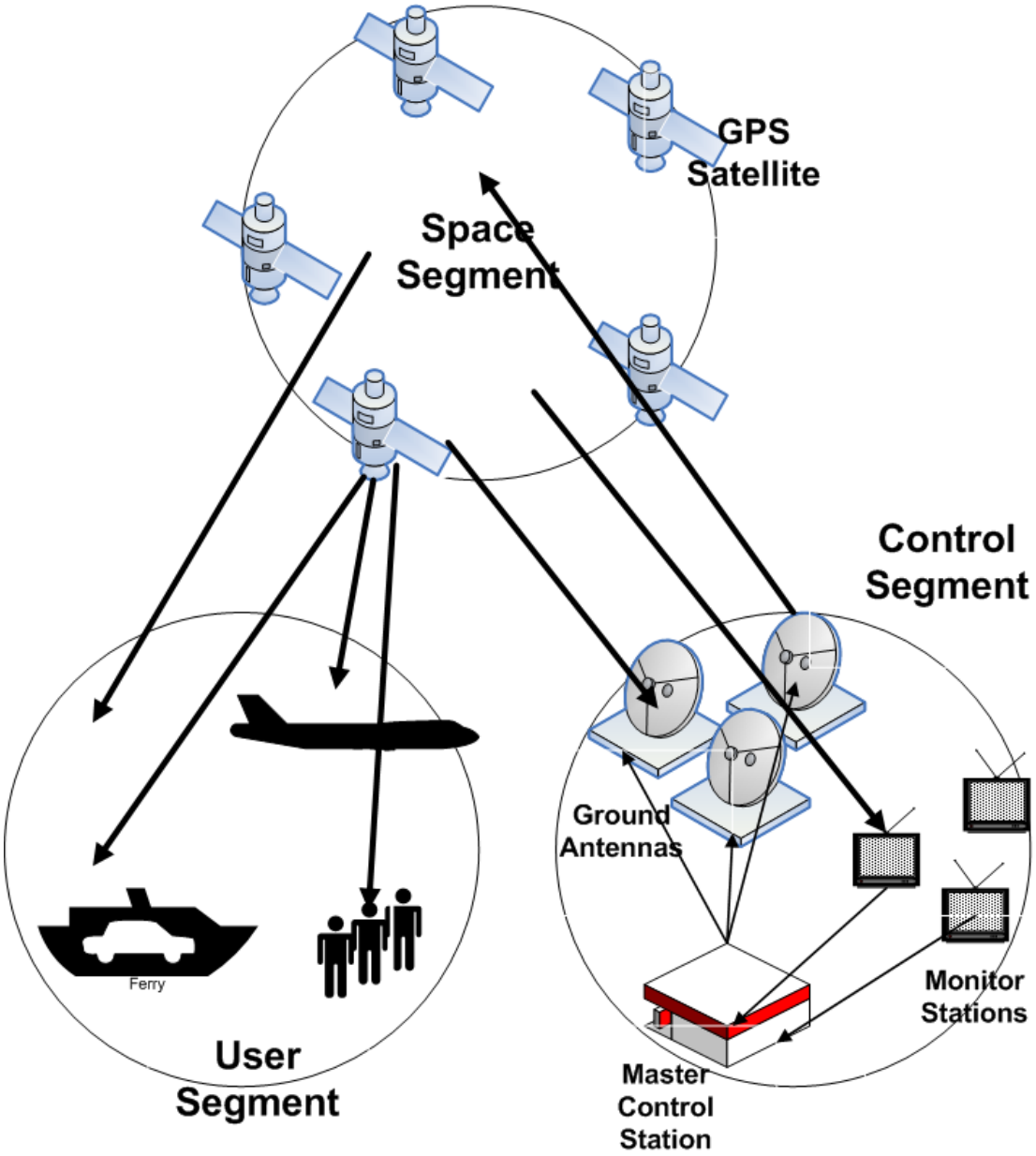


Figure 3.1: Overview of the GPS segments [US.Army (1996)].

This measurement includes various propagation delays, as well as satellite and receiver clock errors. Since the measurement is not a true geometric range, it is known as a pseudorange. The receiver processes these pseudorange measurements along with the received ephemeris data (satellite orbit data) to determine the users three-dimensional position. A minimum of four pseudorange observations are required to mathematically solve for four unknown receiver parameters (i.e. latitude, longitude, altitude, and clock offset). If one of these parameters is known (for example, altitude fixed) then only three satellite pseudorange observations are required and thus only three satellites need to be tracked [Strang and Borre (1997)]. However in the literature (see [Stewart et al. (1995)] ,[Montillet et al. (2007b)]), it is recommended to use at least 5 well distributed satellites for a precise positioning (e.g. RTK GPS [Strang and Borre (1997)]) in practical scenarios. This important point is explained in detail later on.

3.3 Positioning with GPS

3.3.1 Pseudorange and Carrier-Phase Observables

Pseudoranges and carrier-phase measurements are the two types of GPS observables used for positioning. They can be used together or separately to compute the position of the receiver. As previously underlined, the carrier-phase observations are used for precise positioning at the centimetre level. During the last three decades, processing algorithms have been developed to constantly improve the navigation solution using those observables. An example is the double and triple difference algorithms developed to detect some issues related to the carrier-phase measurements [Eren (1987)]. These issues are explained in the following sections. Moreover, GPS receiver architecture includes a great deal of advanced signal processing algorithms and electronics to extract the observables from the satellites' signals [Parkinson and Spilker (1996)]. It is well known that the signal power transmitted from the satellites is severely attenuated ($-135dBm$), because of travelling through the different atmospheric layers of the earth (e.g. Troposphere and Ionosphere).

In the remainder of this part, the errors and phenomena affecting the two observables are discussed in detail with the mathematics to triangulate the receiver's position. It ends with the review of the main GPS technologies (e.g. standalone, Real Time Kinematic GPS).

3.3.1.1 Pseudoranges Ranging

The pseudorange is the distance between a satellite and the receiver's antenna calculated between the epochs of emission and reception of the code. This time is measured during the correlation of the identical Pseudo Random Noise (PRN) codes in the receiver. The code tracking loop within the receiver shifts the internal replica of the PRN code in time until the maximum correlation occurs. The equation of the pseudoranges is :

$$\rho^p(t_k) = \frac{R^p}{c} + dt_k + (dI^p_\rho + dT^p_\rho) + \epsilon^p_{\rho k} \tag{3.1}$$

with $\rho^p(t_k)$ the pseudorange value (in second) at the epoch t_k from the p-th satellite, R^p the geometrical distance between the receiver and the p-th satellite, dI^p and dT^p are respectively the Ionosphere and Troposphere delays, dt_k is the clock drift of the receiver at the k-th epoch and finally $\epsilon^p_{\rho k}$ is the signal propagation error (e.g. shadowing, multipath fading) [Hoffmann-Wellenhof et al. (2001)]. This mathematical expression of the pseudorange shows the different errors to model for a more precise accuracy of the receiver's location. The clock drift (dt_k) is an unknown variable that is directly linked to the hardware of the receiver. The more expensive the receiver is, the smaller is this error (e.g. atomic clock in GPS satellites). As dI^p_ρ and dT^p_ρ are the kind of error that is intrinsic to the atmospheric layers, many models may be used to remove these errors accurately. The Ionosphere is extended in various layers from about 50 km to $1,000$ km above earth. It is modelled as a dispersive medium with respect to the GPS radio signal. Common models are described in [Seeber (1993)] or [Klobuchar (1986)]. Tropospheric delay may also be modelled following various models such as the Hopfield model [Hopfield (1969)] or the Saastamoinen model [Saastamoinen (1973)]. Actually, $\epsilon^p_{\rho k}$ is the only error very difficult to cancel out in practical scenarios [Weill (2003)]. As previously said, it is a term to take into account the signal fading errors

(multipath and shadowing). However, this phenomenon may be modelled in very few and specific scenarios when the surroundings of the GPS antenna are stationary [Ge et al. (2000)].

3.3.1.2 Carrier-Phase Ranging

Carrier-phase is the second type of observable provided by the GPS technology. This observable contains less noise than the pseudorange and so it is possible to locate a GPS receiver with a higher precision. When calculating the carrier-phase measurement, the order of magnitude of the accuracy is about 0.01 cycles, which gives the receiver's position at the millimetre level. The equation of the carrier-phase signal is described in:

$$\phi^p(t_k) \quad = \quad \lambda(\frac{R^p}{c} + dt_k + (dI^p_{cp} + dT^p_{cp})) + \lambda N^p + \epsilon^p_{\phi k} \tag{3.2}$$

With $\phi^p(t_k)$ the carrier-phase measurement in cycles at the epoch t_k; dt_k,dI^p_{cp} and dT^p_{cp} are respectively the receiver's clock drift, the Ionosphere and Troposphere delays. $\epsilon^p_{\phi k}$ is the carrier-phase signal error in cycles. It is common knowledge that the signal transmitted from the p-th satellite is reflected on the ground or on the scatterers before the GPS's antenna received it, which results in some shadowing and multipath effects [Misra and Enge (2001)]. The error $\epsilon^p_{\phi k}$ is much smaller than $\epsilon^p_{\rho k}$, that is one reason why carrier-phase measurement is more accurate than pseudorange.

Finally N^p is the integer ambiguity between the receiver and the $p-$th satellite. When a GPS receiver locks onto a given satellite's signal, it is then possible to measure how many cycles there are between the receiver and the satellite. The ambiguity value is the unknown number of cycles accumulated before the signal was locked by the receiver. This number should remain constant through the measurements until the receiver losses the lock. To calculate this unknown variable, techniques differ depending on whether the GPS receiver is single or dual frequency.

- In the first case, the user needs to initialise the GPS receiver on a known point to calculate the ambiguity values. The ambiguity values are averaged on the values calculated during a couple of epochs for each satellite. Every time the loss of

lock loop occurs the rover needs to come back to the known point (initialisation point) to recalculate the ambiguity [Leick (2004)]. This method is also called the Stop-and-Go technique, because if inside the trajectory of the rover there are a couple of points with known accurate coordinates, the user may stop to those points to reset the ambiguities [Hoffmann-Wellenhof et al. (2001)].

- When using a dual frequency receiver, the ambiguity resolution changes significantly. The advantages result from the various possible linear combinations that can be formed with the carrier-phase equations of the two GPS signals (L1 and L2). Different techniques were developed such as the narrow and wide lane techniques. The wide lane technique may also use the code data in addition to the dual frequency to solve the ambiguities [Misra and Enge (2001)]. When the GPS satellites will transmit a third signal (L5), the Three-Carrier Ambiguity Resolution (TCAR) may be used to resolve instantaneously the ambiguities by using data of a single epoch unless very short baseline is considered [Hoffmann-Wellenhof et al. (2001)].

Once the ambiguities are resolved, the values have to be converted from float to integer values in order to get a more accurate rover's position. This is called the search technique. The search technique may be a long process depending on the standard deviation of the ambiguity. For example, if an ambiguity is estimated to be -87457341.88 cycles with a standard deviation of 0.3 cycles, all the integer ambiguities that fall within $+/-3$ standard deviations of that value should be searched. This would be a search of potential integer ambiguities of -87457340.0 to -87457343.0. Here again, some powerful techniques were developed to calculate the integer ambiguities such as the On-The-Fly (OTF) ambiguity resolution [Roberts (1997)] and the Least-squares AMBiguity Decorrelation Adjustment (LAMBDA) method [Teunissen (1995)]. The OTF technique is well know to solve the integer ambiguities for kinematic cases (see [Roberts (1997)]). The latter method (LAMBDA) is also referred in the literature as the integer least-squares estimator. In other words, it is the least-squares estimator that has the highest probability of correct integer estimation among all possible admissible integer estimators. This technique has gained a great deal of

interest in dual frequency GPS products, which is perhaps due to the probabilistic justification of this method and the speed of the calculations [Leick (2004)].
However, the navigation software in GPS single frequency does not solve generally the ambiguity as an integer, but as a float, because of the long time of the search technique [Hoffmann-Wellenhof et al. (2001)]. It will be explained later in this work why the navigation software inside the LOCATA technology solves the ambiguities as float values.

Furthermore, cycle slip is also a large source of error while positioning with carrier-phase measurements if it is not detected by the navigation receiver's software. A cycle slip is a sudden jump in the observable by an integer number of cycles. Cycle slip is caused by the loss of lock of the phase lock loops. Loss of lock may occur briefly when the signal does not reach the GPS receiver's antenna due to signal obstruction such as foliage or walls [Leick (2004)]. If the receiver software does not correct this error, the carrier-phase signal is shifted by the same integer, which causes this jump on the receiver's position. The common way to detect a cycle slip on a signal is by double difference.

$$\frac{\delta^3 \phi^p}{\delta t_k^3}(t_k) \quad = \quad (\phi^p(t_{k+1}) - \phi^p(t_k)) - (\phi^p(t_k) - \phi^p(t_{k-1})) \tag{3.3}$$

where $\phi^p(t_{k+1})$ is the carrier-phase measurement at the epoch t_{k+1}. The double or triple difference technique is used to get rid of the biases due to mainly the clock drift of the receiver. This technique and its applications to detect cycle slips are described in Section 7.3.1.1.

3.3.2 Receiver's Position

The position of the receiver is calculated by triangulation, which needs the measurements from four well distributed satellites generally [Montillet et al. (2007b)]. This also called point positioning. Using the simplified point positioning assumptions, the receiver clock drift is calculated epoch-by-epoch from least-squares, whereas the satellite's clock drift is neglected (atomic clock). The ionospheric and tropospheric delays are estimated from models as explained previously. Let us consider the example

of positioning with pseudoranges (or code solution). According to Equation (3.1), the pseusdorange measured from the p-th satellite can be written as:

$$\rho_k^p - c\delta t_k \;=\; ||x^p - x^k|| - c\delta t_k \tag{3.4}$$

with x^p being the coordinates in WGS84 Cartesian of the p-th satellite and x^k the coordinates (in WGS84 Cartesian) of the receiver at the k-th epoch. Because the satellite moves at a high speed (2000 miles per hour [Leick (2004)]), x^p should also depend on the epoch. For clarity, let us consider that at each epoch the position of the satellites are updated. Taking the full derivative of the Equation (3.4) with regards to the rover's coordinates $[X^k, Y^k, Z^k]$ and its clock offset δt_k with the following linearisation:

$$-\frac{X^p - X^k}{\rho_k^p}dX^k - \frac{Y^p - Y^k}{\rho_k^p}dY^k - \frac{Z^p - Z^k}{\rho_k^p}dZ^k + c(\delta t_k) \;=\; (\rho_k^p)_{obs} - (\rho_k^p)_0 - \epsilon_i^p \tag{3.5}$$

with $(\rho_k^p)_0$ the first estimation of distance rover-(p-th)satellite. $(\rho_k^p)_{obs}$ is the pseudorange measurements at the k-th epoch. The coordinates of the p-th satellite together with the satellite clock offset are written epoch by epoch in the ephemeris file downloaded by the receiver preliminary to the triangulation of its position [Strang and Borre (1997)]. ϵ_i is the residual error between the pseudorange and the true range.

After writing the Equation (3.5) for each satellite in Line-of-Sight with the receiver, a matrix equation may be written as:

$$\mathbf{Ax} \;=\; \mathbf{b} - \epsilon \tag{3.6}$$

with:

$$\mathbf{A} = \begin{pmatrix} -\frac{X^1 - X^i}{\rho_i^1} & -\frac{Y^1 - Y^i}{\rho_i^1} & -\frac{Z^1 - Z^i}{\rho_i^1} & 1 \\ -\frac{X^2 - X^i}{\rho_i^2} & -\frac{Y^2 - Y^i}{\rho_i^2} & -\frac{Z^2 - Z^i}{\rho_i^2} & 1 \\ \vdots & \vdots & \vdots & \vdots \\ -\frac{X^m - X^i}{\rho_i^m} & -\frac{Y^m - Y^i}{\rho_i^m} & -\frac{Z^m - Z^i}{\rho_i^m} & 1 \end{pmatrix}$$

and $\mathbf{x}$ is the column vector $[dX^k, dY^k, dZ^k, c\delta t_k]^T$. T is the matrix transpose operation. In Equation (3.3.2), there are m satellites used in the triangulation. As $\mathbf{A}$ is

not a singular matrix, the least-squares solution is :

$$[dX^k, dY^k, dZ^k, c\delta t_k]^T = (\mathbf{A}^T\mathbf{\Sigma}\mathbf{A})^{-1}\mathbf{A}^T\mathbf{\Sigma}^{-1}\epsilon \quad (3.7)$$

By iteratively computing the receiver's position, the solution converges to the final solution. For each epoch the rover's coordinates are:

$$\begin{aligned} X_k &= X_k^0 + dX^k \\ Y_k &= Y_k^0 + dY^k \\ Z_k &= Z_k^0 + dZ^k \end{aligned} \quad (3.8)$$

$$(3.9)$$

with $[X_k^0, Y_k^0, Z_k^0]$ the initial estimate of the rover's position. This initial position does not need to be very accurate, and generally it is taken from a previous navigation solution [Strang and Borre (1997)]. It is obvious that the accuracy of the final solution is directly linked to the pseudorange errors. Beside, another factor is the number of satellites used in the triangulation. It is well known that the number of satellites determines the Dilution-Of-Precision (DOP) value: a high DOP value may mean a bad 3D solution [Leick (2004)]. A definition of this parameter is written in the following section. This factor will be underlined in the results shown later in this work.

Finally, triangulation using the pseudoranges for positioning the GPS rover employs the same process using carrier-phase measurements. The difference is that before the computation of the rover's position with carrier-phase observations, the navigation software needs to solve the ambiguity value (float or integer) for each satellite in LoS.

3.3.3 Different Positioning Solutions in GPS Technology

Until now in this chapter, different accuracies have been given under the same generic name: GPS technology. Behind it, many techniques using the GPS observables (carrier-phase and/or pseudorange) have been developed through the evolution of this technology.

- GPS standalone is the first technique. This is the simplest way to use a GPS receiver. The GPS is set up and calibrated to triangulate the position of the

receiver. The accuracy varies a lot with the type of GPS standalone used: a cheap hand-held receiver using pseudoranges may give a position not better than 10 m (e.g. GARMIN GPS 76), whereas a single frequency receiver for geodetic applications (e.g. LEICA system 500 GPS receiver) may triangulate the position of the receiver at the sub-metre level (using pseudoranges smoothed with carrier-phase) [Hoffmann-Wellenhof et al. (2001)]. With the latter type of receiver used in a static scenario with a special receiver's antenna to cancel the fading on the GPS signal, the accuracy may reach the centimetre level by post-processing the carrier-phase observables during a long period of time (ideally more than 60 minutes) [Montillet et al. (2007b)].

- Differential GPS is another technique based on the use of two (or more) receivers, where one (stationary) reference is located at a known point and the position of the (mostly moving) remote receiver is to be determined. At least four common satellites need to be tracked simultaneously at both sites. The basic of DGPS is that the baseline between the GPS receivers is very small comparing with the distance GPS receiver-satellite. Thus, the Ionosphere and Troposphere delays may be considered as the same value epoch-by-epoch at both receivers' antenna. The known position of the reference receiver is used to calculate corrections in the observables (e.g. Ionosphere and Troposphere delays). Then, those corrections are transmitted to the remote receiver by radio link [Lachapelle et al. (1992)]. It is generally possible to get an accuracy around 1 to 5 m with this technique using only pseudoranges. The sub-metre accuracy may be achievable if the pseudoranges are smoothed with carrier-phase measurements [Hoffmann-Wellenhof et al. (2001)].

  The limitations of this technique comes from the baseline length. If the baseline is greater than approximately 50 km, the accuracy degrades at the rate of 1 cm per 1 km; unless special corrections on the observables are applied [Mohino et al. (2007)]. Finally, it exists a network of GPS reference stations for DGPS technique called Wide Area DGPS (WADGPS). The main advantage is that this technique covers a larger territory than a single reference station.

- For very precise positioning, when the accuracy of a receiver has to be better than the centimetre, Real Time Kinematic (RTK) GPS technology is widely used in geodesy. The applications are mainly focused on earth monitoring (e.g. sea level monitoring, open-pit mining), streetworks (e.g. mapping assets, city modelling), and building constructions [Roberts et al. (2002b)], [Ge et al. (1999)], [Pirti (2007)]. This high accuracy is achieved in the relative positioning mode with observed carrier-phase measurements. It requires that the phases are observed at both the reference and remote receivers (ends of the baseline). With the progress of the technology over the recent years, the data are transfered (radio link or General Packet Radio Service in the latest receivers) and calculations are computed in real time (i.e. Real Time Kinematic GPS).
  Finally, some companies have installed (or used) a network of fixed GPS receivers such as the LEICA SmartNet. LEICA Geosystems became the first company to acquire the raw data stream from Ordnance Surveys OS Net, a network of 120 reference stations around Great Britain, each streaming raw data, second by second, from Ordnance Surveys head quarter in Southampton. This technique builds a model of the Troposphere and Ionosphere delays in a server receiving data corrections from the surrounding GPS stations and sends the resulting corrections via GPRS link in real time to the user [Meng et al. (2007)], [Leica (2006)].

3.4 Challenges in Urban Canyons

It is well known that GPS technology suffers from additional errors in urban canyons, which lead to a lack of reliability and degrades the performances of GPS technology. In this part, we review those various challenges.

3.4.1 Satellite Geometry

The triangulation of the GPS receiver was explained in Section 3.3.2. The accuracy of the receiver's position is directly linked to the observable errors and the geometry of the satellites' network. Receivers calculate the dilution-of-precision (DOP) value

for each epoch, which gives an indication of the GPS accuracy. The DOP value is defined as:

$$DOP = \sqrt{\frac{q_x + q_y + q_z + q_t}{\sigma_0}} \tag{3.10}$$

with q_x, q_y, q_z and q_t are the errors related to the X, Y, Z coordinates, t the satellite clock error and σ_0 the variance of the uncorrelated observations. Generally with a DOP value greater than 2, the position may not be accurate at the centimetre level using carrier-phase observables. That is why it is often underlined that GPS technology is accurate with a minimum of 4 well distributed satellites generally [Montillet et al. (2007b)]. In addition, the DOP may be defined in the (X,Y) plan as the Horizontal DOP or in the (X,Z) plan as the Vertical DOP. The HDOP and VDOP will be used to underline the link between the accuracy of the technologies used and the geometry of the transceivers in the next chapters.

The present work is focused on the use of GPS technology in difficult environments like the urban canyons. In typical urban canyons, the streets are narrow and the signal is reflected (many times) on the surrounding scatterers before reaching the receiver's antennas. This phenomenon is called multipath. Furthermore, the receiver may not see enough satellites to triangulate its position, because the buildings obstruct the signal from the satellites, or may have sufficient satellites but with a poor DOP value.

3.4.2 Signal Multipath

In Line-Of-Sight between a GPS receiver and a satellite, two kinds of signals are coming to the receiver's antenna: the direct path and the reflected paths. The reflected paths are called multipath phenomenon, and they come from the multiple reflection of the GPS signal on the scatterers surrounding the receiver's antenna. Multipath is unique to each receiver location and cannot then be removed by differential GPS [Hoffmann-Wellenhof et al. (2001)].

To reduce the multipath error on the incoming GPS signal, several techniques have been developed: choke ring antenna, signal processing techniques, and antenna location strategies [Xia (2004)]. A choke ring antenna eliminates the multipath from below the antenna and also at the sides, but not the multipath coming from above. An array

of antennas can also be used to mitigate the multipath. Due to different multipath geometry, each antenna sees the multipath effect differently. Combined processing of signals from all antennas may mitigate the multipath effect [Misra and Enge (2001)]. Algorithms to mitigate multipath are presented in the appendices in Section F. The family of algorithms is based on the MUltiple SIgnals Classification (MUSIC) algorithm and it is particularly useful to decrease the multipath phenomenon applied on the output of the correlation function inside the receiver's software. Much research is done at the moment to develop more signal processing algorithms to process in real time the multipath [Zahidul et al. (2007)] . In static scenarios, new techniques based on adaptive filters have also been developed [Ge et al. (2000)].

3.5 Summary

This research does not work directly on how to improve the GPS signal, but on the coupling of GPS technology with others. In the next chapter, some simulations are developed to test the accuracy of coupling GSM and GPS technologies to solve the lack of GPS availability in urban canyons. This work includes a description of the simulators used to extract the results. In the second part of this thesis, a new positioning technology (LOCATA) is comprehensively studied from the positioning time series to the statistics on the signal.

This chapter is an overview of the Global Positioning System navigation technology. It emphasises how the GPS receiver works to triangulate its position. The mathematics are explained. This is important to understand the navigation software detailed in the remainder of this work. Nevertheless, this section is also showing the limits of the GPS technology and the various challenges in difficult areas. To achieve the centimetre level positioning accuracy required for mapping precisely the buried assets in the VISTA project, only RTK GPS may be able to do it. Even though the accuracy of the RTK GPS technology in land surveying is established, its performances are severely degraded in narrow streets and urban canyons. This introduces the core of this research work and the solutions developed in the next chapters are an attempt to improve or complete this technology.

Chapter 4

Ubiquitous Positioning

4.1 Introduction

Ubiquitous positioning is a generic name for all positioning technologies: starting with satellite constellations (e.g. GPS, GLONASS), including ground-based positioning networks (e.g. UbiSense using Ultra wide Band signal, cellular networks, Radio Frequency IDentification (RFID)), and imaging sensors [Hightower and Boriello (2001)], [Moore et al. (2007)]. As described in Chapter 2, the general aim of this thesis is to locate precisely buried assets (e.g. sewer, gas pipes, telecoms wires) in urban canyons by improving and integrating state-of-the-art commercial technologies. This kind of application typically requires the centimetre level of accuracy.

Today, such a performance may only be possible using Real Time Kinematic (RTK) GPS networks in open field. However, GPS reception may be severely degraded by multipath and lack of satellites availability in areas where the view of the sky is limited by trees and/or buildings (see Chapter 3). A GPS receiver needs at least five well distributed satellites to achieve a high level of accuracy (centimetre).

Meanwhile, since 1996 and the urge from the American FCC (Federal Communications Commission) to implement enhanced 911 (999 in the United Kingdom) emergency calling systems in cellular networks, the research community has revisited and developed algorithms to locate any handset. In the proposal, the requirements imposed by the FCC were for the accuracy to be within 100 m for 67% of all calls and 300 m for 95% of all calls in network-based methods. Handsets-based methods must be accurate to within 50 m for 67% of calls and 150 m for 95% of all calls. But ten years after, some companies advertise that their solutions may achieve an accuracy of 35 m for all calls using (modifying) a cellular network only [Duffet-Smith and Craig (2004)]. However this accuracy is still not high enough to meet of the requirements of the VISTA project.

Another way of looking at the problem is summarised in Assisted GPS[Krzysztof and Kolodziej (2006)]. This technology integrates GPS and a cellular network, in that the ephemeris data are transmitted to the GPS receiver via the cellular networks. This technology does not improve the positioning accuracy, but the initialisation time is reduced (time-to-first-fix).

This chapter should be seen as a preliminary study of the integration of different technologies. It starts with an overview of the architecture of cellular technologies (GSM, UMTS). Then, Section 4.3 emphasises the problem of synchronisation in those cellular network architectures. It also details the main algorithms developed to locate a handset. Section 4.4 starts with the introduction of the Assisted-GPS (A-GPS) technology. It then explains comprehensively the simulator and the algorithms developed by the author to carry out this research, in order to integrate a cellular signal with the GPS carrier-phase measurements. Finally, a conclusion ends this chapter.

4.2 UMTS and GSM Network Architecture

This section starts with a fundamental definition of the cellular network. Then the architecture of the GSM network is explained. The last part focuses on the new functions introduced in the Universal Mobile Telecommunications System (UMTS) network.

4.2.1 General Definition of a Cellular Network

A cellular network is formed by a number of radio cells, where a base station takes place geographically at the middle of it. A cell radius varies typically from 100 m in urban areas to tens of kilometres in the countryside. The maximum cell size is 35 kilometres in GSM networks. The shape of a cell is not a perfect circle and it generally overlaps with neighbouring cell which means certain positions in space may be covered by more than one base station.

As a matter of fact, the cell radius is directly linked with the power transmitted by the base station. The power control algorithm ensures that each user in the network receives and transmits just enough power to maintain communication links with adequate signal quality while causing minimal interference to other users. This interference phenomenon is the well known near-far problem in wireless communications. Moreover, power control helps to the reduction of battery consumption in the terminals.

The Mobile Station (MS), or User Equipment (UE) in UMTS terminology, communicates with the nearest base station using a dual uplink-downlink channel. In the downlink, the terminal scans the signals from all surrounding base stations and monitors their signal qualities. Depending if the MS is in idle or busy mode, it either listens to the broadcast transmission and receives the payload data from the base station, or it transmits the payload data to the network which contain various parameters (e.g. signal quality) [Kupper (2005)].

4.2.2 GSM to UMTS Architecture

GSM network is a circuit-switched (CS) telephony service. It consists of several access networks, which includes the radio interface to interconnect a Mobile Station (MS) with the core network. It also enables interoperability with external telephone networks (fixed telephone network). The connection between the MS and the network is managed by the Base Station Subsystem (BSS) and the core network is denoted as Mobile Switching and Management Subsystem (SMSS). The BSS is composed of a BTS linked to a BSC. The Base Transceiver Station (BTS) is the official name for a Base Station that transmits and receives a signal to communicate with the MS, whereas the Base Station Controller (BSC) performs the typical cell management tasks (i.e allocation and release of channels at the air interface, handover,..). The goal is to keep a BTS as simple as possible for economical reasons. The SMSS consists mainly of the Mobile Switching Centre (MSC) and a Gateway MSC (GMSC). They both contain additional functions to support the mobility of the subscribers , localisation and handover. A MSC may be connected to several BSC defining a local area, whereas the GMSC is a central component that may serve an entire GSM network. MSC and GMSC are both linked to a Home Location Register (HLR), in addition the MSC is also linked to a Visitor Location Register (VLR). HLR and VLR play essential roles in the localisation of subscribers to manage mobile terminated calls. A MS is identified with a number (MSISDN), stored in the HLR when the MS is turned on. ISDN stands for Integrated Services Digital Network. After the MSISDN is registered in the HLR, the paging procedure starts in order to receive or dial calls to/from the MS. The VLR is needed to identify the MS in the local branch of

a GSM network [Borkowski (2004)]. Figure 4.1 shows both the GSM and the UMTS architecture.

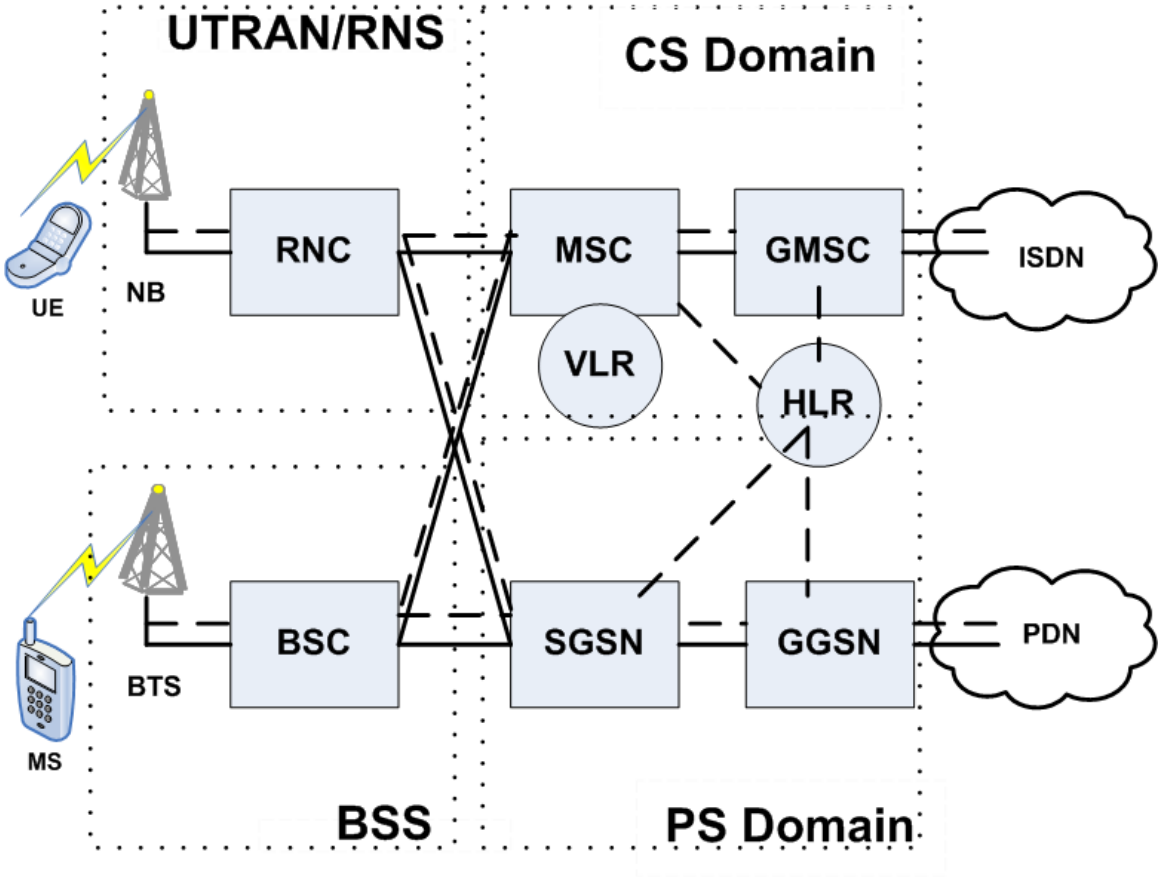


Figure 4.1: Overview of the GSM and UMTS architecture [Kupper (2005)].

ISDN means the fixed telephone network, PDN means Packet Data Network, CS stands for Commercial Service and finally PS for Packet Switched. The UMTS architecture is detailed below. The GSM (900) air interface is a combination of FDMA (Frequency Division Multiple Access) and TDMA (Time Division Multiple Access). Uplink and downlink are separated by FDD (Frequency Division Duplex). A frequency channel (or carrier) in each direction has a bandwidth of 200 KHz.
UMTS architecture has been designed to migrate smoothly the 2 Generation (G) to 3G systems. In other words, the 3G terminals work using UMTS or GSM architecture. It incorporates two access networks: GSM/EDGE Radio Access Network (GERAN) and UMTS Terrestrial Access Network (UTRAN). The former basically corresponds to the original GSM access network as well as the extended version EDGE (Enhanced

Data for GSM Evolution). In the UMTS terminology, a BTS is called a Node B (NB) and it is controlled by a Radio Network Controller (RNC), which is the counterpart of the GSM's BSC. Furthermore, the MS is called a User Equipment (UE). Even though there is a clear parallel between the UMTS and GSM architecture, important differences exist in the design of the air interface. For clarity, the author does not explain those modifications. A reader interested in the air interface may find information in [Holma and Toskala (2005)]. The major difference is the GSM network is a circuit-switched (CS) and UMTS is a packet-switched (PS) domain. In a Circuit-Switched network, the telephone calls go through the different modules of the GSM network presented earlier in this section using the subscriber's address (SIM) to be recognised by the network. PS differs in the type of data transferred along the network: data is segmented into several packets, either of fixed or variable size, which are passed through the network independently from each other.
UTRAN air interface is based on WCDMA (Wide band Code Division Multiple Access). It exists in two modes: UTRAN-FDD (Frequency Division Duplex) and UTRAN-TDD (Time Division Duplex). In UTRAN-FDD uplink and downlink are separated by frequency, that is, in each direction a 5 MHz carrier is required. In UTRAN-TDD downlink and uplink use the same carrier, but are separated in the time domain. For both air interfaces, the time domain is divided into frames of length 10 ms and each frame turn into 15 time slots. Actually, the UTRAN-TDD multiple access scheme is a combination of CDMA and TDMA [Holma and Toskala (2005)].

4.3 Synchronisation and Location Algorithms

4.3.1 GSM Network

There is no timing synchronisation between a BTS and a MS with respect to positioning. According to the description of the uplink-downlink mode of transmission between MS and BTS, BTS cannot hear terminals in idle mode (terminals listening to the network) until they perform an action (e.g. data transfer, location update).

This makes it difficult to measure the range between terminals and different BTS in order to triangulate the MS position. In addition, transmission times from MS and BTS suffer from significant clock drifts which make the synchronisation even harder. Research scientists together with the industries developed some solutions in order to locate precisely a user, based on adding new network components called Serving Mobile Location Centre (SMLC) and Location Measurement Unit (LMU). Those methods are called Enhanced-Observed Time Difference (E-OTD) and uplink Time Difference of Arrival (U-TDoA).
An LMU observes the transmission of data bursts either from different BTS or from terminals in its surrounding area in order to perform timing measurements. An access network usually comprises several LMUs depending on the positioning method that is to be supported and a single SMLC. Two types of LMUs exist: Type *A* LMU is connected to the access network over the air interface without any wired connection appearing as a terminal, whereas Type *B* LMU is integrated to the network either as a standalone unit or linked to the BTS. The SMLC controls the entire positioning process, including allocation of resources, evaluation of timing measurements, and calculation of position fixes. Depending on the positioning method used, it controls one or several LMUs and advises them how to measure transmissions in the uplink or downlink. SMLCS from different networks need to interact with each other in order to coordinate the position of a MS moving through them [Borkowski (2004)].

- Cell-Id combined with Timing Advance (or also called Round Trip Time in UMTS definition) is a method based on proximity sensing and optionally the consideration of the timing advance value that is continuously measured by a base station during a connection or packet transfer. This technique is the simplest algorithm to locate a subscriber within a given cell. The calculus of the range (MS-BTS) [timing advance] is done by the network.

- For E-OTD, the target terminal applies circular hyperbolic lateration based on pulse ranging in the downlink. In GSM, no dedicated pilot signals are used for positioning. The structure of the TDMA frame is the basis for the ranging measurements. The terminal observes the first arriving pulse of a predefined

time slot and timestamps. Furthermore, for circular lateration it is required that the MS and the BTS are synchronised, while for hyperbolic lateration the BTS have to be synchronised with each other. Unfortunately, both of these are not fulfilled in GSM networks (no synchronisation).

- U-TDoA utilises hyperbolic lateration based on observing the arrival of time slots, but unlike E-OTD, it is a network based method. The distance measurements are carried out in the uplink. The transmission of the terminal is also observed by a number of LMUs for timing measurements. As a matter of fact, a sufficient number of LMUs have to be in the range of the terminal in order to triangulate its position.

Figure 4.2 is a scheme of three algorithms: Round Trip Time (or Timing Advance), OTDoA (Observations Time Difference of Arrival) and Assisted-GPS.

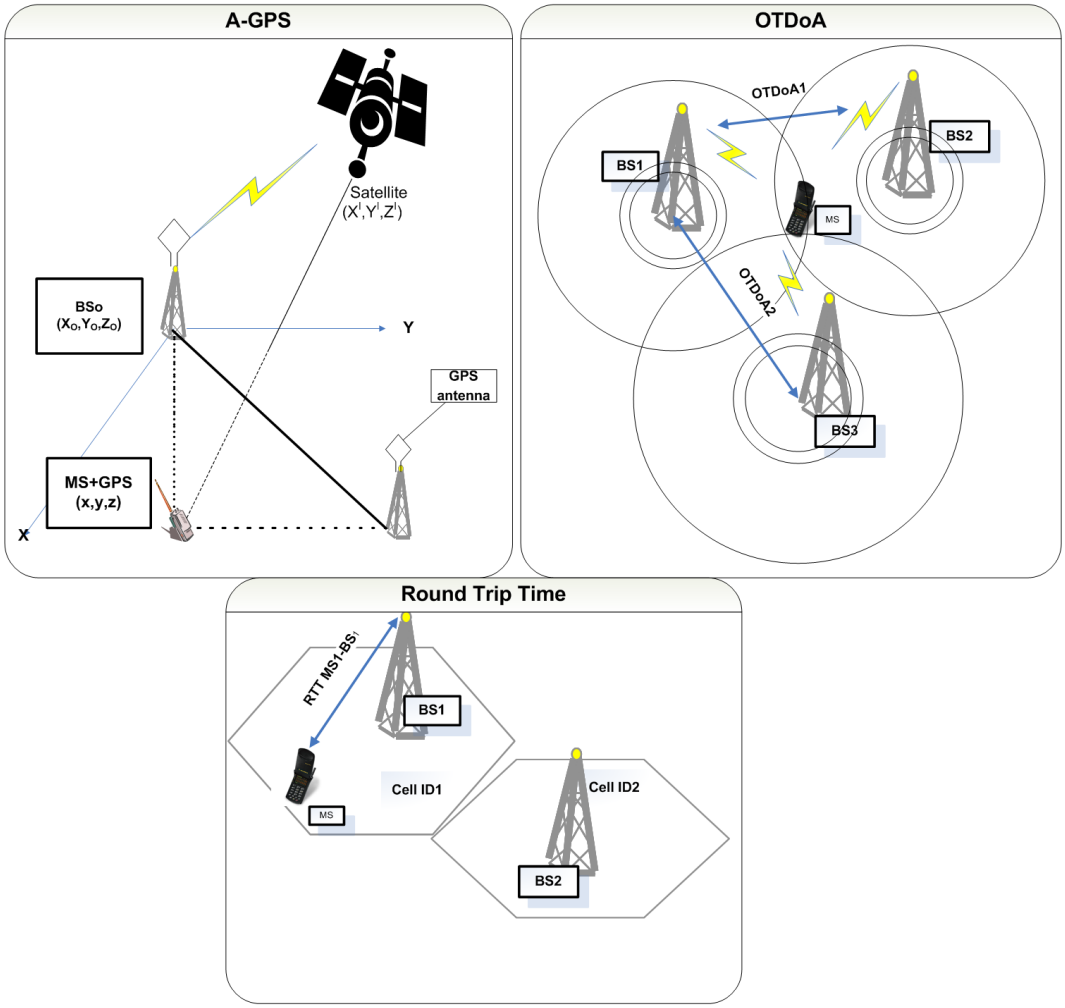


Figure 4.2: Schemes of three algorithms for precise positioning in cellular networks.

The OTDoA scheme gives an overview of the main mechanisms common in E-OTD, OTDoA-IPDL and U-OTDoA algorithms. The latest will be explained in the next paragraph.

4.3.2 UMTS Network

Similar to GSM, UMTS needs specific components for controlling positioning. Nevertheless, one difference with GSM is that most of them do not appear as stand-alone components. They are integrated either in the base stations or RNCs (see Figure 4.1). In the UTRAN-FDD standard, the LMU is associated with the BTS for timing and

synchronisation with neighbouring BTSs. In the case of Non Line-of-Sight (NLoS) between measuring and neighbouring BTSs, the measurements will not be as accurate as in LoS (Line-of-Sight) case which can be an issue in the timing synchronisation and then in the position accuracy of the UE. Operators can alternatively establish stand-alone LMUs at places with better radio conditions. Base stations in UTRAN-TDD are synchronised (a priori) and they do not require any LMU. There is no standard in the integrations of SMLCs to the UMTS architecture. Figure 4.1 shows also the UMTS architecture. Depending on the network operator, the SMLCs are directly coupled with RNCs or sometimes are set up in stand-alone mode. The channel used in UMTS for positioning is the Common Pilot Channel (CPICH), which is arranged in the downlink and does not carry any transport channel. In addition to the ability of calculating the distance BTS-UE, a BTS is also able to calculate the Angle-of-Arrival (AoA). The three main positioning algorithms implemented in UTRAN architecture are: Cell based method, OTDoA-IPDL and Cumulative Virtual Blanking [Kupper (2005)].

- In the cell based method, the coordinates of the terminal are derived from the coordinates of the serving BTS. The position can be further refined by taking into account the distance BTS-UE (Round Trip Time) and the AoA of the incoming signal to the BTS. This algorithm is very similar to the [Cell-ID+Timing Advance] explained in the previous paragraph.

- The Observed Time Difference of Arrival with Idle Period DownLink (OTDoA-IPDL)is basically the UTRAN counterpart of E-OTD. The same options are available in the UTRAN network: circular or hyperbolic laterations, and terminal or network based positioning calculations. IPDL means that the downlink transmission has to be interrupted periodically due to the so-called hearability problem. The hearability problem is similar to the near-far effect, but appears in the downlink transmission. If a terminal stays close to a base station, the signals from this base station may drown out signals from base stations farther away. This makes the need of having 4 BSs hearing one UE in practice difficult and indeed new problems such as traffic congestion appear.

- Cumulative Virtual Blanking (CVB) is an alternative solution to avoid both the hearability problem and using Idle Period-Down Link, which has been developed by Cambridge Positioning Systems Ltd. (CPS) [Duffett-Smith and Macnaughtan (2002)]. This technique removes strong (BSs) interferer. An UE sends a request to the network to get its position to a SMLC. The Serving Mobile Location Centres (SMLC) record the snapshots from each BSs and the UE, then it send the snapshot of the received signal to the Location and Calculation Servers. When the Location and Calculation server has received all the data, it processes the co-incident snapshots from the UE and each relevant BSs by successively cross-correlating the UE snapshot with the BSs snapshots and removing the strongest BS signal from the UE signal by estimation and subtraction. Finally, after this pre-processing, the time delay between each BS and the MS is calculated and the position of the UE may be triangulated.

During the study of the last algorithm, the author found a way to decrease the error on the Time-of-Arrival calculated using the last technique (CVB). The main idea is to apply a super-resolution algorithm such as MUltiple Signals Classification (MUSIC) to the output of the match filter at the physical layer of either the Base Station (Network-based positioning method), or to the mobile phone (handset-based positioning method) [Li and Pahlavan (2004)],[Saarnisaari (1997)]. For this work, the author simulated the scenario with one Base Station and a number of handsets, greater than two in order to be in the case of a near-far effect between multiple transmitters and one receiver. The physical layer of both handsets and BS were developed using Direct Spread Spectrum technology. The results from the simulator show that applying those algorithms on top of the CVB algorithm helps to position more precisely the handsets further away from the BS. This technique shows particularly good results in the case of near-far effect when one transmitter is further away from the receiver than another one. This work has been published in [Montillet et al. (2007a)] (Proceedings of the American Institute of Physics) and a copy can be found in Appendix F.

4.4 Hybrid Systems

Following closely the development of GPS for the Location Based Services market, researchers have developed some algorithms to integrate GPS and cellular networks technologies (GSM/UMTS). The main ideas are Assisted-GPS (A-GPS) and hybrid GPS-GSM signals for localisation. The two solutions suggest that the next generation of mobile phones will integrate a GPS receiver in addition to the GSM/UMTS technology. In A-GPS, the MS position is triangulated only using GPS technology, whereas the hybrid GPS-GSM signal algorithm uses both the signal coming from GPS satellites and GSM/UMTS signals from the base stations as explained in the previous sections of this chapter.

In the following sections, first A-GPS features are underlined and then the hybrid signal positioning solution is investigated. The last solution has been partially developed by the author and published in [Montillet et al. (2007b)]. The research community has developed many algorithms to integrate GSM signals and GPS measurements. Readers interested in further details of those algorithms may refer to [Spirito (2001)], [Son et al. (2003)], [Drakoulis et al. (2000)], [Fischer et al. (1999)] or [Caffery and Stuber (1995)].

4.4.1 Wireless Assisted GPS

GPS technology has already been introduced in Chapter 3. To summarise, GPS receivers need at least 4 well-distributed satellites in order to triangulate their positions to within 10 to 20 m of accuracy in standalone mode in plenary environments. This can be an issue in terms of satellites availability and Dilution-Of-Precision, especially in built up areas.

On top of that, multipath fading occurs by reflection of the signal on buildings and anything in the vicinity of the receiver. In urban canyons and dense multipath areas, carrier phase smoothing or choke ring antenna are not enough to mitigate the multipath phenomenon [Montillet et al. (2006)].

Moreover, the Time -To-First-Fix (TTFF), the time for the GPS receiver to calculate its first position, is an important parameter. Basically, there are three steps when a

GPS receiver is switched on: acquiring the signal, tracking the signal and downloading the navigation information. The downloading can only occur if the GPS receives a minimum level of signal from the satellite of about 28dB-Hz and at this level the signal will be clear enough so as not to require a lot of signal processing power for the correlation to occur and the fix to be established. It results that TTFF is relatively close from one GPS to another with values inside the interval 35-40 seconds [GPSPassion (2005)]. In typical urban areas mentioned earlier, if LoS conditions are lost, the TTFF might be too long in the case of emergency applications. The information received by the satellites is the ephemeris, valid for 4-6 hours, and every slot of 6 hours necessitates a *fresh* batch of new *synthesised* ephemeris. The size is quite large for one week prediction (about 50 KB), which creates issues on how to transmit it to the GPS client.

Thus, A-GPS has been developed to increase the sensitivity of the GPS by providing ephemeris via cellular networks [Garin and Gupta (2007)]. Position calculation can be done either in the MS or in the SMLC. The latter categorisation is also called a network based GPS solution. Figure 4.3 shows the overview of the A-GPS technology.

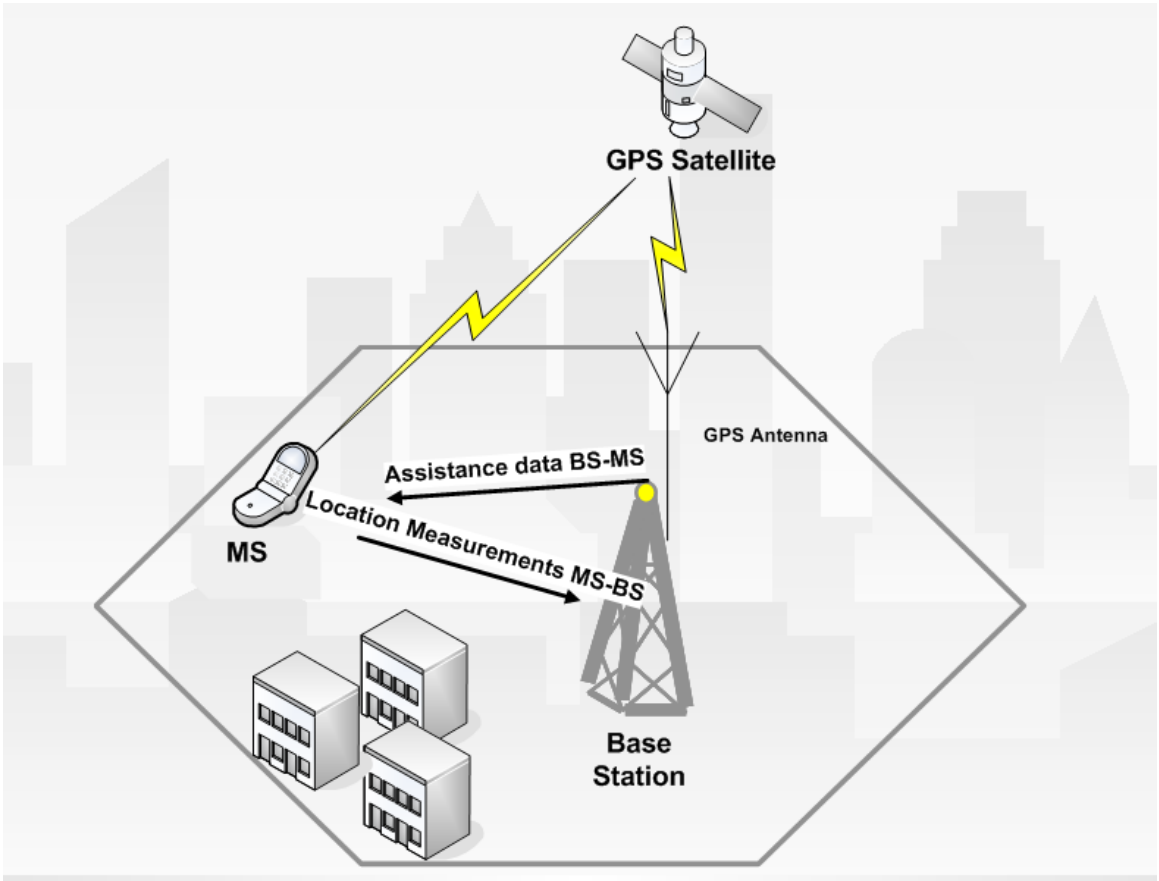


Figure 4.3: Overview of the A-GPS technology.

The base station needs to integrate a GPS antenna in order to receive the ephemeris from the GPS satellites. The acquisition message sent by the network to the MS gives a hint of which frequency/code to search. With this assistance, the search window becomes smaller since the GPS receiver has fewer frequencies to search, and thus TTFF is improved significantly [Syrjarinne (2000)]. The sensitivity is improved due to the MS receiving the information message (i.e. ephemeris, almanac, navigation data,...) via the cellular network. To improve the accuracy of the MS position, the cellular network can also provide Differential GPS corrections, also called DGPS, to the mobile receiver. The accuracy can go down to 10 m for 67%, but in dense multipath areas the accuracy is around 30 m (for 67%). Finally, A-GPS does not only improve MS accuracy in outdoor scenarios, but also indoor measurements are promising.
In conclusion, A-GPS has been standardised by the European Telecommunications Standards Institute (ETSI) and the report is available in [ETSI (2001)]. Nowadays, lots of mobile phone constructors and cellular network providers are modifying their installations worldwide in order to give to their customers the new options gathered under the general name Location Based Services applications [Sun et al. (2005)], [Agarwal et al. (2002)].

4.4.2 Precise Positioning in Urban Canyons using GPS and GSM

This section is divided in three parts. It begins with the explanation on how to integrate the different measurements from the GPS satellites and GSM/UMTS base stations. Then, a Kalman filter is applied to track and smooth the estimated position of the MS. Finally, the simulator and results are explained.

4.4.2.1 Mixing GPS and GSM Measurements

Let us assume a GPS receiver computes the $i-th$ pseudorange (ρ^i) from the $i-th$ satellite. The pseudorange (ρ^i) is composed of the true range ($\| \mathbf{x} - \mathbf{x^i} \|$) plus the receiver clock error ($\Delta\tau$) and a global error (ν) that groups the tropospheric and

$$\mathbf{h}(\mathbf{x}') = \begin{bmatrix} \mathbf{h}_{GPS}(\mathbf{x}') \\ ... \\ \mathbf{h}_{TDOA}(\mathbf{x}') \end{bmatrix} = \begin{bmatrix} \| \mathbf{x} - \mathbf{x^1} \| + \Delta\tau \\ \vdots \\ \| \mathbf{x} - \mathbf{x^j} \| + \Delta\tau \\ ... \\ \| \mathbf{x} - \mathbf{x}_1 \| - \| \mathbf{x} - \mathbf{x}_0 \| \\ \vdots \\ \| \mathbf{x} - \mathbf{x}_m \| - \| \mathbf{x} - \mathbf{x}_0 \| \end{bmatrix} \tag{4.4}$$

ionospheric delays, multipath component and satellite's clock error.

$$\rho^i = \| \mathbf{x} - \mathbf{x^i} \| + \Delta\tau + \nu, \quad i = 1, ..., l \tag{4.1}$$

where $\mathbf{x}$ is the position of the receiver and $\mathbf{x^i}$ is the position of the $i-th$ satellite. In the same way, TDOA can be computed between the $j-th$ BS and the reference BS(0).

$$\zeta_{j,0} = \| \mathbf{x} - \mathbf{x}_j \| - \| \mathbf{x} - \mathbf{x}_0 \| + \mathbf{w}_{j,0}, \quad i = 1, ..., l \tag{4.2}$$

$\mathbf{x}_j$ is the position of the $j-th$ BS, $\mathbf{x}_0$ is the coordinates of the reference BS and $\mathbf{w}_{j,0}$ is the random noise together with possible NLoS biases if the MS and either the reference BS or the $j-th$ BS are not in direct LoS.

In the situation where not enough satellites are in view of the GPS receiver, GPS pseudoranges and GSM TDOA measurements can be combined, as for example $\mathbf{r} = [\rho^1, \rho^2, ..., \rho^l, \zeta_{1,0}, ..., \zeta_{m,0}]$. The equation of combined measurements is displayed in (4.3) and (4.4) (next page).

$$\mathbf{r} = \mathbf{h}(\mathbf{x}') + \mathbf{v} \tag{4.3}$$

$\mathbf{x}'$ is the state vector $\mathbf{x}' = [\mathbf{x}, \Delta\tau]$. $\mathbf{v}$ is the measurement noise. $\mathbf{h}$ is defined as: The location of $\mathbf{x}$ is recursively estimated via least squares (4.5).

$$\hat{\mathbf{x}}' = \mathbf{x}'_0 + (\mathbf{H}_0^T \mathbf{H}_0)^{-1} \mathbf{H}_0^T (\mathbf{r} - \mathbf{h}(\mathbf{x}'_0)) \tag{4.5}$$

where $\mathbf{x}'_0$ is the first estimate and $\mathbf{H}_0$ is the Jacobian matrix of $\mathbf{h}(\mathbf{x}')$. In the same way, a weighted LS can be implemented [Strang and Borre (1997)].

$$\mathbf{\Phi}_{k-1} = \begin{bmatrix} 1 & 0 & 0 & \Delta t & 0 & 0 \\ 0 & 1 & 0 & 0 & \Delta t & 0 \\ 0 & 0 & 1 & 0 & 0 & \Delta t \\ 0 & 0 & 0 & 1 & 0 & 0 \\ 0 & 0 & 0 & 0 & 1 & 0 \\ 0 & 0 & 0 & 0 & 0 & 1 \end{bmatrix}, \mathbf{B}_{k-1} = \begin{bmatrix} 0.5\Delta t^2 & 0 & 0 \\ 0 & 0.5\Delta t^2 & 0 \\ 0 & 0 & 0.5\Delta t^2 \\ \Delta t & 0 & 0 \\ 0 & \Delta t & 0 \\ 0 & 0 & \Delta t \end{bmatrix} \tag{4.9}$$

4.4.2.2 Kalman Filter Smoothing

In this part, we only remind readers of the basic theory on Kalman filtering based on [K. Yu and Oppermann (2005)]. Once the position of the MS is found, a Kalman filter smoother may be used to refine the location based on the previous estimates. Let us define the vector at time t_k

$$\mathbf{x}_k = [x_k, y_k, z_k, v_{x,k}, v_{y,k}, v_{z,k}]^T, \tag{4.6}$$

where $v_{x,k}$ is the velocity component along x axis. The observation vector is defined as

$$\mathbf{P}_k = [x_k, y_k, z_k]^T. \tag{4.7}$$

Then the system dynamic model is

$$\mathbf{x}_k = \mathbf{\Phi}_{k-1}\mathbf{x}_{k-1} + \mathbf{B}_{k-1}\mathbf{w}_{k-1}, \tag{4.8}$$

where the state transition matrix $\mathbf{\Phi}_{k-1}$ and $\mathbf{B}_{k-1}$ are given by (4.9). Δt is the time increment and $\mathbf{w}_{k-1}$ is the acceleration noise assumed to be white Gaussian random vector of mean zero and covariance $\mathbf{Q}_{k-1}$. The measurement model is defined by:

$$\mathbf{p}_k = \mathbf{H}_k\mathbf{x}_k + \mathbf{n}_k \tag{4.10}$$

$\mathbf{H}_k$ is the observation matrix given by

$$\mathbf{H}_{k-1} = \begin{bmatrix} 1 & 0 & 0 & 0 & 0 & 0 \\ 0 & 1 & 0 & 0 & 0 & 0 \\ 0 & 0 & 1 & 0 & 0 & 0 \end{bmatrix}, \tag{4.11}$$

and $\mathbf{n}_k$ is the observation noise vector also assumed to be Gaussian with zero mean and covariance $\mathbf{R_k}$. Implementation of Kalman filtering can be summarised as follows. The initial estimate $\hat{\mathbf{x}}_0$ and its error covariance $\mathbf{C_0}$ are first given. Let (-) and (+) represent the a priori (before update) and the a posteriori (after update) values respectively. The state estimate extrapolation is given by:

$$\hat{\mathbf{x}}_k(-) = \mathbf{\Phi}_{k-1}\hat{\mathbf{x}}_{k-1}(+), \tag{4.12}$$

and the error covariance extrapolation is performed by:

$$\mathbf{C}_k(-) = \mathbf{\Phi}_{k-1}\mathbf{C}_{k-1}(+)\mathbf{\Phi}_{k-1}^T + \mathbf{B}_{k-1}\mathbf{Q}_{k-1}\mathbf{B}_{k-1}^T. \tag{4.13}$$

Then the Kalman gain matrix can be computed according to:

$$\mathbf{K}_k = \mathbf{C}_k(-)\mathbf{H}_k^T[\mathbf{H}_k\mathbf{C}_k(-)\mathbf{H}_k^T + \mathbf{R}_k]^{-1}. \tag{4.14}$$

The state estimate is updated by:

$$\hat{\mathbf{x}}_k(+) = \hat{\mathbf{x}}_k(-) + \mathbf{K}_k[\mathbf{p}_k - \mathbf{H}_k\hat{\mathbf{x}}_k(-)], \tag{4.15}$$

And the error covariance is updated by:

$$\mathbf{C}_k(+) \quad = \quad [\mathbf{I} - \mathbf{K}_k\mathbf{H}_k]\mathbf{C}_k(-). \tag{4.16}$$

Therefore, the Kalman filter is updated from (4.12) to(4.16).

4.4.2.3 Results

In this section, we examine the proposed position location system as shown in Figure 4.4. We use two simulators: one to simulate the GPS pseudoranges and the other one to get the Time-of-Arrival (ToA) measurements from the BSs. The scenario is a simple track where the MS moves along the path. Figure 4.6 gives an idea of the track followed by the MS. The GPS simulator outputs a RINEX observations file and a broadcast ephemeris. In the RINEX file, the pseudoranges are given for each epoch and each satellite in view; the ephemeris gives the satellites' positions and the satellites' clock offsets for each epoch. The ToA simulator outputs an observation file with the ToA for each BS around the MS at a given epoch. Then all these files

are loaded using a Matlab code (using Matlab 7.0 software) and the position is post-processed.

The GPS simulator is comprehensive and takes into account all the biases introduced by the Troposphere, the Ionosphere, the satellite clock offset and the receiver clock-offset. This simulator has been developed in a previous project at the Institute of Engineering Surveying and Space Geodesy [Noakes (2003)].

In the ToA simulator, six BSs are selected randomly at each epoch around the MS position in a 1 km radius. The error on the Time-of-Arrival measurements is zero-mean Gaussian distributed with a variance σ^2. The parameters of the simulators are given in Table (4.1) in standard deviation. The satellite clock error is the offset

	GPS
$Sat.\ Clock\ Error\ [s]$	$1e-12$
$GPS\ Pseudoranges\ [m]\ (L1/C1/L2/P2)$	0.001/1/0.001/1
$Ionosphere\ [m]$	0.05
$Troposhere\ [m]$	0.05

Table 4.1: GPS simulator parameters.

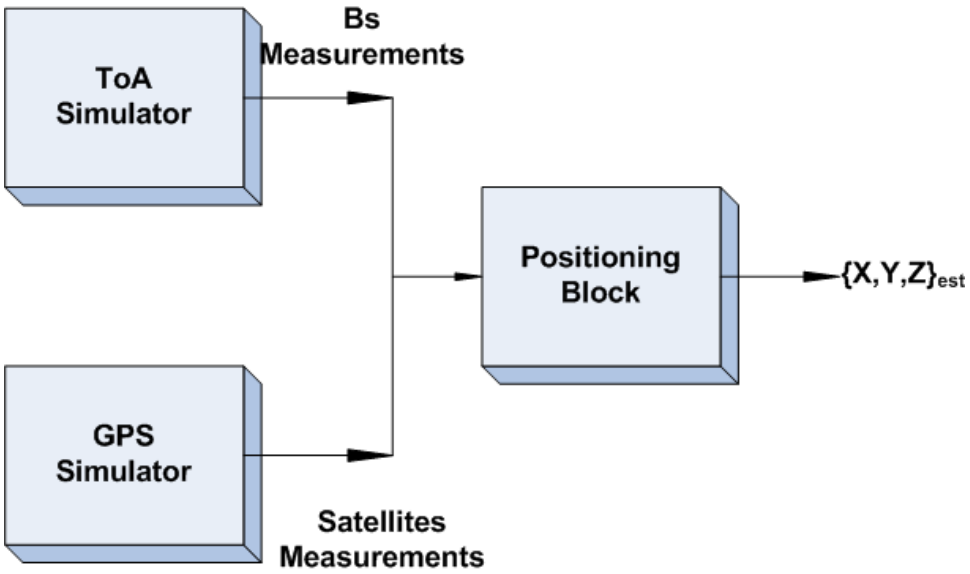


Figure 4.4: Block diagram.

written in the ephemeris file. Different biases are used to simulate the GPS pseudoranges. The Ionosphere effect is modelled using the Klobuchar model [Klobuchar (1996)]. EGNOS (European Geo-stationary Navigation Overlay System) models the Troposphere effects on the pseudoranges. The error may be as small as 0.05 m on the pseudoranges measurements in open sky.

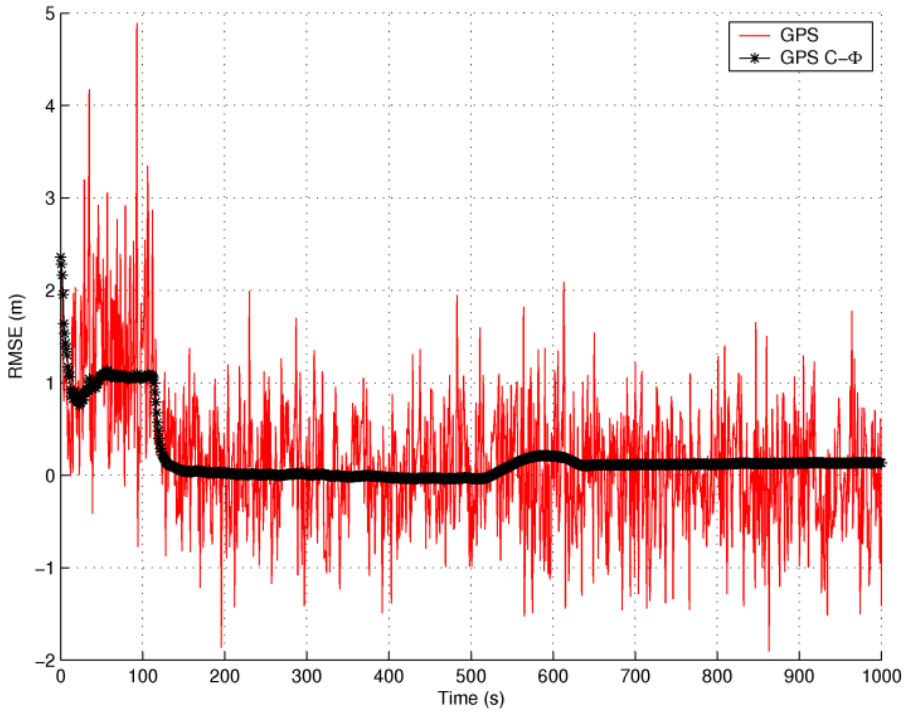


Figure 4.5: Position of the MS estimated using only GPS pseudoranges and then smoothed by carrier-phase measurements.

Figure 4.5 shows the RMSE (Root Mean Square Error) of the position of the MS epoch by epoch using GPS standalone and GPS carrier-phase smoothing ($C - \Phi$). The position of the MS is triangulated using eight satellites. The remaining error is due to multipath.This figure shows carrier-phase smoothing helps to reduce multipath on satellites pseudoranges.

In Figure 4.6 the ToA from BSs around the MS at each epoch are introduced in the matrix of the Least-squares to triangulate the position of the receiver.

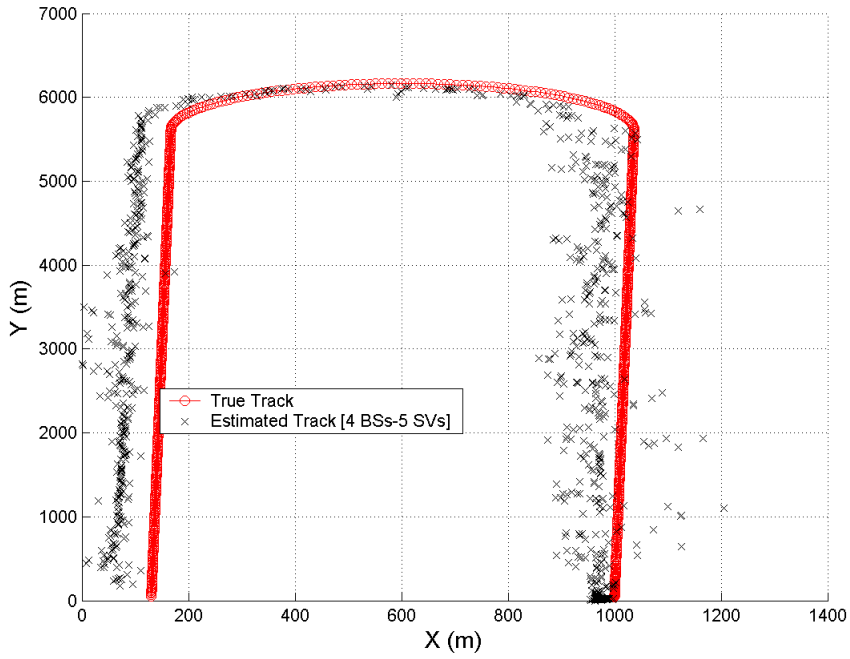


Figure 4.6: True track and track estimated by Hybrid GPS/GSM measurements.

	${\sigma_1}^2$	${\sigma_2}^2$	${\sigma_3}^2$	${\sigma_4}^2$
(μ) $[m]$	54.75	3.42	2.08	0.18
StD $[m]$	71.93	7.58	3.69	0.802

Table 4.2: Mean and variance of hybrid GPS/GSM.

The variance σ^2 is around $10^{(-6)}$ seconds. A set of simulations has been run and the mean and variance on the position of the MS is gathered in Table (4.2). ${\sigma_1}^2$, ${\sigma_2}^2$, ${\sigma_3}^2$, and ${\sigma_4}^2$ are equal respectively to $10^{(-6)}$, $10^{(-7)}$, $10^{(-8)}$ and 0 seconds. These values were chosen as test samples to see how much the position of a MS is improved in meters when the ToA error is reduced. The mean (μ) and standard deviation (StD) of the position of the mobile is extracted after one run. For all the simulations 5 satellites and 5 BSs were used to triangulate the MS position. It can be seen that the variance of the ToA error influences greatly the accuracy of the MS position. Some simulations using carrier-phase smoothing technique were also run. For example, with σ on ToA error equal to 1 microsecond, the mean error of the MS position is equal

to 54.75 m and the standard deviation of 71.93 m. In general It is observed that the carrier-phase smoothing reduces by a few metres the error on the position of the MS as expected. This error reduction depends on the number of satellites involved in the triangulation of the MS position.

The next step was to examine the accuracy of the MS position when a Weighted Least-Squares (WLS) is used. In order to implement it, the variance of the measurements has to be calculated. Thus, before triangulating the position of the MS at each epoch, 100 ToA measurements are gathered from each BS. Then, the variance is calculated for each BS. The results show that with σ^2 on ToA error equal to 1 μm, the mean error of the MS position is equal to 0.469 m with standard deviation of 3.315 m. This result is good, but we also observe that the Weighted Least-Squares diverges when the ToA error becomes smaller and smaller such as 10 ns. This value of ToA error would mean a precise synchronisation into the cellular network architecture which may be achievable by using location measurements units, but this not a cost efficient solution [Duffett-Smith and Macnaughtan (2002)]. Finally, a Kalman filter was used as a well-know technique for smoothing the estimated MS positions. The ToA error is zero-mean distributed ($\mathcal{N}(0, 10^{-6})$). The covariance of the acceleration noise ($\mathbf{Q_k}$) is equal to the identity matrix multiplied by 0.0001, the covariance (C_0) of the first position estimated (x_0) is equal to the identity matrix. Figure 4.7 shows the result. The Kalman filter smoother tracks the MS position reducing the standard deviation (StD) of the error. But the mean accuracy is not influenced by the Kalman filter smoothing algorithm. The accuracy varies from 20 m to 200 m.

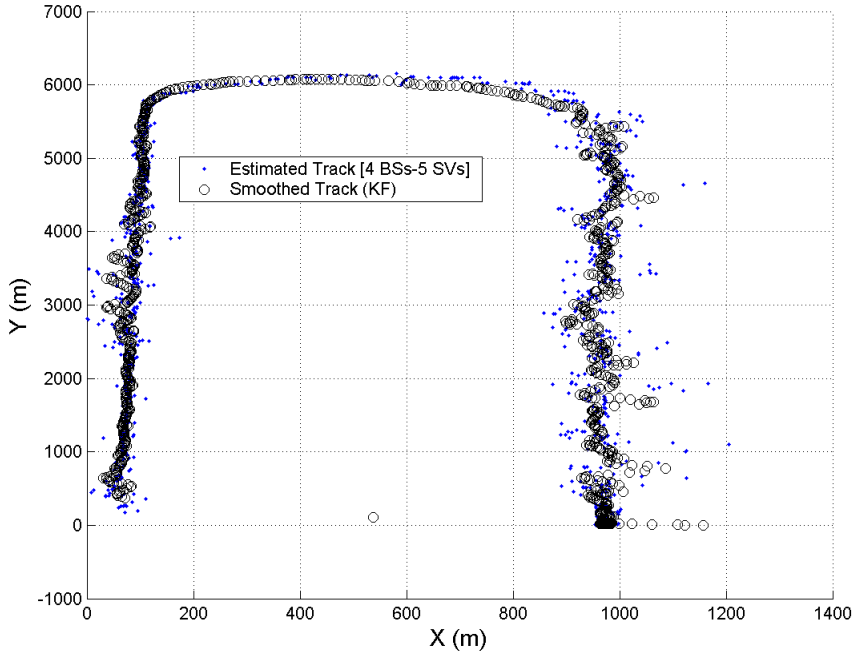


Figure 4.7: Track estimated hybrid GPS/GSM measurements and smoothed with Kalman filter.

4.4.3 Validation of the Results

In order to check the trustworthy of the results, the simulations have to be validated. One may replace the parameters of the GPS or/and GSM simulator by some values used in previous research papers and check the error on the ToA and GPS pseudoranges. Unfortunately, most of them do not describe the simulator in details and the parameters given are not enough to go through this validation way. Thus, we chose to gather some results from previous research work published in scientific papers. Those results are then compared with our simulations. Table (4.4.3) shows the various

	Accuracy	Simulator
[Kabalan and Mounsef (2003)]	100 m to 1 km	GSM
[Fischer et al. (1999)]	80 to 120 m	UMTS
[Syrjarinne (2001)]	10 to 30 m	A-GPS
[Drakoulis et al. (2000)]	30 to 550 m	GPS+GSM
[Son et al. (2003)]	24 to 195 m	GPS+GSM
Our Simulations	20 to 200 m	GPS+GSM

Table 4.3: Validation of the simulations.

accuracy displayed in the literature. In the column Accuracy, the results are averaged on the simulations carried out for 67% and 90% of the time. This is necessary, because our simulator did not introduce additional errors (e.g. signal blocked by walls and buildings) to separate the case when the receiver cannot triangulate its position. In [Kabalan and Mounsef (2003)], the authors triangulated the position of a user using the received signal strength from the transmission of a mobile phone. The simulator developed in [Fischer et al. (1999)] is comprehensive. It takes into account various techniques for positioning in cellular networks (e.g. ToA, TDOA, AoA) and the number of BSs involved in the location of the user. The results in [Syrjarinne (2001)] are based on differential GPS using pseudoranges and they look very good for location based services market, but the simulator does not take into account the major challenges in urban environment (e.g. limited signal availability, multipath). The hybrid GPS-GSM scheme in [Drakoulis et al. (2000)] is not developed

to locate directly the receiver using GPS and GSM signals, but the GPS is used to synchronised the GSM cellular network. As said in Section 4.2, the BSs are not synchronised among them in the GSM cellular network. Once done, the authors used the OTDoA algorithm to locate the MS. Finally, [Son et al. (2003)] develops an algorithm to mix GPS and GSM similar to what is done in this research work. However, they validated the algorithm via real time measurements in the city center of Seoul in Korea. Comparing all the results from the literature to our simulations show that our results are close to [Son et al. (2003)]. However, our GPS and GSM simulator is comprehensive and takes into account different satellite and BS geometries.

4.5 Summary

This chapter explained the basics of how the cellular network operator can locate a subscriber using only the features of the GSM and/or UMTS technologies. Some algorithms have been explained (e.g. E-OTD, U-TDoA, cell-Id). The goal of this chapter was to show the main positioning algorithms, but as previously mentioned new algorithms are flourishing regularly in scientific papers. This makes it difficult to have a comprehensive list of all location techniques, and it is not the goal of this chapter. Moreover, the positioning algorithms presented in this chapter use Time Difference Of Arrival (TDOA) for the ranging between the MS and the base stations. Beside, some other techniques are also available such as Received Signal Strength (RSS) and Angle-of-Arrival (AoA). Readers interested in these technologies may refer to [Ertel and Reed (1999)] or [Rappaport et al. (1997)]. Outside of his project focus, the author has developed a technique to refine the position of a handset on top of the Cumulative Virtual Blanking (CVB).

The last part shows the possible integration of the satellite based positioning technology (GPS) and the cellular network. On one hand, Assisted GPS has already been standardised by the European Telecommunications Standards Institute (ETSI), but it does not solve the GPS reliability and accuracy in urban canyons. On the other hand, the author has developed an algorithm to directly reuse the signal (ranging measurements) between the MS and the base stations in addition to the pseudoranges

between a terrestrial receiver and the different satellites in the sky. This technique is called a hybrid solution using GPS and GSM measurements and it shows some interesting results. However, the simulator would have to be improved to reduce the mean error in order to achieve some results better than 20 m accuracy. This work has to be considered as an introduction of merging different positioning technologies and a basis for the project development. The strong points of this work are based on the fact that lots of research is till on going in the industries world wide and the cellular network operators keep adding new base stations to improve the coverage of the network (indoors and outdoors) [Duffett-Smith and Macnaughtan (2002)]. Furthermore, the research community is now looking for reusing not only GSM signal, but also different technologies such as TV, Radio and Ultra Wide Band to mix with GPS technology [Meng et al. (2007)].

In the following chapters, the work focuses on an alternative solution called LocataLites or LOCATA technology. It is a network of base stations transmitting a GPS-like signal. The features are explained in the next chapter.

Chapter 5

LOCATA Technology

5.1 Background and Definition of the LOCATA Technology

5.1.1 Introduction

Since the earliest days of the GPS concept (1978), ground-based transmitters have been under development to complete a satellites constellation. These ground based transmitters were called *Pseudo-Satellites* quickly renamed as *Pseudolites*. They have been used to test GPS system elements and to enhance GPS in certain applications by providing better accuracy, integrity and availability through the use of Pseudolite signals in addition to the GPS signals. Pseudolites are also a promising technology for providing positioning in high multipath environments where GPS signals are generally unavailable or severely attenuated and of questionable quality. Thus, they have the potential to be used for both indoor and outdoor positioning applications transmitting a GPS-like signal [Cobb (1997)]. Pseudolites work in unsynchronised mode and double differencing is used to eliminate the Pseudolites and receiver clock biases. In the mid 1990s growing interest foresaw Pseudolites technology as the next big thing. Since then, numerous Pseudolites applications have flourished: Local Area Augmentation Systems (LAAS), plane landing, bridge deformation monitoring, open pit-mining, reducing streetworks [Cosser (2004)],[Misra and Enge (2001)] ,[Kanli (2005)], [Van Dierendonck (1997)], [Roberts et al. (2006)].

However, there are some fundamental issues that limit the effectiveness of a Pseudolite system using C/A code on L1/L2. These include the legality of transmitting on L1/L2, cross-correlation between Pseudolites and GPS signals (GPS jamming), saturation of GPS receiver front-ends, and the limited multipath mitigation offered by C/A codes. When combined with other problems inherent to all Pseudolite systems such as near-far, multipath, and synchronisation, the issues in using L1/L2 C/A code Pseudolite systems further complicates the design and deployment of such systems and places limits on their operational effectiveness [Kanli (2005)]. However, if Pseudolites can be synchronised, stand-alone positioning can be achieved without base station data (and without the radio modem data link) [Barnes et al. (2003b)]. Until recently attempts

to synchronise Pseudolites have resulted in position solutions that are up to six times worse in comparison to an unsynchronised approach using double-differencing [Yun and Kee (2002)].

Recently, two positioning solutions have emerged from the Pseudolite technology: *Terralites* and *LocataLites*. LOCATA is welcomed as a new break-through in the ground-based positioning world.

Terralites are developed by Novariant (formerly IntegriNautics). Terralites technology triangulates the position of a receiver using both the GPS and XPS signals. The XPS signal frequency is in the 10GHz band [Novariant (2005)]. Thus it does not interfere with the GPS L-band signal. Their business area is oriented on open-pit mining and Auto farm tractors [Novariant (2004)].

LocataLites is based on LOCATA technology developed by *LOCATA Corporation* from Australia. The technology consists of a network (LocataNet) of time-synchronised transceivers (LocataLites) allowing point positioning of a rover with centimetre accuracy (using carrier-phase) [Barnes et al. (2006)]. In February 2007, the IESSG (University of Nottingham) received a prototype system to demonstrate the proof-of-concept of the LOCATA technology. this is described in the following sections of this chapter.

In the next section, the LOCATA signal is investigated together with the frequency band, antennas, multiple access scheme and network synchronisation. Section 5.3 emphasises the different softwares in the LocataLites firmware and particularly the main parameters in the Setup file. A potential user interested in manipulating the LOCATA technology needs to read Section 5.4. Section 5.5 focuses on the Signal-to-Noise Ratio displayed by the LOCATA technology, the distance tests and some basic statistics to model the multipath distribution.

5.1.2 A Definition of the LOCATA Technology

As explained previously in 5.1.1, the LOCATA technology is built on the knowledge of, and to overcome the challenges addressed by Pseudolites, a decade earlier. LocataLites transmit a signal modulated in the same way as the GPS code, which enable the triangulation of a mobile user at the centimetre level of accuracy. A LocataNet is

a network of Locatalites. It is formed of two kinds of devices: the LocataLites and the LOCATA receiver (or rover). The LocataLite transmitter generates a carrier-phase signal modulated with a proprietary ranging code in the 2.4GHz Industrial Scientific Medical (ISM) band. At the time of writing, the LocataLites can transmit two positioning signals at the same frequency with different Pseudo Random Noise ranging codes from the two transmit antennas. A third antenna is used as receiver. The receiver chipset and the transmitters share the same clock, which is a cheap temperature-compensated crystal oscillator (TCXO) according to [Barnes et al. (2003b)]. Figure 5.1 shows a LocataLite with different setup scenarios.



Figure 5.1: Typical setup of a LocataLite on a tripod (left) or on a roof (right).

On the left picture the LocataLite is mounted on a tripod, and on the right one the LocataLite is mounted on a pole on the roof of the University of New South Wales (UNSW). The waterproof metallic box (circle on the left picture) protects the hardware.

5.2 Characteristics of the LOCATA Signal

5.2.1 The IEEE 802.11 Standard and the ISM Frequency Band

In the field of WLAN the IEEE 802.11 standard is among the most well known standards. This project was initiated in the 1990s and several draft standards have been published for reviewing. The original IEEE802.11 was issued in July 1997. Subsequently, the IEEE802.11b and the IEEE802.11a were issued in September 1999. All drafts of the IEEE802.11 standard have an identical MAC sub-layer, they use a Carrier Sense Multiple Access/ Collision Avoidance method to share the medium. Differences between the versions of the IEEE802.11 standards appear at the physical layer. The maximum data rate possible in the first version was 2 Mb/s, and this rate was improved in the following versions: IEEE802.11b can reach 11 Mb/s. This improvement reflects the -always increasing- need, for high data rates in (wireless) communications [Prasad (1998)].
The IEEE802.11b standards specify at the physical layer (PHY) three methods:

- the Frequency Hopping Spread Spectrum (FHSS)
- the Direct Sequences Spread Spectrum (DSSS)
- the Infra Red (IR)

All these radio modes operate in the ISM band. The common ISM bands used worldwide are 902-928 MHz, 2.4-2.4835 GHz and 5.725-5.850 GHz. Note the 5 GHz band is also called the Unlicensed National Information Infrastructure band (UNII). The 2.4 GHz ISM band is practically attractive because first it enjoys worldwide allocations for unlicensed operations. Therefore these bands can be deployed everywhere without going though a long and expensive license application. It also has a good balance of equipment performance and cost compared with the 5.725 GHz bandwidth. In other words, it allows more bandwidth to support higher data rates and number of channels. Finally, the IEEE802.11 is the global WLAN standard. The spectrum allocation in Europe and USA for the ISM band is 2.400-2.4835 GHz. According to

the Federal Communication Commission regulations (FCC 15.247) for operations in the 2.4 GHz ISM band the nominal power of the transmitter is 100 mWatt or 20 dBm. This signal strength was chosen to accommodate coverage of approximately 35/100 metres radius areas for indoor/outdoor applications and to limit the battery power consumption. The 2.4 GHz band is broken down into 11 channels for the FCC or North American domain and 13 channels for the European or ETSI domain. These channels have a center frequency separation of only 5 MHz and an overall channel bandwidth (or frequency occupation) of 22 MHz [Fainberg (2001)]. The most common wireless access scheme implemented into the Physical layer (PHY) is the Direct Sequence Spread Spectrum (DSSS). The LocataLites PHY is based on DSSS technology.

DSSS transmissions multiply the data being transmitted by a noise signal. The noise signal is a pseudo random noise sequence of 1 and -1 values, at a frequency much higher than that of the original signal, thereby spreading the energy of the original signal into a much wider band. The LOCATA PHY uses a spreading code called Gold code [Proakis (2000)]. Note the length of the code is not released by the industry. This allows the devices to communicate in a limited bandwidth and to avoid interference to/from the other users of the spectrum. These unlicensed bands become overcrowded by wireless networking products such as Wi-Fi, Bluetooth, HomeRF and other Wireless technologies (i.e. ZigBee). Table (5.1) makes a comparison of different standards transmitting in the ISM band and the characteristics of the LOCATA technology. N/A means the value is not displayed by the company.

Characteristics	Bluetooth	IEEE802.11b	LOCATA
Spectrum	$2.4 - 2.4835$GHz	$2.4 - 2.4835$GHz	$2.4 - 2.4835$GHz
Max Data Rate	1Mb/s	11Mb/s	N/A
Frequency Selection	FHSS	DSSS or FHSS	DSSS

Table 5.1: Physical layer characteristics of Bluetooth, IEEE802.11 and LOCATA [Crow et al. (1997)].

5.2.2 Antennas

As said previously, the LOCATA technology uses three antennas (two transmitters and one receiver) and then benefits from spatial diversity. It is common knowledge that any radio signal suffers from multipath distortion and scattering effects when travelling. Deploying an antenna array instead of a single antenna at the transmitter side helps to immune the signal radio against the fading effects at the receiver side. In the LOCATA technology, the rover receives two signals distorted differently. This is the basics of the Multiple-Inputs-Multiple-Outputs (MIMO) technology [Proakis (2000)]. Thus, comparing the Signal-to-Noise-Ratio(SNR) of the two incoming signals from the same LocataLites, the rover may detect if one antenna is in a deeper fading zone than the other one and may choose to discard this signal to triangulate its position.

The results presented in [Barnes et al. (2006)] indicate that a TX_1, TX_2 vertical separation of approximately 1-2 m gives sufficient spatial diversity at a LOCATA receiver up to 2 km from the LocataLite. In a LocataNet, two types of antenna can be differentiated: the LocataLites use an antenna developed by *AeroAntenna Technology Inc* [Model AT2400-2] both to receive and to transmit a signal, whereas the rover uses an omnidirectional antenna (in the horizontal plane) commercialised by *HyperLink Technologies* [Model HG2403MGURB]. Figures 5.2 and 5.3 show respectively the LocataLites and rover antennas.

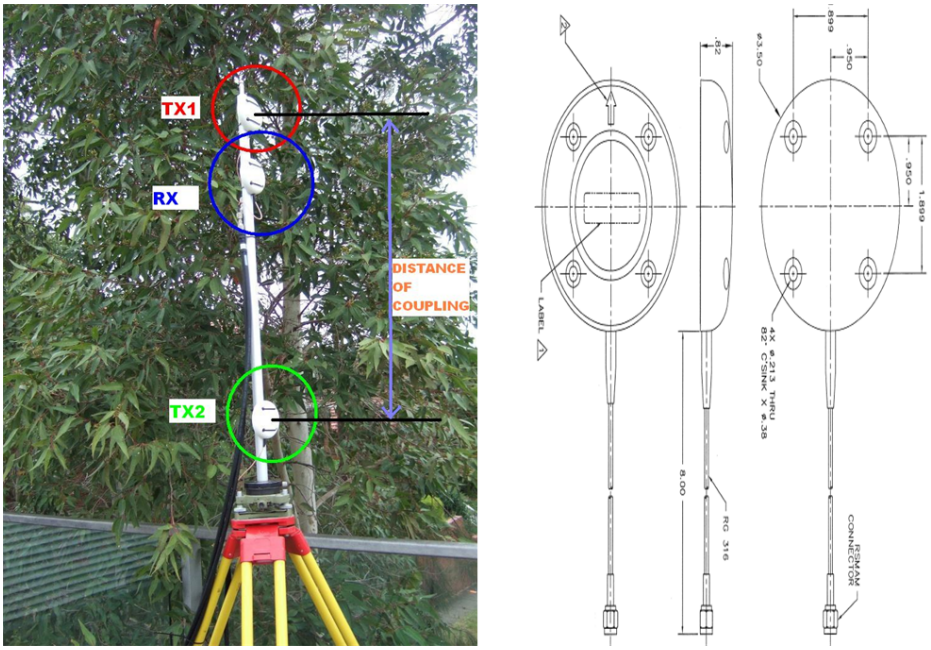


Figure 5.2: LocataLites' antennas mounted on a temporary pole (left) and its specifications (right) [Inc (2004)].

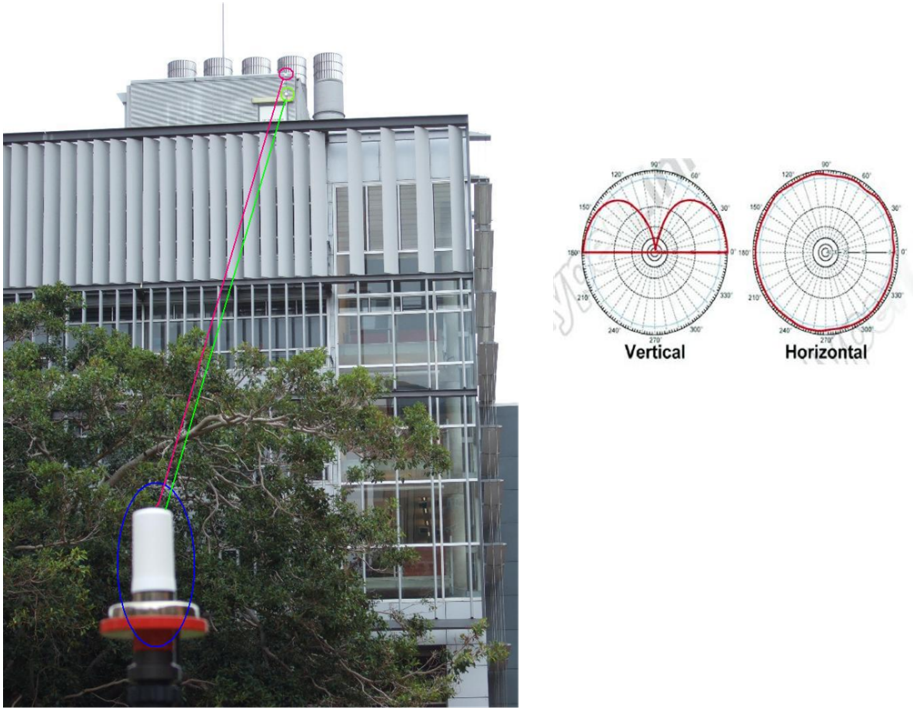


Figure 5.3: Rover's antenna (left) and gain pattern (right) in two planes (vertical and horizontal) [HyperLink (2005)].

The radiation pattern of the LocataLite antennas shows a beamwidth of 70 degrees turned to the front. When designing a LocataNet careful consideration must be taken to direct the LocataLites patch antennas into the desired work area. If it is required to have LocataLites at the centre of a network, the two transmit patch antennas can be replaced with the omnidirectional antennas (used on the rover).

5.2.3 Multiple Access Schemes and Near-Far Effect

Because the radio spectrum is a scarce resource, its usage must be carefully controlled. Wireless systems use various techniques to allow multiple users to access the same radio spectrum at the same time. In fact, many systems employ several techniques simultaneously. The four well known techniques are: Frequency-division multiple access (FDMA), Time Division Multiple Access (TDMA), Code Division Multiple Access (CDMA) and Space-division multiple access (SDMA). The TDMA system is designed for use in a range of environments and situations, from hand portable in a downtown office to a mobile user traveling at high speed on the freeway. In 1989, the Cellular Telecommunications Industry Association (CTIA) chose TDMA over Motorola's FDMA narrow band standard as the technology of choice for existing 800 MHz cellular markets and for emerging 1.9 GHz markets. TDMA offers a flexible air interface, providing high performance with respect to capacity, coverage, and unlimited support of mobility and capability to handle different types of user needs. However, Qualcomm has pushed in favor of CDMA for GSM mobile Communication systems. Thus in the past years, the wireless community has been debating the merits of using either the TDMA or CDMA multiple access scheme [Korhonen (2003)]. Nowadays, the two majors systems are TDMA and CDMA. LOCATA technology uses a hybrid CDMA/TDMA scheme.

In a CDMA system, all users occupy the same frequency at the same time, no time scheduling is applied, and their signals are separated from each other by means of special codes. Each user is assigned a code applied as a secondary modulation, which is used to transform a users signals into a spread-spectrum-coded version of the users data stream. The receiver then uses the same spreading code (PRN) to transform the spread-spectrum signal back into the original users data stream.

In a TDMA system, the entire available bandwidth is used by one user, but only for short periods at a time. The frequency channel is divided into time slots, and these are periodically allocated to the same user so that other users can use other time slots. In order to transmit in the ISM band, LocataLites PHY has to respect the IEEE802.11b standard specifications described Section 5.2.1. That is why the multiple access scheme of the LOCATA technology is a DS-CDMA/TDMA. But we may wonder why a hybrid CDMA/TDMA scheme is used? The answer is found in the so called Near-Far Problem.

The Near-Far effect occurs when one transmitter is much closer to a receiver than others. The consequence is the signal-to-noise-ratio increases and the other signals from the transmitters further away are hidden in the receiver's noise floor. Thus, it makes it difficult for the receiver to detect those signals [Duffett-Smith and Macnaughtan (2002)]. We explained previously in Section 5.2.1 that using the PRN sequence should prevent any interferences, because the multiplication of the data by the CDMA Gold code makes the transmitted signal appeared as a noise, and then the cross-correlation with any other signals is null. But in the specifications, the CDMA Gold code is limited to within 23 dBm dynamic range for a pulsing technology [Barnes (2006)]. In other words, if the difference of power between two received signals is up to 23 dBm, the receiver is not able to detect the weakest signal, and then the CDMA Gold code is not enough to avoid the Near-Far effect. In addition, LOCATA Engineers implemented a TDMA Time Slot to tackle this problem. Nevertheless, TDMA has to be carefully designed to avoid aliasing effect.

Aliasing is also called spectral overlapping: if a signal is not filtered around its central frequency, the transmitter may transmit in other frequency bands that produces interferences with surrounding receivers [Delmas (1995)]. Thus inside each time slot (T_S) the LOCATA pulse starts randomly (pseudo random pulse scheme). It is important to underline that this new technology differs from GPS in the transmission mode: while GPS is transmitting continuously, LOCATA is pulsing. The frame's length (T_f) of the LOCATA TDMA is 1 ms, divided in 30 slots, which allows in theory a network of 30 LocataLites with a duty cycle of 1%. The duty cycle is the ratio of the pulse duration to the pulse period for an ideal time frame. If there are

only 5 LocataLites in the network, each pulse can be transmitted within 6 slots and then the duty cycle is equal to 20%. At the time of writing this section, a LocataNet cannot exceed 10 LocataLites. Figure 5.4 is the drawing of the TDMA frame used by the LocataLites to send data to the rover.

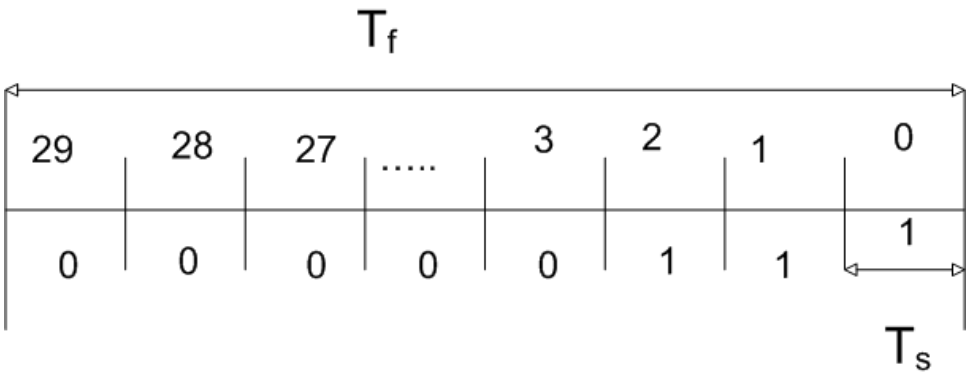


Figure 5.4: TDMA frame used in the LOCATA technology [Barnes (2006)].

In this example, the device transmits in the first 3 time slots. In the next generation of the LOCATA technology, LocataLites may share slots allowing a larger LocataNet than there are slots in the time frame. The design of the time frame is flexible as long as the LOCATA technology takes into account the near-far dynamic of the signals if both signals are required to be tracked simultaneously. In the LocataLite parameters, every time slot is characterised by an hexadecimal number called a bit mask (i.e. 0×00000007) [Barnes (2006)].

5.2.4 Network Synchronisation

In Section 5.1.2, the LocataNet was introduced. In addition, two kinds of LocataLites have to be distinguished: master and slaves. All the slave LocataLites are synchronised with the reference PRN of the master LocataLite, generally $PRN1$. This information is displayed in the field $ReferencePRN$ in the header of the rover/LocataLite setup files. Thus the user decides which ones are either the master or the slaves manually during the LOCATA network setup. The synchronisation process is called *TimeLoc*. Note if the slave cannot directly be synchronised with the master, due to Non Line-Of-Sight (NLoS) or deep fading area, the synchronisation can be done with

another slave by cascade synchronisation. Albeit, it is worth underlining that all the formulas used to explain formally the *TimeLoc* process in the following, are developed by the author through correspondence with Dr. J. Barnes. The general overview of the process is described in [Barnes et al. (2003a)].

We saw in Section 5.2.3 that every transmitter has a dedicated time slot to communicate. However the transmitters clock-offset has to be corrected. This correction is called the network synchronisation. Figure 5.5 describes the *TimeLoc* process. The example involves a master named A, and a LocataLite slave B.

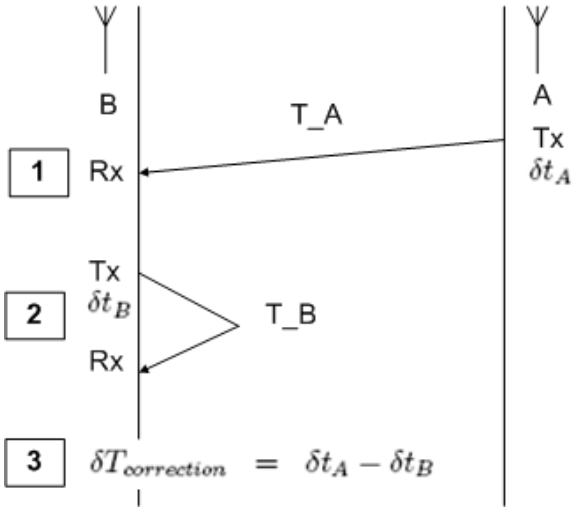


Figure 5.5: Different steps in the TimeLoc process.

Worthwhile highlighting that the *TimeLoc* process involves only the reference PRN transmitter (master) and a single transmitter- receiver from the slave LocataLite, since the two transmitters of the same LocataLite share the same clock. In the first step, the master transmits a signal received by the slave. To simplify, the time delay (T_A) is due to the separation distance TX_A-RX_B and the clock drift of the master (neglecting any troposphere effects and random errors due to signal propagation). In the second step, the slave transmits its own signal at a low power in order to avoid the near-far effect phenomenon with the signal coming from the master, and receives it. This time delay (T_B) is also correlated with the slave's transmitter clock offset. Mathematically the problem can be viewed as:

$$T_A = \delta t_A + R_A/c$$

$$T_B = \delta t_B + R_B/c \tag{5.1}$$

where R_A and R_B are respectively the geometrical separation distances TX_A-RX_B and TX_B-RX_B. The distance between the slave's transmitter and slave's receiver is geometrically very small ($R_A >> R_B$). In the final step, the slave subtracts the two time delays ($T_A - T_B$) and it corrects this value by the geometrical range R_A, as it knows the precise position of the transmitters from the setup files. The reader may wonder how the coordinates of the receiver are calculated. The author assumes that the transmitter and the receiver from the slave's LocataLite are coupled, then the separation distance (R_B) is equal to zero; R_A is calculated replacing the coordinates of the receiver by those of the slave's transmitter. Finally, using Direct Digital Synthesis (DDS) technology [Barnes et al. (2003c)], the slave's transmitter adjusts its local oscillator in order to have:

$$\begin{aligned} \delta T_{correction} &= T_A - T_B - R_A/c \\ \delta T_{correction} &\simeq \delta t_A - \delta t_B \end{aligned} \tag{5.2}$$

The master and slave are now synchronised. Note that in the following (and the remainder of the section), the X, Y and Z coordinates are in ENU referential, not WGS84.

A valuable example is to consider the special case when the antennas (transmitter and receiver) are on the same pole and the clock drift of the master is very small compared to the pseudorange T_A. The geometrical range can be calculated as:

$$\begin{aligned} (X_A - X)^2 + (Y_A - Y)^2 + (Z_A - Z)^2 &= (c \times (T_A))^2 \\ (X_B - X)^2 + (Y_B - Y)^2 + (Z_B - Z)^2 &= (c \times (T_B - \delta t_B))^2 \end{aligned} \tag{5.3}$$

with $[X_A, Y_A, Z_A]$, $[X_B, Y_B, Z_B]$ and $[X, Y, Z]$ being the coordinates of the master, the slave's transmitter and the slave's receiver. c is the velocity of light. The slave's receiver is on the same pole as the slave's transmitter assuming the support of the antennas is exactly vertical, thus $[X, Y]$ is equal to $[X_B, Y_B]$. Then the clock synchronisation of the slave is calculated from:

$$\begin{aligned} \delta T_{correction} &= \delta t_B \\ \delta T_{correction} &= \frac{1}{c}(Z_B - Z_A + c \times T_B + \sqrt{(c \times T_A)^2 - (X_A - X_B)^2 + (Y_A - Y_B)^2}) \end{aligned} \tag{5.4}$$

The carrier-phase *TimeLoc* process is done after the pseudorange is synchronised. The carrier-phase synchronisation must calculate the integer ambiguities in addition to the errors affecting also the pseudoranges for each LocataLite.

$$\begin{aligned} \hat{T_A} &= \delta t_A + R_A/c + N_A \times \lambda/c \\ \hat{T_B} &= \delta t_B + R_B/c + N_B \times \lambda/c \qquad (5.5) \\ (N_A - N_B) \times \lambda/c &= \hat{T_A} - \hat{T_B} - (\delta t_A - \delta t_B) - (R_A - R_B)/c \qquad (5.6) \end{aligned}$$

In Equation (5.5), N_A and N_B are the integer ambiguities of the master and slave carrier-phase signal; λ is the wavelength of the signal. First, the quantity $(N_A - N_B)$ is calculated replacing $(\delta t_A - \delta t_B)$ by $\delta T_{correction}$ calculated using the pseudoranges (i.e. Equation (5.2)). As a result, the value found for the quantity $(N_A - N_B)$ is a float. Thus, iteratively the clock of the slave decreases this quantity and checks if it can synchronise with the master (using DSS). The lower bound is given by the field $fcodelockthreshold$ and it is set to 5 nanoseconds. In other words, $\delta T_{correction}$ cannot be inferior to this value. Finally, $TimeLoc$ is not one step in the LocataNet configuration, but it is a continuous process where the LocataLites perform a synchronisation check repetitively during the time of the test. It has to be continuous, because the clock of the master drifts continuously over time.
The main advantages of this time-synchronisation are:

- The network is synchronised at the sub-nano second level. Thus the signal transmission is precisely controlled to ensure that transceivers do not transmit at the same time, minimising interference between signals from different transceivers (intelligent signal transmission).

- As the network is synchronised, the rover does not need to wait for any additional data to start processing its position.

- As demonstrated later in this thesis, the Carrier Point Positioning (CPP) with LOCATA technology may achieve the centimetre level of accuracy without using double difference measurements.

In fact, it was shown in GPS studies that the precision of the double difference measurements is two times worse than a single carrier-phase measurement assuming that all measurements are uncorrelated and have equal precision [Teunissen (1997)].

5.2.5 L1/C1 Characteristics

After studying the multiple access scheme and the synchronisation process of the LOCATA technology, the focus is the type of GPS-like signals generated by the transmitters. Actually, the LocataLites radiate both a C/A code pseudorange and a carrier-phase signal, single frequency, in the 2.4 GHz licence free band (Section 5.2.1). The pseudorange signal (C1) radiated by the receiver A at the transmitter j is described in the equation below:

$$\rho_A^j = r_A + \tau_{trop} + c\delta T_A + \epsilon_\rho^j \tag{5.7}$$

where r_A is the geometrical range between the LocataLites A and the rover, τ_{trop} is the error due to the troposphere propagation effect, δT_A is the clock drift of the rover for the transmitter A, and ϵ_ρ^j is the propagation error (i.e. multipath, scattering). The troposphere is modelled using the RTCM LAAS model for radio communication. τ_{trop} is proportional to a gradient of temperature according to [Barnes (2006)]. But for most of the LocataLite networks the height difference between the rover and the transmitters is in the order of magnitude of 50 m maximum [Barnes (2006)]. Thus, the troposphere error may be negligible in those measurements. The static tests show that the precision achieved with the C/A code is roughly 3 m. This result is traditionally the 1% of the chip length in the GPS transmitter [Hoffmann-Wellenhof et al. (2001)]. Using the previous notations, the carrier-phase equation is equal to:

$$\phi_A^j = \frac{1}{\lambda}(r_A + \tau_{trop} + c\delta T_A) + N_A^j + \epsilon_\phi^j \tag{5.8}$$

with N_A^j the integer ambiguity and ϵ_ϕ^j is the propagation error on the phase measurement (L1). It is well known that the precision of the carrier-phase measurements is better than the pseudorange measurements ($\epsilon_\phi^j << \epsilon_\rho^j$). Roughly, the carrier-phase error is proportional to 0.01 cycle or 0.001 m [Hoffmann-Wellenhof et al. (2001)]. But in Equation (5.8), we notice that there is also the integer ambiguity to estimate in

addition to the receiver's clock drift (δT_A) and the coordinates of the rover. At the time of writing, the LOCATA technology uses only a single frequency to transmit the data. Thus it does not allow On-The-Fly kinematic ambiguities resolution. Nevertheless, as the rover is initialised statically on a precisely known point, the integer can be solved in a pre-processing step. The integers remain constant as long as the carrier tracking loop maintains lock. Any break in tracking, no matter how short, could change the integer values. That happens if the rover and the transmitter are not in Line-of-Sight (LoS) or if the rover enters a deep fading zone (e.g. obstruction by foliages, strong scattering). The rover is then reinitialized on a known point (the starting point).

5.3 The LOCATA Setup Files

This paragraph deals with how experimentally a LOCATA user modifies the LocataLite/rover settings to configure a LocataNet. There is almost no literature and very few reports published about the technical manipulation of the LocataLites. Most of this section is based on the experience the author received during training at the University of New South of Wales (UNSW) in January 2007, the experience gained in the field during the measurements and the introduction manual released by the UNSW and *LOCATA Corp.* [Barnes (2006)].
The LocataLites and the rover both uses a Field-Programmable Gate Array (FPGA) chipset and thus they load their settings from the flash MC card. On the LocataLites'

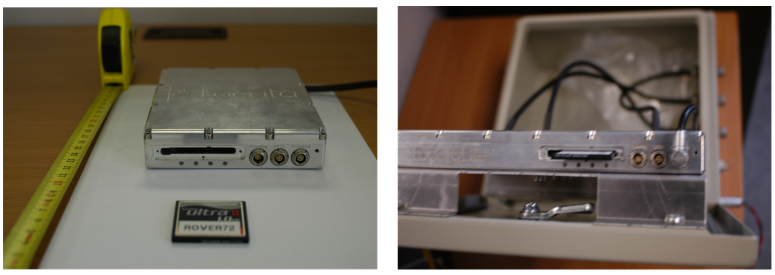


Figure 5.6: Rover (left) and LocataLite (right) with a flash memory card.

flash card, two types of file are loaded: *setup.txt* and $XXX.ace$, with XXX either

being the LocataLite's or rover's name. The latter file contains the firmware. In addition, the rover memory card contains also an executable file (*exec.elf*). The remainder of this paragraph focuses on the *setup.txt* and the main parameters to manipulate in order to calibrate a LocataNet.

The first parameter is the *DEVICE TYPE*, which is either master, slave or rover, according to the LocataNet definition given in Section 5.2.4. The second parameter to specify is the *Reference PRN*, or the Pseudo Random Noise (PRN) of the LocataLite to be synchronised with. The reference PRN is generally the one from the master LocataLite. The reference PRN would be the one from a slave, only if the user wants to do cascade synchronisation with another slave Locatalite. The user allocates on which PRN the LocataLite transmits by filling in the field *Tx PRN*. For example, if *Tx PRN* is equal to $[1, 2]$, then it means that the LocataLites transmit using PRNs 1 and 2. As explained previously, PRN value cannot exceed 20.

Figure 5.7 shows some parameters in the setup file.

```
################################################################################
# Setting for Locata devices
# init version

################################################################################
# DEVICE_TYPE could be MASTER, SLAVE, ROVER
#
DEVICE_TYPE = ROVER;

################################################################################
# Reference PRN
# The PRN of the Locata signal that this device will TimeLoc to. Current
# valid PRN range is 1-16.
#
Reference_PRN = 1;

################################################################################
# Tx PRN
# The PRN or PRNs that this device will transmit. For dual transmit function
# use a comma to separate values, for example:
#         Tx_PRN = 3,4;
# The first (reading left to right) PRN specified in the order will be
# transmitted via Tx antenna 1. Current valid PRN range is 1-16.

# Roof of the IEssg - SN00107
Tx_PRN = 9,10;

################################################################################
# Rover coordinates are in format: x, y, z;
#
# Permanent NTF Rover locations without precise orbit corrections

#Rover in the parking - UoN
Rover_Coordinates = 3851134.41005942, -80112.7593967668,  5066595.10890174;
```

Figure 5.7: Example of LocataLites setup file.

The next parameters are the rover and Locatalite coordinates (*Rover Coordinates*,

Network Coordinates). Those coordinates have to be very precise, because they play key roles in the TimeLoc process and the initialisation of the rover. Usually, they are monitored using either Real Time Kinematics GPS or a total station. The coordinates needs to be converted to the World Geodetic System 1984 (WGS84) or also called XYZ Cartesian coordinates. Figure 5.8 emphasises that in the *Network Coordinates* field the user needs also to attribute for each transmitter the LocataLite number (first pair of brackets), the PRN number (second pair of brackets) and finally the bit mask (blue circle).

```
##############################################################################
# Rover coordinates are in format: x, y, z;
#
# Permanent NTF Rover locations without precise orbit corrections

#Rover in the parking - UoN
Rover_Coordinates = 3851134.41005942, -80112.7593967668,  5066595.10890174;

##############################################################################
# Below is an array of coordinates and slot allocation of all devices in the network includi
# The array index is the PRN for the device.
# The coordinates are in format: x, y, z.
# The final argument is the slot allocation, given as a bitmask.
# currently the max devices is 20.
#
# NOTTINGHAM UNIVERSITY - IESSG Locatanet Locations

#Position 1 (Master SN0085)
Network_Coordinates[1][1] = 3851170.65389686, -80093.4522098472, 5066633.07091184, 0x0000000
Network_Coordinates[1][2] = 3851170.23515122, -80093.443501123, 5066632.51629372, 0x00000007

#Position 2 (Parking lab SN0071 )
Network_Coordinates[2][3] = 3851165.06760286, -80135.1649724665, 5066640.0070038, 0x00000038
Network_Coordinates[2][4] = 3851164.66994588, -80135.1566980075, 5066639.4803156, 0x00000038

#Position 3 ( SN00116 in the Grass)
Network_Coordinates[3][5] = 3851144.06880091, -80130.4860376163,  5066658.51272749, 0x000001
Network_Coordinates[3][6] = 3851143.70428413, -80130.478453141, 5066658.02992837, 0x000001C0

#Position 4 (SN0100 - tripod 2m)
Network_Coordinates[4][7] =  3851183.10525976, -80129.4699517189, 5066626.27560985, 0x00000E
Network_Coordinates[4][8] =  3851182.67747523, -80129.4610510392, 5066625.70902254, 0x00000E
```

Figure 5.8: Example of LocataLites setup file.

The maximum transmitted power in the ISM band allowed by the International Telecommunication Union (ITU-R) is 100 mW or 20 dBm in the United Kingdom. The transmitted power is regulated with two parameters: *TXPower Setting* and *TXVGA LNA Setting*. The latter field controls the variable Linear Gain Amplifier (LNA). The power values are in hexadecimal.

The rover's position is computed in 3D only if the Vertical Dilution of Precision (VDOP) is better than a specified threshold. The dimension of the rover's position may be an issue for a quick setup scenario when all the LocataLites are set up at the

same height. Figure 5.9 shows not only the VDOP parameters, but that it is also

```
Msg_Latency = 400;

# number of succussful searches completed less than
Num_Searched = 11;

# Solution type of Incoming TPV Message considered Valid
Msg_Solution_Type = 254;

# Quality of latitude (less than) in meters
lat_quality = 0.05;

# Quality of longtitude (less than) in meters
lon_quality = 0.05;

# Quality of height (less than) in meters
height_quality = 0.05;

# Speed over ground less than in knots
Sog = 0.5;

# HDOP less than
HDOP = 5;

# TDOP less than
TDOP = 5;

# VDOP less than
VDOP = 5;

# Number satellites in Pos Computation more than
sats_used = 4;

################################################################################
```

Figure 5.9: Example of LocataLites setup file.

possible to control the Horizontal DOP (HDOP) and Time DOP (TDOP).

Let us consider a vector of the estimated rover's coordinates in WGS84 and clock drift $V = [X, Y, Z, \delta T_{clock}]$. Then the covariance matrix is equal to ([Kreyszig (1992)]):

$$Var(\mathbf{V}) \quad = \quad E\{[\mathbf{V} - E\{\mathbf{V}\}][\mathbf{V} - E\{\mathbf{V}\}]^T\} \tag{5.9}$$

with $E\{\}$ denoting the expectation of a random variable and T the matrix transpose. Then, the covariance matrix (5.9) is converted to the East North Up (ENU) reference. The new covariance matrix is then equal to :

$$\mathbf{Co}_{ENU} = \begin{pmatrix} \sigma_E^2 & \sigma_{EN} & \sigma_{EU} \\ \sigma_{NE} & \sigma_N^2 & \sigma_{NU} \\ \sigma_{UE} & \sigma_{UN} & \sigma_U^2 \end{pmatrix}$$

According to [Strang and Borre (1997)] and [Massat and Rudnick (1990)], the VDOP, HDOP and TDOP are defined by:

$$HDOP = \sqrt{\frac{\sigma_E^2 + \sigma_N^2}{\sigma_0^2}} \tag{5.10}$$

$$VDOP = \frac{\sigma_U^2}{\sigma_0^2} \tag{5.11}$$

$$TDOP = \frac{\sigma_{\delta T_{clock}}}{\sigma_0} \tag{5.12}$$

with σ_0^2, the variance of the uncorrelated observations (C/A code or carrier-phase). Finally, a user interested in recording more data for a specific utilisation of the LocataNet, may modify the measurement rate (*Meas Rate*) and the data output rate (*Data Output Rate*). A user can display in real-time the data registered on the flash card, by simply plugging a laptop to the COM port of either the rover or the LocataLite. For the bandwidth restriction specified by the $RS232$ port standard, increasing the data output rate of up to 5Hz reduces the number of channels displayed by the devices. Finally, not all the parameters of the setup file have been explained in this section. Some parameters controlling the triangulation of the rover's position are explained later in Chapter 6.

5.4 A Dedicated LocataNet

5.4.1 The Different Steps to Set Up the Network

This section describes step-by-step how to set up a LocataNet starting from the very beginning and taking into account the network limitations. This part is based mainly on the experience of the author gained by manipulating the LOCATA technology. Some technical details can be found in [Barnes et al. (2003b)] and in [Barnes (2006)]. The network design is the first step. The position of the LocataLites are determined taking into account the area to cover, the size of the LocataNet (number of LocataLites) and the fact that the antennas are not omni-directional (see Section 5.2.2). The limitations imposed by the narrow beamwidth of the LocatLites is partially solved by the omni-directional rover's antenna and the small size of the area where our experiments took place. For the purposes of our experiments, the monitored areas

were chosen for a small scale network ($A = 100\ m^2$). As the antennas are not perfect, there are some sidelobes around the main lobe. The effect of those additional lobes allows the radiation of the energy in other directions than the main lobe [Balanis (2005)]. Thus, this phenomenon helps to cover the area under study.
The right hand side of Figure 5.10 shows a LocataNet in construction.



Figure 5.10: Orthophoto of a locataLites network with $LL1$ the master node (left), LocataLites setup (right).

For a temporary setup, the antennas are mounted on a tripod, whereas a metal pole is preferred in a longer measurements campaign (Figure 5.1). Once the antennas are fixed, taking into account the coupling distance between the two transmitters, they are plugged to the LocataLite hardware (metal box) using a 20 dB cable loss. LocataLites are powered either on a 12 V battery as shown on the left hand side of Figure 5.11 , or using a transformer if they are near an electricity point.
After the installation step, the user elects the master, checking that all the slave receivers are in LoS with the reference PRN transmitter for the synchronisation step. Then, the user monitors precisely the LocataLites transmitters. Depending on the size of the LocataNet and the environment, the antennas position can be calculated using either a total station or by putting a GPS antenna on top of the LocataLites as shown in Figure 5.11. Both the GPS receiver and the total station are precise at the centimetre level of accuracy in the three dimensions. The GPS technology may



Figure 5.11: A LocataNet (left), LocatLites mounted with GPS antennas on top (right).

be even precise down to the millimetre level using a special setup (e.g. RTK GPS with choke ring antenna). During our LocataNet setup, we used the Total Station *LEICA Geosystems TCR705*.

The next step is to write the setup files for each LocataLite and the rover. All the details to perform this task are investigated in Section 5.3. The reader may see the direct relationship between the accuracy of the LOCATA technology and the need to precisely monitor the LocataLites antennas. Once the setup files are ready, it is time to power on the LocataLites and to check the network synchronisation.

Figure 5.12 shows the colour of the different LED (Light Emitting Diode) representing the different phase a LocataLite follows in order to synchronise with the master.

The different synchronisation phases are summed up as:

- Orange (solid) LED : the LocataLite is powered up.
- Green (flash) LED : the LocataLite loads the firmware.
- Red (flash) LED : the LocataLite is synchronising with the master.
- Red (solid) LED : the LocataLite is synchronised with the master.



Figure 5.12: The different LED colours after powering up the LocataLites.

It generally takes a couple of minutes for a LocataLite to perform the last two steps if the LocataLites work in an open area (e.g. downs). In difficult environments, the network synchronisation may take a longer time. The master does not follow step 3 and thus the LED turns directly to solid RED. Finally, a parallel should be made with the setup of the rover. We saw in the previous section that the rover setup file differs of few parameters with a LocataLite setup file. However, the rover is not synchronised with the LOCATA transceivers. It just receives the data sent to it.

5.4.2 Check and Run of the LocataNet

This part starts with the frequent problems any user may meet during the manipulation of the LOCATA technology. In a second paragraph, some hints are given to detect a LocataLite turned off during the measurements.
Here are some possible problems:

- ◇ The orange LED does not appear: check if the battery is empty, or if the

transformer is working.

- ◇ The green LED does not blink and only the orange one is on: the device cannot load either the firmware or the setup file. Check that there are no errors in the setup file (i.e. forgot to put the coordinates of the rover/LocataLites, error of character). Check that all the required files are copied on the memory flash card (see Section 5.3). Sometimes it may happen that there is a problem while formatting the memory card, especially when the equipment is new. The best way is to format the card selecting the parameter FAT 16 (16 bits). The author used the free software MKDOSFS.

- ◇ The red LED keep blinking: sometimes the LocataNet synchronisation lasts for a while. After approximately 13 minutes, it means that the LocataLite cannot synchronise with the master due to either fading problem or (light) obstruction. The quickest solution is to reorientate the receiver antenna of this LocataLite and point it in the direction of the nearest slave in direct LoS. Then, the user performs a cascade synchronisation as explained in Section 5.3.

- ◇ When I plug my laptop to the COM port of a LocataLite/rover, I do not recognise either the NMEA code, or the ASCII code. In this case, the hyperterminal parameters are wrong and an user should Follow the procedure given by Figure 5.13.

From the beginning of this chapter, it was shown that the need for precise synchronisation is directly linked with the accuracy of the rover's position. Thus the major problem during a measurement session is the loss of one or several LocataLites. The only solution is to detect this problem as early as possible by plugging a laptop into the COM port of the rover and displaying the ASCII code (hyperterminal function). Figure 5.14 shows a LOG file. The LOG file is the ASCII code registered by the LOCATA devices on their flash card and also what the COM port displays. The green numbers are the *tracking state field*. The LocataLite is correctly synchronised if the numbers are up to 90. Thus, the loss of base-stations can be directly checked by reading the *tracking state field* in real-time.

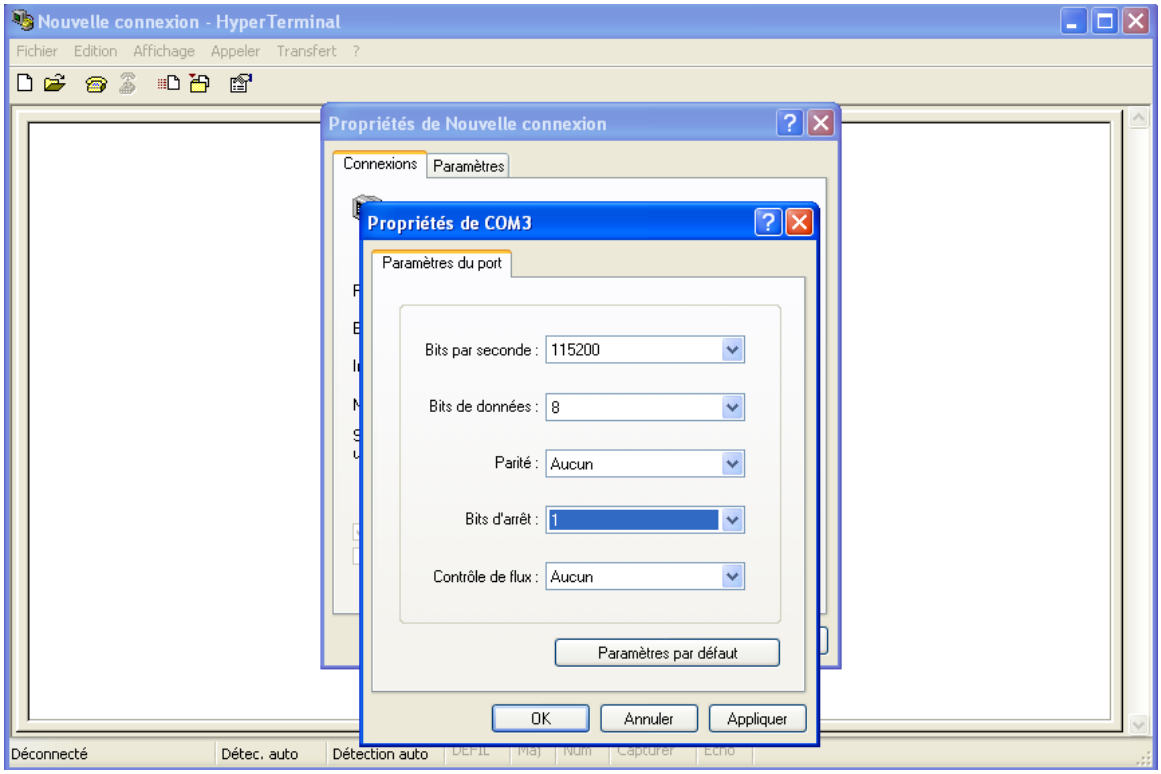


Figure 5.13: Hyperterminal parameters.

LOG3

	A	B	C	D	E	F	AA	AB	AC	AD	AE	AF	AG	AH	AI	AJ	AK	AL
1	0	40	0	0	55	7	28	0	0	0	0	0	0	0	60	9	-16	0
2	$GPLOC	ASC2	0	0	F		99	674	-406	-16965.3	-10019.3	0	11.7	72	13	4	99	-20
3	$GPLOC	ASC2	0	0	F		99	-49	-78	-16975.2	-10192.5	0	0	9	16	0	32	54
4	$GPLOC	ASC2	0	0	F		99	402	-45	-17003.8	-10364.7	0	4.7	39	40	5	41	-32
5	$GPLOC	ASC2	0	0	F		99	162	95	-17001.6	-10536.6	0	0	84	62	12	42	-59
6	$GPLOC	ASC2	80	0	F		99	545	36	-17054	-10705.8	0	8.4	35	97	16	56	123
7	$GPLOC	ASC2	0	0	F		99	-255	301	-17069.6	-10874.9	0	4.7	10	1	0	91	88
8	$GPLOC	ASC2	0	0	F		99	52	-59	-17081.1	-11043.5	0	0	9	31	4	91	148
9	$GPLOC	ASC2	0	0	F		99	-269	66	-17084.5	-11211.8	0	3	38	32	7	91	132
10	$GPLOC	ASC2	0	0	F		99	-331	-24	-17102.9	-11380.3	0	4.7	13	2	0	91	238
11	$GPLOC	ASC2	0	0	F		99	442	164	-17158.1	-11549.2	0	8.4	2	31	3	91	-196
12	$GPLOC	ASC2	0	0	F		99	-470	-25	-17140.1	-11718.7	0	8.4	48	61	11	99	299
13	$GPLOC	ASC2	0	0	F		99	578	-97	-17180.6	-11886.9	0	10.7	1	0	0	99	-166
14	$GPLOC	ASC2	0	0	F		99	-303	66	-17137.9	-12055.4	0	4.7	0	0	0	99	181
15	$GPLOC	ASC2	0	0	F		99	-580	93	-17183.7	-12222.4	0	11.4	8	3	0	99	26
16	$GPLOC	ASC2	0	0	F		99	536	-75	-17217.9	-12390.3	0	11.1	0	0	0	99	-70
17	$GPLOC	ASC2	0	0	F		99	385	141	-17266.9	-12557.5	0	8.4	11	0	0	99	40
18	$GPLOC	ASC2	0	0	F		99	249	-100	-17294.7	-12728.2	0	3	14	29	11	99	-22
19	$GPLOC	ASC2	0	0	F		99	-233	115	-17234.5	-12896.4	0	3	29	39	6	99	130
20	$GPLOC	ASC2	0	0	F		99	218	63	-17229.6	-13064.8	0	3	14	107	49	99	116
21	$GPLOC	ASC2	0	0	F		99	-51	7	-17266.7	-13232	0	0	44	37	12	99	-89
22	$GPLOC	ASC2	0	0	F		99	-345	34	-17299.7	-13399.6	0	7.7	20	4	0	99	25
23	$GPLOC	ASC2	0	0	F		99	-384	70	-17325.2	-13566.9	0	9	2	3	1	99	-114
24	$GPLOC	ASC2	0	0	F		99	193	-67	-17343.3	-13734.6	0	3	0	2	1	99	76
25	$GPLOC	ASC2	0	0	F		99	239	242	-17433.4	-13902.1	0	9	9	34	1	99	49
26	$GPLOC	ASC2	0	0	F		99	364	-122	-17484.4	-14070	0	8.4	15	20	0	99	-66
27	$GPLOC	ASC2	0	0	F		99	-249	263	-17487.7	-14238.6	0	8.4	24	81	0	99	-110
28	$GPLOC	ASC2	0	0	F		99	-528	49	-17510.6	-14407.1	0	11.4	73	39	0	99	-180
29	$GPLOC	ASC2	0	0	F		99	-71	-53	-17548.8	-14574.9	0	0	44	55	16	99	-164
30	$GPLOC	ASC2	0	0	F		99	-35	141	-17560.6	-14742.2	0	0	74	38	1	99	-186
31	$GPLOC	ASC2	0	0	F		99	190	-136	-17604.3	-14911.8	0	3	65	144	76	99	-168
32	$GPLOC	ASC2	0	0	F		99	-116	126	-17583	-15080.8	0	0	19	3	0	99	189
33	$GPLOC	ASC2	0	0	F		99	-201	155	-17636	-15250.6	0	3	53	54	7	99	108
34	$GPLOC	ASC2	0	0	F		99	-203	-267	-17668.3	-15420.2	0	6.9	33	51	11	99	-5
35	$GPLOC	ASC2	0	0	F		99	279	-239	-17661	-15589	0	7.7	48	59	17	99	76
36	$GPLOC	ASC2	0	0	F		99	223	-79	-17675.5	-15756.2	0	3	17	5	2	99	-57
37	$GPLOC	ASC2	0	0	F		99	165	-130	-17681	-15924.6	0	0	28	102	36	99	101

Figure 5.14: LOG file.

On Figure 5.14, the blue and red numbers are respectively the pseudorange and carrier-phase values. The reader may wonder why those two last fields have so high values considering the distance rover-LocataLites (couple of hundred metres). This is due to the clock error and the rollover. The rollover occurs when the pseudorange value exceeds a certain threshold which is the limits of the rover's memory ($+/-29979.248$ metres).

5.5 Range Tests

5.5.1 The LOCATA Radio Channel

Positioning systems ideally operate in free space environments. The path between the LocataLites Tx antenna and the rover may be (lightly) obstructed by natural structures (e.g. trees, vegetation). The presence of these obstacles to the received signal manifests itself in several ways such as pathloss, distortion or spreading of the received signal, multipath fading, ...etc. The Maxwell's theory defines an electrical signal as the result of the propagation of electromagnetic waves in a medium from a transmitter to a receiver. In wireless communications, the medium is often composed of multiple environments (i.e. ground, Troposphere, Ionosphere, man-made obstacles), which results in the waves bouncing on the different scatters along the path transmitter-receiver as shown in Figure 5.15.

When the Tx/Rx antennas are high enough, the simple propagation model is the so called single bounced scattering model, which takes into account the direct path between the transmitter and receiver plus the reflected path by the ground [Ramakrishna (2000)]. Generally, the scattering cross section of the scatterers is assumed to be isotropic, but their density is assumed to vary from location to location. The research community has developed several geometric models such as the ring model [Jakes (1994)] and the circular scattering model [Ertel and Reed (1999)]. Each model is applicable to a specific environment type (i.e. circular scattering model for macrocell environments).

The LocataLites experiments are done in a microcell environment. Thus the main

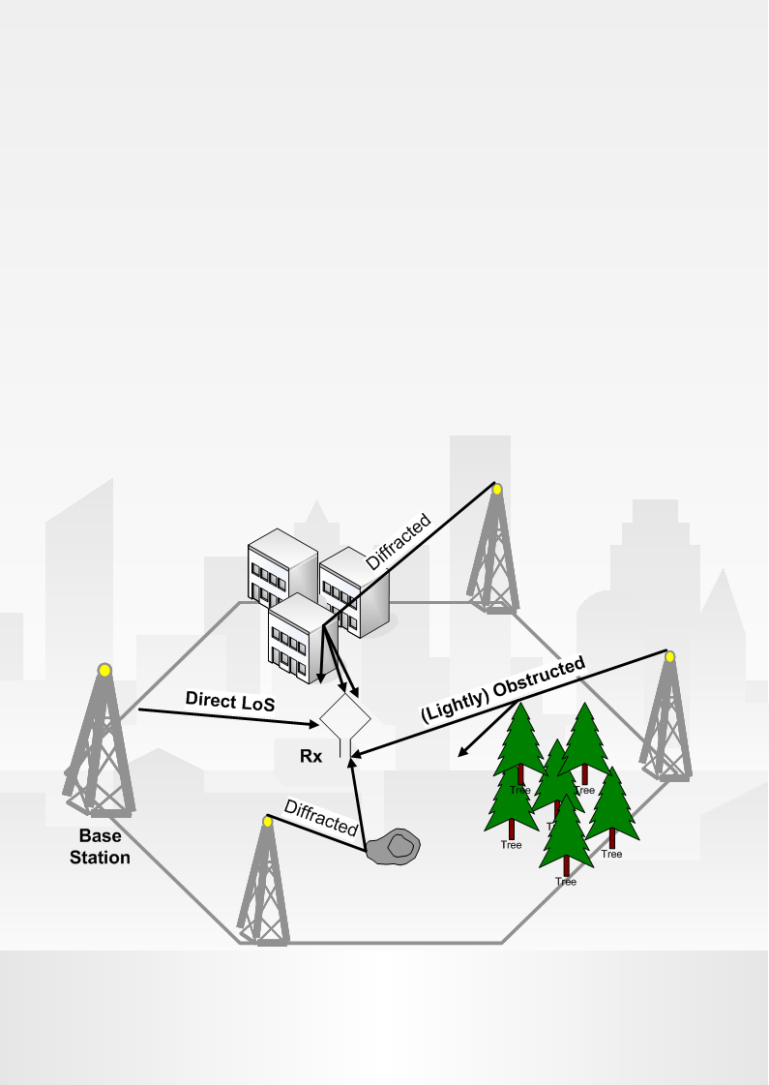


Figure 5.15: Signal propagated in urban areas.

propagation phenomena are the scattering and multipath fading as the transmitter and receiver should always be in direct LoS in order to achieve the centimetre level accuracy in the rover's position. According to [Gibson (2002)], the signal is distorted differently by these effects depending on its bandwidth. The larger the bandwidth is, the more multipath components are received. The goal of the distance test is to model statistically the distribution of the different scatters surrounding the Tx and Rx antennas using the Signal-to-Noise Ratio (SNR). The SNR values are displayed in the second column after the carrier-phase column value (red numbers) in Figure 5.14. However, the LOCATA technology does not record the SNR defined by the

general definition, but as a post-correlation SNR. In the current standard, the SNR is measured at the Rx antenna, whereas in the LOCATA technology the signal is measured at the output of the correlator. Beforehand, the Adaptive Gain Control (AGC) regulates the power of the received signal whether it is too weak or too strong to be correlated [Ko et al. (2005)]. The AGC is a narrow band model, and then the power calibration is done on the raw distance between the rover and the LocataLites calculated with the Tx/Rx coordinates in the Setup files. The role of the AGC is to keep the SNR values around the same mean value. Only if the rover is moved hundreds of metres away, the user may notice a variation in the SNR mean value. Figure 5.16 shows the overview of the PHY of a receiver with an AGC.

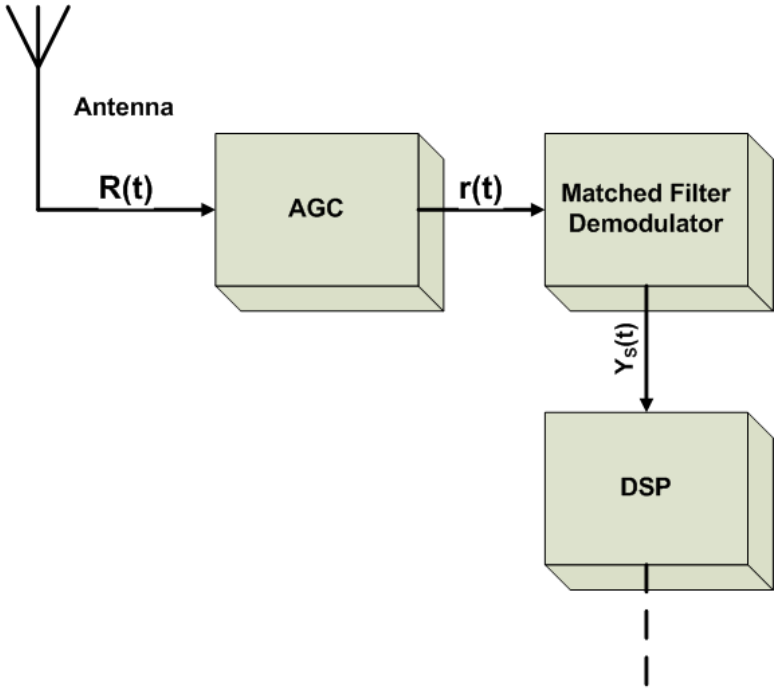


Figure 5.16: Receiver physical layer.

As a result, the slow fading effect is removed from the signal energy and the monitored SNR variations are due to the correlation noise on top of the multipath fading. Figure 5.17 shows some typical SNR values.

The slow and multipath fading characterises a radio communications channel and are correlated in the received signal. Based on Figures 5.16 and 5.17 , the received signal

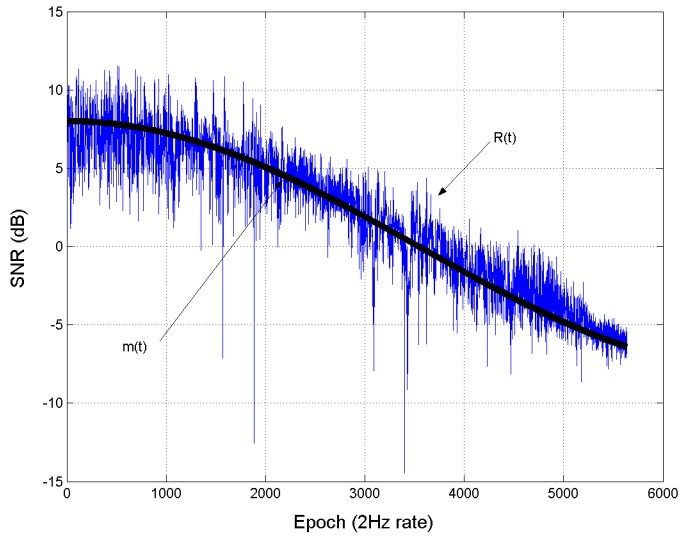


Figure 5.17: Signal-to-Noise Ratio(SNR) and slow fading.

$R(t)$ is partitioned in two terms:

$$R(t) \quad = \quad m(t) \times r_0(t) \tag{5.13}$$

with $m(t)$ the pathloss and $r_0(t)$ the small scale fading (or multipath). Equivalently, $r_0(t)$ is calculated from $R(t)$ when the slow fading is taken out ($m(t)$). Figure 5.17 shows the received signal and the pathloss phenomena. $m(t)$ is also referred to as the local mean or log-normal fading because the magnitude is described by a log-normal pdf (or, equivalently, the magnitude measured in decibels has a Gaussian pdf). The most important parameters are the pathloss exponent n and the power intercept at some reference range (d_0). The mean pathloss ($\bar{L}_p$) is defined by (5.14).

$$\bar{L}_p(d)[dB] \quad = \quad L_s(d_0)[dB] + 10n \log \frac{d}{d_0} \tag{5.14}$$

A considerable interest has been generated in finding quick solutions for predicting average field strengths and multipath signals in macrocells [Hashemi (1993)], [Lee and Lee (2000)], [Gibson (2002)]. A number of research groups have carried out measurements in outdoor environments of which the most extensive set of measurements was carried out by Okumura [Okumura et al. (1968)] in the city of Tokyo. Various empirical models exist to model this phenomenon such as the Hata and Okumura

model [Hashemi (1993)] for urban macrocells environment. *LOCATA Corp.* claims that their technology is based on the pathloss model (L_{50}) developed in the COST 231-Hata (European Cooperation in the Field of Science and Technology) model:

$$\begin{aligned} L_{50}(urban) &= 46.3 + 33.9 \log f - 13.82 \log h_{BS} \\ &\quad -a(h_{rover}) + (44.9 - 6.55 \log h_{BS}) \log d + C_m \end{aligned} \tag{5.15}$$

with C_m equal to {0,3} if the measurements take place either in medium city/suburban area, or metropolitan centre. f is the center frequency of the transmitted signal. The model was originally developed for signals inside the frequency band [1500 − 2000] MHz. h_{BS} and h_{rover} are the antenna heights of the LocataLites and rover, respectively. The validity of the COST 231-Hata model is for Base station antenna height (h_{BS}) from 30 to 200 m where the antenna is above the roof-top level, and h_{rover} values are inside the interval [1 m-10 m] according to [Ramakrishna (2000)].
The next section focus on applying any existing channel models from the literature to check its validity with the LOCATA technology. We characterise the channel in terms of modelling the multipath phenomenon and calculating some relevant parameters.

5.5.2 SNR and Multipath Fading Model

Multipath fading may seriously degrade the performance of communication systems depending on the environment in the vicinity of the transmitter/receiver. Unfortunately, one can do little to eliminate multipath disturbances. However, if the channel is well modelled, the transmitter and receiver can be designed to reduce the fading effect.
The common model for narrow band communication systems is the impulse response approach modelling the channel as a time varying filter [Proakis (2000)]. Equation (5.16) is the mathematical formula of the time varying filter with the assumption that the channel is stationary.

$$h(t) = \sum_{k=0}^{N-1} a_k \delta(t - t_k) e^{i\theta_k} \tag{5.16}$$

N is the number of multipath components, a_k, t_k, θ_k are the random time-varying amplitude, arrival-time, and phase sequences, respectively, and δ is the Kronecker

symbol. When the time varying impulse response is assumed to have stationary fluctuations in time and frequency, the channel is said to be wide sense stationary with uncorrelated scattering (WSSUS).

Following the studies of [Zepernick and Wysocki (1999)], [Woodward et al. (1999)] and [Huang and Khayata (1992)], research work has already been done on 2.4 GHz radio channel model parameters. The distribution of the amplitude of the fast fading may follow different statistical distributions depending on the area covered by the measurements, the presence of a dominating strong path (LoS) and some other conditions. Many distributions have been developed and studied to model the radio communication medium such as Rayleigh, Rician, Lognormal, Nakgami (m-distribution), Binomial, Maxwell, ...etc. [Papoulis and Pillai (2002)],[Zepernick and Wysocki (1999)]. But the Rician ($Pr(a, \sigma^2)$) distribution is of greater interest in the present work:

$$Pr(a, \sigma^2) \quad = \quad \frac{x}{\sigma^2} e^{\frac{-(x^2+a^2)}{2\sigma^2}} \mathbf{I}_o(\frac{ax}{\sigma^2}) \tag{5.17}$$

x takes the values in the interval $[-\infty, +\infty]$, and a in $[0^+, \infty]$ according to [Papoulis and Pillai (2002)]. $\mathbf{I}_o$ is the zero th -order modified Bessel function of the first kind. A search in the literature indicates that the application of the Rician distribution to multipath amplitude distribution occurs when a strong path exists in addition to the low level scattered paths [Hashemi (1993)], [Rice (1944)]. This strong path is generally a LoS between the receiver and transmitter, or a path much less attenuated than the other reflected/diffracted paths. [Rice (1944)] has shown when a strong path exists, the multipath amplitude distribution can be considered as the sum of two vectors: a scattered Rayleigh vector with random amplitude and phase, and a vector with deterministic amplitude and phase. But in the previous section, it was explained that the SNR values recorded by the LocataLites/rover are correlated by the noise from the correlator. Based on this observation, it is not possible to model directly the multipath fading from the SNR values. However it is possible to study some properties of the multipath fading phenomenon. In Equations (5.7) and (5.8), one way to extract multipath may be calculated by differencing pseudoranges and carrier-phase measurements:

$$\Delta^j_A(t) \quad = \quad \phi^j_A(t) \times \lambda - \rho^j_A(t)$$

$$\Delta_A^j(t) \quad = \quad \epsilon_\rho^j(t) - \lambda \times (N_A^j + \epsilon_\phi^j(t)) \tag{5.18}$$

The subscript A means *at the receiver* A and j is for the j-th LocataLites. From the Equation (5.18), the term $N_A^j \times \lambda$ is the integer ambiguity and thus it does not vary with time. The multipath fading is described in the time dependent variables ϵ_ρ^j and ϵ_ϕ^j. Those variables are related to the pseudorange and carrier-phase random propagation errors. As stated in Section 5.2.5, the carrier-phase values are more accurate and less sensitive to multpath. In other words, given the inequality $\epsilon_\rho^j >> \lambda \times \epsilon_\phi^j$, one can extract the multipath fading from the Equation (5.18). The following study of the multipath fading statistics is based on the difference between the phase and pseudorange data recorded for a each LocataLite.

In early March 2007, the author conducted a series of distance test experiments in urban canyons and open field scenarios. Figure 5.18 shows the two environments where the experiments took place.



Figure 5.18: Snapshots of the scenarios for the open field (left) and urban canyon (right) scenarios.

Only one LocataLite was set up for this kind of test. The distance rover-LocataLite varied from 50 m to 200 m. Tables 5.2 and 5.3 display the mean and standard deviation (StD) values of the multipath fading distribution along the distance. On one hand, the mean values are not given much information, because the biases due to the distance are correlated with the integer ambiguity from the phase measurements on top of some additional biases from the LocataLites technology (e.g. pseudorange and phase rollover). Reader interested in extracting the exact distance Rx-Tx should pre-process the measurements to extract those biases. This issue is investigated in

Chapter 6. Note for the same reason, it is not possible to extract the slow fading effect from the difference between the phase and pseudorange values. The mean and StD values are calculated using the software Matlab (7.0) developed by *Mathworks* [*www.mathworks.com*].

On the other hand, the StD values for the urban canyon scenario are almost twice the values calculated for the downs measurements. The explanation comes from the density of the scatterers surrounding the receiver antenna being higher in urban canyons than in the downs [Ramakrishna (2000)], [Lutz et al. (1991)], [Akturan and Vogel (1997)].

To conclude, the SNR values displayed by the LocataLites/rover are used as a signal quality check. According to a SNR threshold, the rover may discard some LocataLites in the triangulation of its own position.

Urban	50	100	150	200
μ (m)	-0.034	-0.161	-0.157	-0.28
StD(m)	0.693	0.664	0.638	1.51

Table 5.2: Mean and standard deviation of the measurements recorded during the urban canyon trial.

Urban	50	100	150	200
μ(m)	-0.013	-0.094	-0.028	-0.072
StD(m)	0.44	0.304	0.48	0.351

Table 5.3: Mean and standard deviation of the measurements recorded during the downs trial.

5.6 Summary

The LOCATA technology has been reviewed in detail from the physical layer (PHY) to the Multiple Access scheme (MAC). Throughout this study, some weaknesses have been identified such as the careful design of the network, the limited number of LocataLites in a LocataNet, the advantages and drawbacks of transmitting in the ISM band. These weaknesses appear at the time of writing this thesis and with the version of the firmware used in the various trials (version $20061114_2222_L R\, timing fix_3 rdorder\ limiter_l oclite.ace$). Before going further, this new ground-based positioning devices should be seen as a prototype of which a new version of the firmware is released every six months. Inside the firmware, the positioning algorithm (LINE) is of particular interest. LINE and the performances of the LOCATA technology, in terms of position accuracy, are studied in the next chapter through static and kinematics tests.
In the last section, the SNR values were explained and related to the statistical distribution of the scatterers surrounding the Tx-Rx antennas. It was not possible with the values output by the LocataLites/rover to model this distribution and then to demonstrate statistically that this technology is narrow band. However, it was shown that the type of environment influences the multipath extracted from the subtraction of the pseudoranges to the carrier-phase observables. In the future, the robustness of LOCATA technology to multipath fading may take advantage of the antennas diversity in addition to some improvements in the channel model.

Chapter 6

Achieving Centimetre Level Positioning Accuracy with LOCATA

6.1 Introduction to the Experiments

6.1.1 General Comments

As a reminder, this work is motivated by the need for precise location in urban canyons when GPS solutions are sporadically available. The aim of this project is to reduce streetworks in difficult areas by mapping precisely buried assets from a metre wide sewer pipe to a thin telecoms wire. From the numerous discussions with the VISTA board members and companies involved, it was decided that the accuracy of the location solutions should be about the centimetre level for this kind of application. Thus, several trials have been carried out on the main campus of the University of Nottingham to test and analyse the performance of the LOCATA technology. Based on the pseudoranges and carrier-phase measurements output by the rover, the navigation software triangulates the position (in real time if it is required). This software is called LINE standing for LOCATA Inline Navigation Engine. In the first part of this chapter, the position accuracy is analysed as a function of the LINE parameters. The understanding of the navigation software requires a more in depth study of the Setup.exe file than the previous explanations given in Chapter 5. Statistics of the position accuracy are studied through static and kinematic experiments in various environments. The results in both Sections 6.2.2 and 6.2.3 are based on three dimensional analysis of the error. Furthermore, the accuracy (mean and standard deviation values) is in absolute value throughout this chapter and the future analysis in the next chapters, except if any additional information is given. This chapter ends with a statistical analysis of the errors and the best fitting distribution (see pdf). The error ellipse is also calculated and some explanations are given to link it to the geometry of the network.

Note that the terminology of the parameters written in the Setup.exe file and used through this chapter may vary in the future with the new updated versions of the firmware released by *LOCATA Corp.*

6.1.2 Extraction of the Data

It is always difficult to quantify the hours spent to post-process, reprocess and extract data from the output files recorded on the memory card of the LOCATA rover (e.g. LOG files). here it is important to make a brief statement on the hidden work, generally difficult to show through scientific publications, which are the code lines written either in language *C* [Kernighan and Ritchie (2000)] or Matlab [www.mathworks.com]. Those small softwares are necessary to study, analyse and display the data.
In Chapter 5, the format of the LOCATA files were analysed. From them, the user can reprocess the carrier-phase measurements or the pseudoranges code. But a user may also record the rover's position in real time if a laptop is connected to the COM port. It is also possible to extract the measurements (e.g. pseudoranges, carrier-phase, SNR) for each LocataLite at a given epoch.
Through this chapter, the results are sometimes extracted after post-processing the LOG files. In other words, some of the results were obtained after reprocessing the LOG files with a version of LINE (mini LINE) compatible with the software *Windows XP Pro*. For each experiment, the author wrote some functions to read, extract and calculate the accuracy of the rover position. Some examples of the scripts written are in the Appendices Section B.

6.2 Position Analysis with the LINE Software

6.2.1 Block Diagram of LINE

As previously stated, the rover records both the carrier and pseudorange code measurements for each LocataLite in the LocataNet, and then triangulates its own position. The navigation software follows a three-stages process: Measurements Correction, Select LocataLites and Navigation Algorithm. The block diagram of the LINE software is sketched in Figure 6.1.
The common error in both carrier and pseudoranges code measurements is the rollover. Due to internal memory limitations, pseudoranges have a maximum value of $+/-$ 29979.248 metres and the carrier measurements cannot exceed in absolute value

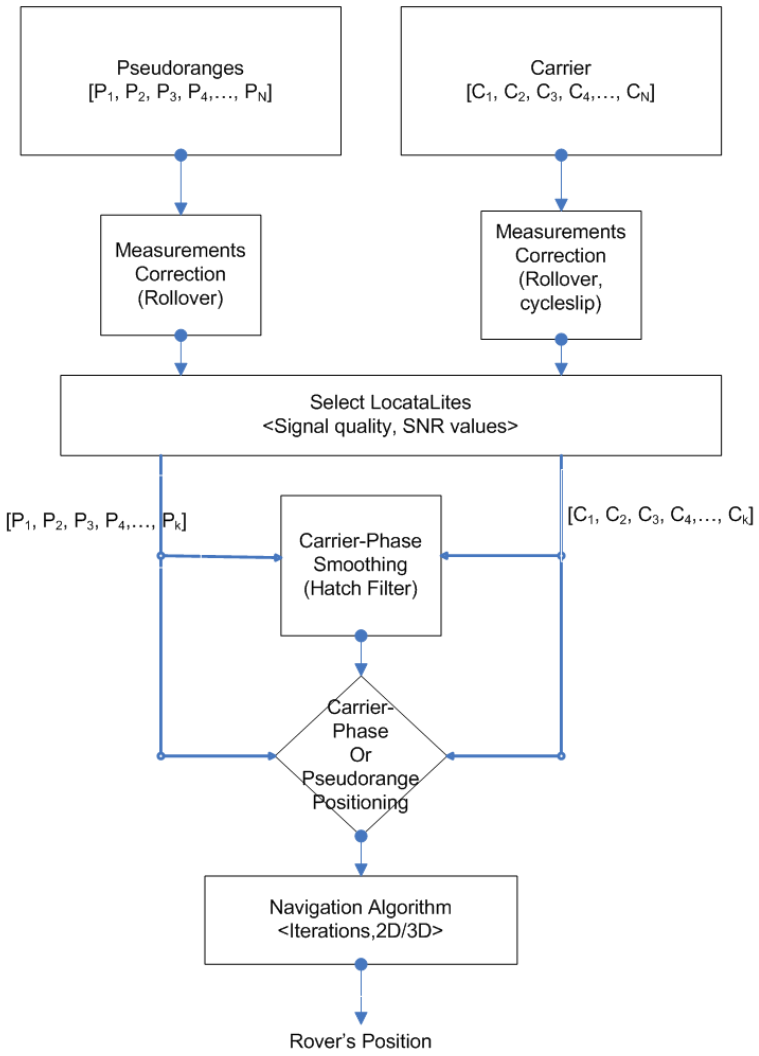


Figure 6.1: Overview of the LINE software.

250000 cycles. When the pseudoranges or carrier measurements get more or less a maximum value at a given epoch, the measurements are wrap round (subtraction of the measurement with this limiting value). Figure 6.2 shows an example of a rollover on pseudoranges.

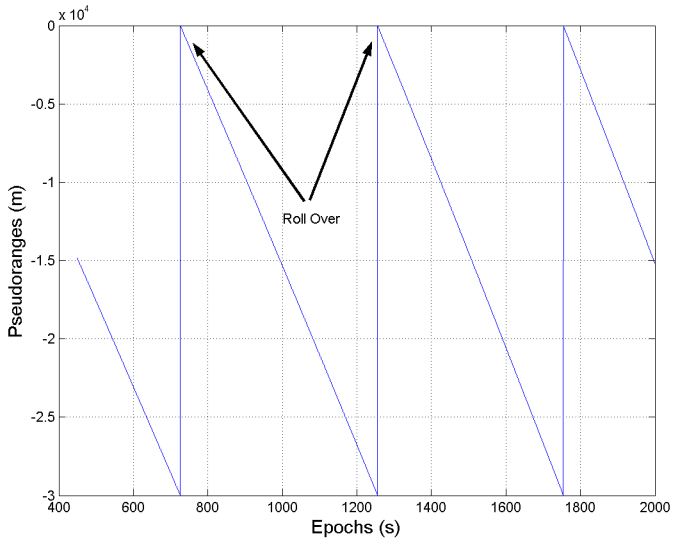


Figure 6.2: Pseudoranges and rollover for a dedicated LocataLite.

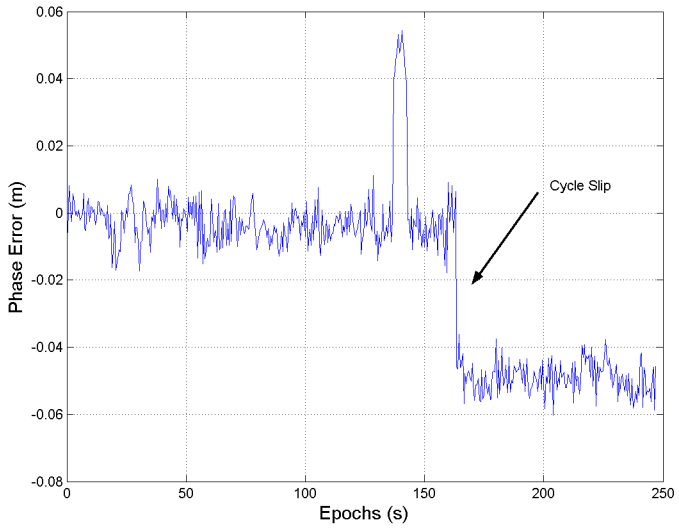


Figure 6.3: Phase error in meters and a cycle slip.

In addition, carrier measurements suffer from cycle slips. This phenomenon was already explained in Chapter 3 when presenting the GPS technology (see Section 3.3). As a reminder, cycle slip occurs when the integer ambiguity changes due to momentary loss of phase lock. Figure 6.3 shows a cycle slip. Note on this Figure, the phase error is normalised to zero. Thus the initial integer ambiguity and the

geometrical distance between the transmitter and the rover are removed. The cycle slip is detected by differentiating the carrier-phase epoch-by-epoch and then the value is compared to a threshold. The Equation (6.1) explains mathematically the process for detecting a cycle slip.

$$\Delta\phi \;=\; (\phi_1^j - \phi_2^j) - (\phi_1^{j-1} - \phi_2^{j-1}) \tag{6.1}$$

where ϕ_1^j is the carrier measurement at the j-th epoch from the transmitter 1. If $\Delta\phi$ is greater than the threshold $SignalQualityMaxIcpDeltaDiff$ (in cycles), as written in the Setup file, a cycle slip is found. Using the initial values, the rover is able to detect cycle slip in the carrier-phase measurements as small as 0.333 cycles or 4.16 centimetres. At the time of writing this thesis, the post-processing of the measurements shows that LINE is able to repair a cycle when it is detected. The algorithm to repair the cycle slip recomputes the (float) ambiguity with the current navigation solution as soon as the signal from the LocataLite is reintroduced. It is worth underlining that in Equation (6.1), the detection process uses both the carrier measurements from the two transmitters (Tx1-Tx2) of a same LocataLite. Using measurements of two transmitters converges to the idea of antennas diversity exposed in Section 5.2.2.

Once the measurements are corrected, the software selects the LocataLites measurements according to different thresholds. The first parameter to look at is the SNR value for each LocataLite in the network. This absolute input value is compared with the threshold $SignalQualityMinSnr$: if the value is less, the rover discards the measurements from this transmitter only at this epoch. The initial threshold is set to 0.0. In other words, LocataLites powered off are ignored.

$SignalQualityMaxPrIcpDeltaDiff$ is the second threshold to check the signal quality for a given LocataLite. This parameter can be explained by the Equation (6.2).

$$\Delta\rho \;=\; (\rho_1^j - \lambda \times \phi_1^j) - (\rho_1^{j-1} - \lambda \times \phi_1^{j-1}) \tag{6.2}$$

where ρ_1^j is the pseudorange at the j-th epoch from the transmitter 1, ϕ_1^j is the carrier measurement at the j-th epoch from the transmitter 1, and λ is the wavelength.

An intermediate stage is the pseudorange smoothing filter, also called Hatch filter

([Hatch (1982)]). If the user wants to get the rover position using pseudoranges smoothed with carrier values. According to [Hoffmann-Wellenhof et al. (2001)], the principle of the code pseudoranges smoothed by means of carrier-phase values is:

$$\begin{aligned} \rho(t_1)_i &= \rho(t_i) + \lambda \times (\phi(t_i) - \phi(t_1)) \\ \rho(t_1)_{ex} &= \frac{1}{p}\sum_{i=1}^{p} \rho(t_1)_i \\ \rho(t_i)_{sm} &= \rho(t_1)_{ex} + \lambda \times (\phi(t_i) - \phi(t_1)) \end{aligned} \tag{6.3}$$

where $\rho(t_i)$ is the code pseudorange at the i-th epoch, $\phi(t_i)$ is the carrier value at the i-th epoch, $\rho(t_i)_{sm}$ is the smoothed code pseudorange at the i-th epoch, λ is the wavelength, and p is the so called epoch in the Hacth filter. In Equation (6.3), the filter starts at the first epoch ($\rho(t_i)_{sm} = \rho(t_1)$). However, carrier data are sensitive to cycle slips. When detected, the Hatch filter is restarted ($\rho(t_1) = \rho(t_j)$). The filter is based on the fact that carrier measurements are much less sensitive to multipath than code pseudoranges.

Finally, if there are at least 4 valid measurements, the position of the rover can be computed ([Barnes et al. (2003d)]). The triangulation is based on a least-squares algorithm estimating four unknowns $[X, Y, Z, c\delta t]$ as described in [Strang and Borre (1997)]. $[X, Y, Z]$ are the coordinates of the rover in the $WGS84$ (World Geodetic System 1984). In the navigation algorithm, two parameters are important: $NavSolverMax3DVDOP$ ($NavSolverMaxPDOP$) and $MaxIterations$. If the Vertical Dilution of Precision (VDOP) value is up to $NavSolverMax3DVDOP$ (or $NavSolverMaxPDOP$), the position is calculated only in 2 dimensions, according to the definition given in Section 5.3. $NavSolverMax3DVDOP$ is also called $VDOPlessthan$ in some Setup files. But $NavSolverMax3DVDOP$ is not the only parameter that controls the position calculated in 2D or 3D: if the least-squares algorithm does not converge in 3D, then the software switches to 2D mode. This is underlined later in this thesis. Last but not least, $MaxIterations$ controls the number of iterations in the least-squares algorithm. More details will be given in the next sections of this chapter.

6.2.2 Static Positioning

Static tests show the accuracy of the LocataLites and the evolution of the error epoch-by-epoch. For six months, the author made several measurement campaigns with LocataLites around the campus of the University of Nottingham (main campus, University Park). In the appendices Section A.8, the orthomap of the main campus of the University of Nottingham describes the places where the experiments took place. The different environments sum up the various applications where LOCATA technology may be used in the future. In this part, the results are averaged from four trials: the downs (05/04/07), the car park of the IESSG (22/02/07), and a yard close to the George Green Library (GGL) [28/03/07 and 26/04/07]. Each result gathered in the following tables is averaged on 2000 epochs. The two first places symbolise light multipath environments, whereas the GGL yard is surrounded by multiple scatterers (trees and buildings). Note that the car park trial was done at daybreak when few cars moved in or around the network. Figures 6.4 and 6.5 show the different places selected for the measurement campaigns.



Figure 6.4: Parking of the IESSG (left) and yard close to the George Green library (right).

In the following tables, the statistics of the error (mean and standard deviation) are extracted for each scenario. Although the rover's coordinates output by the LOCATA technology are in Latitude, Longitude and Altitude reference system (LLA), internally the navigation software converts all of them to Easting Northing and Up (ENU). This translation is justified in order that the least-squares computations can easily be done in a horizontal 2 dimensions model when the VDOP value is too high, in other words



Figure 6.5: Downs scenario.

for a better convergence of the least-squares. The results are extracted based on the estimated rover's coordinates in ENU. Mean (μ) and standard deviation (StD) are calculated over the 3 dimensions according to the equations:

$$\begin{aligned} \mu &= \frac{1}{N}\sum_{i=1}^{N}\sqrt{(\hat{E}_i - E_0)^2 + (\hat{N}_i - N_0)^2 + (\hat{H}_i - H_0)^2} \\ \mu &= \frac{1}{N}\sum_{i=1}^{N} RMSE(i) \\ StD &= \sqrt{\frac{1}{N}\sum_{i=1}^{N}(RMSE(i) - \mu)^2} \end{aligned} \tag{6.4}$$

where N is the number of samples ($Epochs$) used to average the statistics, $[\hat{E}_i, \hat{N}_i, \hat{H}_i]$ are the estimated rover's coordinates at the i-th epoch, and $[E_0, N_0, H_0]$ are the true coordinates. The true coordinates are calculated using a long survey of a point with a GPS RTK receiver or using the CUPT method explained in Section 7.4. The doublets (μ_E, StD_E), (μ_N, StD_N) and (μ_H, StD_H) are the computed statistics of the error in only one dimension. Table (6.1) shows the results using only pseudoranges.

RMSE (m)	DOWNS $05-04-07$	G.G.L1 $26-04-07$	G.G.L2 $28-03-07$	Parking $22-02-07$
LocataLites	8	7	7	5
HDOP/VDOP	0.79/9.39	1.02/4.99	0.79/1.28	1.91/10.95
Epochs	2000	2000	2000	2000
μ	3.110	5.202	4.583	2.629
StD	0.820	2.478	1.519	0.415
μ_E	1.515	3.347	3.540	2.199
StD_E	0.449	1.780	1.339	0.409
μ_N	2.703	1.891	2.810	1.312
StD_N	0.906	1.365	1.032	0.499
μ_H	N/A	2.731	N/A	N/A
StD_H	N/A	1.887	N/A	N/A

Table 6.1: Position and coordinates accuracy in metres of the rover using pseudoranges.

The mean (μ) is approximately equal to 3 m in light multipath environment (Downs, Parking), whereas 5 m in dense multipath (GGL). The standard deviation is also high, with a maximum of approximately 2.5 m in the GGL trials. The results converge to the general conclusion: pseudoranges are not precise enough for very accurate positioning. In the appendices, Figures A.1 and A.2 show the accuracy of the rover's position epoch-by-epoch using or not using a Hatch filter.

Note the error in the H coordinate was unacceptably low (under the millimetre), except for the GGL1 trial. May this result be explained by the value of the VDOP for each experiment? When looking at the VDOP, the values are high for the first and last trials in the tables. Thus the answer is the least-squares triangulation does not converge in 3D, then LINE makes the calculus of the position in 2D. For the same reason, the software is able to calculate the height coordinate of the rover for the $GGL1$ trial. On the other hand, in the GGL2 trial, the VDOP value is low and the error on the H coordinate diverges. At the time of doing those early experiments close to the GGL building, the author did not suspect any possible interference

between LOCATA and other technologies transmitting also in the 2.4 GHz band. After later investigations, it was found that the data recorded during the test at GGL2 may have been more corrupted than when the test was done at the time of GGL1. Following the study about the Wi-Fi interference in Section 7.2, the side effect of the interference may make the accuracy of the rover diverge. The interference with LOCATA technology are explained comprehensively in the next chapter.
Tables (6.2) and (A.1) give the accuracy of the LOCATA technology with pseudoranges smoothed using a Hatch filter (e.g. Section 6.2.1).

RMSE (m)	DOWNS $05-04-07$	G.G.L1 $26-04-07$	G.G.L2 $28-03-07$	Parking $22-02-07$
LocataLites	8	7	7	5
HDOP/VDOP	0.79/9.39	1.02/4.99	0.79/1.28	1.91/10.95
Epochs	2000	2000	2000	2000
μ	3.070	3.775	4.434	2.594
StD	0.392	2.230	1.173	0.236
μ_E	1.504	2.662	3.414	2.189
StD_E	0.284	1.836	1.120	0.231
μ_N	2.663	1.531	2.731	1.315
StD_N	0.428	1.267	0.762	0.270

Table 6.2: Position and coordinates accuracy in metres of the rover using pseudoranges smoothed with carrier-phase measurements using 50 epochs.

According to Equation (6.3), p is equal to 10 and 50 epochs, respectively in Tables (6.2) and (A.1). The results globally demonstrate that the mean errors remain approximately the same as in Table (6.1), but only the standard deviation would decrease to 47% of the initial value (Downs, StD_N). When comparing the results of Tables (6.2) and (A.1), the difference in terms of StD values are small (i.e. $StD^{10}_{GGL1} = 1.285 \sim StD^{50}_{GGL1} = 1.173$). Note that *LOCATA Corp.* sets up the number of epochs in the Hatch filter to be equal to 50.

Finally, Table (6.3) sums up the results using carrier measurements. Looking at the mean values, the best accuracy is around 3 cm (Downs) and the worst is 8 cm (Parking) in $3D$, although this is mostly height error with about 1 cm in plan in both cases. The accuracy is down to the millimetre level averaging on the East coordinate for three trials (e.g. $\mu_E^{GGL1} = 0.003$m). The experiments in the Downs show also an accurate position on the North coordinate ($\mu_N^{Downs} = 0.010$ m). The opposite is true with the results obtained using pseudoranges. The H coordinate has

RMSE (m)	DOWNS $05-04-07$	G.G.L1 $26-04-07$	G.G.L2 $28-03-07$	Parking $22-02-07$
LocataLites	8	7	7	5
HDOP/VDOP	0.79/9.39	1.02/4.99	0.79/1.28	1.91/10.95
Epochs	2000	2000	2000	2000
μ	0.034	0.049	0.041	0.084
StD	0.023	0.001	0.004	0.057
μ_E	**0.004**	**0.003**	0.022	**0.009**
StD_E	0.002	0.008	0.004	0.005
μ_N	**0.010**	0.034	0.034	0.012
StD_N	0.002	0.004	0.003	0.008
μ_H	0.031	0.046	N/A	0.082
StD_H	0.025	N/A	N/A	0.058

Table 6.3: Position and coordinates accuracy in metres of the rover using carrier-phase measurements.

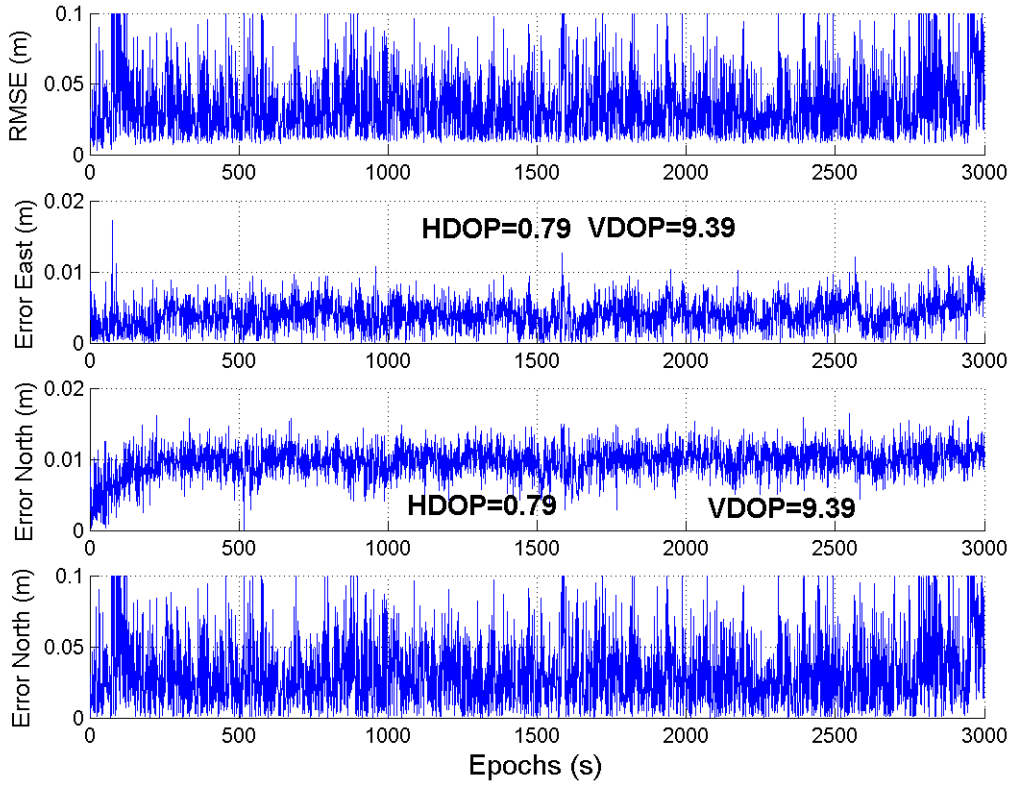


Figure 6.6: Absolute value of the accuracy of the rover's position using carrier-phase measurements $[05-04-07]$.

a trustworthy error when computing the rover position with carrier measurements. But the experiments with a high VDOP value (e.g. $VDOP^{Downs} = 9.39$) demonstrate that the error is bigger in the Height than in the East and North coordinates ($\mu_H^{Downs} = 0.031$ m). Moreover, the standard deviation and mean values of the estimated Height in the GGL2 scenario are still very low. As previously stated, the interferences are the only explanations. Figure 6.6 shows the time series of the positioning error on each coordinate over time for the experiments carried out the $[05-04-07]$, whereas Figure A.3 (in the appendices) shows the time series of the error for the Height coordinates during the $[28-03-07]$ experiments. Note that the error is in absolute value in the East, North and Height coordinates. That may justify why in Figure 6.6 the time series of the error in the North coordinate appeared to have a bias.

In practice, the user can switch between the different positioning solutions (pseudo-

ranges or carrier-phase measurements) by plugging a laptop into the COM port of the rover. According to Section 5.3, on the screen a comma separated ASCII format should be displayed. If nothing has been previously done, the header format is of this form: $GPLOC, ASC2, 0, 0, F, , ...,$ as seen in Section 5.4 in Figure 5.14. Then, typing p on the laptop's keyboard makes the rover triangulates its own position using pseudoranges. Depending on whether the parameter $SmoothPR$ is set to on or off in the rover Setup file, the pseudoranges will or will not be smoothed using the Hatch filter. After typing p, the user should see on the screen $GPLOC, ASC2, 0, 0, F, p, ...$ To use only the carrier measurements in the navigation algorithm, the user needs to type p and then i.

6.2.3 Kinematic Positioning

Unlike in the previous section, the rover was now moving. The results were extracted based on two different scenarios: the first one was performed in the same yard at the University of Nottingham used for the GGL1 scenario , whereas the second scenario took place in a yard at the University of New South Wales in Australia (UNSW).

In the scenario at the University of Nottingham, the difference with GGL1 is that there were now three LocataLites set up on the roof of one of the buildings. Let us call this modified scenario GGL1b. Figure 7.1 is the orthophoto of the place where the experiments are carried out. Note that the picture is in the next chapter, because the same testbed will be used to study the interference with the LOCATA signal. The red crosses symbolise the LOCATA antennas, whereas the purple dots are the test points. The trajectory followed by the LOCATA rover starts at *Tree*, goes to *Hole*, it then comes back to the initial point. The pictures of the LocataNet set up at the University of Nottingham are displayed in the Appendices (i.e. Figure A.7). In both experiments, the rover is initialised on a known point before moving away. As already underlined, the LOCATA technology is single frequency at the time of writing this thesis and the ambiguities may be solved only as float values by averaging over a number of epochs (e.g. 50 epochs).

In the scenario at the University of New South Wales, the rover is initialized on

the point *REF* and it moves close to the left wall referring to the orthophoto 5.10 presented in Chapter 5.4. It follows the path *REF*-*B*6-*B*5-*REF*.
Tables (6.4) and (6.5) show the results in terms of accuracy in the Easting, Northing and Height coordinates for the two scenarios.

GGL1b	$Tree$	$Hole$	$Tree_b$
HDOP	0.602	1.253	0.602
VDOP	2.76	2.68	2.76
D_{TS-Pt}	0	17.04	0
μ	0.020	0.131	0.075
StD	0.013	0.033	0.036
μ_E	0.004	0.048	0.014
StD_E	0.002	0.013	0.007
μ_N	0.002	0.101	0.013
StD_N	0.002	0.036	0.005
μ_H	0.019	0.051	0.070
StD_H	0.014	0.039	0.040

Table 6.4: RMSE in metres of the rover's coordinates using carrier-phase measurements averaged on 60 epochs for the GGL1 scenario.

UNSW (m)	**TS**	**B5**	**B6**	**TS**
HDOP	0.66	0.829	0.743	0.66
VDOP	2.279	1.885	2.05	2.279
$\mathbf{D_{TS-Pt}}$	0	11.50	4.96	0
μ	*0.016*	*0.086*	*0.157*	*0.025*
StD	0.010	N/A	N/A	0.003
$\mu_{\mathbf{E}}$	**0.006**	**0.009**	0.049	0.017
$\mathbf{StD_E}$	0.008	0.004	0.021	0.002
$\mu_{\mathbf{N}}$	**0.007**	0.016	0.129	0.014
$\mathbf{StD_N}$	0.008	0.003	0.002	0.003
$\mu_{\mathbf{H}}$	0.012	0.085	0.060	0.012

Table 6.5: RMSE in metres of the rover's coordinates using carrier-phase measurements (results averaged on 60 epochs) for the UNSW scenario.

The statistics are averaged over 60 epochs; in addition eight LocataLites were used in the two scenarios. The number under the point ID, in both tables, is the distance in metres between the point and the reference point TS. In three dimensions, the accuracy is better than 2 cm at the initial point for both scenarios. Moving further away, the accuracy degrades: the value reaches approximately 9 cm at $B5$ for the experiments in Australia, and 13 cm at *Hole* at the University of Nottingham .

Figure 6.7 shows the time series of the RMS error at the point $B6$ and when we come back on TS. A similar figure is in the appendices (Figure A.6), showing the time series of the RMSE for the experiments at the University of Nottingham at *Hole* and *Tree*. The reader may wonder whether the error propagates while moving further away from the initial point. The survey errors do not justify this result as [Montillet et al. (2007c)] and [Montillet (2007)] showed through using various techniques to survey the coordinates of the reference points (i.e. total station and long survey with RTK GPS receiver).

On one side, the errors may partially come from the environment around the points and the network geometry. The environment does not only include the phenomena

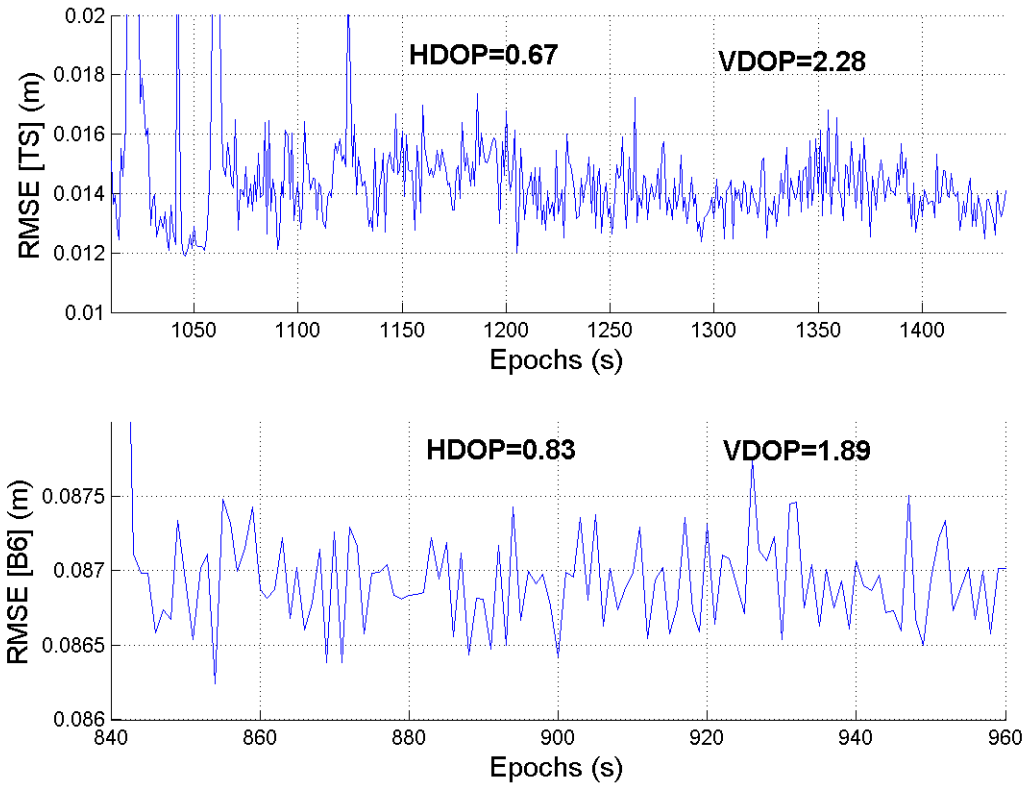


Figure 6.7: Accuracy of the kinematic test at the UNSW.

linked to signal propagation such as multipath, scattering and shadowing (fading environment), but also the variation of network geometry when the rover moves from the initial point. Furthermore, during the experiments the rover was not in Line-of-Sight with all the LocataLite antennas, due to obstructions caused by the trees or foliages. Note that the fluctuation of the values of the Horizontal DOP (HDOP) and VDOP along the path followed by the rover increases the error sometimes more in the North coordinates than in the Height.

On the other hand, the analysis of the carrier-phase measurements epoch-by-epoch reveals that cycle clips did occur whilst moving the rover. Figure 6.8 shows the RMSE and the double difference of the carrier-phase measurements ($\delta^2\phi/\delta t^2$) for $LL1$ and $LL6$. $M1$ and $M2$ are the periods when the rover moves from $Tree$ to $Hole$ and back ($Tree_b$). The dash-dot lines are the threshold for the navigation software to detect the cycle slips. Any measurements up to this threshold in absolute value is considered

as a cycle slip. This threshold can be modified by the user. In this experiment, the threshold was equal to 0.33 cycles. The figure shows clearly that cycle slips appeared when the rover starts to move. Thus, it results that the navigation software resets the ambiguity each time a cycle slip is detected for a given LocataLite's received signal. Note that the ambiguities are calculated using the last estimated rover's position. The result may be interpreted as the LOCATA firmware needs some time to receive and process the signals from each LocataLite before it is able to calculate precisely the carrier-phase measurement (e.g. signal acquisition in [Cavicchi (2001)]). This problem may be solved in the next update of the LOCATA firmware when the technology will become dual frequency. Last but not least, it has already been said that the yard where we performed the measurements at the University of Nottingham (GGL1, GGL1b) is surrounded by Wi-Fi access points. Thus the researcher has to take into account that the accuracy of the rover was also influenced by this phenomenon.

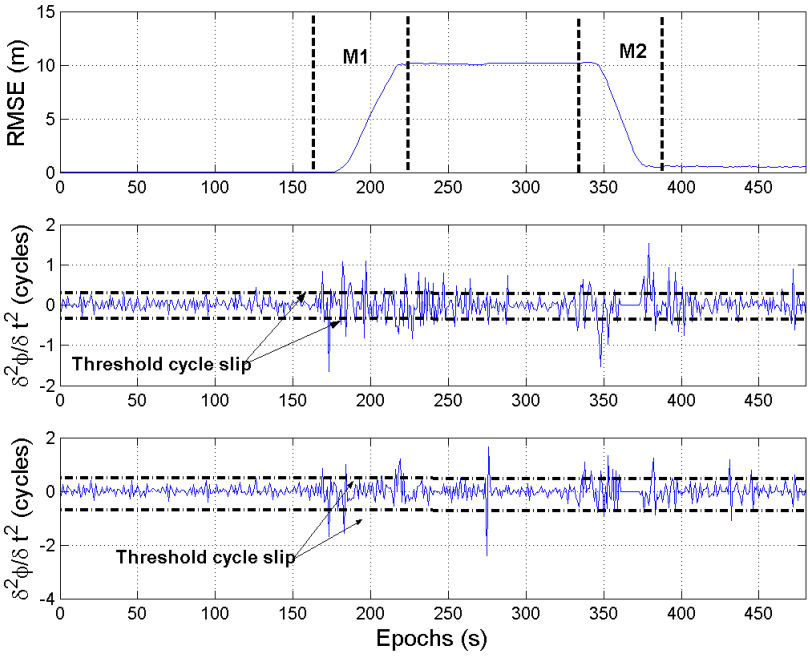


Figure 6.8: RMSE and double difference of the carrier-phase measurements for the LocataLites $LL1$ and $LL6$ during the kinematic test.

6.3 Error Analysis

In Section 2.1.4, the performances of a positioning technology were defined from its accuracy and precision. Thus, the study of the statistics of the error is now investigated one step further by modelling the RMSE with the best fitting distributions and extracting the statistical parameters from the error time series. The second part discusses the confidence ellipses and the attempt to link to the geometry of the network.

6.3.1 Statistical Distribution

In Section 6.2.2, the mean and standard deviation of the estimated coordinates by the LOCATA technology were extracted from several trials. The three dimensions are thus considered as random variables (rv). A reasonable assumption is to consider the three dimensions as independent rvs according to [Strang and Borre (1997)] and [Kleusberg and Teunissen (1996)]. However, one can check this assumption by forming the covariance matrix of the estimated coordinates:

$$\begin{aligned} \sum_E &= E\{(\mathbf{E}_{es} - \mu_{es})(\mathbf{N}_{es} - \mu_{es})^T\} \\ \sum_E &= \begin{bmatrix} \sigma_{EE}^2 & \sigma_{EN} & \sigma_{EH} \\ \sigma_{EN} & \sigma_{NN}^2 & \sigma_{NH} \\ \sigma_{HE} & \sigma_{HN} & \sigma_{HH}^2 \end{bmatrix} \end{aligned} \tag{6.5}$$

with $\mathbf{E}_{es} = [\hat{E}, \hat{N}, \hat{H}]$, the vector of the rover's estimated coordinates; $\mu_{es} = [\mu_E, \mu_N, \mu_H]$ the vector of the means; σ_{EE} is the variance of the E coordinate and σ_{EN} is the cross-covariance between E and N. Checking if the off diagonal terms (e.g. σ_{NH}, σ_{EN}) are very small, it demonstrates whether the rvs are independent stochastic processes in theory [Strang and Borre (1997)]. The author did some random checks of the off diagonal terms using some recorded data and it may be seen that those terms are much smaller (i.e. ten times less) than the diagonal terms. The following study is based on the same scenarios described earlier in Section 6.2.2 (Downs, GGL1, GGL2 and Parking).

The results are shown in Tables (6.6) and (6.7). Only the errors using pseudoranges

	Parameters	DOWNS $05-04-07$	G.G.L1 $26-04-07$	G.G.L2 $28-03-07$	Parking $22-02-07$
RMSE	μ	3.12	5.19	4.92	3.02
	StD	0.85	2.48	1.73	0.43
	ρ	0.97 [N]	0.97 [N]	0.98 [N]	0.99 [N]
		0.96 [Ri]	0.93 [Ri]	0.8 [Ri]	0.98 [Ri]
E	μ_E	1.52	3.21	3.93	2.7
	StD_E	0.41	1.91	1.63	0.45
	ρ_E	0.96 [N]	0.89 [N]	0.97 [N]	0.98 [N]
		0.94 [Ri]	0.81 [Ri]	0.82 [Ri]	0.97 [Ri]
N	μ_N	2.72	1.86	2.81	0.12
	StD_N	0.76	1.42	1.049	0.54
	ρ_N	0.97 [N]	0.94 [N]	0.97 [N]	0.97 [N]
		0.96 [Ri]	0.92 [Ri]	0.83 [Ri]	0.95 [Ri]
H	μ_H		3.1		
	StD_H		2.1		
	ρ_H		0.97 [N]		
			0.93 [Ri]		

Table 6.6: Statistical model of the error using pseudoranges on the East, North, Height (Up) coordinates. [Ri]= Rician distribution, [N]= Normal distribution.

without Hatch filter or carrier-phase measurements are modelled. The influence of a Hatch filter on the estimated rover position makes the data difficult to model.

In order to check whether a distribution fits to a given data set, the correlation coefficient test was applied. According to [Papoulis and Pillai (2002)], the definition of the coefficient correlation test applied to two rvs (E, N) is:

$$\begin{aligned} \rho_{EN} &= \frac{E[(E-\mu_E)(N-\mu_N)]}{\sigma_E \sigma_N} \\ |\rho_{EN}| &< 1 \end{aligned} \tag{6.6}$$

In the tables, ρ_E, ρ_N, ρ_H and ρ are the correlation coefficient values of the different rvs for each scenario and for a given distribution, whereas the mean values (μ, μ_E, μ_N and μ_H) and standard deviation (StD_E, StD_N, StD_H, StD) values are the ones found as degrees of freedom of the distribution functions to well fit the data. According to the definition of a precise technology, the higher the correlation coefficient value is, the more precise is the technology.

The values of correlation coefficient vary slightly with the values exposed earlier (i.e. Table (6.1)). During the data processing, two distributions best model the data: the

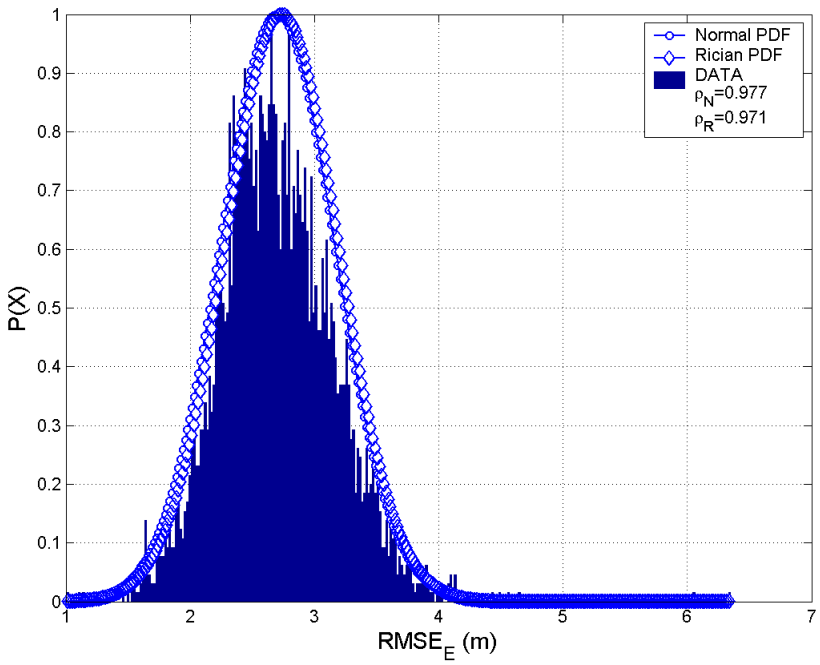


Figure 6.9: Rician and Normal distribution fitting the data ($\mu = 2.7$, $StD = 0.5$).

Rician/Rayleigh and Normal distributions. The Rician distribution was previously presented (e.g. Equation (5.17)) and the Normal or Gaussian distribution is defined by:

$$\mathcal{N}(\mu, \sigma^2) \quad = \quad \frac{1}{\sqrt{2\pi\sigma^2}} \exp -(x-\mu)^2/2\sigma^2 \tag{6.7}$$

The Rayleigh distribution is the same as the Rician distribution, except that the distribution is centred in zero (zero mean distribution).

Comparing the Tables (6.1) and (6.3), the Ricean/Rayleigh and Normal distributions better fit the data on the error calculated with the pseudoranges code (higher cross-correlation values). This is due to the fact that the pseudorange measurements are smoothed with a Hatch filter. Thus, the standard deviation of the error is smoothed. Secondly, the error (mean and standard deviation) with the pseudoranges is obviously much higher than with the carrier-phase values.
As the Normal distribution fits to the data, it means that the error distribution is homogeneous. In fact, the error component is spread equally on both side of the mean error value. The geometrical interpretation is that the scatterers in the vicinity of the rover's antenna are isotropically distributed and no main scatterers may have corrupted the data. This result agrees with where the static rover was placed: in any of the experiments, the rover was not close to a scatterer (e.g. tree, wall).
The Rician distribution fits the data when replacing its parameters (a, σ^2) by the mean and standard deviation of the data measurements $(\mu_{data}, \sigma_{data})$. With these parameters, the shapes of the Rician and Normal distributions are close. Figure 6.9 shows the Rician and Normal probability density functions on top of the data, and ρ_N and ρ_R are respectively their correlation coefficient values.

Moreover, Table (6.7) shows that the error in the height is best modelled with an exponential distribution. An exponential distribution is modelled by the equation:

$$\mathcal{N}(\mu, \sigma^2) \quad = \quad \frac{1}{\sigma^2} \exp -(x-\mu)/\sigma^2 \tag{6.8}$$

Figure A.9 shows the data of the height error recorded in the Downs scenario ($[05-04-07]$) modelled with either a Normal or an Exponential distribution. The meaning of this result may be viewed as the extreme case of a Rayleigh/Rician distribution,

	Parameters	DOWNS $05-04-07$	G.G.L1 $26-04-07$	G.G.L2 $28-03-07$	Parking $22-02-07$
Epochs		2000	1000	1000	1000
RMSE	μ	0.034	0.004	0.065	0.056
	StD	0.023	0.002	0.050	0.041
	ρ	0.65 [N]	0.7 [N]	0.76 [N]	0.6 [N]
		0.7 [R]	0.8 [R]	0.7 [R]	0.6 [R]/0.7 [EXP]
E	μ_E	0.004	0.003	0.003	0.010
	StD_E	0.002	0.002	0.003	0.005
	ρ_E	0.95 [N]	0.84 [N]	0.75 [N]	0.72 [N]
		0.27 [R]	0.82 [R]	0.71 [R]	0.7 [R]
N	μ_N	0.010	0.002	0.003	0.010
	StD_N	0.002	0.001	0.002	0.006
	ρ_N	0.95 [N]	0.81 [N]	0.65 [N]	0.7 [N]
		0.32 [R]	0.79 [R]	0.63 [R]	0.6 [R]
H	μ_H	0.031	N/A	0.066	0.051
	StD_H	0.002	N/A	0.002	0.040
	ρ_H	0.71 [N]	0.77 [N]	0.68 [N]	0.61 [N]
		0.5 [R]	0.7 [R]	0.4 [R]	0.5 [R]
		0.8 [Exp]	0.83 [Exp]	0.76 [Exp]	0.9 [Exp]

Table 6.7: Statistical model of the error using carrier-phase measurements on the East, North and Height. [R]= Rayleigh/Rician distribution, [N]= Normal distribution and [Exp]= Exponential distribution.

where the error is spread only above the mean error value. One may suggest that even though the rover antenna is omnidirectional, but not in both the horizontal and vertical plans. This result is agreed with the diagram of the antenna's power pattern (see Figure 5.3) where it is shown that the antenna does not radiate (receive) any signal in the lower part ($[\pi - 2\pi]$) of the vertical plan. Thus any direct or reflected signal arriving with a certain angle is not received by the receiver's antenna. In addition to in the Downs scenario, this result may also be explained by the fact that there were not many scatterers surrounding the receiver.

Finally, the RMS Error is most likely described by either a Normal or a Rician distribution. This result is predicted by the theory of probability: according to [Papoulis and Pillai (2002)], a rv equal to $\sqrt{E^2 + N^2}$ with E and N two rvs modelled by a normal distributions (μ_E, σ_E, μ_N, σ_N), its distribution follows a Rician shape. However, if the height error is much bigger than the error in the other coordinates, then the RMSE distribution follows the distribution of the height error. That is why sometimes the exponential distribution fits the RMSE data.

6.3.2 Confidence Ellipse

Let us consider the error estimate of a point (Δ_E, Δ_N) in two dimensions in the Easting Northing Up referential defined by the equations:

$$\begin{aligned} \Delta_E &= E - \hat{E} \\ \Delta_N &= N - \hat{N} \end{aligned} \tag{6.9}$$

with ($\hat{E}$, $\hat{N}$) the estimated coordinates and (E, N) the true coordinates of a particular point. The covariance matrix may be defined as:

$$\mathbf{\Sigma} = \begin{pmatrix} \sigma_E^2 & \sigma_{EN} \\ \sigma_{NE} & \sigma_N^2 \end{pmatrix} \tag{6.10}$$

$\mathbf{\Sigma}$ is a 2-by-2 positive definite matrix, so its inverse exists and it is also positive definite. In the previous Section, it was shown that Δ_E and Δ_N are two random variables (r.v.), following a normal distribution with means (μ_E, μ_N), and variances (σ_E^2, σ_N^2). Let us consider now, a new referential with origin at (mean(Δ_E), mean(Δ_N)). Then, in this

new referential, (Δ_E, Δ_N) has a two dimensional normal distribution with zero mean and covariance matrix $\mathbf{\Sigma}$ ($\mathcal{N}(\mathbf{0}, \mathbf{\Sigma})$). Let us look for the points on the curve described by:

$$\begin{aligned} f(\mathbf{X}) &= cte \\ Q &= cte \end{aligned} \tag{6.11}$$

with Q is equal to $[\mathbf{X} - \mu]^T\ \mathbf{\Sigma}^{-1}\ [\ \mathbf{X} - \mu\ ]$, $\mathbf{X}$ is the vector $[\Delta_E,\ \Delta_N]^T$ and μ the vector $[\mu_E, \mu_N\ ]^T$. Equation (6.11) is a quadratic form, and the points solution of this equation describes an ellipse. Figure 6.10 shows the confidence ellipse on top of the error in Easting and Northing coordinates for different values of $\mathbf{\Sigma}$.

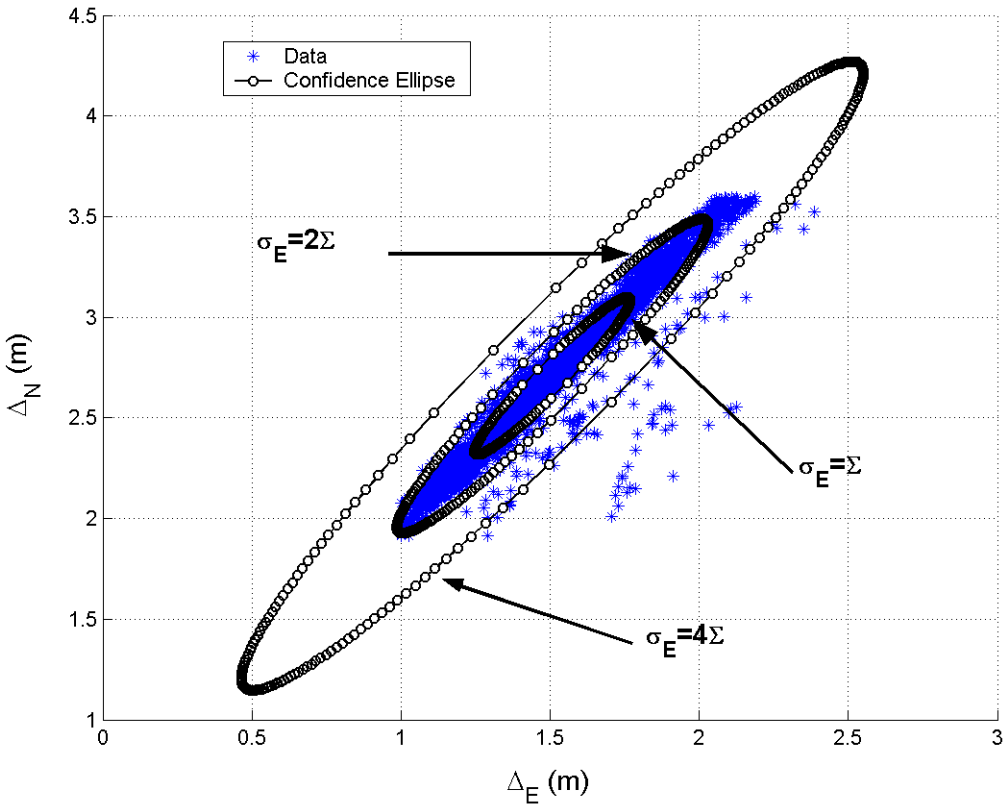


Figure 6.10: Confidence ellipse for various values of σ_E.

The experiment took place in the Downs (e.g. static scenario 05/04/2007). Note the Equation (6.11) is solvable, because $\mathbf{\Sigma}^{-1}$ is positive definite. Following the studies of [Strang and Borre (1997)] and [Dupraz and Stahl (1995)], the confidence ellipse is

defined by:

$$\begin{aligned} A &= \sqrt{0.5(\sigma_E^2 + \sigma_N^2 + w)} \\ B &= \sqrt{0.5(\sigma_E^2 + \sigma_N^2 - w)} \\ w &= \sqrt{(\sigma_E^2 - \sigma_N^2)^2 + 4\sigma_{EN}} \\ \phi &= 0.5 \times arctan(\frac{2\sigma_{EN}}{\sigma_E^2 - \sigma_N^2}) \end{aligned} \tag{6.12}$$

A is the semi major axis, B the semi minor axis and ϕ is the angle between the semi major axis and the N-axis in the ENU referential (or Y-axis in the Cartesian referential). According to Equation (5.10), the covariance matrix in (6.10) can be redefined as $\sigma_0^2 \times \mathbf{\Sigma}_0$ and thus the Horizontal Dilution of Precision is equal to:

$$\begin{aligned} HDOP &= trace(\mathbf{\Sigma}_0) \\ HDOP &= \sqrt{\sigma_E^2 + \sigma_N^2} \end{aligned} \tag{6.13}$$

with σ_0^2, the variance of the uncorrelated observations (pseudoranges or carrier-phase measurements). Inserting (6.13) in (6.12), the angle ϕ is redefined as:

$$\phi = 0.5 \times arctan(\frac{2\sigma_{EN}}{HDOP^2 - 2\sigma_N^2}) \begin{cases} \phi > 0 & \text{if} \frac{HDOP^2}{2\sigma_N^2} > 1 \\ \phi < 0 & \text{if} \frac{HDOP^2}{2\sigma_N^2} < 1 \end{cases} \tag{6.14}$$

Equation (6.14) shows that the semi major axis A of the confidence ellipse rotates in the direction of the E-axis if $\frac{HDOP^2}{2\sigma_N^2} > 1$. However, the HDOP is also defined as a measure of the geometry of the network according to [Massat and Rudnick (1990)].

$$\mathbf{V} = \begin{pmatrix} \hat{E} - BS_{E1} & \hat{N} - BS_{N1} \\ \dots & \dots \\ \hat{E} - BS_{EP} & \hat{N} - BS_{NP} \end{pmatrix} \tag{6.15}$$

with (BS_{E1}, BS_{N1}) being the coordinates of the Base Station 1 (LocataLite). The covariance matrix and the HDOP are then redefined as:

$$\begin{aligned} \mathbf{\Sigma_2} &= (\mathbf{V}^T\mathbf{V})^{-1} \\ HDOP &= trace(\mathbf{\Sigma}_2) \end{aligned} \tag{6.16}$$

Then, the HDOP is a key parameter to define the confidence ellipse and also in the network design (LocataNet). Figure 6.11 explains the boundaries of the rotation of

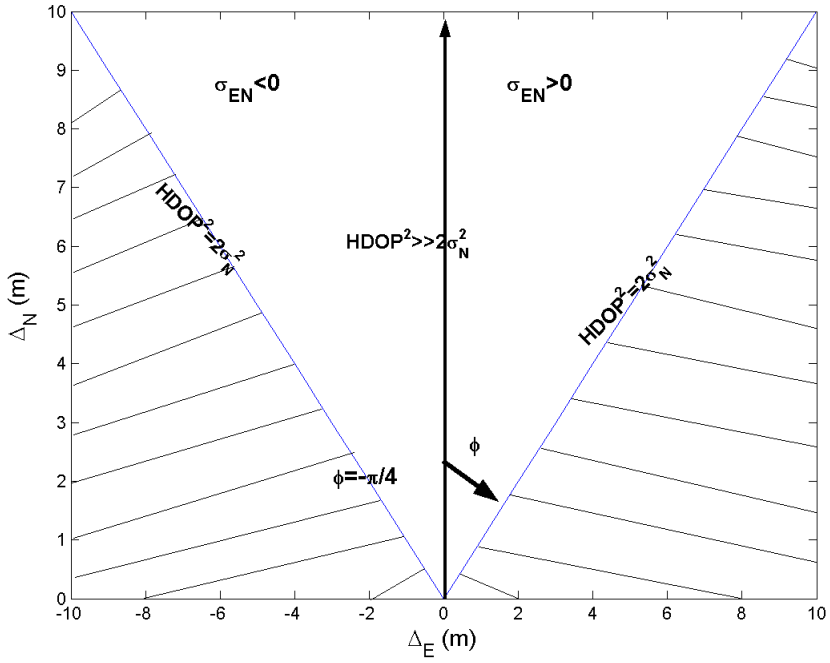


Figure 6.11: Rotation of the confidence ellipse following the HDOP values.

the confidence ellipse based on the raport $\frac{HDOP^2}{2\sigma_N^2}$.

The space shaded with lines indicates in which the space the ellipse cannot rotate. In other words, in this space $HDOP$ is smaller than $2\sigma_N^2$, which is not possible in real life experiments. Thus, the ellipse is a circle with the axes merged with the Cartesian referential.

The angle of rotation of the ellipse (ϕ) varies in the interval $[-\pi/4, \pi/4]$. From (6.14), ϕ is equal to $\pi/4$, meaning that $HDOP^2$ is equal to $2\sigma_N^2$. This result is also confirmed when looking in the appendices at Figure A.10. Finally, the confidence ellipse rotates in $+\phi$ or $-\phi$ plan depending on the sign of the covariance σ_{EN}. Respectively the same study is applied if in Equation (6.14) the denominator $HDOP^2 - 2\sigma_N^2$ is replaced by $2\sigma_E^2 - HDOP^2$.

As a practical example of the theory developed above, Figure 6.12 shows the data (estimated positions with LOCATA technology) for the measurements $[28 - 03 - 07]$ with on top the confidence ellipse for different values of σ_E (radius of the ellipse).

In this case, σ_{EN} is negative and the ellipse rotates in the counter-clockwise direction.

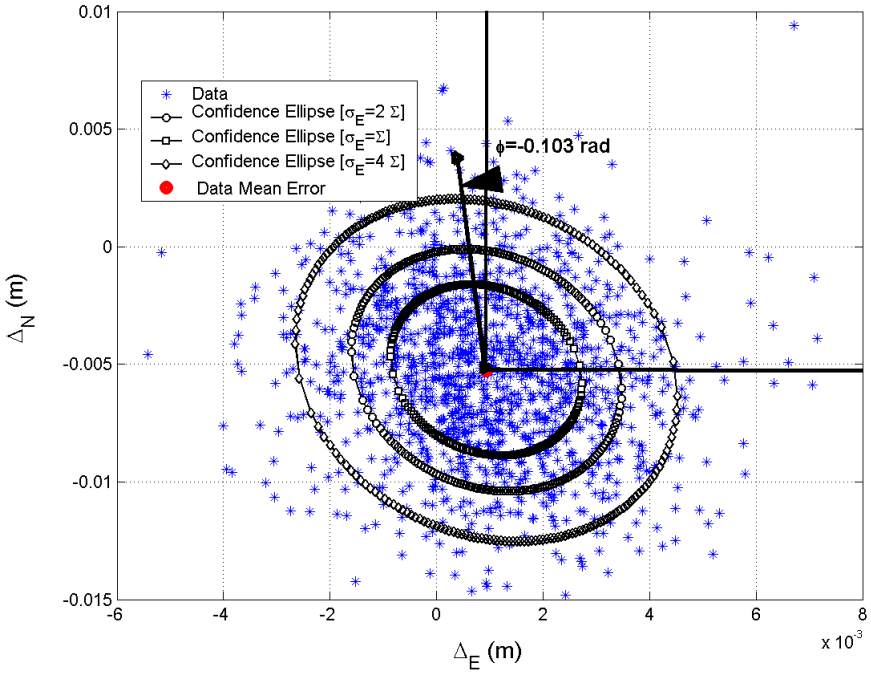


Figure 6.12: Confidence ellipse applied to the data from the experiment $[28-03-07]$.

The angle ϕ defined by Equation (6.14) is equal to -0.013 radians ($6deg$). Unlike in Figure 6.10, the data used in this particular case are the real coordinates (in ENU referential) and not the error. The calculus of the error uses a square root, thus the data are translated to the positive axes part of the referential. It has just been shown that the confidence ellipse may be applied either on the error measurements, or the ENU coordinates. Finally, the author warns the difficulty of fitting the confidence ellipse to the measurements, especially if there are multiple biases or when the standard deviation of the error is large ($\sigma_{Error} > cm$).

6.4 Summary

This chapter starts with a comprehensive definition and study of the navigation software (LINE) triangulating the rover's position using the signals coming from the various LocataLites.

Moreover, the first results obtained with LOCATA technology were analysed. The

author made some measurements around the campus of the University of Nottingham in 2007. The accuracy of this new technology was tested in various scenarios: in an open field environment with low multipath received by the rover antenna, and in urban canyons where the locations are surrounded by buildings and trees. The error was analysed through static and kinematic tests. In the static experiments, the best accuracy is around 3 centimetres in three dimensions (Downs [05 − 04 − 07]) using carrier-phase measurements, and the worst value is between 4.5 cm to 8.4 cm in urban canyons (GGL - Parking). Furthermore, in open environment, the results showed also that the LOCATA technology may triangulate the rover's position at better than the centimetre level of error in $2D$ (East and North coordinates). The kinematic tests underline that the vertical and horizontal dilution of precision values may change from one test point to another and sometime leads to a degradation of the accuracy (to a few centimetres). The surrounding area around the rover and the LocataLites plays an important role, in order to get a trustworthy accuracy all around the monitored area. All information points out the need to adapt and carefully design the LocataNet depending on where the survey takes place. It also shows the difficulty in monitoring the area with a single frequency LOCATA receiver. If the rover loses the lock, the user needs to come back to the initial point to calculate the ambiguity values. Furthermore, the author thinks that the cycle slip detected when the rover starts moving, may be fixed when the LOCATA prototype will become dual frequency. The LOCATA navigation engine may then calculate the ambiguities as integer values and use some powerful algorithms to quicken the processing time.In the next chapter, the author sets up some LocataLites on the roof of a building at the University of Nottingham to improve the position dilution of precision.

The last part of this chapter focused on a statistical study of the error. The author wanted to show another way of looking at the LOCATA performances rather than studying only the time series. Some distributions were studied and applied to the data. Without any surprise, the Normal distribution is the most relevant and shows that the error is well distributed around the mean value. Finally, the confidence ellipse was redefined to fit to the data distribution. An attempt was also made to link the angle of rotation of the confidence ellipse (ϕ) and the HDOP value. The theory was

validated by applying the equations to real data sets.

Chapter 7

LOCATA Technology: Issues and Solutions

7.1 Preamble

This chapter aims at analysing the LOCATA technology beyond the basic tests done through Chapters 5 and 6. The first part analyses the interferences between LOCATA signals and other technologies transmitting in the ISM band. As a reminder, the Wi-Fi phenomenon has already been underlined in the previous chapters during the static and kinematic tests around the University Park at the University of Nottingham. Thus, a comprehensive analysis is given. Furthermore, a special setup of the LocataNet used to prepare this analysis is described.
Section 7.3 is another approach to characterise the LOCATA signal: until now the LOCATA technology has been studied through the time series of the accuracy of the rover's position, thus we need to do some statistics on the double difference of the carrier-phase measurements and the Signal-to-Noise-Ratio distribution. This allows the distribution of the carrier-phase measurements (and cycle slip) for each test to be seen. A complete study is made on when the LOCATA signal passes through foliage and the effect of the Wi-Fi interference on the carrier-phase measurements. At the end of this section, some comments are written on the SNR referring to some experiments. Lastly, a comparison of LOCATA technology and RTK GPS in terms of accuracy is presented in Section 7.4. A summary concludes this chapter.

7.2 Wi-Fi Interference

This part analyses the interferences between the LOCATA technology and the Wi-Fi signals. In the first part, a general description of the interferences is given based on the LOCATA hardware characteristics discussed in the previous chapters. Then, this section details the LOCATA network established at the University of Nottingham in order to study the Wi-Fi interference on the LOCATA signal. Section 7.2.3 is focused on the study of the Wi-Fi affecting the LOCATA accuracy through static and kinematic tests. The interferences are modelled using the data available from the Wi-Fi Access points (AP) surrounding the test area. This phenomenon is presented as a function of different parameters (e.g. signal strength, throughput of the access

points). Note that in the following study, the x-axis of some figures is labeled Samples which means Epochs in seconds.

7.2.1 Overview of the Problem

LOCATA physical layer is transmitting and receiving in the 2.4 GHz (ISM) band. As this band is license free, some existing technologies are already using it. The current users are Wi-Fi and Bluetooth. Bluetooth is a peer-to-peer technology and may not jam the LOCATA signal, unless there is a bluetooth user nearby. Therefore, the tests of this technology were outside the scope of this study.

A Wi-Fi network is higher power than Bluetooth and operates as point-to-multipoint. As the Internet has become wireless, thousands of user services have flourished either to ease our daily life (i.e. directions, addresses, information, TV) or to keep businesses running (i.e. email, addresses). This phenomenon has motivated the rapid expansion of Wi-Fi networks from inside industrial premises, Universities and private properties. This expansion is still on going with Internet operators promoting the installation of private Wi-Fi piconets inside homes. That is why in urban environments or densely populated areas, when turning on a laptop with a Wi-Fi card it may be observed that several Wi-Fi piconets may overlap each other at a given place [Smith (2003)]. Once a Wi-Fi network is installed, the Access Points (APs) transmit continuously and even increase the transmitting power (of a few dB) when a wireless connection is set up between an AP and a laptop for example. For information, Wi-Fi physical layer is built on the IEEE 802.11b and 802.11g standards. The two standards have both 13 transmitting channels, but in the countries following the FCC regulations only channels 1 to 11 are used. A typical deployment uses only channels 1, 6 and 11 in order to avoid any overlap which may cause unacceptable degradation of signal quality and throughput. In addition, a Wi-Fi piconet radius may vary from 35 m (indoor) and to 100 m (outdoor) according to [Ferrari et al. (2006)].

From the LOCATA specifications, the analogue front-ends of the LocataLites and rover, filtering the signal from the receiving antenna, have been designed to be wide enough to sweep the whole ISM band. Thus any devices transmitting in this band may interfere with the LOCATA technology. Using the area described in Section

7.2.2, experiments were carried out.

7.2.2 A Dedicated LocataNet at the University of Nottingham

The author has installed the LocataNet in a courtyard surrounded by buildings at the University of Nottingham. The purpose of these experiments is to test LOCATA in a difficult environment where Real Time Kinematic (RTK) GPS is not reliable enough for precise surveying. This setup opens new applications of the LOCATA technology and points out the drawbacks and advantages of deploying a ground based network technology. As shown later on, it provides an opportunity to study the effects of other wireless technologies operating in the same frequency band on the LOCATA transceivers and rover. Figure 7.1 shows the test area at the University of Nottingham.

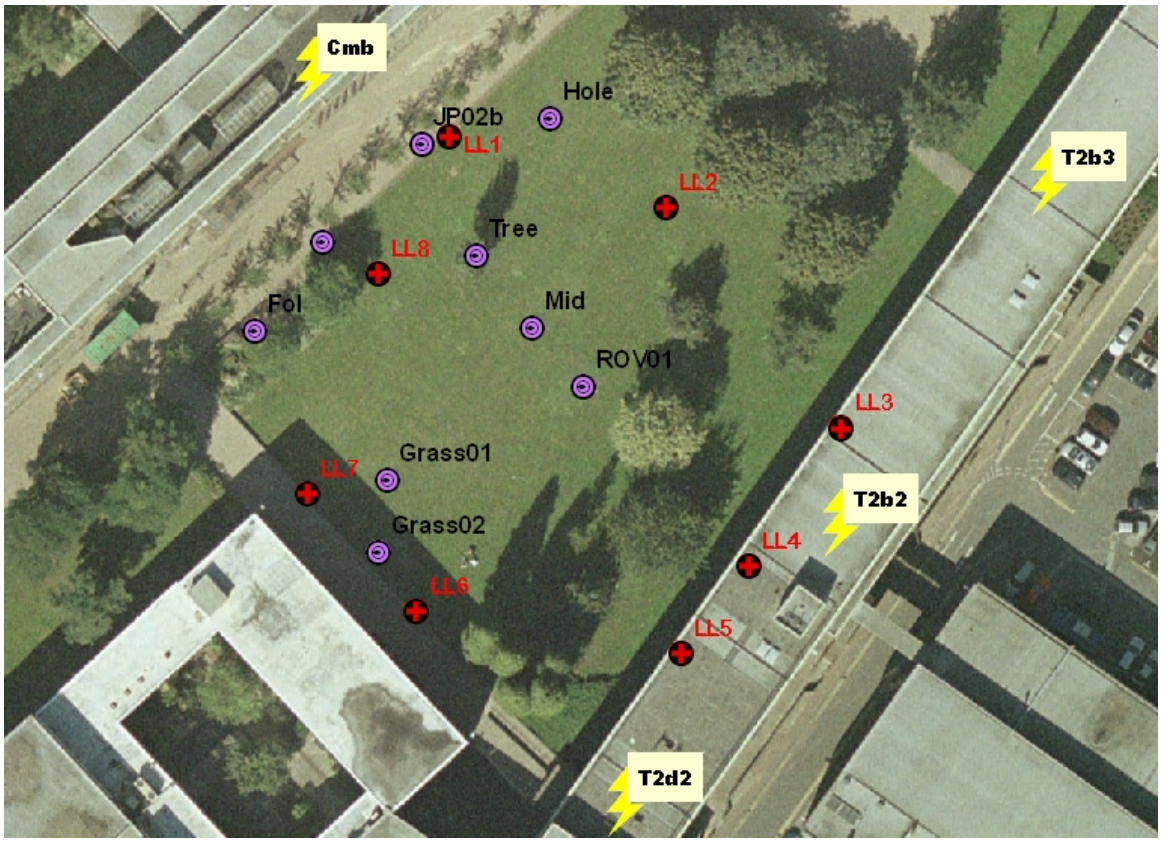


Figure 7.1: Test area to analyse the Wi-Fi interference on the LocataLites.

Through the past summer, three LocataLites (crosses: $LL3$, $LL4$, $LL5$) were installed on the roof and five more were set up on the ground (crosses: $LL1$, $LL2$, $LL6$, $LL7$, $LL8$). Six tests points are selected ($Tree$, $Hole$, $Grass01$, $Grass02$, $Rov01$, Mid) to measure the accuracy of the LOCATA technology (purple dots). Figure 7.1 also shows the Wi-Fi Access Points (APs, yellow bolts). The signal strength of each AP was monitored using a laptop DELL Latitude $D505$ with a Wi-Fi card - $DELL\ True Mobile\ 1300\ WLAN\ Mini-PC$ and using a software called $Network\ Stumbler$.

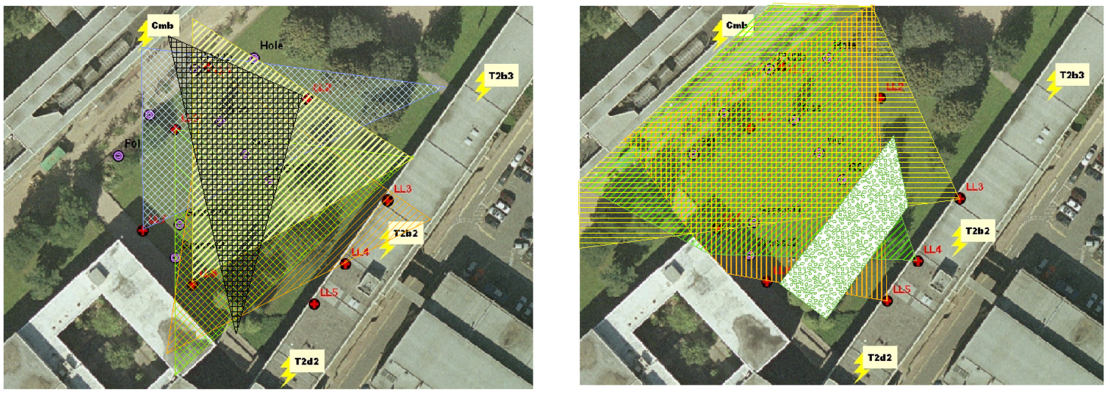


Figure 7.2: Test area showing the coverage of each antenna on the ground (left) and on the roof (right).

The APs were selected taking into account that only the ones with a received power of -75 dBm may potentially disrupt the LOCATA signal. This hypothesis is based on many observations the author did preliminary to the LOCATA experiments. It may appear that below this threshold the Wi-Fi effect may hide in the noise floor of the LOCATA received signal.

Figure 7.2 shows the coverage of the test area by superimposing the radiation pattern of the antennas. Each LoactaLite antenna has a main beamwidth of 70 degrees turned to the front, whereas the rover antenna is omni directional [Montillet (2007)]. But there are also some side lobes which appear in the design of any directional antennas [Balanis (2005)] making the LocataLite's beamwidth wider than it appears in the LOCATA antenna's specifications. Thus, even if the rover is not geographically in the main beamwidth radiated by the antenna, it may still receive the signal as

long as there is a Line-of-Sight (LoS) between the rover and the LocataLite. The coverage is also a function of the transmitted power by the base station. During the experiment, the power was set up at 100 mW, the maximum allowed in the United Kingdom. Nevertheless, the LocataNet must be carefully designed and adapted to the measurements scenario. In the right hand side of Figure 7.2, the white-green polygon represents some trees and foliages which block partially or totally the LoS depending where the rover moves in the field.
Note that preliminary to the setup of the network, the author investigated by reading the specifications of other devices transmitting in or close to the testbed whether any other technologies may have also interfered with the technology under study. The investigations conclude that only the Wi-Fi may be a potential interferer with the LOCATA signal.

7.2.3 Degradation of the LOCATA Accuracy

7.2.3.1 General Observations

The evolution of the interference through time is compared to the accuracy of the rover's coordinates at different days ($15-08-07$, $30-08-07$ and $10-08-07$) monitoring the same point (Mid). Figure 7.3 shows the total Root Mean Square Error (RMSE), and then the error on each coordinate in absolute value.
The circles underline typical jumps due to Wi-Fi interference. Although the jump is clearly seen on the height coordinates, it is much more difficult to assimilate the spikes on the East and North coordinates (circles) as Wi-Fi interference. Figure 7.4 shows the results of the rover's position error measured at a different day $[15-08-07]$.

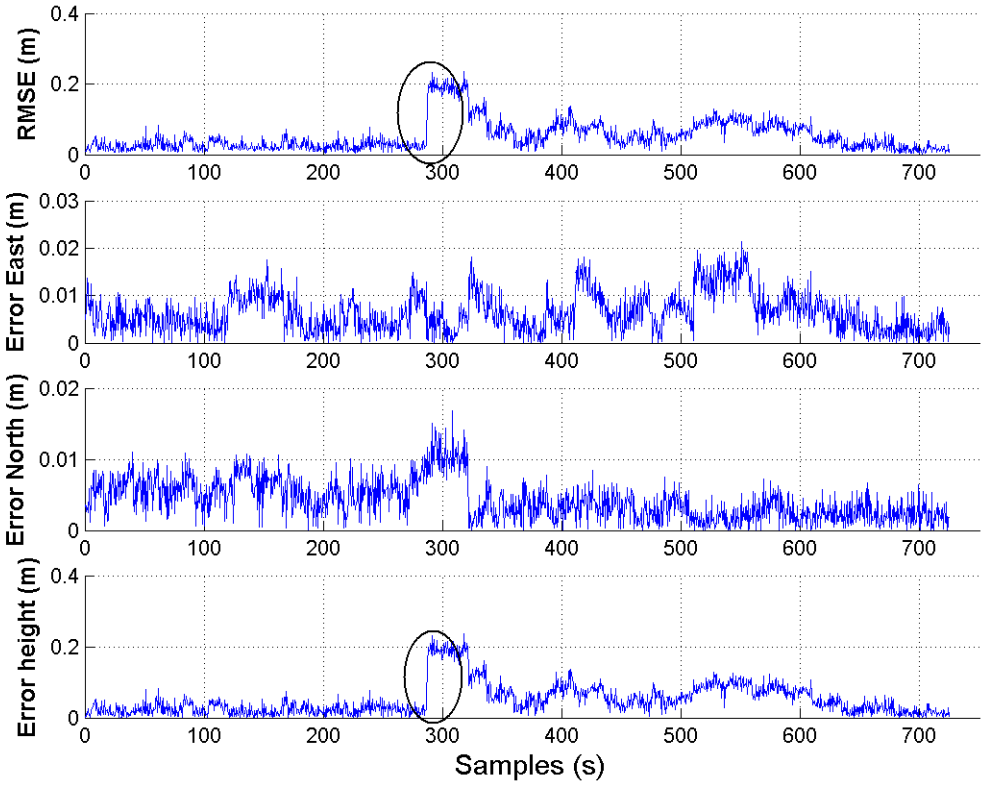


Figure 7.3: Rover's position error measured at midfield test point ($VDOP = 2.99$-$HDOP = 0.69$) $[30 - 08 - 07]$.

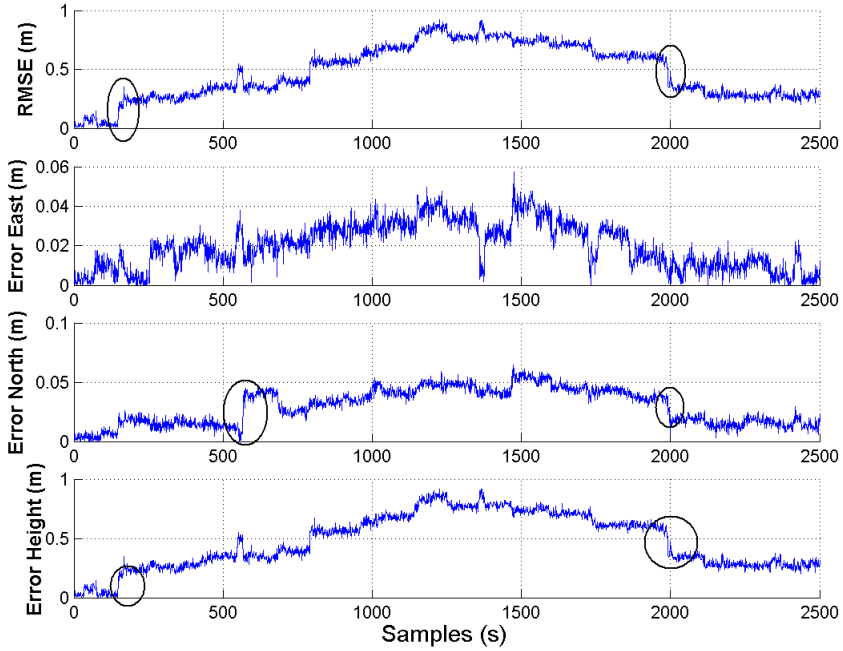


Figure 7.4: Absolute value of the rover's position error measured at midfield test point ($VDOP = 2.82$-$HDOP = 0.65$) $[15 - 08 - 07]$.

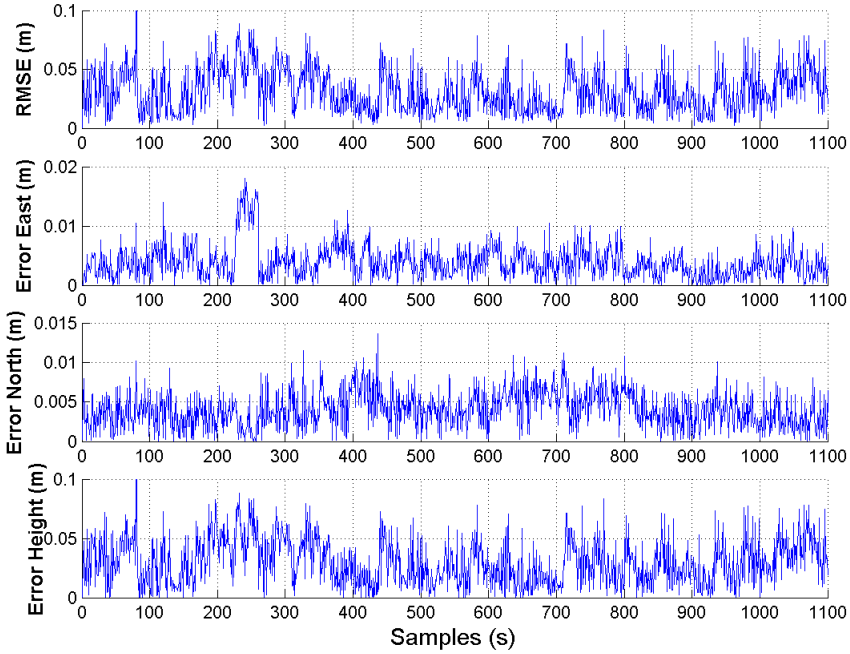


Figure 7.5: Absolute value of the rover's position error measured at midfield test point($VDOP = 2.94$-$HDOP = 0.66$) $[10 - 08 - 07]$.

On the total RMSE and the height error, several jumps are seen (circles) making the accuracy of the LOCATA technology diverge over time. The same conclusions may be drawn for the North coordinate: the jumps on the total RMSE and the height error are of a few millimetres. The East coordinate seems to be less affected by the Wi-Fi signals and the jumps cannot be directly attributed as Wi-Fi interference. Although the test point, *Mid* on Figure 7.1, is situated in the middle of the test area, the rover is not in direct Line-of-Sight with the 8 LocataLites due to the foliages and the trees according to Table (7.1). Note that Table (7.1) displays the number of Wi-Fi Access Points covering different test points in the testbed and the number of LocataLite antennas in direct LoS with the LOCATA rover. The results come from the monitoring of the APs with the software *Network Stumbler* and the user's check while recording the measurements. Again, the height error is more affected by the Wi-Fi interference than the other coordinate components. Figure 7.5 illustrates the results monitored on the $[10 - 08 - 07]$.

From those results, the Wi-Fi interference seems to have a little effect on the estimated rover's coordinates with the RMSE value better than in Figures 7.3 and 7.4.

To conclude, when looking at the time series of the error on the East, North and Height coordinates, it is observed that in presence of Wi-Fi, the position error may jump. The order of magnitude varies from small size jumps (few millimetres) to jumps of a few centimetres. It looks like the software did not detect and repair the cycle slip on the phase measurements.

Now the comparison in time is generalized to other test points. Tables (7.2), (7.3) and (D.1) [in the appendices] display the results. For both days 8 LocataLites were used. Note that all the test points were monitored again and there is no relationship with the previous figures. In addition, during the experiments the height of the rover's antenna varied between 1.60 m and 2.10 m. This variation is small compared with the network size, and there is little difference in the number of LocataLite antennas seen by the rover between those two heights.

	Mid	ROV01	Grass01	Grass02	Tree	Hole
number of WiFi APs	3	3	2	2	3	2
WiFi Id	cmb/t2-b2 /t2-d2	cmb/t2-b2 /t2-d2	cmb /t2-d2	cmb /t2-d2	cmb/t2-b2 /t2-d2	cmb /t2-b2
LoS Antennas	13	12	14	12	13	12
NLoS Antennas	3	4	2	4	3	4

Table 7.1: Number of antennas in LoS or Non LoS with the rover for each test point.

$30-08-07$	Mid	ROV01	Grass01	Grass02	Tree	Hole
Epochs	750	750	750	750	750	750
VDOP/HDOP	2.99/0.69	3.3/0.9	3.0/0.66	2.88/0.78	2.75/0.602	2.69/1.25
Number of Jumps $[R\|E\|N\|H]$	[1|0|0|1]	[4|3|6|9]	[3|3|3|3]	[5|5|5|5]	[3|3|1|3]	[4|1|1|4]
μ	0.051	0.257	0.105	0.076	0.081	0.185
StD	0.043	0.187	0.072	0.064	0.062	0.096
μ_E	0.006	0.049	0.019	0.018	0.009	0.013
StD_E	0.004	0.020	0.025	0.016	0.007	0.008
μ_N	0.004	0.052	0.033	0.014	0.004	0.035
StD_N	0.003	0.039	0.025	0.013	0.003	0.026
μ_H	0.050	0.243	0.095	0.068	0.079	0.176
StD_H	0.044	0.187	0.067	0.066	0.062	0.10

Table 7.2: Position error in metres of the rover in Wi-Fi area (R =total Error).

$15-08-07$	Mid	ROV01	Grass01	Grass02	Tree	Hole
Epochs	750	750	750	750	750	750
VDOP/HDOP	2.82/0.65	3.1/0.83	2.99/0.65	2.85/0.77	2.76/0.59	2.9/1.23
Number of Jumps $[R\|E\|N\|H]$	[6|6|3|6]	[4|4|3|4]	[3|3|1|3]	[10|8|4|10]	[0|0|0|0]	[0|0|0|0]
μ	0.260	0.110	0.170	0.160	0.031	0.027
StD	0.125	0.076	0.160	0.127	0.020	0.013
μ_E	0.014	0.021	0.012	0.026	0.003	0.003
StD_E	0.008	0.015	0.012	0.024	0.002	0.003
μ_N	0.018	0.016	0.007	0.021	0.003	0.013
StD_N	0.012	0.013	0.003	0.015	0.002	0.007
μ_H	0.259	0.106	0.170	0.150	0.031	0.021
StD_H	0.124	0.080	0.160	0.130	0.020	0.014

Table 7.3: Position error in metres of the rover in a Wi-Fi area.

In Table (7.2) the field *Number of Jumps* shows that the number of jumps may not be comparable between the test points, and between two points covered with the same number of Wi-Fi APs (i.e. *Mid*, *Rov*01). Note that R means RMSE in the legend of the tables. Looking at this field, the results confirm that the jumps are of different sizes and the accuracy of the rover's position only diverges with high jumps similar to the one shown in the RMSE of Figure 7.3. For example in Table (7.2), the accuracy of the LOCATA rover is down to the two centimetre level on both the East and North coordinates for the point *Grass*02, whereas the number of jumps recorded in the first 750 epochs is 5 on these two coordinates. In the same way, we may observe for the point *Grass*01 that the mean of the RMSE is approximately 10.5 cm but only 3 jumps were counted.

In an attempt to understand better the jumps potentially resulting from the Wi-Fi interference, we now focus on the carrier-phase measurements.

Figure 7.6 shows the double difference of the carrier-phase signal ($\Delta^2\phi$) for the LocataLites $LL2$ and $LL6$ and the corresponding time series of the rover's position for the experiments $[15-08-07]$.

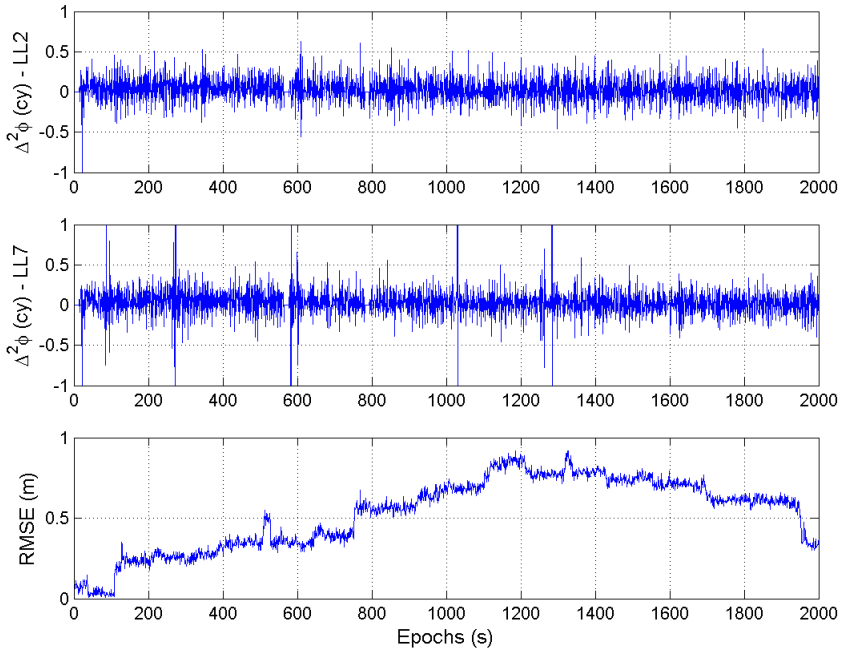


Figure 7.6: Double difference of the carrier-phase signal (in cycles) for $LL2$ and $LL7$ $[15-08-07]$.

In the legend of this figure *cy* means cycles. This figure underlines the difficulty of directly correlating the time of the jumps in the RMSE graph and the cycle slips in the carrier-phase measurements, because some cycle slips (e.g. first jump) may appear on all 16 carrier-phase measurements at the same time of the jump and some other cycle slips may appear on a restricted number of some carrier-phase measurements. Therefore, this analysis of the carrier-phase signal in various experiments may justify that the Wi-Fi interference increases the number of cycle slip. Making the hypothesis that the cycle slips may be the result of a miscalculation of the carrier-phase measurements, it may be concluded that the Wi-Fi interference increases the level of noise in the Adaptive Gain Control (AGC).

To justify the previous hypothesis, let us remind ourselves that an AGC normalizes the probability density function of the input signal (see [Sklar (2001)]). According to its design, the AGC scales the input signal removing the bias due to distance propagation and normalize it. Thus in the normalization process, the signal and the noise are amplified. If the output of the AGC is match filtered with a template signal, the estimated time delay is corrupted with some additional errors coming from the additional noise from the Wi-Fi interference. This may be the same problem as in the near far effect phenomenon [Duffet-Smith and Craig (2004)] when the nearest transmitter to a receiver hides the other transmitted signals in its noise floor. As a result, the pseudorange codes and carrier-phase measurements appear to have some additional errors.

However when looking at Table (7.3), for the last two points ($Tree$, $Hole$) the rover's position is accurate on the first 750 epochs even with the Wi-Fi technology surrounding the area. The RMSE is approximately 3 centimetres. The major source of error is in the estimation of the height, which is understandable when comparing the VDOP with the HDOP for each point. This shows that even if the Wi-Fi APs are radiating in the test area, they may not corrupt the LOCATA measurements all the time. It then suggests a relationship between the variation of the noise floor in the AGC and the transmitted power of the Wi-Fi APs.

Moreover, another way to see the Wi-Fi interference is to turn on the Wi-Fi card on a laptop and then monitoring the divergence of the LOCATA accuracy, as seen in

Figure 7.7. Note that in this experience, the laptop was at a metre away from the rover's antenna.

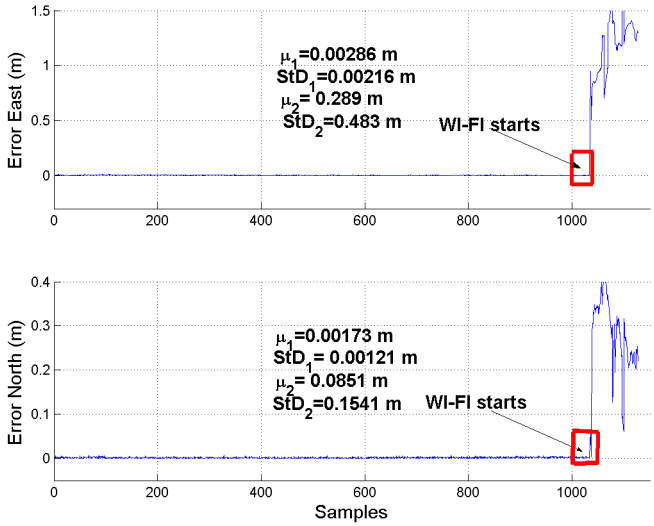


Figure 7.7: Interference when the Wi-Fi card is turned on the laptop.

7.2.3.2 Influence of the Data Throughput of the Wi-Fi APs

The following section will compare the data throughput of the different APs surrounding the test area. Figure 7.8 shows the data rate in terms of packets and bytes per second for each AP. The name of the APs follows the label given in Figure 7.1. The

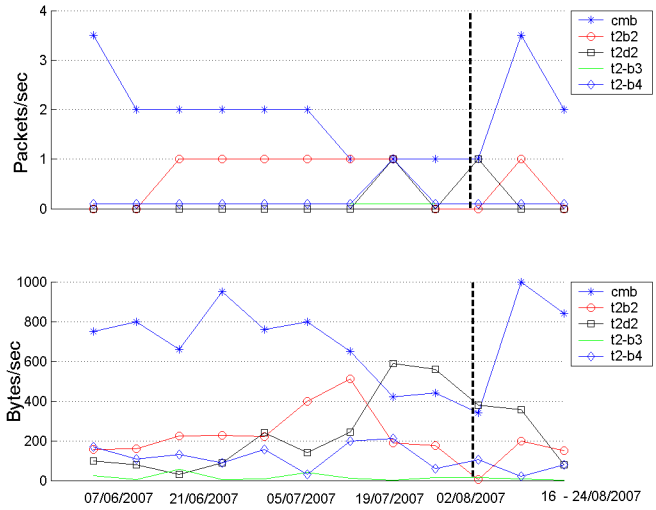


Figure 7.8: Data throughput for each Wi-Fi access point surrounding the test area.

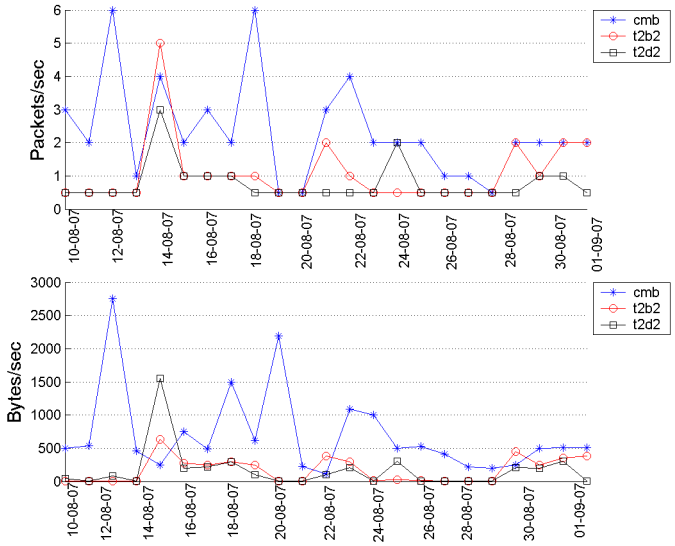


Figure 7.9: Data throughput for 3 Wi-Fi access points (cmb, $t2-d2$ and $t2-b2$) over August 2007.

period of interest is only the time interval 8−08−2007 to 24−08−2007 (right hand side of the dashed -line). During this period, the drawing shows clearly that cmb, $t2-d2$ and $t2-b2$ APs transmitted at a data rate up to 100 bytes/sec. Moreover, following the configuration of the APs given in the previous sections, the channel in which the Wi-Fi transmitted were configurated again after the $24-08-07$. The accuracy of the rover's location is similar for the different experiments before and after changing the transmitting frequency of the Wi-Fi APs. This is supported when comparing the results displayed in Tables (7.2) and (D.1) [in the appendices]. Figure 7.9 displays the data throughput averaged on each day of August 2007. The data throughput for the days $15-08-07$ and $22-08-07$ is under 500 bytes/sec for two APs and the third one is between 500 and 1000 bytes/sec. It confirms the probability of the Wi-Fi interference phenomenon influencing the LOCATA measurements. Unfortunately, the x-axis scale in these figures of the data throughputs for each AP is not precise enough (day-by-day) to match directly the accuracy of the rover and the LOCATA's accuracy.

Note that the Wi-Fi interferes also with the data transmitted by the LocataLites, even if for a matter of clarity the whole study of the interference was based on the data recorded by the rover.

7.3 Statistics from the SNR and Carrier-Phase Measurements

In this section, the study of the LOCATA signal is analysed from another point of view by looking at the carrier-phase measurements and the SNR values. The results from this study are based only on the basic statistics applied to the LOCATA signal. In the first part, the effects of the signal passing through foliage are analysed, then the Wi-Fi interference is studied in another way, doing some statistics on the carrier-phase measurements rather than looking at the LOCATA accuracy itself (time series of the error). Finally, this part ends with some general comments on the SNR values through the experiments.

7.3.1 Statistics of a Signal Blocked by Foliage

7.3.1.1 General Results

The dedicated LocataNet described in Figure 7.2 and used in the previous part to study the Wi-Fi interference allows the extraction of data related to foliage effects on the LOCATA signal. This study focuses on the scenario $[05-04-07]$, $[15-08-07]$ $(Hole)$, $[30-08-07]$ $(Tree)$ and $[30-08-07]$ (Mid). For a matter of clarity, the reader needs to look in the Appendix D, to get the results related to the last two experiments ($[30-08-07]$). Furthermore, the first one is the reference scenario, because the measurements were realised in an open field (downs) and all the LocataLites were in LoS with the rover. No leaves or foliage were in the vicinity of the transmitting antennas. The accuracy calculated from this scenario was explained in the first column of Table (6.3). As a reminder, Tables (7.2) and (7.3) are the accuracy for the experiments done during the days $[15-08-07]$ and $[30-08-07]$. Those experiments are selected because the accuracy is good enough to make the hypothesis that the Wi-Fi does not interfere with the LOCATA signal.

The LOCATA carrier-phase signal is studied by calculating the double difference of the carrier-phase measurements as explained in the Equation (7.1).

$$\frac{\delta^2}{dt^2}\phi_i \quad = \quad (\phi_{i+2}-\phi_{i+1})-(\phi_i-\phi_{i-1}) \tag{7.1}$$

where ϕ_i is the the carrier-phase measurement at the i-th epoch. Because of the biases in the carrier-phase observables modelled as a polynomial function of power 2 ($\delta f(t_k) = at_k^2 + bt_k + c$) [Eren (1987)], the double difference gets rid of the clock bias, the integer ambiguity and the geometrical distance in the carrier-phase equation (e.g. Section 5.5). Thus a double difference residual looks like a constant in time with some spikes, whereas a triple difference residual is a zero mean variable with some spikes. Figure 7.10 shows the double difference of the LOCATA carrier-phase signal ($\delta^2\phi(t)/\delta t^2$). The interest is to number the spikes by their heights. It was explained in Chapter 6 that LINE detects cycle slip as small as 0.3 cycles. Thus, spikes equal or greater than this value are considered as cycle slips.

Tables (7.4) and (7.5) show the results. The field $R.$ means double difference residual. Equally, the field is the number of spikes with a height between $a < x < b$. The

$05-04-07$	Loc	R. $0.1 < x < 1$	R. $x > 0.3$	$\frac{\delta^2}{dt^2}\phi_i$ or SNR $= 0$	Comments
	1	641	15	3/0	$\rho = 0.97$ — t=[-0.5,0.5]
	2	648	18	2/0	$\rho = 0.98$ — t=[-0.4,0.4]
	3	741	88	4/0	$\rho = 0.96$ — t=[-0.4,0.6]
	4	756	89	5/0	$\rho = 0.96$ — t=[-0.4,0.6]
	5	739	98	2/0	$\rho = 0.95$ — t=[-0.4,0.6]
	6	744	101	4/0	$\rho = 0.95$ — t=[-0.4,0.6]
	7	727	70	1/0	$\rho = 0.96$ — t=[-0.4,0.4]
	8	723	71	3/0	$\rho = 0.96$ — t=[-0.4,0.4]
	9	745	66	4/0	$\rho = 0.95$ — t=[-0.5,0.5]
	10	751	63	2/0	$\rho = 0.95$ — t=[-0.5,0.5]
	11	733	71	5/0	$\rho = 0.94$ — t=[-0.4,0.4]
	12	724	74	4/0	$\rho = 0.96$ — t=[-0.4,0.4]
	13	740	72	3/0	$\rho = 0.95$ — t=[-0.4,0.4]
	14	732	80	3/0	$\rho = 0.95$ — t=[-0.4,0.4]
	15	714	60	4/0	$\rho = 0.96$ — t=[-0.4,0.4]
	16	729	62	2/0	$\rho = 0.96$ — t=[-0.4,0.4]

Table 7.4: Characteristics of the LOCATA signal [$t = 2200$].

$15-08-07$ Hole	Loc	R. $0.1 < x < 1$	R. $x > 0.3$	$\frac{\delta^2}{dt^2}\phi_i$ or SNR $= 0$	Comments
	1	424	24	4/0	$\rho = 0.91$ — t=[-0.4,0.4]
	2	416	26	3/0	$\rho = 0.95$ — t=[-0.5,0.5]
	3	528	60	2/0	$\rho = 0.93$ — t=[-0.4,0.4]
	4	520	54	39/0	$\rho = 0.94$ — t=[-0.6,0.6]
	5	**542**	68	3/0	$\rho = 0.93$ — t=[-0.5,0.5]
	6	**550**	67	2/0	$\rho = 0.95$ — t=[-0.8,0.7]
	7	**647**	130	1/0	$\rho = 0.92$ — t=[-0.8,0.7]
	8	**639**	131	3/0	$\rho = 0.90$ — t=[-0.6,0.6]
	9	**623**	129	1/0	$\rho = 0.92$ — t=[-0.6,0.6]
	10	**644**	164	3/2	$\rho = 0.95$ — t=[-0.8,0.8]
	11	508	56	0/0	$\rho = 0.91$ — t=[-0.5,0.5]
	12	533	64	1/0	$\rho = 0.94$ — t=[-0.6,0.4]
	13	486	45	1/0	$\rho = 0.92$ — t=[-0.5,0.5]
	14	488	42	3/0	$\rho = 0.93$ — t=[-0.4,0.4]
	15	505	50	3/0	$\rho = 0.95$ — t=[-0.8,0.4]
	16	513	47	1/0	$\rho = 0.93$ — t=[-0.4,0.4]

Table 7.5: Characteristics of the LOCATA signal [$t = 1952$].

column ($\frac{\delta^2}{dt^2}\phi_i$ or $SNR = 0$) is the number of times that the $\Delta\phi$ or SNR is null during the measurement time. In the particular case of $SNR = 0$, it may also mean that the given LocataLite fails to synchronise during the experiments. Finally, in the field *Comments*, ρ is the correlation coefficient explained previously in this thesis (see Equation (6.6)). Thus, the distribution of the spikes around the mean of the residual is compared with the Normal distribution (e.g. Equation (6.7)). The numbers inside the brackets are the tails of the distribution in cycles.

Comparing the values in Tables (7.4) and (7.5), the column $x > 0.3$ numerates the cycle slips detected by the navigation software. Given a LOCATA transceiver and according to Section 6.2.1, each time a cycle slip is detected, LINE automatically recalculates the ambiguity value based on the latest navigation solution. In the first table, the values in this column are close. There is no large jumps between the slave transmitters (Master - LocataLites PRN 1 and 2). However, it is interesting that all tables show the values for the master LocataLite being smaller than the slaves. As the synchronisation is a continuous process during the experiments, this may suggest that the synchronisation process may add some small cycle slips.
On the other hand, Table (7.5) shows a jump between transmitter 4 and $5, 6, 7, 8, 9, 10$. The values for the remaining LocataLites $(11, 12, 13, 14, 15, 16)$ are close to $3, 4$. Remembering Section 7.2 and in particular Figure 7.1, transceivers $5, 6, 7, 8, 9, 10$ are the ones on the roof. $7, 8, 9$ and 10 are blocked by the foliage (trees) during the summer 2007. A jump in the values (column $x > 0.3$) is also noticeable between $5, 6$ and $7, 8, 9, 10$. In the experiments $[15 - 08 - 07]$ (Hole), there are two results. The first one is related to the height, whereas the second one is related to the foliage blocking the LoS between the rover and the transmitting antenna. In other words, the position on the roof and the foliage add small cycle slips. The tables of the other experiments shown in the appendices (e.g. Table (D.4) and (D.3)) confirm the cycle slips due to the foliage, but it is more difficult to support the first result. This may be due to the fact that the three experiments took place at different test points in the yard. The test point $Hole$ on $[15 - 08 - 07]$ is in direct LoS with transmitters $5, 6$, whereas Mid and $Tree$ on $[30 - 08 - 07]$ is in LoS but with a different view of the transmitters $5, 6$.

7.3.1.2 Statistics of the Carrier-Phase Signal

Another way to look at the effect of the LoS obstruction by foliage is to see the distribution of the spikes of the carrier-phase signal around the mean value (approximately zero in the case of double differencing the signal).

Figures 7.10 and 7.11 show the Normal distribution on top of the carrier-phase measurements (left hand side of the Figures). A value of the correlation coefficient

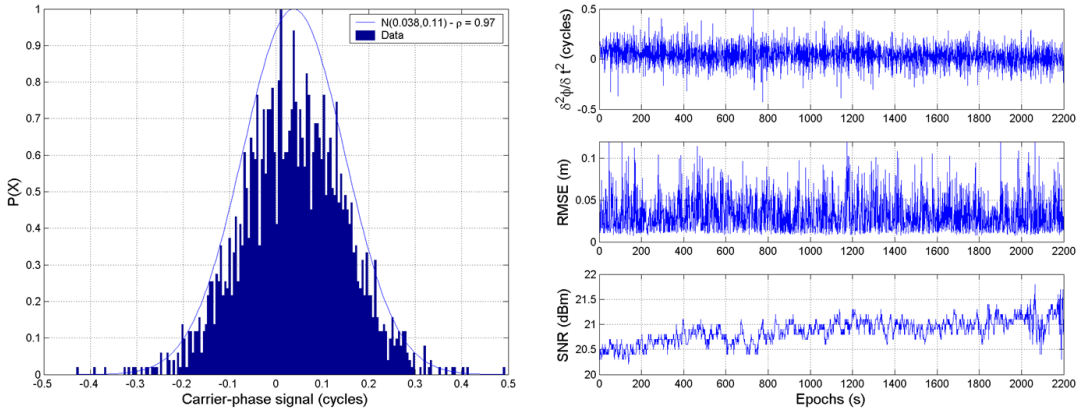


Figure 7.10: Distribution of the carrier-phase measurements (left)and the LOCATA signal (right) for the experiments $[05-04-07]$ (transmitter 1).

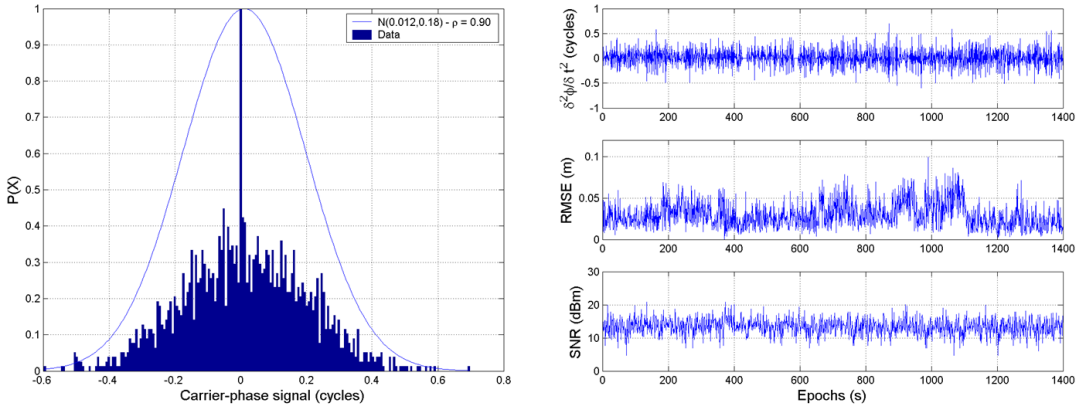


Figure 7.11: Distribution of the carrier-phase measurements (left)and the LOCATA signal (right) for the experiments $[15-08-07]$ (transmitter 8).

(ρ) is also given in the legend. When looking at the correlation coefficient values in the

Tables (7.4) and (7.5), the low values (e.g. 0.56) mean that the Normal distribution does not seem to fit the data all the time. Figure 7.11 shows that when there are a large number of zero values in the double difference of the carrier-phase measurements, the data may not be Normally distributed. Thus, what does a large number of zero values mean? The first explanation comes if the given LocataLite fails to synchronise with the network. Then, no carrier-phase measurement is calculated by the rover. In the same way, it occurs if the LocataLite is powered off by a battery failure or a manipulation mistake. These issues may be detected by checking the SNR value for each epoch. If the SNR value is also zero, it confirms either the battery failure hypothesis or the problem of synchronisation.

It is also interesting to underline that in Table (7.5) the tail of the distribution is slightly bigger for the transceivers on the roof. For example, the tail of the Normal distribution of transceiver 6 is from $[-0.8, 0.7]$ cycles, whereas the tail of the data from transceivers 1 is between $[-0.4, 0.4]$. But this result is also linked to the surrounding of the transmitters. For example, in the same table, transmitter 15 also has a long distribution tail ($[-0.8, 0.4]$ cycles), which may come from the foliage above it and may be a source of fading effect.

The results from Table (D.4) support what was previously explained. Note that transmitters $9, 10$ have a small data tail compared with $7, 8$ even considering that from the test point of view (Mid) all those transmitting antennas are in fading areas due to foliage. In addition, LocataLite $15, 16$ should be discarded in this study, because the number of SNR values equal to zero is big. After a check with the LocataLite set up file, the LocataLite was not working properly due to a battery failure.

Thus, the tail of a distribution helps to see if the transmitter is in a fading area, but generally the signal reflection due to foliage is also correlated with the other surrounding scatterers (e.g. edge, wall, rock).

7.3.2 Another Approach to the Wi-Fi Interference

The carrier-phase measurements are extracted from the rover LOG file. This file was previously described in Figure 5.14. From the previous experiments in the previous section, Table (D.3) shows another kind of information behind the foliage effect. Focusing on the column ($\frac{\delta^2}{dt^2}\phi_i$ or $SNR = 0$), for every LocataLite the numbers are not close to zero compared with the time series (1355 epochs). When $SNR = 0$ during a couple of epochs, it means that there was a problem of synchronisation. In addition, if $\frac{\delta^2}{dt^2}\phi_i$ is equal to zero, then it means during a couple of epochs the carrier-phase measurements were equal. In other words, the receiver failed to calculate the carrier-phase measurements during these epochs. This may be another effect of the Wi-Fi interference on the LOCATA signal.
Let us focus on the scenario $[22-08-07]$ at point $ROV01$ with the accuracy exposed in Table (D.1). Let us focus on the LocataLite number 4, where in column ($\frac{\delta^2}{dt^2}\phi_i$ or $SNR = 0$) the number of zeros either on the carrier-phase measurement or the SNR is high.
Figure 7.12 is the LOCATA signal from the LocataLite number 4. The LocataLite number 4 shows a SNR pattern with some values equal to zero. This pattern is typical of a LOCATA signal degraded by the Wi-Fi interference, causing some short time failures in the synchronisation of a slave and the master.

Now if we come back to the experiment $[15-08-07-Mid]$. During the previous analysis performed in Section 7.2 and Figure 7.4 , it was shown that the degradation of the LOCATA accuracy was due to the addition of small jumps over the time. It was then demonstrated that these jumps were produced by the increase of the noise in the AGC. Looking now at the double difference of the carrier-phase measurements in Table (7.7) and comparing with Table (7.4), there is not a high number of zero values. Nevertheless, the values in the columns $0.1 < x < 1$ and $x > 0.3$ are higher than in the previous experiments. Even though the LINE navigation software may repair cycle slips greater than 0.333 cycles, the smaller jumps may be the results of undetected cycle slips ($0.1 < x < 1$). Adding those two results together, it means that the Wi-Fi interference induces a miscalculation of the carrier-phase measurements. The

$22-08-07$ $Rov01$	Loc	R. $0.1 < x < 1$	R. $x > 0.3$	$\frac{\delta^2}{dt^2}\phi_i$ or SNR $= 0$	Comments
	1	212	3	15/0	$\rho = 0.94$ — t=[-0.3,0.4]
	2	212	6	0/0	$\rho = 0.94$ — t=[-0.5,0.5]
	3	265	70	0/37	$\rho = 0.96$ — t=[-1.5,1.5]
	4	255	112	21/84	$\rho = 0.93$ — t=[-2,2]
	5	261	147	0/32	$\rho = 0.97$ — t=[-2,2]
	6	246	185	0/66	$\rho = 0.91$ — t=[-2,2]
	7	285	106	0/12	$\rho = 0.95$ — t=[-1,1]
	8	277	108	0/2	$\rho = 0.96$ — t=[-1.5,1.5]
	9	264	46	0/2	$\rho = 0.93$ — t=[-0.8,0.8]
	10	265	26	0/0	$\rho = 0.90$ — t=[-0.4,0.6]
	11	260	96	0/22	$\rho = 0.79$ — t=[-4,4]
	12	259	86	0/35	$\rho = 0.80$ — t=[-4,4]
	13	272	38	0/0	$\rho = 0.90$ — t=[-0.4,0.6]
	14	282	32	0/0	$\rho = 0.90$ — t=[-0.6,0.6]

Table 7.6: Characteristics of the LOCATA signal [$t = 1952$].

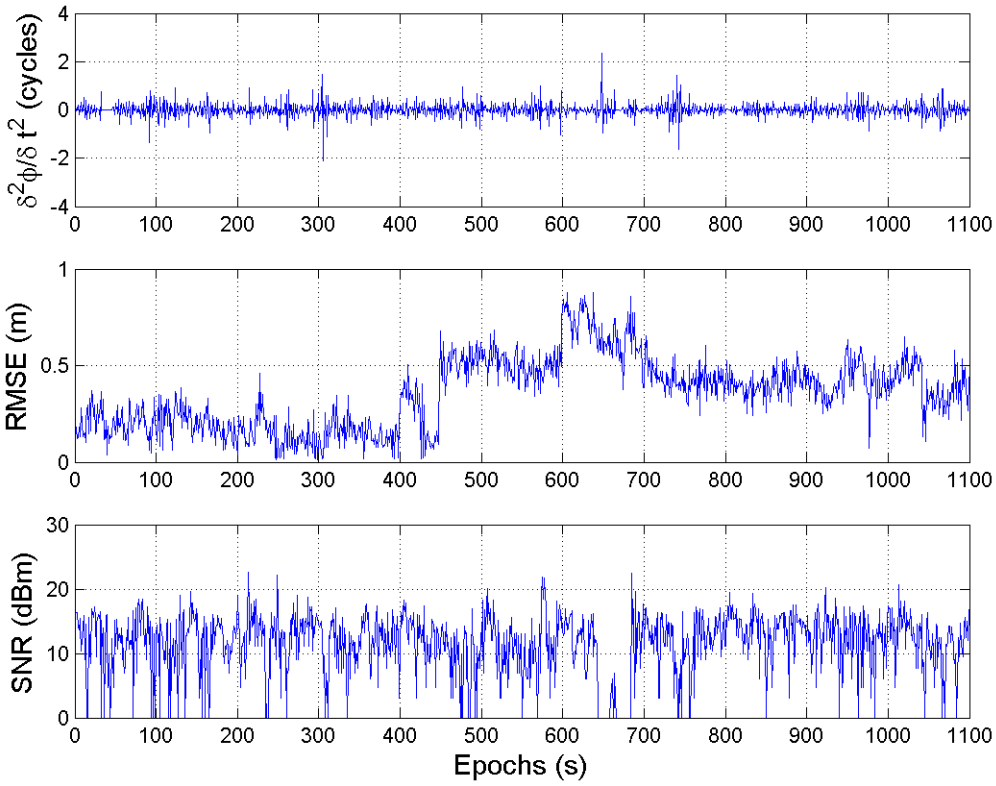


Figure 7.12: LOCATA signal from LocataLite number 4 ($22-08-07$).

$15-08-07$ Mid	Loc	R. $0.1 < x < 1$	R. $x > 0.3$	$\frac{\delta^2}{dt^2}\phi_i$ or SNR $= 0$	Comments
	1	935	21	8/0	$\rho = 0.96$ — t=[-0.3,0.3]
	2	989	72	8/0	$\rho = 0.98$ — t=[-1,1]
	3	968	51	50/0	$\rho = 0.98$ — t=[-1,1]
	4	1261	144	51/0	$\rho = 0.98$ — t=[-1,1]
	5	1226	161	5/0	$\rho = 0.98$ — t=[-1,1]
	6	1355	455	3/140	$\rho = 0.78$ — t=[-4,4]
	7	1484	422	6/16	$\rho = 0.66$ — t=[-15,10]
	8	1551	518	12/244	$\rho = 0.90$ — t=[-5,5]
	9	1498	416	7/67	$\rho = 0.75$ — t=[-10,10]
	10	1433	358	4/10	$\rho = 0.93$ — t=[-10,10]
	11	1397	268	4/0	$\rho = 0.85$ — t=[-10,10]
	12	1356	236	1/0	$\rho = 0.98$ — t=[-1,2]
	13	1278	154	7/2	$\rho = 0.98$ — t=[-1,1]
	14	1287	151	7/25	$\rho = 0.87$ — t=[-10,6]
	15	1305	196	5/0	$\rho = 0.98$ — t=[-5,4]
	16	1324	242	5/0	$\rho = 0.94$ — t=[-5,4]

Table 7.7: Characteristics of the LOCATA signal [$t = 4400$].

more the noise level increases in the AGC, the more the error in the carrier-phase measurement increases.
Nevertheless, as LINE uses the last navigation solution to recalculate the float ambiguities after detecting a cycle slip, the repetition of the cycle slips may make the solution diverge over time. Even though the robustness of the LINE software should take this error into account, this is the result of the jumps over time (e.g. Figure 7.4).

7.3.3 Comments on the SNR

In Section 5.5.2, the basic definitions concerning SNR were explained. Here are some comments from the analysis of the various experiments.
As the SNR values in the LOG file are the post-correlated data, or the correlation between the fading from the surrounding of the transmitter-receiver and the noise of the receiver, it is hard to see from the SNR values the influence of the environment. This was already demonstrated in Section 5.5.2.
Figure 7.13 compares the SNR threshold among several LocataLites for different experiments and Table (7.8) shows the mean (μ) and standard deviation (StD) of the SNR for the 16 transmitters used in the reference experiments.

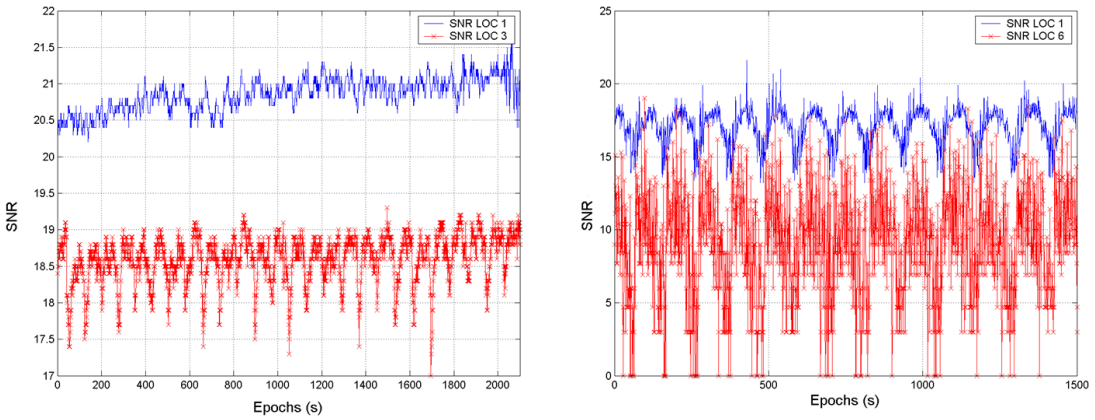


Figure 7.13: Signal-to-Noise-Ratio for different LocataLites at $[5-04-07]$ (left) and $[15-08-07-Mid]$ (right).

The first comment regarding the values in the table is that the SNR threshold is higher in the experiment $[05-04-07]$ than in the other scenario. As a reminder, $[05-04-07]$ is the reference test, because not much Wi-Fi was observed during the measurements. In addition, the size of the two networks were close. This supports that the post-correlated SNR values are the difference between the noise of the rover and the transmitted LOCATA signal, rather than the fading effect in the vicinity of the receiver-transmitter.

Regarding the kinematic experiments, it has previously been demonstrated that while moving with the rover, some cycle slips appear on the carrier-phase measurements. Figure 7.14 shows the SNR of the experiments $[30-08-07]$. The experiment starts at *Tree* and the rover moves to *Mid*, and then it comes back to the initial point. In the appendices, the track followed by the rover is shown in Figure D.7. It means that the AGC needs some time to receive the signal and process it (e.g. removing pathloss) before the rover is able to calculate precisely the carrier-phase measurements (ambiguity resolution). Thus, it follows that some cycle slips were recorded while the rover was moving. Figure 7.15 shows the double difference of the carrier-phase measurement during the kinematic test for LocataLite 1 (left) and 6 (right). It is clearly seen that there are formations of large peaks as soon as the rover moves (in both direction) for the two LocataLites carrier-phase measurements. However, there

SNR	Loc	$[05-04$ μ	$-07]$ StD	$[15-08$ μ	$-07]$Mid StD
	1	20.86	0.23	17.13	1.24
	2	21.81	0.31	16.28	1.21
	3	18.59	0.34	15.04	2.65
	4	17.54	0.29	14.18	2.24
	5	19.19	0.39	12.18	3
	6	19.7	1.01	9.22	3.77
	7	19.7	0.30	13	3.66
	8	19.21	0.24	11.88	5.07
	9	21	0.36	12.55	3.75
	10	19.65	0.32	12.60	3.14
	11	17.11	0.24	11.69	2.67
	12	16.73	0.22	12.82	2.44
	13	20.29	0.32	14.88	3.19
	14	18.17	0.44	13.81	3.65
	15	20.52	0.29	13.71	2.66
	16	16.86	0.95	11.60	2.7

Table 7.8: Signal-to-Noise-Ratio values for various experiments.

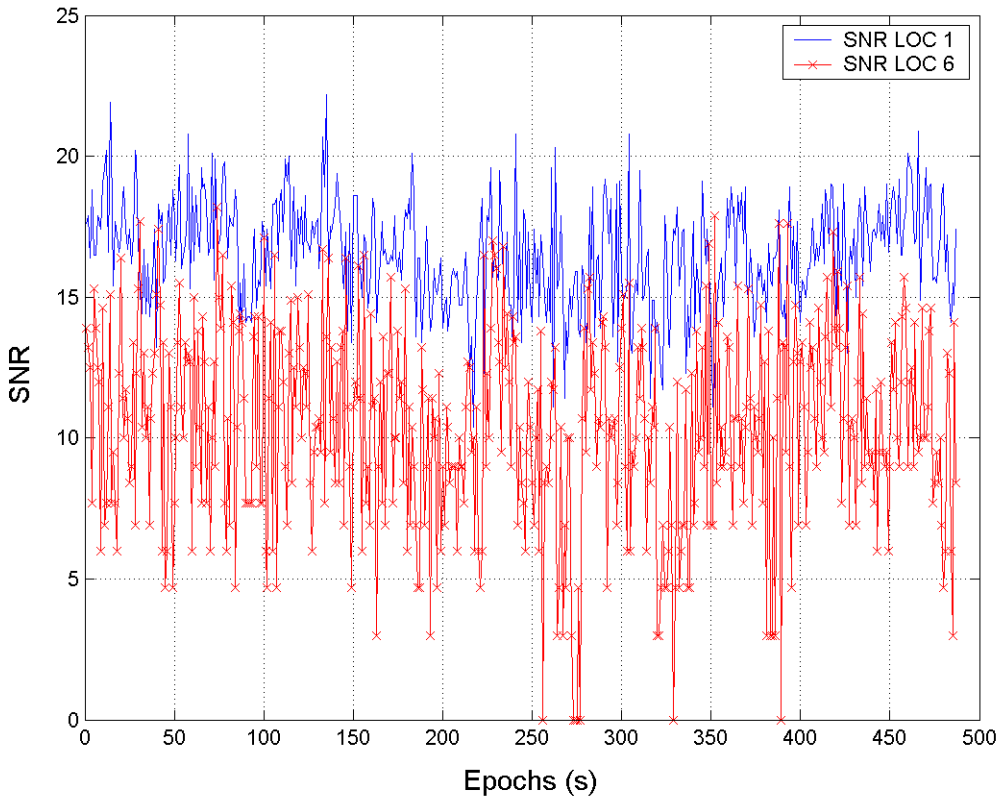


Figure 7.14: Signal-to-Noise-Ratio for different LocataLites at $[30-08-07]$ during a kinematic experiment.

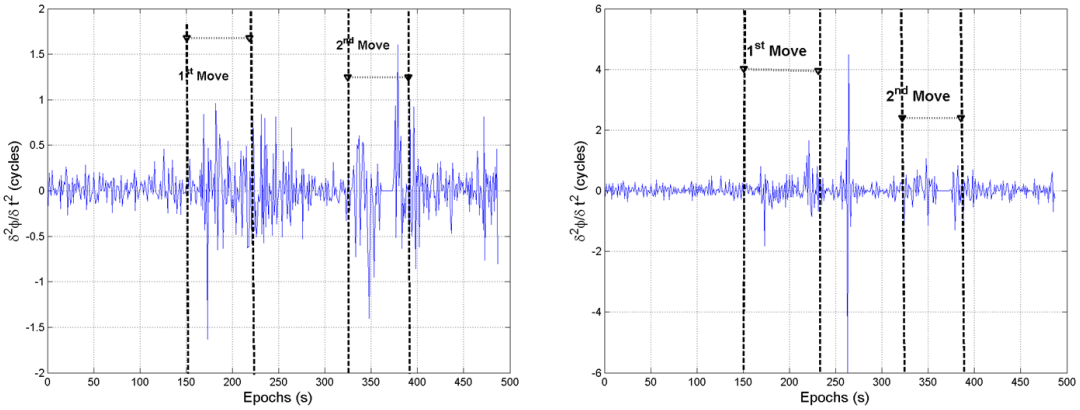


Figure 7.15: Delta carrier-phase measurements for the LocataLites 1 (left) and 6 (right) during the kinematic test $[30-08-07]$.

are also spikes when the rover is stationary for a few minutes and thus that may be due to the Wi-Fi interferences. It is also underlined in those figures that it takes time for the rover's software (LINE) to recover after a move. These results converge to the results obtained with another LOCATA setup in the study of the kinematic rover in Chapter 6.

7.4 Real Time Kinematic GPS and LOCATA Technology

In Section 7.2, the testbed of the experiments was described. The focus of this part is the comparison of Real Time Kinematic GPS and LOCATA technologies. The RTK GPS measurements were carried out using a $GPS\ LEICA\ 500\ dual\ frequency$, monitoring the same test points in the area. The data were post-processed using the software $LEICA\ GEO-Office$ Version 1.1.0.0 released 2004. The first part deals with the concepts of relative and absolute positioning. Then the results are explained.

7.4.1 Absolute and Relative Positioning

Preliminary to the comparison, it is required to measure accurately the test points. The results already shown earlier in this chapter and in the previous ones are obtained using a relative positioning. Let us define what the absolute and relative position are. An absolute position is obtained using beacons, landmarks or satellite based systems, whereas a relative localisation is evaluated from the position, orientation, angles or ranging techniques (e.g. Time-Difference-of-Arrival, laser) as it is performed in a total station and in LOCATA technology [Goel et al. (1999)]. In other words, a relative position is calculated in a coordinate system which can be qualified as local one (e.g. ENU).

In Section 5.4, it was explained how to monitor precisely the antennas of the LocataLites using a total station [Lavine et al. (2003)]. A total station is an accurate tool that provides a precision down to the millimetre level. But this accuracy is relative to the accuracy of the two points necessary for the initialisation (reference and back sight points). In other words to achieve millimetre accuracy of any points measured with a total station, the reference points have to be measured very accurately. Following [Taha et al. (2006)] and [Montillet et al. (2007b)], the authors demonstrated the discontinuity of the GPS phase solutions around the test area due to satellite availability and multipath. Thus two solutions are identified: surveying for a few hours the various test points and LocataNet, or using a novel technique called the

Continuous UPdate Technique developed by Mr A. Taha [Taha (2007)]. As this work is motivated by research, the second choice was used.

The first step is to measure a couple of very precise points around the area and the setup of the total station [Montillet et al. (2007b)]. Then, Mr J.P. Montillet and Mr C. Hancock have conducted multiple measurements of both the LOCATA antennas and the test points. The purpose of the CUPT technique is to combine multiple

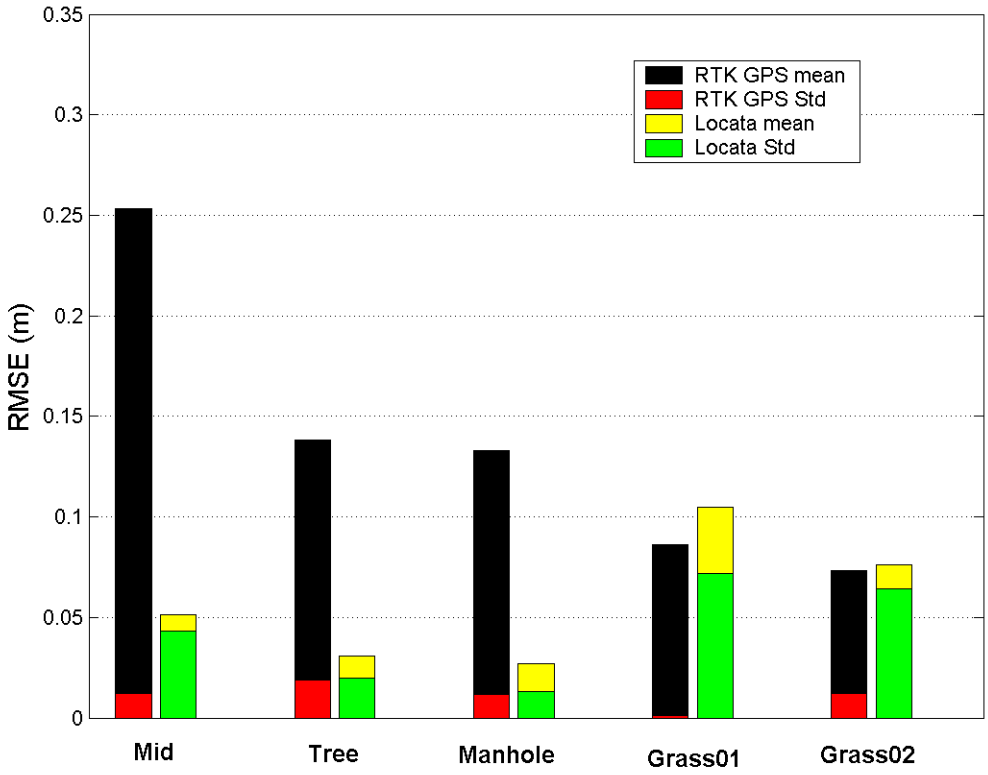


Figure 7.16: A comparison between the RMSE of the LOCATA and RTK GPS technologies.

measurements of same point using various geometrical setups of the total station. The very precise coordinates of the monitored points are then extracted using the software of the CUPT technique coded by Mr Taha [Taha (2007)]. In the appendices, Figure D.5 shows the output of Taha's software in terms of absolute accuracy of the network (in millimetres) and ellipse error. The readers interested in the details of this novel technique may refer to [Taha (2007)].

7.4.2 Results

Once the test point coordinates are evaluated, the users then start successively the survey using On-The-Fly kinematic GPS and LOCATA technologies. The baseline between the reference station and the RTK GPS rover antenna is approximately two hundred metres and the type of GPS receiver was a *Leica Geosystems* dual frequency 500. In Figure 7.1, the reference station is outside of the frame of the picture, but not far from the top left corner. During the experiments with the On-The-Fly kinematic GPS, an important parameter is the time spent to monitor each point. As it is a difficult area, a time period less than 15 minutes is not enough to get comparable results with the LOCATA accuracy. Nevertheless, a longer time is not realistic in

		Mid	Tree	Hole	Grass01	Grass02
LOCATA	μ	0.05	0.02	0.017	0.11	0.08
	StD	0.04	0.01	0.009	0.08	0.07
RTK GPS	μ	0.253	0.138	0.133	0.086	0.073
	StD	0.012	0.018	0.012	0.001	0.015

Table 7.9: Accuracy of LOCATA and RTK GPS technologies averaged on the three coordinates.

terms of process efficiency. 15 minutes represent approximately 900 epochs. Thus, the LOCATA accuracy is averaged on the same number of epochs.

Figure 7.16 shows the bar chart of the accuracy of the two technologies for each test point in the field. The accuracy is displayed in Root Mean Square Error calculated on the three coordinates. The first information is the high standard deviation of the LOCATA accuracy (yellow) compared with the mean error (green). When looking at the previous results (i.e. static tests in Chapter 6), the high standard deviation of the RMSE is due to the high standard deviation of the Height coordinate. It is also important to underline that generally in the same static scenarios the standard deviations of the East and North coordinates are much smaller (e.g. millimetres compared to the centimetres in the standard deviation of the Height). In the case of possible Wi-Fi interferences, Tables (7.3) and (D.1) show that the standard deviations in the East and North coordinates are sometimes higher than the mean values. This

is a consequence of the jumps in the time series of the rover's location.

The overall results show that RTK GPS and LOCATA are two comparable technologies. This result can be explained with the number of LocataLites in direct Line-of-Sight with the rover antenna. For those points in the middle of the test area, at least five base stations on the ground and two antennas on the roof (one LocataLite) cover them . When moving from Mid to $Grass01$, the rover loses the LoS with one LocataLite on the ground and the foliage fades the antennas on the roof. As a result, the LOCATA accuracy degrades when the rover moves to the right hand-side of the field.

Moreover, the reader may ask why the RTK GPS technology does not achieve the centimetre level accuracy in the middle of the field in Figure 7.16. This result was previously investigated in [Taha et al. (2006)] in the same testbed. From the measurements, the main problem is the satellite geometry has a Position Dilution of Precision value of 4. The position of the RTK GPS receiver was averaged using carrier-phase measurements with float ambiguities. Thus, it was required to stay more than 20 minutes to achieve the centimetre level of accuracy and then fixing the ambiguity values as integer numbers. Note that the results may be improved by averaging the measurements at different periods of a day. However, this comes back to the fundamental problem of this work, the main challenge of precise positioning in an urban canyons and the efficiency of monitoring accurately a point in dense multipath area. To conclude this comparison study, Table (7.9) shows the results of the two technologies averaged in the plane component.

7.5 Summary

This chapter mainly focuses on the Wi-Fi interference effects on the LOCATA signal through experiments using the latest LOCATA firmware (March 2007). Thus, a dedicated network was installed through the summer 2007 at the University of Nottingham, to deal with this issue and many data were recorded in various experiments. The results show how complex is this phenomenon, because the interference is a function of many parameters (e.g. the Wi-Fi access point location, data throughput

during the measurements, transmitted power of the LOCATA transceivers) through the study of the accuracy of the rover's coordinates. In a separated section, statistics are extracted on the LOCATA carrier-phase measurements perhaps corrupted by Wi-Fi interference. This shows the increase of cycle slips on the LOCATA carrier-phase measurements.
To summarise, it was shown in presence of Wi-Fi transmitters that the level of noise in the AGC may increase. The direct result is that the LOCATA observables may be less accurate. Then, in presence of strong Wi-Fi signal, the LINE software may detect repetitive cycle slips which may make the time series of the rover's coordinates diverge.

On the other hand, the LOCATA signal received from each LocataLite is analysed closely by double differencing the carrier-phase measurements. A part focuses on the signal blocked by foliage/trees. Through the study, it shows that the obstruction adds cycle slips in the carrier-phase measurements. Some statistics and Normal distribution fitting tests are applied to the data in order to see if any remarks may be made on the vicinity of the receiver-transmitter. The length of the Normal distribution tail gives some interesting results on whether the transmitter is in a fading area or its signal is corrupted by interferences.
Furthermore, the value and shape of the SNR is discussed through the scenarios with and without Wi-Fi interference. It completes the preliminary study done at the end of Chapter 5. In addition, the interferences may also be detected while monitoring this parameter. The interference also affects the synchronisation between the LocataLites and the rover, which sometimes ends up with no measurements (or SNR $= 0$) during a very short time (few epochs).
Finally, a study to compare RTK GPS and LOCATA technology was done in the urban canyon scenario defined at the beginning of this Chapter. The two technologies have close accuracy with sometimes one better than the other.

Chapter 8

LOCATA Technology: Further Tests

8.1 Preamble

This chapter starts with an overview of software developed by the author of this thesis for a better understanding of how LINE (embedded in the LOCATA firmware) triangulates the rover's position. As a reminder of Chapter 1, there was no industrial disclosure signed between the IESSG and *LOCATA Corp.* Thus, it was decided to code a navigation software to better understand it. Following two sections are then dedicated to some experiments when deploying a LocataNet in a work site, which shows the application of this new technology in a type of environment defined in the VISTA project (i.e. [Research (2005)]), and indoors.
The last section is focused on some simulations to study the future integration of a Global Navigation Satellite System and the LOCATA technology. A summary of the results ends this chapter.

8.2 The In-House Software

8.2.1 Block Diagram

The presented software has an architecture similar to that of the LINE software explained in Section 6.2.1. The input files are the measurements in the LOG file registered by the LOCATA rover during the experiments (see Section 5.4.2), and the precise coordinates of each LocataLite synchronised in the LocataNet (file called xyz_coor;). In addition the second file needs to contain the rover initialisation point. All those points should be preliminarily converted to the ENU referential. The block diagram of the software is shown in Figure 8.1.
The first loop extracts the measurements (carrier-phase in cycles and pseudorange in metres) for each LocataLite, the corresponding SNR and epochs (in seconds) and also a synchronisation number called *tracking state field* explained in Section 5.4.2. As a reminder, if this number is up to 90, it means the given LocataLite is correctly synchronised with the master. The generic function extracting the data epoch-by-epoch for each LocataLite is called *ReadData*.
Then, another function is used to select the valid LocataLites (the function *SelectLocatalites*

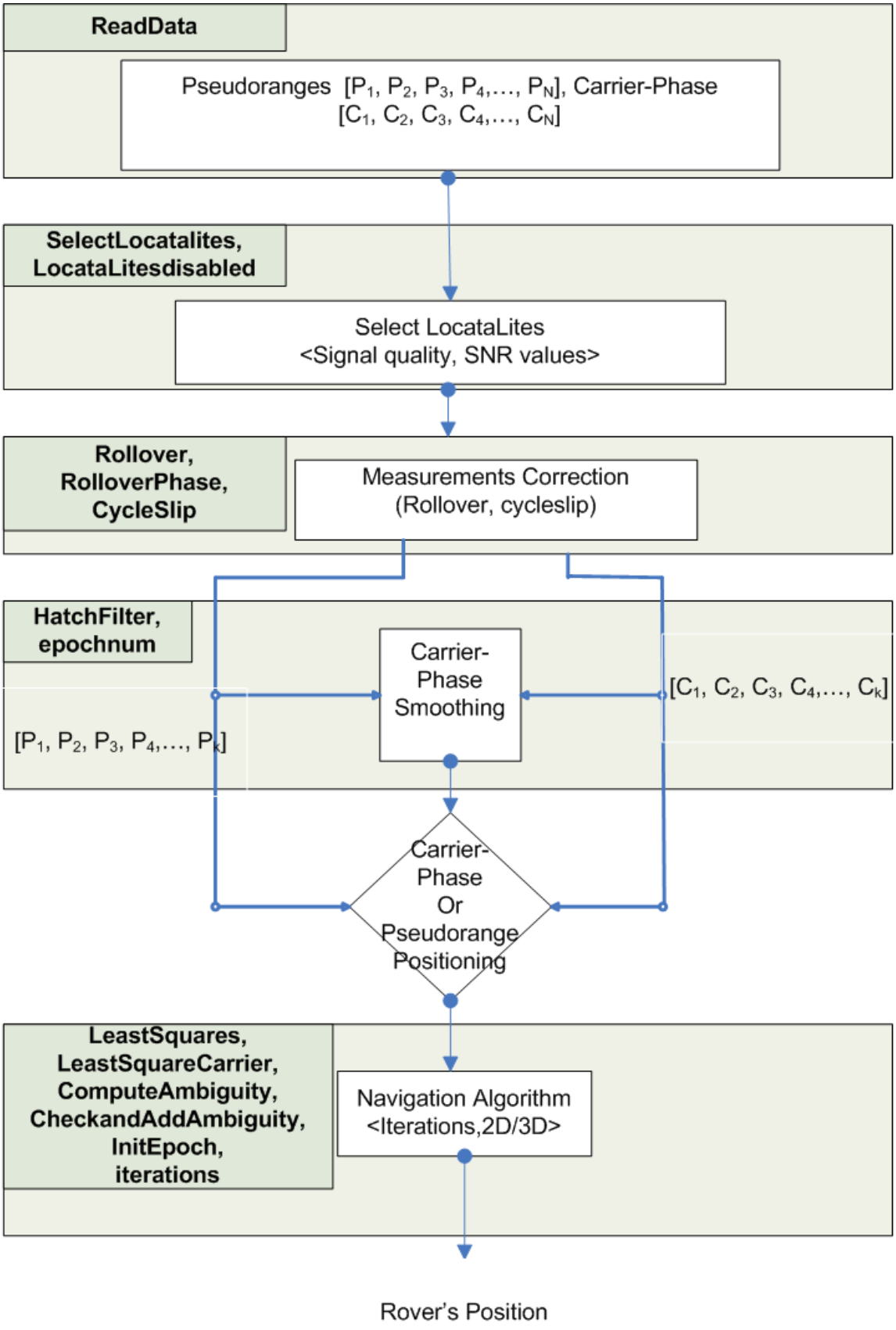


Figure 8.1: Block diagram of the in-house software.

returns an integer value) depending on some criteria: if the value of the SNR is up to a threshold (zero as default) and if the carrier-phase measurements or pseudoranges are not null for the given epoch. If the number of LocataLites is up to a certain threshold (4 is the default value), a flag is set equal to 1 to go further. An option is available in the case that the user wants to disable some LocataLites in the triangulation of the receiver's position (function *LocataLitesdisabled* returns an array of integer values). The remainder of the software varies if the user wants to triangulate the position of the rover using pseudoranges or carrier-phase measurements. Thus, let us differentiate each case study: pseudorange, carrier-phase measurements and navigation algorithm.

- Pseudorange: The first step is to check if there are no rollovers (function *rollover*). The rollover occurs when the pseudorange value exceeds a certain threshold which is the limits of the rover's memory ($+/-$ 29979.248 metres). This was explained in Section 6.2.1. This function detects the rollover for each LocataLite by comparing the pseudorange value at a given epoch and at the previous epoch. The function is also able to repair the rollover when detected. The rollover reparation is simply adding this memory limit number. Note that in the case of the value at the previous epoch is equal to zero, the software does not understand it as a rollover. This may occur either when the rover starts to output the measurement values or when the measurements are reset (see Section 5.4.2).

  Before the triangulation of the rover's coordinates, the user may also choose to smooth the pseudoranges with the carrier-phase measurements. This is carried out by using a Hatch filter as described in Section 6.2.1 (see Equation (6.3)). In the Hatch filter (function $HatchFilter$), the carrier-phase measurements are not corrected by the ambiguities, because the filter needs, as input, the carrier-phase measurements of the given and previous epochs. There is a parameter (*epochnum*) which means the maximum consecutive epochs that a Hatch filter can use to smooth the pseudorange. If the number of epoch is exceeded, the Hatch filter selects the carrier-phase measurements for the smoothing process as done in a sliding window process. In other words, the right number of measurements is selected by shifting the measurements [Feigenbaum et al. (2004)]. The

default parameter is 40 epochs. However, if a cycle slip is detected in the carrier-phase value, the Hatch filter is reset. It means that the filter restarts to the epoch where the cycle is detected and no previous carrier-phase measurements are taken into account to smooth the pseudoranges. As a reminder, the Hatch filter uses the carrier-phase measurements in a difference epoch-by-epoch which cancelled out the ambiguities for each LocataLite.

- Carrier-phase measurement: The carrier-phase measurements are also corrected for the possible rollover epoch-by-epoch for each LocataLite in an identical way to the pseudoranges (function *rolloverPhase*). The memory limitation for the carrier-phase measurements is equal to 250000 cycles (see Section 6.2.1). In addition, for each LocataLite selected, the software looks for any cycle slip. The cycle slips are detected via the function *CycleSlip*. The function calculates first the double difference (see Equation (3.3)) of the carrier-phase measurements and the result is compared to a threshold. The default value is 0.3 cycles, but the user can change it in the parameter inside the function *CycleSlip*. When a cycle slip is detected, the ambiguity value is recalculated using the previous rover's position solution. The cycle slip is NOT repaired in this software and only the ambiguity value is reset for this LocataLite.

  How does the software calculate the ambiguity value for each LocataLite? For a given LocataLite, this number is calculated taking into account that the rover is initialised on a known point (known coordinates) for a few epochs. The ambiguities are then calculated using the function *ComputeAmbiguity* based on the following equation:

$$N_L^j(t) \;=\; \lambda_L \times \phi_L^j(t) - \rho_L^j - c \times \delta t_{sy-L}^j \tag{8.1}$$

  where N_L^j is the ambiguity of the j-th LOCATA transceiver; λ_L is the wavelength of the LOCATA signal; ϕ_L^j is the carrier-phase measurement of the j-th LOCATA transceiver; ρ_L^j is the true distance rover to j-th transmitter; and δt_{sy-L}^j is the clock drift of the rover estimated in the least-squares process. Then, the ambiguity value is averaged on number of epochs, a parameter chosen by the user (see the variable *InitEpoch*). The default value is 50. The ambiguity value is a

float value and it remains constant till a cycle slip is detected. Once the carrier-phase measurements are corrected of any rollovers, cycle slips and ambiguity values, they can then be used to triangulate the rover's position. However, the ambiguities are checked at each epoch in case of new LocataLites synchronise or whether due to disruptions (e.g. manipulation error, fading) some LocataLites (re)synchronise with the LocataNet. This is taken into account via the function *CheckandAddAmbiguity*. Note that in the Equation (8.1), the carrier-phase measurements are not corrected of any tropospheric delay. It was decided that taking into account the small size of the LocataNet installed to carry out the measurements, the error introduced by the tropospheric delay may be negligible (see [Leick (2004)] for a definition of the tropospheric delay).

- Navigation algorithm: The code of the navigation algorithm is based on the equations developed in Section 3.3.2. It uses the general least-squares formula. However, the difference is that we do not need to correct the pseudoranges and the carrier-phase measurements with the LocataLites' clock offset, because of the very precise network synchronisation (see Section 5.2.4).
  The triangulation of the rover's position with the pseudoranges (function *LeastSquares*) requires only the pseudoranges (corrected of any rollovers and/or smoothed by carrier-phase measurements) and the accurate position of the LocataLites (written in the second input file xyz_coor;). In Section 7.4, we explained that the LocataLites' position were measured using either a total station or via RTK GPS to get an accuracy of the order of magnitude of the centimetre level. In addition, the coordinates (in ENU referential) of the initialisation point are required to start the least-squares iterations. That is the same process used in the LINE software (see input parameters in the rover setup file in Section 5.3). The parameter *iterations* means the number of iterations that the least-squares algorithm does to compute the final rover's coordinates. 6 iterations is the default value used in many GPS software [Strang and Borre (1997)].
  It is approximately the same method to triangulate the position of the rover using the carrier-phase measurements (function *LeastSquareCarrier*). The

difference is that the carrier-phase measurements have to be corrected for any rollovers, cycle slips and (float) ambiguities before inserting them in the matrix of the least-squares process.

8.2.2 Results

This section presents the results obtained using the in-house software to post-process the measurements (i.e. LOG file) and to triangulate the rover's position. The software is tested only through static scenarios. As previously said, the development of this software should be seen as a way to validate the many hypotheses on how the LINE commercial software works. Thus, it was decided that the results are analysed in three scenarios: $[22-02-07]$, $[05-04-07]$ and $[28-03-07]$. The results are directly compared with the ones shown in Chapter 6 output by the LINE software. The results shown in Table (8.1) are the RMSE and the error in each coordinate using pseudoranges, smoothed pseudoranges with a Hatch filter and using only carrier-phase measurements.

RMSE (m)	DOWNS	G.G.L 2	Parking
	$05-04-07$	$28-03-07$	$22-02-07$
LocataLites	8	7	5
HDOP/VDOP	0.79/9.39	0.79/1.28	1.91/10.95
Epochs	500	500	500
μ	3.317/3.107/0.054	5.804/5.80/0.163	2.126/2.106/0.007
StD	1.262/0.783/0.004	0.144/0.124/0.003	0.317/0.152/0.005
μ_E	2.251/2.053/0.031	0.822/0.823/0.066	1.119/1.116/0.004
StD_E	0.690/0.450/0.006	0.137/0.083/0.002	0.333/0.173/0.004
μ_N	1.693/1.433/0.036	5.734/5.73/0.142	1.565/1.578/0.003
StD_N	1.024/0.756/0.004	0.146/0.125/0.002	0.269/0.092/0.002
μ_H	1.681/1.587/0.023	0.516/0.516/0.047	0.821/0.817/0.003
StD_H	0.513/0.314/0.004	0.104/0.063/0.002	0.252/0.130/0.003

Table 8.1: Position and coordinates accuracy in metres of the rover using pseudoranges without Hatch filter / with Hatch filter [50 *epochs*] / and only carrier-phase measurements.

Note that the Hatch filter was explained in Section 6.2.1 and only 50 epochs are used to smooth the pseudoranges. The accuracy is averaged on 500 epochs, because the in-house software is coded in the Matlab language and the performing time to process the LOG files is fairly high. For example, it may take more than one hour to process a LOG file of more than 10 mega bytes.

The results confirm the general conclusions while studying the static experiments: the pseudoranges perform worse than the pseudoranges smoothed and the carrier-phase measurements when triangulating the rover's position. Secondly, the pseudoranges smoothed improve the standard deviation of the time series of the coordinates, but the mean accuracy remains approximately the same value as with the pseudoranges. It is interesting to underline that the results from the in-house software are more accurate for the Parking scenario than the Downs. When comparing these results with the ones exposed in Tables (6.1), (6.2) and (6.3), the overall comment is that they are comparable in terms of RMSE. For example, the RMSE is equal to 3.317 m using the in-house software and 3.110 m using LINE in the $[05-04-07]$ scenario. The difference of accuracy may be explained, because of the lack of routines to switch between the 2D and 3D mode of triangulation (see explanations in Section 6.2.1). In other words, the in-house software forces the triangulation in 3D without any regards to the DOP value. The proof of this result is given when looking at the error on each coordinate: while positioning the rover with the carrier-phase measurements the mean error is 0.0039 m with LINE and 0.031 m with the in-house software in the $[05-04-07]$ experiment.
Taking into account the error for all types of measurements (pseudoranges, smoothed pseudoranges and carrier-phase), it shows that the accuracy of the in-house software in $[05-04-07]$ is closer to what LINE output with the same LOG file; in $[22-02-07]$ the in-house software performs better than LINE; and in $[28-03-07]$ the results are worse than expected (especially with the carrier-phase measurements). The distance between the two software in the $[28-03-07]$ experiment may be explained by the sensitivity of our software to the strong interferences described comprehensively in Chapter 7. Figure 8.2 shows the time series of the accuracy of the rover's coordinates

for the $[05-04-07]$ scenario.

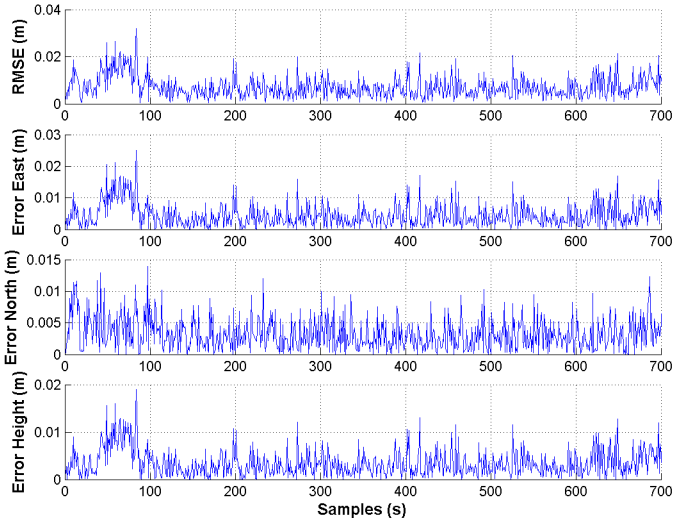


Figure 8.2: Rover's position error output by the in-house software using carrier-phase measurements $[05-04-07]$.

To conclude, the performance of the in-house software in static scenario is comparable to LINE. However, implementation of complex techniques such as the LAMBDA method may improve the accuracy. That is planned as a future work beyond this thesis.

8.3 Test Trial of the LOCATA Technology for the VISTA Project

During February 2008, the author together with Mr C. Hancock and Mr H. De Ligt installed a network of five LOCATA transceivers in a construction site to test this technology in the conditions defined in the VISTA project proposal [Research (2005)]. Figure 8.3 shows the testbed of the measurements. The goal of this work is to map the buried asset (gray pipe on the left picture of Figure 8.3) within the same conditions as it would be during streetworks, taking into account the limited space available to set up the network of transceivers. In this section, all the results were pocessed using the LINE software (not the software developed by the author of this thesis).

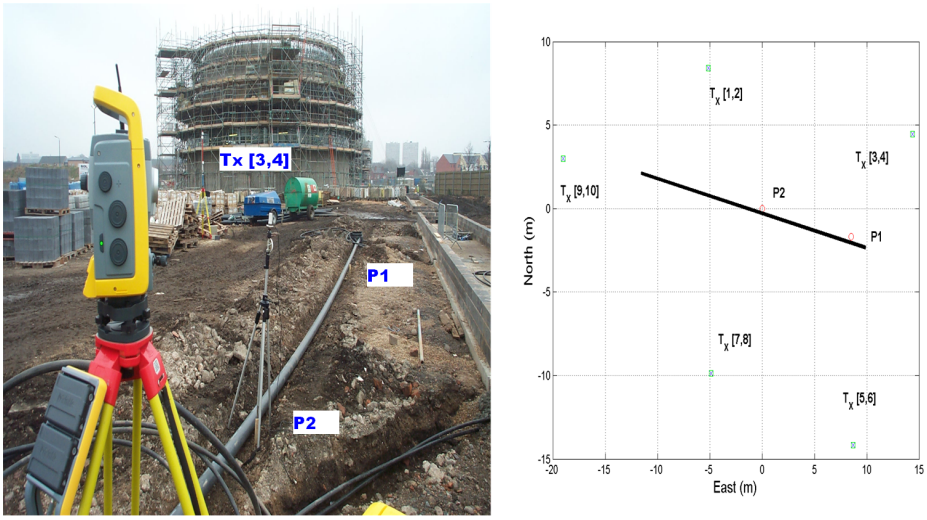


Figure 8.3: The buried asset in the construction site (left) and the scheme of the LocataNet.

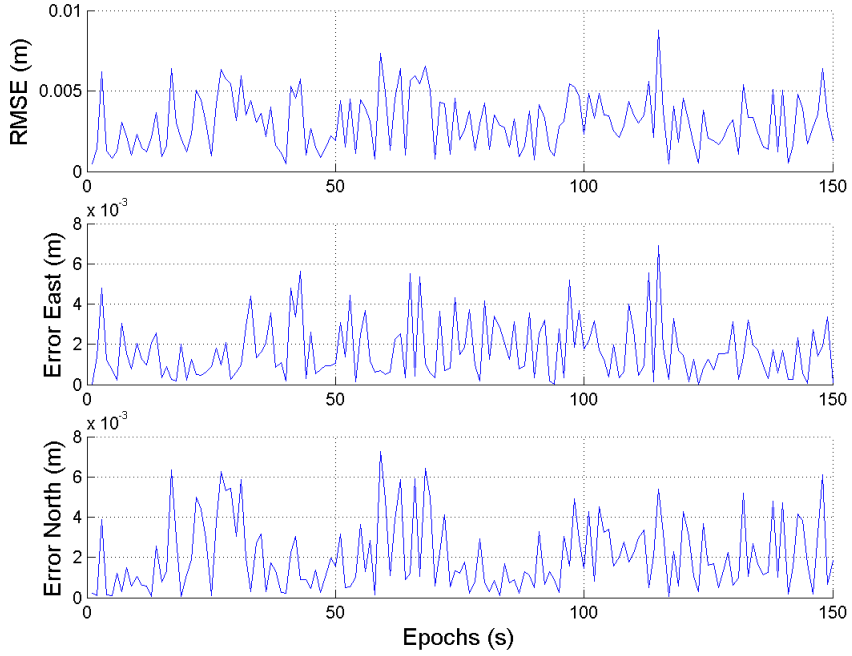


Figure 8.4: Time series of the rover's position error during thes trial $[14-02-08]$.

Note that the asset is a plastic pipe which gathers a bundle of electrical cables. That is why only five LocataLites are deployed in order to symbolise those limitations. Some more pictures of the experiments are gathered in the appendices in Section E. In the preamble to the measurements, the author checked the presence of any Wi-Fi transmitters using a laptop DELL Latitude $D505$ with a Wi-Fi card - $DELL\ TrueMobile\ 1300\ WLAN\ Mini-PC$ and using software called $NetworkStumbler$ (see *www.netstumbler.com*). No APs were found on the test site.

Following the comments about the installation of the LocataNet given in the previous chapters (i.e. Chapter 6), the first important parameter is the geometry of the network in order to have an accurate rover position. From the network schematic in the right picture of Figure 8.3, the DOP values are approximately 0.67 in the horizontal plane and 10.31 in the vertical plane at the initialisation point P2. The value of the VDOP is high, because the antennas of the LOCATA transceivers were all set up approximately at the same height. This setting issue has already been developed in Section 6.2.2. It justified why the rover does not triangulate accurately its position in the third dimension. Thus, the following results are only focused on the error on the East and North coordinates. In addition, the true coordinates were measured using a robotic total station ($Trimble\ S6$) and averaging over face left and face right measurements. Figure 8.4 shows the time series of the rover's position in a static test. The rover was initialised in $P2$ according to Figure 8.3. The mean accuracy of the total error is approximately 3 millimetres with a standard deviation of 1.7 millimetres. When looking at the curves, the curves are steady over the epochs, without showing any jumps characteristic of possible interferences (i.e. Chapter 7).
After the initialisation of the rover, some measurements were carried out while moving the rover along the asset. The rover started the movement from $P2$ to $P1$ and then come back to the first point. The distance between the initial point and the other point is approximately 30 m. Figure 8.5 shows the root mean square error of the rover's coordinate when moving from $P2$ to $P1$ and back ($P2b$). When moving the rover, the error is maximum in $P1$ with a RMSE value around 11 cm. This jump in the accuracy was noticed in the previous chapters. Mainly, there are two phenomena:

on one hand the HDOP value increases slightly to 0.841, on the other hand it was established in Section 7.3.3 that the processing of the signal was low enough to induce cycle clips in the carrier-phase measurements in the kinematic tests. The proof of the second phenomenon is given in appendices Section E - Figure E.1. $T1$, $T2$, $T3$ and $T4$ are the periods when the rover moves to one point to another. The figure shows the cycle slips appearing during the movement of the rover.
Finally, Table (8.2) shows the results for all the points monitored during the kinematic test. The overall result is that the total error and the error on each coordinate are within the margin defined by the VISTA project in 2D. It is interesting that the accuracy of the initialisation is at the millimetre level on both the East and North coordinate.

In parallel of the LOCATA experiments, the author and his colleagues carried out some RTK GPS measurements. The reference station was set up in a 100 m radius around the asset under study. Thus, the baseline used in the RTK GPS measurements was short. Table (8.3) shows the results averaged on 100 epochs. Although the table displays the error in 2D, it was possible during the experiments to monitor each point on the pipe in 3D. The test site was a sort of open field, because no major obstacles could have obstructed the GPS signal. In addition, the position dilution of precision value was approximately equal to 0.5 on each point $P1$ and $P2$.

$14-02-08$	$P2$	$P1$	$P2b$
HDOP/VDOP	0.670/10.310	0.841/9.980	0.670/10.310
RMSE(μ)	3.10^{-3}	0.117	0.072
RMSE(Std)	10^{-3}	7.10^{-3}	0.005
E(μ_E)	10^{-3}	0.018	5.10^{-3}
E(Std_E)	10^{-3}	0.012	2.10^{-3}
N(μ_N)	2.10^{-3}	0.115	0.072
N(Std_N)	10^{-3}	8.10^{-3}	2.10^{-3}

Table 8.2: Error (in metres) on each coordinate averaged on 150 epochs using LOCATA technology.

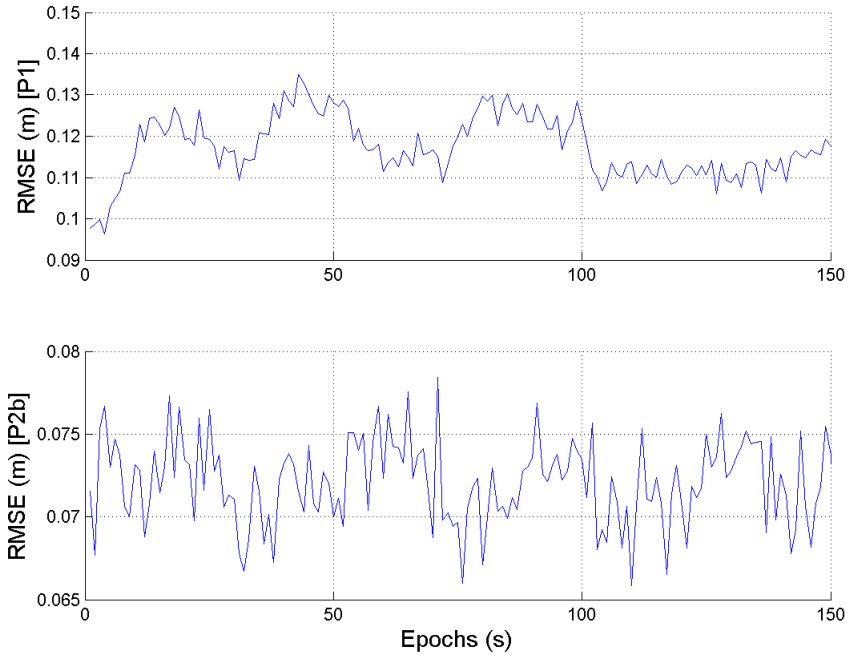


Figure 8.5: Time series of the rover's position error at different points $[P1]$ and $[P2]$ during the trial $[14-02-08]$.

$14-02-08$	$P2$	$P1$
RMSE(μ)	0.012	0.052
RMSE(Std)	0.001	0.010
E(μ_E)	0.001	0.033
E(Std_E)	0.001	0.009
N(μ_N)	0.012	0.0410
N(Std_N)	0.007	0.006

Table 8.3: Error (in metres) on each coordinate averaged on 100 epochs using RTK GPS.

From the table, the results are comparable with the ones obtained with the LOCATA technology. The mean error at the initial point $P2$ is 1.2 cm which is four times the error of that with LOCATA, whereas for at $P1$ the RTK GPS error is half that of the accuracy obtained with the ground-based technology (5.2 cm). Thus, the overall conclusion is that the two technologies have similar performances in this environment and converges to the discussion in Section 7.4.

8.4 LOCATA Technology Performances Indoors

It was planned to carry out a set of experiments with the LOCATA technology in an indoor environment (warehouse). Few studies are published deploying a LocataNet for indoors measurements ([Barnes et al. (2003a)]). An indoor environment may be of interest in the challenges addressed by the VISTA project, because the scenario is comparable to the conditions in very narrow urban canyons (e.g. high multipath). The scenario took place in a warehouse on the campus of the University of Nottingham. The author would like to thank Mr H. De Ligt and Dr S. Waugh for their help in the setup of the LocataNet.

The scheme of the LocataNet is shown in Figure 8.6.

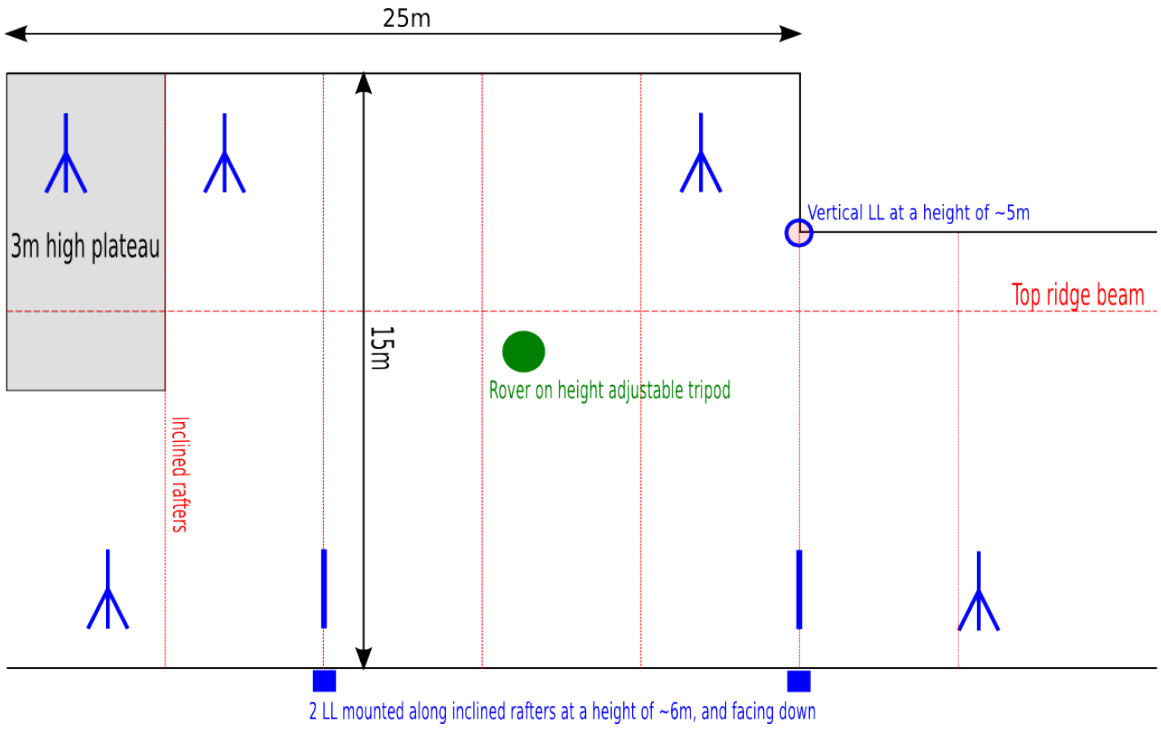


Figure 8.6: LocataNet scheme [20 – 11 – 2007].

Eight LocataLites were involved in the measurements: 5 installed on tripods and 3 on the wall of the warehouse. From the scheme, it is worth underlining that the LOCATA transceivers are set up at different heights. Indeed, 3 tripods are installed on the ground floor, one LocataLite is on a 3 m high plateau, 2 transceivers are

attached to some surrounding rafters at approximately 6 m above the ground, and the last one is attached to the wall at 5 m high. On the scheme, the green point is where the rover took place for the static experiments. This configuration of the LocataNet gives a VDOP value of 1.76 and a HDOP of 0.59. Note that no multipath mitigation antenna are used at the rover or at the transceivers.

Figure 8.7 shows the time series of the error in each coordinate. The East and North coordinate errors show steady error over the time.

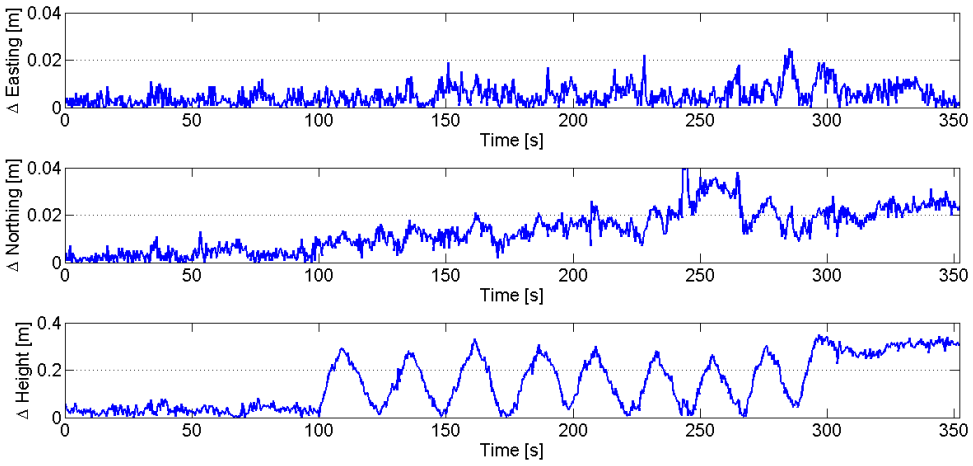


Figure 8.7: Time series of the rover's accuracy $[20-11-2007]$.

The purposes of this experiment is to measure the accuracy of the LOCATA technology in this type of environment when moving up and down the rover's antenna of a few centimetres. As a result, it is clearly noticeable several jumps in the Height coordinate.

The results show that the mean of the East and North coordinate error is respectively 0.011 cm and 0.018 cm. It seems that the North coordinate diverges with time. It may be partially due to an effect of moving the rover up and down. However from all the experiments carried out during this work, this one was the most accurate. The analysis of the data may suggest that multipath may be the major source of error in this environment. Thus, this kind of experiment may be a good testbed for the performances of the multipath mitigation algorithms embedded in the LOCATA firmware.

8.5 Simulations on the Future Integration of GNSS and LOCATA Technologies

8.5.1 Simulator: Integration of the LOCATA and the GNSS Signals

The simulator is designed using the same principles as the software developed for the integration of the Global Navigation Satellite System and the cellular signal (i.e. Chapter 4). As a result, the block diagram is the same as in Figure 4.4 in Section 4.4.2.3. Instead of ToA Simulator, the block simulates the positions and the measurements of the LOCATA transceivers.

The first part of the simulator simulates the receiver's trajectory, the GPS satellites' constellation and it generates a RINEX observations file (pseudoranges and carrier-phase measurements). This is performed using the same simulator developed within the IESSG in previous research project (i.e. [Noakes (2003)]). To simplify the simulations, the observations are free of tropospheric and ionospheric errors. As a result, the multipath is the main source of errors in the measurements written in the RINEX observations file. The standard deviation of the multipath error is approximately 2 centimetres in the carrier-phase measurements.

The trajectory is a typical urban canyon scenario, where the number of satellites drops down from 10 to 4 satellites during the movement. This is to simulate the obstruction of the sky by buildings which limits the availability of the GPS technology. Figure 8.8 shows the urban canyon scenario and the trajectory of the rover. Note this picture was generated using the software *ArcGIS* which is independent of the simulator described in this section.

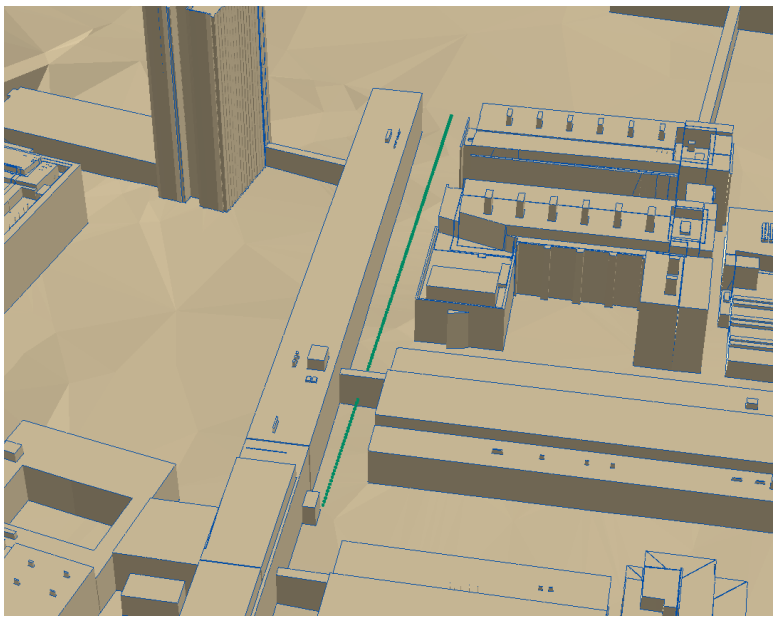


Figure 8.8: 3D model of the trajectory followed by the rover (bold green line) and the urban canyon scenario.

In the second step, a Matlab script was written to add a number of LocataLites to augment the GPS constellations and then to analyse the time series of the rover's position accuracy. The number of LocataLites and their coordinates are chosen at the beginning of each simulation run. This part of the simulator adds a couple of errors with a standard deviation depending on the parameters set up in the simulator. The observations follow the equations:

$$\lambda_s \times \phi_s^i = \rho_s^i + c \times \delta t_{sy-s} + c \times + \delta t_s^i + \epsilon_{\phi_s}^i + N_s^i \tag{8.2}$$

$$\lambda_L \times \phi_L^j = \rho_L^j + c \times \delta t_{sy-L}^j + c \times + \delta t_L^j + \epsilon_{\phi_L}^j + N_L^j \tag{8.3}$$

where c is the speed of light. λ_s and λ_L are respectively the wavelengths from the i-th satellite and the j-th LocataLite. ϕ_L^j and ϕ_s^i are respectively the carrier-phase measurements from the i-th satellite and the j-th LocataLite. ρ_s^i and ρ_L^j are respectively the true ranges between the receiver and the i-th satellite and the j-th LocataLite. δt_{sy-s}^i is the error of synchronisation between the i-th satellite and the rover. This error should be seen as the remainder after subtracting the measurements with the estimated clock drift of the receiver using least-squares method, which may be small (e.g. 10^{-10} s) according to [Misra and Enge (2001)]. This parameter is not simulated in either the GNSS simulator or the Matlab script.

δt_s^i takes into account the time delay from the transmission through Ionosphere and Troposphere and it is NOT simulated in the Matlab manuscript. $\epsilon_{\phi_s}^i$ and $\epsilon_{\phi_L}^j$ are respectively the multipath error in the received signals from the i-th satellite and the j-th LocataLite. $\epsilon_{\phi_s}^i$ is simulated in the GNSS simulator (RINEX observations file), whereas $\epsilon_{\phi_L}^j$ is simulated as a zero mean Gaussian random variable in the Matlab script. The standard deviation is approximately of 10^{-9} s at the beginning of the trajectory and then the standard deviation is multiplied by factor of 3 when the rover entered in the urban canyon.

N_s^i and N_L^j are respectively the integer ambiguities in the received signals from the i-th satellite and the j-th LocataLite. Note that those errors are turned off in both the GPS constellation simulator and the Matlab script ($\forall(i,j)\ N_s^i = N_L^j = 0$). This is justified as these simulations are only to show the feasibility of integrating the two technologies.

δt^j_{sy-L} is the clock drift of the rover. Finally, δt^j_L is the synchronisation error between the i-th satellite and the j-th LocataLite. However, all the Locatalites are synchronised with the master LocataLite, and as a matter of fact this error should be constant for all the transceivers. In other words, δt^j_L is equal to δt_L. A way to cancel out this error is to do a double difference between the measurements from the master and the j-th LocataLite. Neither δt^j_{sy-L} nor δt^j_L are taken into account in the simulator, but a global random variable (zero mean Gaussian distributed) is added to the LOCATA carrier-phase measurements to symbolise the possible synchronisation error in the LocataNet due to some possible effects (e.g. fading, interferences). This synchronisation error will then affect the accuracy of the measurements from all LocataLites and their synchronisation with the GNSS measurements.

Once the observations are simulated, the position of the rover is calculated mixing the measurements following the explanations in Chapter 4 Section 4.4.2.1. The algorithm is based on a least-squares algorithm. However, the TDOA measurements should be replaced by:

$$\zeta_{j,0} = \lambda_L \times (\phi^j_L - \phi^0_L) \tag{8.4}$$

where ϕ^0_L is the carrier-phase measurement from the master LOCATA transceiver. Following the notation given in Section 4.4.2.1, the vector of unknown variables should also include the δt^j_{sy-L} (clock drift of the rover in the LOCATA measurement):

$$\begin{aligned} \mathbf{x} &= [X, Y, Z, c \times \delta t_{sy-s}, c \times \delta t^0_{sy-L}, c \times \delta t^1_{sy-L}, c \times \delta t^2_{sy-L}]^T \\ \mathbf{x}_0 &= [X, Y, Z]^T \end{aligned} \tag{8.5}$$

Note that in the above equation, three LocataLites are used. $\mathbf{x}_0$ is the vector of unknown variables (the coordinates of the rover) estimated by the least-squares process in the simulator following the explanations given above.

8.5.2 Analysis of the Results

This study focuses on the improvement of the accuracy delivered by the GNSS technology when augmenting the constellation with some LocataLites in a difficult

environment. As described in the previous section, the trajectory is the (green) bold line in Figure 8.8. At the beginning, the rover may locate itself by using only the signals from 10 GPS satellites. While moving in the urban canyons, a mask is applied and only a limited number of satellites are available. This number is a parameter in the Matlab script file. Figure 8.9 shows the time series of the rover position accuracy using only the signal from 4 satellites and 4 LocataLites. The values of the $VDOP$ and $VDOP_+$ mean respectively the vertical dilution of precision calculated without and with adding the LOCATA transceivers. Note that the mean and standard deviation of the multipath values in the urban canyon are three times higher when compared at the start of the trajectory (open sky environment). The overall results from this figure show that the centimetre level is achievable.

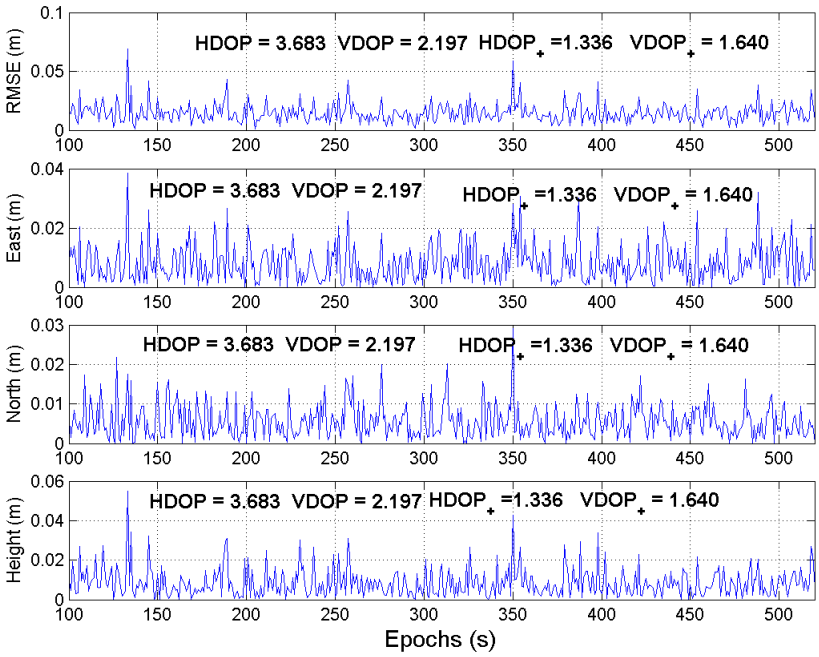


Figure 8.9: Time series of the rover position's error in absolute value using 4 satellites and 4 LocataLites.

To support this result, further simulations are carried out by increasing progressively the size of the LocataNet. Figure 8.10 shows the RMSE and errors in absolute value in the East, North and Height coordinates when increasing the number of LOCATA transceivers. The bold vertical lines are the different standard deviation values for

each point. Those lines end with different symbols as written in the legend of the figure (*tgd* stands for triangle down and *plus* is the positive sign).

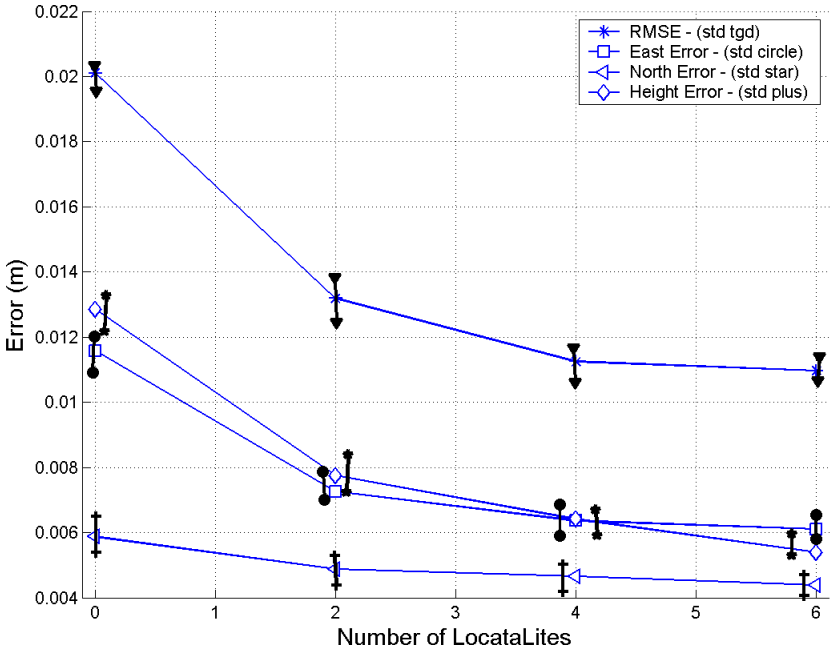


Figure 8.10: RMSE and errors in absolute value in the East, North and Height coordinates - (standard deviations are the vertical bold lines).

Each result is averaged on a 1000 simulations. In other words, for a given scenario (e.g. 4 satellites and 4 LocataLites) the mean RMSE, the associated standard deviation, the mean error on the three coordinates and their standard deviation are averaged on a 1000 runs. This limits the influence of the geometry of the network fluctuating from one simulation to another. The general result is the more LocataLites are added, the better the accuracy of the rover's position. This result agrees with the general definition of the Dilution of Precision given in Chapter 6 or in [Strang and Borre (1997)].

Finally, the influence of the synchronisation error between the satellite constellation and the LOCATA technology is also simulated. As previously explained, this error is not directly shown in the observables described in Equation (8.2). The parameter δt_L^j is cancelled out in the LOCATA observations by double differencing the measurements

between the master and the j-th LocataLite. Following the previous comments on the error models in the LOCATA carrier-phase measurements, a zero mean Gaussian distributed random variable is added to each LOCATA measurement which symbolises the error of synchronisation. Figure 8.11 shows the RMSE and the error in absolute value on the three coordinates when increasing the synchronisation error. Note that the scale on the x-axis is in nano seconds. Each result is averaged on a 1000 siumlations as previously explained. Table (8.4) displays the results of the standard deviation for each point in the previous figure. The results justifies that the error of synchronisation

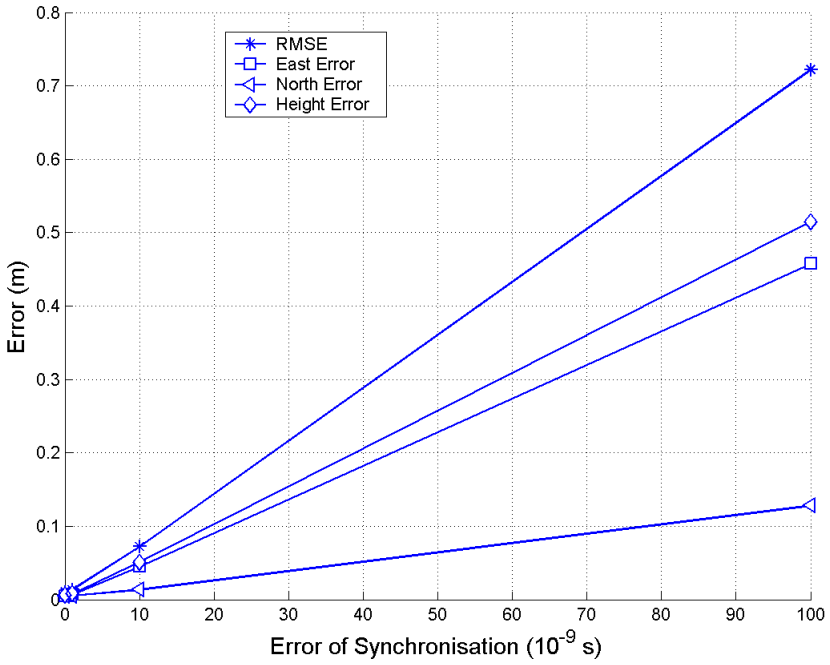


Figure 8.11: RMSE and errors in absolute value in the East, North and Height coordinates while increasing the synchronisation error.

makes the rover's position diverge.

StD (s)	0	10^{-10}	10^{-9}	10^{-8}	10^{-7}
RMSE (m)	0.006	0.006	0.007	0.053	0.546
East (m)	0.004	0.005	0.006	0.036	0.373
North (m)	0.004	0.004	0.004	0.011	0.107
Height (m)	0.005	0.005	0.007	0.041	0.421

Table 8.4: Standard deviation for each value of the synchronisation error averaged on a 1000 simulations.

8.6 Summary

At the beginning of this chapter, the in-house software was explained in detail and its performances were shown to be comparable to the LINE software in the static scenarios. The software was entirely developed and coded by the author of this thesis. This chapter also shows some practical applications of the LOCATA technology (e.g. in work site) beyond the series of tests performed in the last three chapters. These applications are crucial to open the market for this new location technology and may be seen as a proof of concept. Nevertheless, the experiments pointed out the advantages and drawbacks studied in the previous chapters (e.g. time to set up a LocataNet, careful design of the network). The "extreme" scenario is the indoor measurements. This setup shows promising results for this technology and the possibility to achieve the centimetre inside a building. However, the processing of the LOCATA data underlined the need of more multipath mitigation algorithms.
Finally, a simulator was developed to integrate the LOCATA and GNSS measurements using the same architecture as the one studied in Chapter 4 while integrating GNSS and cellular network. The observations (carrier-phase measurements from GNSS and LOCATA technologies) were modelled and the Gaussian error model of some unknown variables was justified. The overall results show that only few LocataLites are required in the augmentation of the GNSS constellation in order to achieve the centimetre level in urban canyons. Beside, the synchronisation of the two technologies would have to be at the nano second level in order to guarantee the error on the rover's position better than few centimetres.

Chapter 9

Conclusion and Recommendations

United Kingdom utility services are faced with the challenge of mapping 4 million kilometres of buried pipes and cables. Disturbances such as accidents, weather conditions, traffic volume, and road work can be detrimental to these buried assets, many of which are not shown precisely on maps. Pipes and cables must be located precisely to increase the efficiency of street works projects. In 2005 the UK Department for Trade and Industry (DTI) along with some industrial partners have commenced funding the VISTA project. The academics at the IESSG, University of Nottingham have been working on how satellite technology may be integrated with other location technologies to deliver information on where utilities are buried, and so provide an accurate location of the assets buried in the ground.

However, precise positioning in difficult environments such as urban canyon scenarios implies that many challenges need to be solved using positioning technologies such as RTK GPS and other satellite positioning systems (e.g. GLONASS). The VISTA project brings the challenge one step further when looking at positioning at the centimetre level, any buried assets, from a bundle of wires to a sewer pipe. The sponsors defined in the early drafts of the project that the positioning accuracy would be better than the centimetre level in 2D, but the limit of the accuracy in 3D was approximately set up at 15 cm, as the frequent street works affect the accuracy in the depth of the buried assets.

This work started with a comprehensive review of existing technologies on the market used by surveying companies in the United Kingdom. Although Global Navigation Satellite Systems are by far the most widely used to survey outdoors. The pipes are generally monitored using ground penetrating radars and cable detectors. Although, it was underlined that the plastic pipes may not be detected, depending on the nature of the soil (conductivity) where the assets are buried. In addition some more invasive technologies may be used such as the CCTV/Light Line. However all those technologies do not provide a precise position of the buried assets.

9.1 Conclusions

While studying the Global Positioning System technology in Chapter 3, a number of challenges were discussed. Although the Real Time Kinematic GPS technology may deliver the centimetre level of accuracy, it suffers from signal fading (e.g. multipath), lack of satellite availability and efficiency in difficult environments such as urban canyons in towns. The narrower the urban canyon is, the less sky the receiver sees. Thus it makes it difficult to triangulate its position.
In order to tackle the urban canyon challenges for precise positioning, the first research study in this thesis was to look at the ubiquitous positioning market and the newly emerging technologies behind it (Chapter 4). It was then decided to study the integration of GNSS and the cellular network through simulations. On one hand, this was motivated by the constant expansion of the coverage and improvement of the cellular technology in cities around the world. On the other hand, there is a still lot of research work on going and new algorithms to position subscribers are designed by researchers and industries. The analyses of the results were carried out via simulations. A comprehensive simulator simulates separately the GPS constellation with a RINEX observations file (this is done using an in-house software developed in a previous project at the IESSG), and the observations coming from the simulated cellular base stations (also called ToA). Finally, the rover's position is triangulated by combining the two types of observations. However, the analysis of the results showed that the centimetre level may be difficult to achieve with the integration of those two technologies. This was mainly due to the lack of synchronisation in the cellular network (even when using the UMTS time frame). The accuracy of the rover position in 3D was found to be not better than 20 m with improvements by introducing a synchronisation error in the cellular network.

By the beginning of 2007, the IESSG received a LOCATA network of 8 LocataLites and 2 LOCATA rovers. LOCATA technology is built on new proprietary synchronisation technology which overcomes the challenges presented when trying to use ground-based transmitters (i.e. Pseudolites technology). LocataLite transceivers transmit and receive a signal modulated in the same way as the GPS technology, allowing a

rover to calculate its position. A LocataNet is a network of LocataLites. It consists of two kinds of devices: the LocataLites and the LOCATA receiver (or rover). This technology is not available on the market yet. It remains at a prototype stage with a firmware update every semester. Chapter 5 describes the technology features such as the synchornisation process in the LocataNet ($TimeLoc$ parameter), the transmission of the LOCATA signal (PRN code), the multiple access layer to avoid the transmitters to jam each other. Some range tests (how far the rover from a LOCATA transceiver can receive the signal) were also carried out at the end of this chapter.

In the following chapter (Chapter 6), tests were carried out in various environments (e.g. open areas, built up areas) to analyse this new technology. The environments were chosen regarding the future deployment of this technology (e.g. cities, urban canyons, more open sky area) and its applications. A series of static tests showed that the LOCATA technology may achieve better than 3 cm using carrier-phase measurements when deployed in Open environments. The analysis of the time series of the rover's position also underlined the need for a careful designed of the LOCATA network (for good values of the HDOP and VDOP) in order to locate the rover in 3D. This problem is justified by describing how the embedded navigation engine work and processes the LOCATA measurements: if the least-squares algorithm diverges, the software then triangulates the position in 2D. With the accuracy of the rover in 2D sometimes better than 1 cm.

The kinematic tests have underlined that the vertical and horizontal dilution of precision values may change from one test point to another and sometime leads to a degradation of the accuracy. The surrounding area around the rover and the LocataLites plays an important role, in order to get a trustworthy accuracy all around the monitored area. All information points out the need to adapt and carefully design the LocataNet depending on where the survey takes place. It also shows the difficulty in monitoring the area with a single frequency LOCATA receiver. If the rover loses the lock on the tracked signal, the user needs to come back to the initial point to calculate the ambiguity values. Furthermore, it was underlined that the cycle slip detected when the rover starts moving, may be fixed when the LOCATA prototype

will become dual frequency. The LOCATA navigation engine may then calculate the ambiguities as integer values and use some powerful algorithms to quicken the processing time.

Following the previous summaries, Chapter 7 is a study of the LOCATA technology when deploying a LocataNet on the roofs of the buildings at the University of Nottingham. Some results in the previous chapter suggested that the network configuration and the position dilution of precision values were not the only causes of the diverging accuracy of the LOCATA rover. A large part of this chapter was dedicated to answering the question of whether Wi-Fi technology interferes with the LOCATA signal, because the test bed is surrounded by many Wi-Fi access points. The Wi-Fi technology was identified as the only technology transmitting in the test bed in the same frequency band (ISM). The study includes the analysis of the measurements at different locations around the area and on different days. To summarise, it was shown that in the presence of Wi-Fi transmitters, the level of noise in the Adaptive Gain Control may increase. The direct result is that the LOCATA observables may be less accurate. Then, in the presence of strong Wi-Fi signal, the LINE software may detect repetitive cycle slips which may make the time series of the rover's coordinates diverge. A strong Wi-Fi signal means that one or more Wi-Fi APs were transmitting at a high data rate while monitoring with the LOCATA technology. Unfortunately, the author could not demonstrate the exact relationship between the level of noise in the AGC and the data rate of the surrounding Wi-Fi APs. This is mainly due to a lack of data from the Wi-Fi network. Any phenomenon experienced during the measurements have been fed-back to *LOCATA Corp.* Thus, the issues are validated with the version of the firmware used during the experiments and at the time of writing this thesis.

On the other hand, the LOCATA technology demonstrated promising performances in the test bed and competes well with the RTK GPS accuracy in difficult environments. While monitoring with the same amount of time different test points, the LOCATA technology was able to provide an accuracy better than 5 centimetres in 3D (using carrier-phase measurements with float ambiguities), whereas the RTK GPS receiver

triangulated its position with an accuracy not better than 10 centimetres for the same test point using carrier-phase measurements with float ambiguities. The PDOP value was around 4 when surveying with the RTK GPS technology.

The last chapter started with the explanations of the development of an in-house software which produces results that are comparable to the LINE software in the static scenarios.
As a proof-of-concept for the LOCATA technology, tests were later carried out on a work site. The performances demonstrated the capacity of this ground-based technology to locate an asset with an accuracy better than 2 cm in 3D.
Another experiment was realised in an indoor warehouse. It shows promising results: this technology may allow a survey inside buildings which is at the moment an even greater challenge for any surveying companies (RTK GPS may not work indoors). However, more work is required on the multipath mitigation algorithms in the LOCATA firmware.
Finally, a simulator was developed with the same architecture as the one used to produce the early results of the integration between GPS and cellular networks. The observables from the GNSS and the LOCATA technologies were modelled by adding different sources of error (i.e. synchronisation, clock drift, multipath) as zero mean Gaussian random variable. The analysis through simulations of the integration of the GNSS and LOCATA technologies then demonstrated the feasibility and the possibility of a 3D positioning at the centimetre level in urban canyons. Nevertheless, the results underlined that a lack of synchronisation (i.e. less than 10 ns) may make the rover position diverges rapidly (i.e. accuracy greater than 10 cm).

9.2 Recommendations for Future Work

The future work following this thesis may focus on some experiments when the LOCATA firmware will be updated and the prototype will use a dual frequency to triangulate the rover's position. Some algorithms should then be developed to solve and fix the integer ambiguities in the LOCATA carrier-phase measurements (e.g.

LAMBDA method). New trials will be planned to test the algorithms and to study the new features and perhaps new phenomenon.

The integration of the GNSS signal with the LOCATA technology will be a milestone to kick-off the technology on the market and this may solve many challenges underlined during this research work. For example, the deployment of a LocataNet may be handier, and it may be then possible to do some measurements in the streets of London, for example. However future research may not only focus on surveying applications such as the ones described in the background of the VISTA project, but it may also explore the LOCATA technology applied to the emerging ubiquitous positioning market (position anywhere, anytime). This will then allow the development of algorithms to integrate the LOCATA technology with other ground based positioning technologies such as the Ubisense positioning system (using Ultra Wide Band signal).
Beside, it may be worth funding a specific project to integrate GPR and positioning systems (e.g. LOCATA, GPS) as the GPR outputs only a picture of what is buried in the soil without giving any coordinates in a global reference frame (e.g. WGS84).

Finally, there is room to improve the multipath mitigation algorithms inside the firmware. The author demonstrated the feasibility of improving the accuracy by using super resolution algorithms (e.g. MUSIC) in the short study published in a conference paper (i.e. appendix F). This requires further collaboration with *LOCATA Corp*, and it is a key factor for the use of LOCATA in high multipath environments. In addition, some more research should focus on how to optimise the use of the two transmitters on each LocataLite to mitigate multipath. At the moment, a simple difference between the carrier-phase measurements (or pseusoranges) indicates if one transmitter is in a deeper fading area than the other one. One possibility may be to look at the multiple inputs single output technology in array antennas technology.

References

Agarwal, N., Basch, J., Bechmann, P., Bharti, P., Casadei, S., Chou, A., Enge, P., Fong, W., Hathi, N., Mann, W., Sahai, A., Stone, J., Tsitsiklis, J., Roy, B. V., 2002. Urban *GPS*: Algorithms for *GPS* operation indoors and downtown. GPS Solutions , 149–160.

Akturan, R., Vogel, W. J., 1997. Path diversity for *LEO* satellite-pcs in the urban environment. IEEE Transactions on Antennas and Propagation 45 (7), 1107–1116.

Balanis, C. A., 2005. Antenna theory: Analysis and Design, 3rd Edition. John Wiley & Sons, New York, NY.

Barnes, J. B., 2006. Ground-breaking ground-based positioning, *LOCATA* training course. Tech. rep., available at `http://www.gmat.unsw.edu.au/snap/staff/joel_papers.htm`.

Barnes, J. B., Rizos, C., Kanli, M., Pahwa, A., July 2006. *LOCATA*: a new positioning technology for classically difficult gnss environments. In: Proceedings of the International Global Navigation Satellite Systems Society (IGNSS Symposium 2006).

Barnes, J. B., Rizos, C., Wang, J., Small, D., Voigt, G., Gambale, N., November 2003a. *LOCATA*: A new positioning technology for high precision indoor and outdoor positioning. In: Proceedings 2003 International Symposium on GPS-GNSS. pp. 9–18.

Barnes, J. B., Rizos, C., Wang, J., Small, D., Voigt, G., Gambale, N., July 2003b. *LOCATA*: the positioning technology of the future? In: Proceedings of the

6th International Symposium on Satellite Navigation Technology Including Mobile Positioning and Location Services.

Barnes, J. B., Van Cranenbroeck, J., Rizos, C., Pahwa, A., Politi, N., May 2007. Long term performance analysis of a new ground-transceiver positioning network (*LocataNet*) for structural deformation monitoring applications. In: Proceedings of the FIG Working Week.

Barnes, J. B., Wang, J., Rizos, C., Small, D., Voight, G., Gambale, N., October 2003c. Guidelites: Intelligent synchronised pseudolites for cm-level stand-alone positioning. In: Proceedings of the 11th International Association of Institutes of Navigation (IAIN) World Congress. pp. 21–24.

Barnes, J. B., Wang, J., Rizos, C., Small, D., Voight, G., Gambale, N., September 2003d. *Locatanet*: A new positioning technology for high precision indoor and outdoor positioning. In: Proceedings of the 16th International Technical Meeting of the Satellite Division of the U.S. Institute of Navigation ION-GPS. pp. 1119–1128.

Bond, A., October 2007. Sahara- the inspection system. Tech. rep., may be obtained at `http://www.vistadtiproject.org/site/vista/public/overview`, [Accessed May 2008].

Borkowski, J. M., 2004. Performance of cell ID+RTT hybrid positioning method for $UMTS$. Master's thesis, Tampere University of Technology, Insinoornikatu 60A 25.

Boukhelifa, N., Duke, D. J., 2007. The uncertain reality of underground assets. In: Proceedings of ISPRS/ICA/DGfK joint Workshop on Visualization and Exploration of Geospatial Data.

Caffery, J. J., Stuber, G. L., 1995. Radio location in urban $CDMA$ microcells. In: Proceedings of the Personal, Indoor and Mobile Radio Communications (PIMRC'95). Vol. 2. pp. 858–862.

Cavicchi, T. J., 2001. Digital Signal Processing, 1st Edition. John Wiley & Sons, New York, NY.

Cobb, H. S., 1997. *GPS* pseudolites: Theory, design and applications. Ph.D. thesis, Stanford University.

Cosser, E., 2004. Bridge deformation monitoring with single frequency *GPS* augmented by pseudolites. Ph.D. thesis, University of Nottingham, Institute of Engineering Surveying and Space Geodesy.

Crow, B., Widjala, I., Kim, J. K., Sakai, P., September 1997. *IEEE* 802.11 wireless local area networks. IEEE Communications Magazine , 116–126.

Daniels, D. J., 2004. Ground Penetrating Radar, 2nd Edition. Institution of Engineering and Technologie.

Delmas, J., 1995. Elements de Theorie du Signal: les Signaux Deterministes, 1st Edition. Ellipses, Paris, Rue Bargue.

Drakoulis, D., Kyriazakos, S., Karetsos, G., 2000. Improving subscriber position location using hybrid satellite-assisted and network-based technique. In: Proceedings of the 52nd IEEE Vehicular Technology Conference. Vol. 4. pp. 1887–1893.

Duffet-Smith, P., Craig, J., May 2004. Matrix, and enhanced satellite positioning. In: Proceedings of the IEE 3G Mobile Communications Technologies conference. pp. 364 – 367.

Duffett-Smith, P., Macnaughtan, M., May 2002. Precise *UE* positioning in *UMTS* using cumulative virtual blanking. In: Proceedings of the IEE 3G Mobile Communications Technologies conference. pp. 355 – 359.

Dupraz, H., Stahl, M., 1995. Theorie des erreurs. Tech. rep., Ecole Polytechnique Federale de Lausanne.

Eren, K., 1987. Geodetic network adjustment using *GPS* triple difference observations and a priori stochastic information. Ph.D. thesis, Institute of Geodesy, University of Stuttgart.

Ertel, R. B., Reed, J. H., 1999. Angle and time of arrival statistics for circular and elliptical scattering models. IEEE Journal on Selected Areas in Communications 17, 18291840.

ETSI, 2001. *ETSI TS* 125 305 *V*3.0.0 (2000-01). Tech. rep., available at `www.ofta.gov.hk/en/ad-comm/tsac/ts-paper/ts2003p23.pdf`.

Fainberg, M., 2001. A performance analysis of the *IEEE* 802.11b local area network in the presence of bluetooth personal area network. Master's thesis, Polytechnic University of Brooklyn, Brooklyn N.Y.

Feigenbaum, J., Kannan, S., Zhang, J., 2004. Computing diameter in the streaming and sliding-window models. Algorithmica 41 (1), 25–41.

Ferrari, P., Flammini, A., Marioli, D., Taroni, A., 2006. *IEEE* 802.11 sensor networking. IEEE Transactions on Instrumentation and Measurements 55 (2), 615–619.

Fischer, S., Koorapaty, H., Larsson, E., Kangas, A., 1999. System performance evaluation of mobile positioning methods. In: Proceedings of the 49th IEEE Vehicular Technology Conference. Vol. 3. pp. 1962–1966.

Garin, L., Gupta, P., 2007. A novel *GPS* satellite ephemeris extension compaction/decompaction method. In: Proceedings of the 63rd ION Symposium.

Ge, L., Chen, H. Y., Hans, S., Rizos, C., 2000. Adaptive filtering of continuous *GPS* results. Journal of Geodesy 4 (7/8), 572–580.

Ge, L., Han, S., Rizos, C., July 1999. Fast *RTK* applications of the leica *CRS*1000 *GPS* receiver. In: Proceedings of the 4th International Symposium on Satellite Navigation Technology and Applications.

Geomatrix, 2004. Geometrics technical note: Ohmmapper theory of operation. Tech. rep.

Gibson, J. D., 2002. The Communications Handbook, 2nd Edition. CRC Press, Boca Raton, London, New York, Washington D.C.

Goel, P., Roumeliotis, S. I., Sukhatme, G. S., October 1999. Robust localization using relative and absolute position estimates. In: Proceedings of the IEEEE International Conference on Intelligent Robots and Systems.

GPSPassion, E., August 2005. *GPS* performance and *TTFF*.
URL `http://www.gpspassion.com/`

Hashemi, H., 1993. The indoor radio propagation channel. Proceedings of the IEEE 81 (7), 943–968.

Hatch, R. R., 1982. The synergism of *GPS* code and carrier measurements. In: Proceedings of the Third International Geodetic Symposium on Satellite Doppler Positioning, New Mexico. Vol. 2. pp. 1213–1232.

Hickinbotham, S. J., Cohn, A. G., 2007. Knowledge-based recognition of utility map sub-diagrams. In: Proceedings of 9th International Conference on Document Analysis and Recognation (ICDAR 2007).

Hightower, J., Boriello, G., 2001. Location systems for ubiquitous computing. IEEE Computer 34 (8), 57–66.

Hoffmann-Wellenhof, B., Lichtenegger, H., Collins, J., 2001. *GPS*: Theory and Practice, 5th Edition. Springer-Verlag Wien New York.

Holma, H., Toskala, A., 2005. *WCDMA* for *UMTS*: Radio Access for Third Generation, 3rd Edition. John Wiley & Sons, New York, NY.

Hopfield, H. S., 1969. Two quartic tropospheric refractivity profile for correcting satellite data. Journal of Geophysical Research 74 (18), 4487–4499.

Horoshenkov, K. V., Tait, S. J., Wood, A. S., Boot, J. C., Ali, T. B., Saul, A., Rogers, C. D., long, R., October 2007. Sonic characterisation of change in sewers. Tech. rep., may be obtained at `http://www.vistadtiproject.org/site/vista/public/overview`, [Accessed April 2007].

Huang, C. C., Khayata, R., June 1992. Delay spreads and channel dynamics measurements at ISM bands. In: Proceedings of the IEEE SUPERCOMM/International Conference on Communications. Vol. 3. pp. 1222–1226.

HyperLink, 2005. 2.4 GHz 3dBi Magnetic Vehicule Mounrt Wireless LAN Antenna - Models: HG2403MGURB and HG2403MGURW, Data Sheet.

Inc, A. T., 2004. Wireless Antenna 2.4GHz Linear, AT2004, Data Sheet.

Jakes, W. C., 1994. Microwave Mobile Communications, 1st Edition. IEEE Press Classic, Piscataway, New Jersey.

K. Yu, J.-P. Montillet, A. R. P. C., Oppermann, I., December 2005. Uwb location and tracking for wireless embedded networks. EURASIP Journal on Advances in Signal Processing .

Kabalan, K. Y., Mounsef, J. L., December 2003. Mobile location in GSM using signal strength technique. In: Proceedings of the 10th IEEE International Conference on Electronics, Circuits and Systems (ICECS 2003).

Kanli, M. O., 2005. Limitations of pseudolites systems using off-the-shelf GPS receivers. Journal of Global Positioning Systems 3 (1-2), 154–166.

Kernighan, B. W., Ritchie, D. M., 2000. Le Langage C: Norme $ANSI$, 2nd Edition. Dunod.

Kleusberg, A., Teunissen, P. J. G., 1996. GPS for Geodesy, 2nd Edition. Springer.

Klobuchar, J., November 1986. Design and characteristics of the GPS ionospheric time-delay algorithm for single-frequency users. In: Proceedings of the Position Location and Navigation Symposium (PLANS'86).

Klobuchar, J. A., 1996. Ionospheric Effects on GPS. Vol. 1 of Global positioning System:Theory and Applications. American Institute of Aeronautics and Astronautics.

Ko, J., Kim, J., Cho, S., Lee, K., 2005. A 19-mw $2.6-mm^2$ $L1/L2$ dual-band $CMOS$ GPS receiver. IEEE Journal of Solid-State Circuits 40, 1414–1425.

Korhonen, J., 2003. Introduction to 3G Mobile Communications, 2nd Edition. Artech House Publishers, New York, London, Boston.

Kreyszig, E., August 1992. Advanced Engineering Mathematics, 7th Edition. John Wiley & Sons, New York, NY.

Krzysztof, W., Kolodziej, J. H., 2006. Local Positioning Systems: *LBS* Applications and Services, 1st Edition. CRC Press.

Kupper, A., 2005. Location-Based Services: Fundamentals and Operation, 1st Edition. John Wiley & Sons, New York, NY.

Lachapelle, G., Cannon, M. E., Erickson, C., Falkenberg, W., March 1992. High precision C/A code technology for rapid static *DGPS* survey. In: Proceedings of the Sixth International Geodetic Symposium on Satellite Positioning.

Lavine, A., Gardner, J. N., Reneau, S. L., October 2003. Total station geologic mapping: an innovative approach to analyzing surface-faulting hazards. Engineering Geology 70 (1).

Lee, W. C. Y., Lee, D. J. Y., May 2000. Pathloss predictions from microcell to macrocell. In: Proceedings of the 51st IEEE Vehicular Technology Conference. pp. 1988–1992.

Leica, 2006. Leica smartnet commercial rtk network solution for great britain. Tech. rep., Leica Geosystems AG, available at `<http://www.leica-geosystems.com/uk/en/2346.pdf>`, [Accessed January 2008].

Leick, A., 2004. *GPS* Satellite Surveying, 3rd Edition. John Wiley & Sons, New York, NY.

Li, X., Pahlavan, K., January 2004. Super-resolution ToA estimation with diversity for indoor geolocation. IEEE Transactions in Wireless Communications 3 (1), 224–234.

Liu, C. J., August 2002. Effects of selective availability on gps positioning accuracy. Southern Journal of Applied Forestry 26 (3).

Lutz, E., Cygan, D., Dippold, M., Dolainsky, F., Papke, W., 1991. The land mobile satellite communication channel-recording, statistics, and channel model. IEEE Transactions on Vehicular Technology 40 (2), 375–386.

Lynch, R. S. J., Willett, P. K., August 1998. Testing the statistical similarity of discrete observations using dirichlet priors. In: Proceedings of the IEEE International Symposium on Information Theory.

Manolakis, D., Ingle, V., Kogon, S., 2005. Statistical and Adaptive Signal Processing, 1st Edition. Artech House.

Massat, P., Rudnick, K., June 1990. Geometric formulas for dilution of precision calculations. Journal of the Institute of Navigation 37 (4), 379–391.

Meng, X., Dodson, A., Moore, T., Roberts, G. W., June 2007. Anyone, anything: Anytime, anywhere. GPS World , 106–113.

Misra, P., Enge, P., 2001. Global Positioning System: Signals, Measurements, and Performance, 1st Edition. Ganga-Jamuna Press.

Mohino, E., Gende, M., Brunini, C., 2007. Improving long baseline (100300 km) differential GPS positioning applying ionospheric corrections derived from multiple reference stations. Journal of Surveying Engineering 133, 1–5.

Montillet, J.-P., 2007. Achieving the centimeter level of accuracy in urban canyons using locatalites. In: Proceedings of the 20th International Technical Meeting of the Satellite Division of the Institute of Navigation ION-GNSS 2007, Fort-Worth.

Montillet, J.-P., Roberts, G. W., Meng, X., 2007a. Super-resolution in cumulative virtual blanking. In: Proceedings of the International e-Conference of Computer Science (IeCCS2007) - In Press.

Montillet, J.-P., Roberts, G. W., Meng, X., Taha, A., 2006. Precise positioning in urban canyons using GPS and GSM. In: Proceedings of the Mobile GIS in eGouvernment conference.

Montillet, J.-P., Roberts, G. W., Meng, X., Taha, A., March 2007b. Buried assets: Testing GPS and GSM in urban canyons. GPS World , 39–43.

Montillet, J.-P., Roberts, G. W., Meng, X., Taha, A., Hancock, C., Ogundipe, O., Barnes, J. B., December 2007c. Achieving centimetre-level positioning in urban canyons with $LOCATA$ technology. Journal of CPGPS - in Press .

Moore, T., Hill, C., Ice, S., Ochieng, W., Feng, S., Ioannides, R., Cross, P., Lau, L., 2007. End-to-end testing of an integrated centimetric positioning test-bed. In: Proceedings of the 20th International Technical Meeting of the Satellite Division of the Institute of Navigation ION-GNSS 2007, Fort-Worth.

Noakes, C., April 2003. The Navigation Sensor Simulator (NSS): Algorithm Description.

Novariant, 2004. Novariant announces industry first terralite XPS positioning infrastructure. Tech. rep., availabe at `http://www.novariant.com/documents/TerraliteAnnounce.pdf`.

Novariant, 2005. Novariant terralite XPS *Deployment* at *Phelps Dodge Morenci* mine. Tech. rep., available at `http://www.novariant.com/mining`.

Okumura, Y., Ohmori, E., Kawano, T., Fukuda, K., 1968. Field strength and its variability in VHF and UHF land-mobile radio service. Review of the Electrical Communication Laboratory 16, 852–873.

Papoulis, A., Pillai, S. U., 2002. Probabilty, Random Variables and Stochastic Process, 4th Edition. Mc Graw Hill, Madrid, London, New York.

Parker, J., Overton, C., 2005. $UKWIRE$ briefing. Tech. rep., may be obtained at `http://www.vistadtiproject.org/site/vista/public/overview`, [Accessed Mai 2008].

Parkinson, B. W., Spilker, J. J., 1996. Global Positioning System: Theory and Applications, 3rd Edition. Vol. 1. Progress in Astronautics and Aeronautics.

Pirti, A., 2007. Performance analysis of the real time kinematic GPS (RTK GPS) technique in a highway project (stake-out). Survey Review 39 (303), 43–53.

Prasad, R., 1998. Universal Wireless Personal Communications, 1st Edition. Artech House Publishers.

Proakis, J. G., 2000. Digital Communications, fourth edition Edition. Mc-Graw-Hill, New York, NY.

Ramakrishna, J., 2000. Radiowave Propagation and Smart Antennas for Wireless Communications, 1st Edition. Kluwer Academic Publishers, Hingham, MA, USA.

Rappaport, T. S., Biedka, T. E., Krizman, K. J., May 1997. Wireless position location: Fundamentals, implementation strategies, and sources of error. In: Proceedings of the 47th IEEE Vehicular Technology Conference (VTC 1997). Vol. 3. pp. 919–923.

Research, U. W. I., 2005. Visualising integrated information on buried assets to reduce streetworks (vista) project proposal. Tech. rep., may be obtained at `http://www.vistadtiproject.org/site/vista/public/overview`, [Accessed Mai 2008].

Rice, S. O., 1944. Mathematical analysis of random noise. Tech. rep.

Roberts, G., 1997. Real time on-the-fly kinematic gps. Ph.D. thesis, Institute Engineering for Surveying and Space Geodesy, University of Nottingham.

Roberts, G. W., Evans, A., Dodson, A. H., Denby, B., Cooper, S., Hollands, R., April 2002a. The use of augmented reality, GPS and INS for subsurface data visualisation. In: Proceedings of XXII Fig Congress.

Roberts, G. W., Meng, X., Montillet, J.-P., Taha, A., October 2006. The location and positioning of buried pipes and cables in built up areas. In: Proceedings of XXIII Fig Congress: Shaping the Change. pp. 1 – 9.

Roberts, G. W., Ogundipe, O., Dodson, A. H., April 2002b. Construction plant control using *RTK GPS*. In: Proceedings of FIG XXII International Congress.

Saarnisaari, H., May 1997. *TLS*-esprit in a time delay estimation. In: Proceedings of the IEEE Vehicular Technology Conference 47th (VTC 1997). Vol. 3. p. 16191623.

Saastamoinen, J., 1973. Contribution to the theory of atmospheric refraction. Bulletin Geodesique 107, 13–34.

Schmidt, R., March 1986. Multiple emitters location and signal parameter estimation. IEEE Journal of Antennas Propagation 34 (3), 276 – 280.

Schwieger, V., December 2003. Using handheld *GPS* receivers for precise positioning. In: Proceedings of the 2nd FIG Regional Conference.

Seeber, G., 1993. Satellite Geodesy: Foundations, Methods, and Applications. Walter de Gruyter.

Sklar, B., 2001. Digital Communications: Fundamentals and Applications, 2nd Edition. Prentice Hall, Inc., Upper Saddle River, New Jersey.

Smith, R. J., 2003. *WiFi* Home Networking, 1st Edition. McGraw-Hill, Chicago, San-Fransisco, London.

Son, H. C., Lee, J. G., Jee, G. I., 2003. Mobile station location using hybrid *GPS* and a wireless network. In: Proceedings of the 57th IEEE Vehicular Technology Conference. Vol. 4. pp. 2716–2720.

Spirito, M. A., May 2001. On the accuracy of cellular mobile station location estimation. IEEE Transactions on Vehicular Technology 50 (3), 674–685.

Stewart, H. C., Lawrence, D. G., Pervan, B., Cohen, C. E., Powell, J., Parkinson, B., September 1995. Precision landing tests with improved integrity beacon pseudolites. In: Proceedings of the Institute of Navigation ION-GNSS 1995.

Strang, G., Borre, K., 1997. Linear Algebra, Geodesy, and *GPS*. Wellesley Cambridge Press, Wellesley, MA.

Sun, G., Chen, J., Guo, W., Liu, K. J. R., July 2005. Signal processing techniques in network-aided positioning [a survey of state-of-the art positioning designs]. IEEE Journal of Signal Processing 22 (4), 12 – 23.

Syrjarinne, J., 2000. Possibilities for GPS time recovery with GSM network assistance. In: Proceedings of the 15th International Technical Meeting of the Satellite Division of the Institute of Navigation ION-GPS 2000, Salt Lake City. pp. 955–966.

Syrjarinne, J., 2001. Studies of modern techniques for personal positioning. Ph.D. thesis, Tampere University of Technologies.

Taha, A., September 2007. A continuous updating technique for loosely coupled RTK GPS with total station observations. In: Proceedings ION-GNSS 2007.

Taha, A., Meng, X., Roberts, G. W., Montillet, J.-P., September 2006. Using smartstation and gps integrated with INS to map underground pipes and cables. In: Proceedings of the Institute of Navigation ION-GNSS 2006.

Teunissen, P., November 1995. The least-squares ambiguity decorrelation adjustment: A method for fast gps integer ambiguity estimation. Journal of Geodesy 70 (1-2), 65–82.

Teunissen, P., February 1997. Gps double-difference statistics: with and without using satellite geometry. Journal of Geodesy 71 (3), 137–148.

US.Army, 1996. Navstar GPS - user equipment introduction. Tech. rep., U.S. Government.

Van Dierendonck, A., 1997. Satellite Radio Navigation, in Avionic Navigation Systems, 2nd Edition. Myron Kayton nad Wlater R. Fried (Eds.), John Wiley & Sons.

Weill, L. R., June 2003. Multipath mitigation: How good can it get with new signals. GPS World , 106–113.

Woodward, G., Oppermann, I., Talvitie, J., September 1999. Outdoor-indoor temporal and spatial wideband channel model for ISM bands. In: Proceedings of the 50th IEEE Vehicular Technology Conference. pp. 136–140.

Xia, L., 2004. Multipath in GPS navigation and positioning. GPS Solutions 8 (1), 49–50.

Yun, D., Kee, C., 2002. Centimeter accuracy stand-alone indoor navigation system by synchronized pseudolite constellation. In: Proceedings of the 15th International Technical Meeting of the Satellite Division of the Institute of Navigation ION-GPS 2002.

Zahidul, M., Bhuiyan, H., Lohan, E. S., Renfors, M., December 2007. Code tracking algorithms for mitigating multipath effects in fading channels for satellite-based positioning. EURASIP Journal on Advances in Signal Processing (in press) .

Zepernick, H. J., Wysocki, T. A., May 1999. Multipath channel parameters for the indoor radio at 2.4 GHz ISM band. In: Proceedings of the 49th IEEE Vehicular Technology Conference. pp. 190–193.

Appendix A

LOCATA: Additional Data

The following information are related to the Chapter 5.

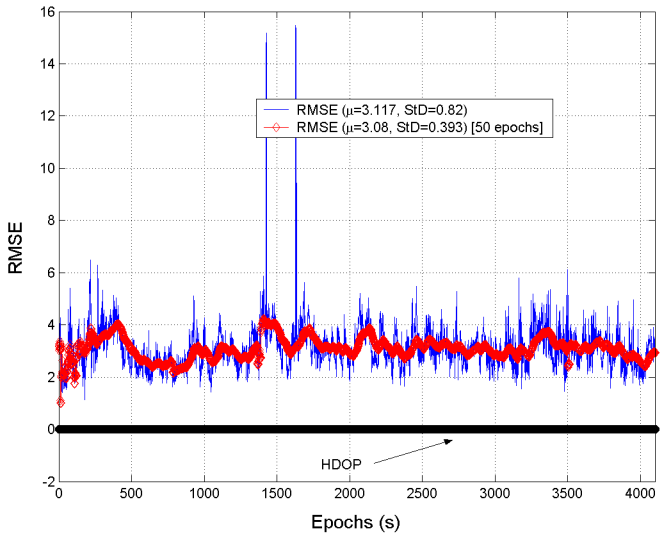


Figure A.1: Accuracy of the rover's position with and without applying a Hatch filter [05 − 04 − 07].

RMSE (m)	DOWNS $05-04-07$	G.G.L1 $26-04-07$	G.G.L2 $28-03-07$	Parking $22-02-07$
LocataLites	8	7	7	5
HDOP/VDOP	0.79/9.39	1.02/4.99	0.79/1.28	1.91/10.95
Epochs	2000	2000	4000	2000
μ	3.070	3.794	4.43	2.594
StD	0.517	1.799	1.285	0.296
μ_E	1.499	2.658	3.412	2.195
StD_E	0.343	1.761	1.186	0.296
μ_N	2.655	1.516	2.741	1.302
StD_N	0.497	1.193	0.886	0.335

Table A.1: Position and coordinates accuracy in metres of the rover using pseudoranges code smoothed with carrier-phase measurements using 10 epochs.

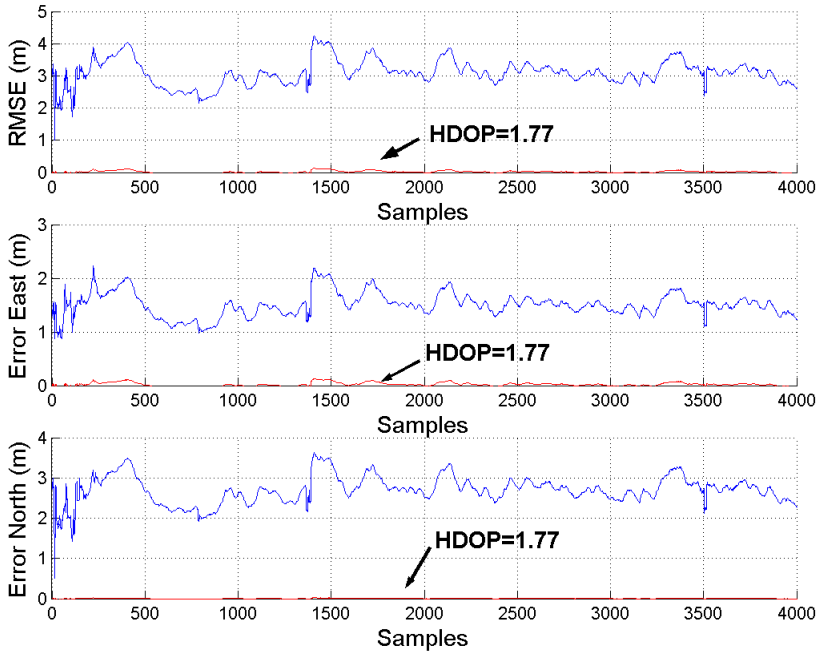


Figure A.2: Accuracy of the rover's position with a Hatch filter (50 epochs).

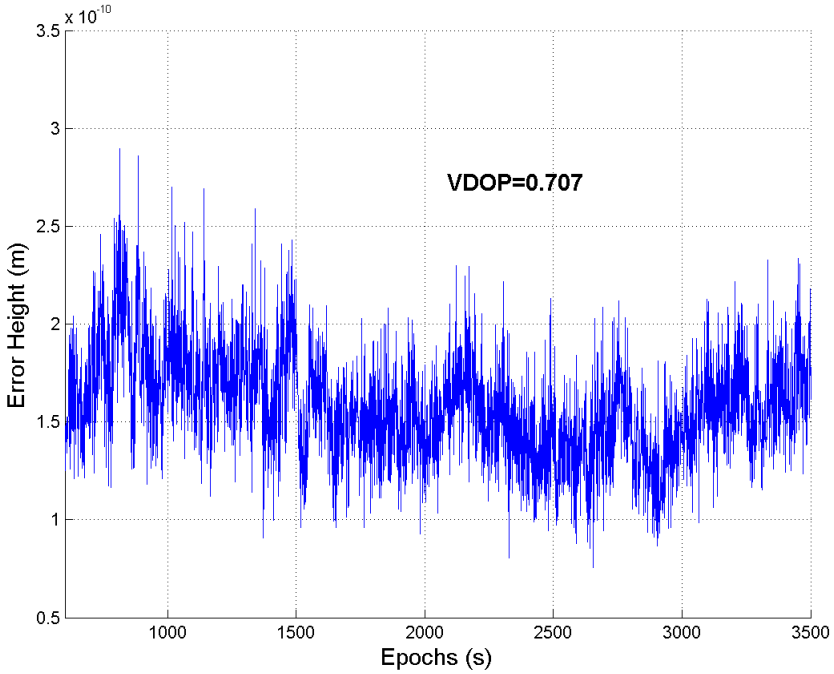


Figure A.3: Height error of the rover's position using carrier-phase measurements [28 – 03 – 07].

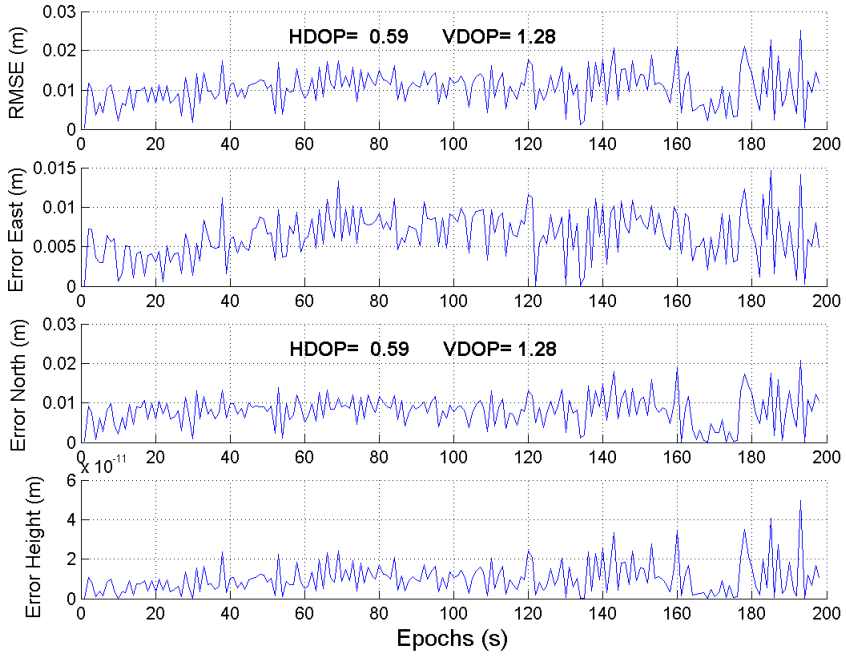


Figure A.4: Time series of the rover accuracy at another test point [28 – 03 – 07].

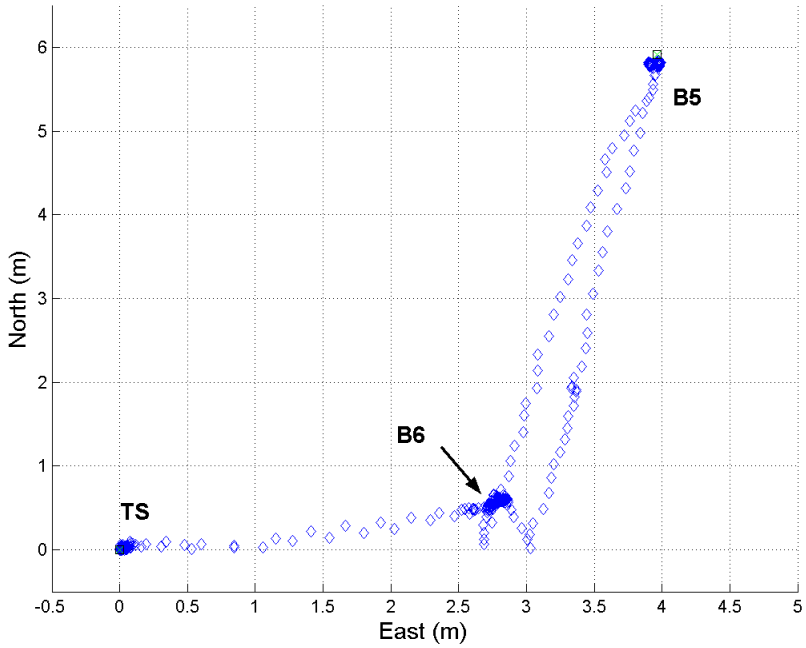


Figure A.5: Kinematic test at the UNSW.

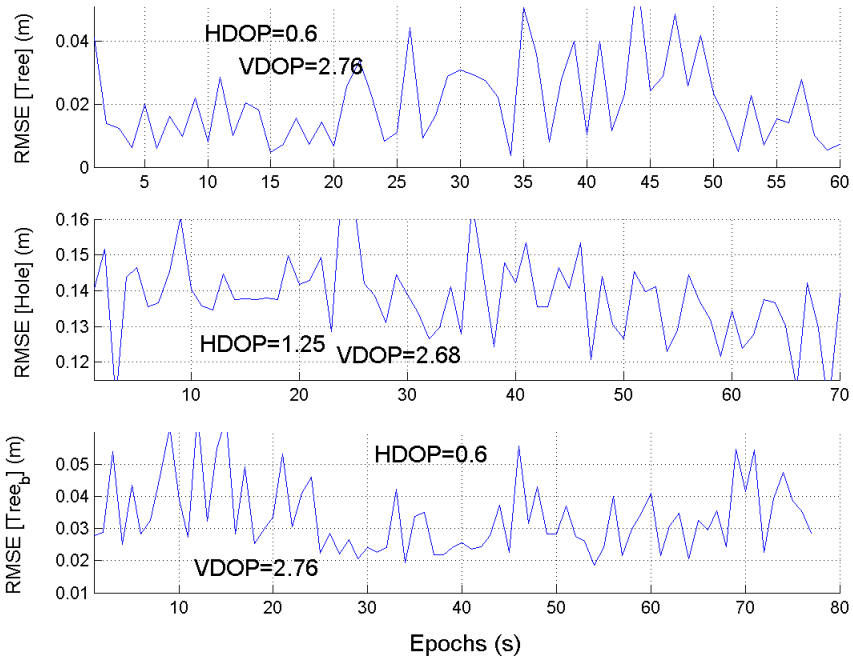


Figure A.6: Accuracy of the kinematic test at the University of Nottingham: the rover moves from *Tree* to *Hole*.

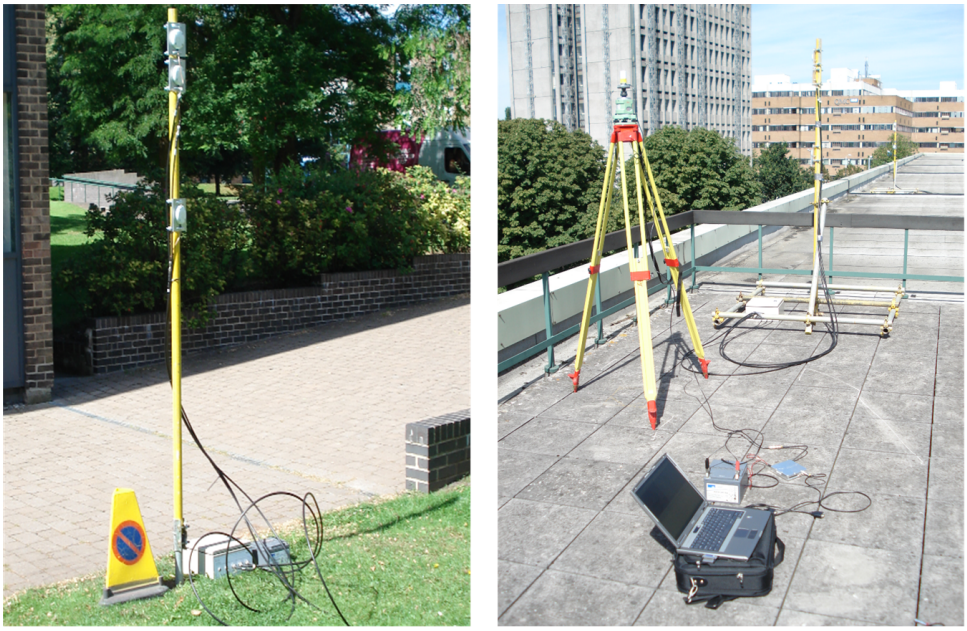


Figure A.7: LocataLites mounted on a metal pole (left), and mounted on the roof (right).

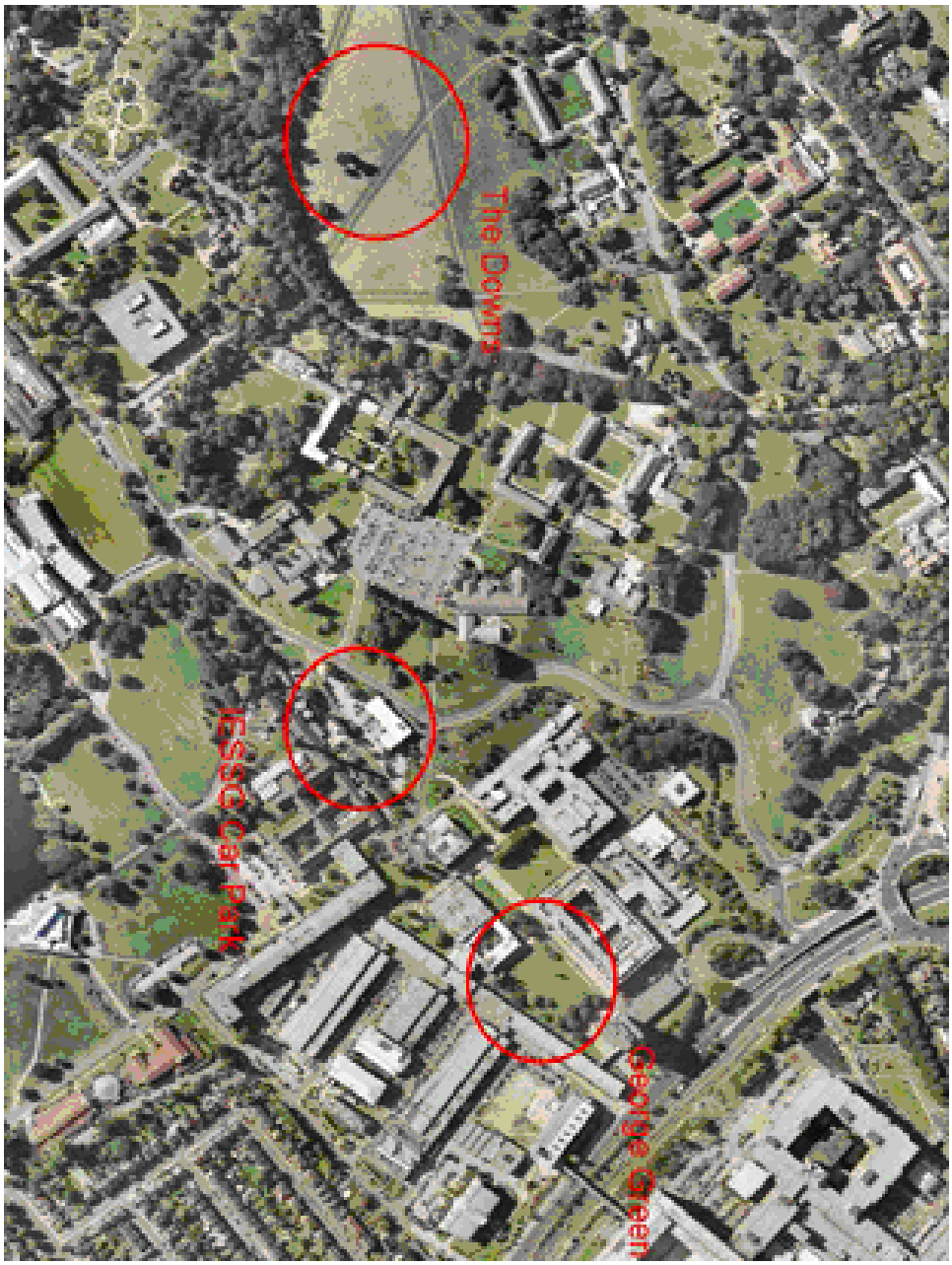


Figure A.8: Overview of the University of Nottingham main campus.

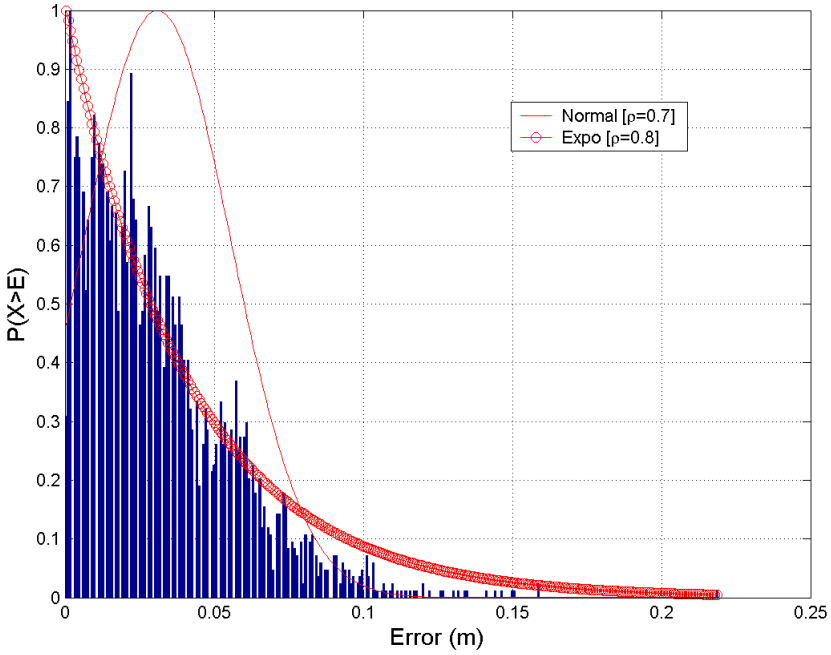


Figure A.9: Histogram of the height error ([05−04−07]) using either the Normal or the Exponential distributions to fit the data.

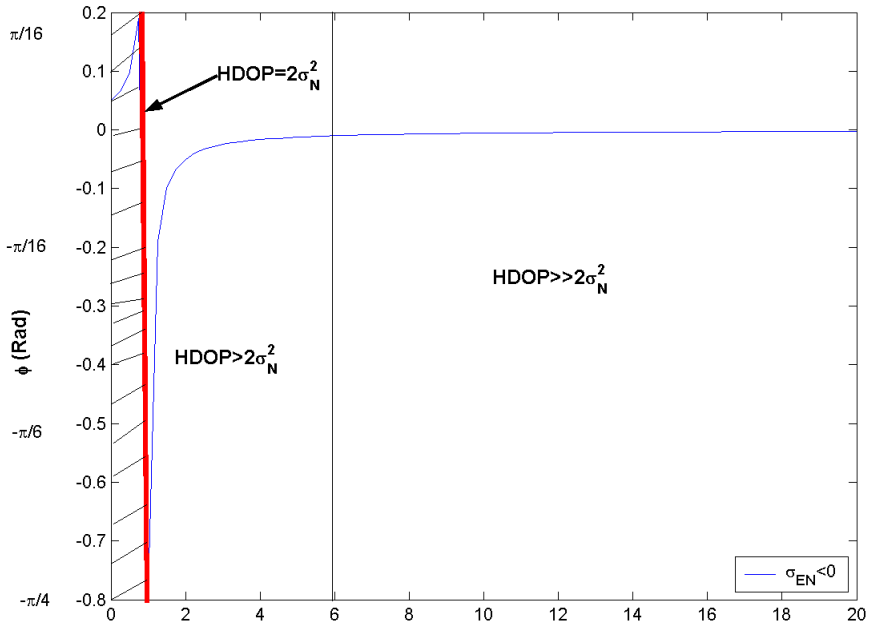


Figure A.10: Another view of the diagram of ellipse angle values shown in Section 6.11.

Appendix B

Matlab Scripts to Extract Data

B.0.1 Master File

File containing the interface to extract the estimated position of the rover from the data file.

File Header.

clear all;

close all;

format long g;

Name of the file containing the estimated position of the rover for a given scenario.

name=$LOG2_05_04_07 - 02.txt$;

Function to extract the estimated position of the rover from the data file.

[Matlla]=processingrover(name);

File containing all the parameters: ref (the reference point to initialise technology), NetworkCoor

GPSRTK03;

ref=GPSlla(2,:);

Mean Error.

[err,errx,erry,errz,MeanErr]=ErrorVector3D(100,Matlla,ref,5000,1);

basestations=NetworkCoordinates;

option=2; $(2 = 2D/3 = 3D)$

ref=GPSlla(end-1,:);

Section to display the results.

figure;

subplot(4,1,1);

hold on;grid on;

plot(err(1:end-op,3));

ylabel('RMSE (m)','FontSize',14);

subplot(4,1,2);

hold on;grid on;

plot((errx(1:end-op,3)));

ylabel('Error East (m)','FontSize',14);

subplot(4,1,3);

hold on;

grid on;

plot((erry(1:end-op,3)));

ylabel('Error North (m)','FontSize',14);

subplot(4,1,4);

hold on;

grid on;

plot((errz(1:end-op,3)));

xlabel('Samples','FontSize',14);

ylabel('Error North (m)','FontSize',14);

B.1 Processing Data File

This MATLAB code extracts the coordinates in ECEF [WGS84] format of the rover from the NMEA str

function [Matlla]=processingrover(file);

fid = fopen(file,'rt');

eof= 0;

k= 1;

```
count=1;
while 1
count=count+1;
line = fgetl(fid);
if (line == −1), eof = 1;break; end;
answer = findstr(line,GPGGA);
if(isempty(answer)== 0)
flag= 0;
i= 1;
while isempty(line)== 0
[delta, line] =strtok(line,',');
if(isempty(str2num(delta))== 0)
if(i== 1)
fg=sscanf(delta,%15f);
HeaderBlock=fg;
elseif(i== 2)
S1=sscanf(delta(1:2),%15f);
S2=sscanf(delta(3:end),%15f);
South=S1+S2/60;
elseif(i== 3)
E1=sscanf(delta(1:3),%15f);
E2=sscanf(delta(4:end),%15f);
East=E1+E2/60;
flag= 1;
elseif(i== 7)
Height=sscanf(delta,%15f);
else
end;
i=i+1;
```

```
end;

end;%While 2

if(flag== 1 && South > 0)
positionf(k,:)=[HeaderBlock,South,East,Height];
k=k+1;
end;

end;

end; %while

fclose(fid);

Coordinates conversion LLA to ECEF

[e1 e2]=find(abs(positionf(:,2))> 0);
Matlla = positionf(e1,:);
```

B.2 Error Function

```
This MATLAB code can calculate the error for the experiments done at the University of Nottingham -
function
[err,errx,erry,errz,MeanErr] =ErrorVector3D(threshold,Matlla,MatRTK2,lines,locataLitestotrack)


Parameters

plot Locatalites solutions
onplot=1;

if(size(Matlla,1)¿lines), Matlla=Matlla(1:lines,:);end;

Latitude, Longitude, height of the estimated points via Locatalites (Nottingham [N,W,H]-¿ mask= [1,-1,1
llh=[Matlla(:,2),-Matlla(:,3),Matlla(:,4)];

Latitude, Longitude, height of the rover position -on TS
llh0=MatRTK2(1,:);
```

Convert llh to E,S,H

denu=dllh2denu(llh0,llh);

Latitude, Longitude, height of the points measured with GPS RTK

llh2=MatRTK2;

Convert llh to E,S,H realpos = dllh2denu(llh0,llh2);

truepoints=size(realpos,1);

numberpoints=size(denu,1);

time=Matlla(:,1);

kk=1;

ji= 1;err= [];errx= [];erry= [];

if(locataLitestotrack> 0 && truepoints>=locataLitestotrack),truepoints= 1;

realpos=realpos(locataLitestotrack,:); onplot= 0; end;

for i = 1:truepoints

for j= 1:numberpoints

Ej=realpos(i,:);

Ei=denu(j,:);

Vect= $(Ej(1) - Ei(1))^2 + (Ej(2) - Ei(2))^2 + (Ej(3) - Ei(3))^2$;

Vectx= $(Ej(1) - Ei(1))^2$;

Vecty= $(Ej(2) - Ei(2))^2$;

Vectz= $(Ej(3) - Ei(3))^2$;

Vect=sqrt(Vect);

Hg(ji)=Vect;

Hgx(ji)=Vectx;

Hgy(ji)=Vecty;

if(Vect<threshold)

err(kk,:)=[i,j,(Vect)];

errx(kk,:)=[i,j,sqrt(Vectx)];

erry(kk,:)=[i,j,sqrt(Vecty)];

errz(kk,:)=[i,j,sqrt(Vectz)];

```
kk=kk+1;
end;
ji=ji+1;
end;
end;
```

Error

```
for l=1:size(err,1)
num=err(1,1);
numel=num;
[e1 e2]=find(err(:,1)>num);
while(isempty(e1)== 0)
num=err(e1(1),1);
[e1 e2]=find(err(:,1)>num);
numel=[numel,num];
end;
end;
```

```
errx(:,2)=time(errx(:,2));
erry(:,2)=time(erry(:,2));
errz(:,2)=time(errz(:,2));
```

```
for jk=1:length(numel)
[f1 f2]=find(err(:,1)==numel(jk));
MeanErr(jk,:)=[numel(jk), mean(err(f1, end)), std(err(f1, end))];
end;
```

labeling

```
label=['TS'];
Result=[];
gh=[];
if(size(MeanErr,1)== 1)
i=locataLitestotrack;
```

num=i;

nume=$(num-2)+num*2$;

lab=label(nume:nume+1);

Result=$[Result,,lab]$;

else

for i=1:size(MeanErr,1)

num=MeanErr(i,1);

nume= $(num-2)+num*2$;

lab=label(nume:nume+1);

Result=$[Result,,lab]$;

end;

end;

Plot Locatalites

if(onplot==1)

hold on;

plot(realpos(:,1),realpos(:,2),$'ok'$);

for i=1:size(MeanErr,1)

plot(realpos(MeanErr(i,1),1),realpos(MeanErr(i,1),2),$'xg'$);

num=MeanErr(i,1);

nume= $(num-2)+num*2$;

lab=label(nume:nume+1);

y=lab;

text(realpos(MeanErr(i,1),1)+0.05,realpos(MeanErr(i,1),2),y);

end;

plot(denu(err(:,2),1),denu(err(:,2),2),$'db'$);

grid on;

else

end;

Appendix C

Example of a LOCATA Rover Setup File

Rover LOG File from the $05-04-07$ experiments

##############

Setting for Locata devices

###

UNIVERSITY DOWNS SMALL SCALE RANGE EXPERIMENT TO HAVE PROOF OF CONCEPT

#

#OMNI ROVER - red

###

DEVICE-TYPE could be MASTER, SLAVE, ROVER

#

#

This is ROVER 02 and it has the Omnidirectional antenna attached

#

#

DEVICE-TYPE = ROVER;

###

Reference PRN

The PRN of the Locata signal that this device will TimeLoc to. Current

♯ valid PRN range is 1-16.

♯

♯

Reference-PRN = 1;

##

♯ Tx PRN

♯ The PRN or PRNs that this device will transmit. For dual transmit function

♯ use a comma to separate values, for example:

Tx-PRN = 3, 4;

♯ The first (reading left to right) PRN specified in the order will be

♯ transmitted via Tx antenna 1. Current valid PRN range is $1 - 16$.

♯

♯

Tx-PRN = 1, 2;

##

♯ Rover coordinates are in format: x, y, z;

♯ Permanent NTF Rover locations without precise orbit corrections

♯ The rover has to be initialized on known coordinates

♯ The rover coordinates will be input before the experiment starts but for

♯ now they are default = 1000000.0000, 1000000.0000, 1000000.0000;

♯

♯rover 01 -total station - sn76

$Rover_Coordinates = 3851141.250, -80647.065, 5066655.297$;

##

♯ Below is an array of coordinates and slot allocation of all devices in the network including Master, Slave

♯ The array index is the PRN for the device.

♯ The coordinates are in format: x, y, z.

♯ The final argument is the slot allocation, given as a bitmask.

♯ currently the max devices is 20.

♯

♯

♯ NOTTINGHAM UNIVERSITY - civil engineering experiment 28/03/07

♯Position 1 - $SN00107$ -Master

Network-Coordinates[1][1] = $3851109.007, -80645.928, 5066685.666, 0x00000007$;

Network-Coordinates[1][2] = $3851108.587, -80645.913, 5066685.110, 0x00000007$;

♯ Position 2 - $SN00096$

Network-Coordinates[2][3] = $3851118.684, -80598.864, 5066682.073, 0x00000038$;

Network-Coordinates[2][4] = $3851118.343, -80598.863, 5066681.625, 0x00000038$;

♯Position 3 - $SN00116$

Network-Coordinates[3][5] = $3851145.744, -80581.389, 5066664.455, 0x000001C0$;

Network-Coordinates[3][6] = $3851145.398, -80581.382, 5066663.980, 0x000001C0$;

♯Position 4 - $SN00094$

Network-Coordinates[4][7] = $3851176.634, -80575.022, 5066644.362, 0x00000E00$;

Network-Coordinates[4][8] = $3851176.180, -80575.013, 5066643.757, 0x00000E00$;

♯Position 5 - $SN00060$

Network-Coordinates[5][9] = $3851196.714, -80650.203, 5066628.434, 0x00007000$;

Network-Coordinates[5][10] = $3851196.286, -80650.189, 5066627.871, 0x00007000$;

♯Position 6 - $SN00071$

Network-Coordinates[6][11] = $3851181.160, -80684.838, 5066634.370, 0x00038000$;

Network-Coordinates[6][12] = $3851180.740, -80684.829, 5066633.833, 0x00038000$;

♯Position 7 - $SN000100$

Network-Coordinates[7][13] = $3851150.409, -80720.841, 5066651.223, 0x001C0000$;

Network-Coordinates[7][14] = $3851150.000, -80720.836, 5066650.675, 0x001C0000$;

♯Position 8 - $SN00085$

Network-Coordinates[8][15] = $3851124.248, -80697.352, 5066669.861, 0x00E00000$;

Network-Coordinates[8][16] = $3851123.771, -80697.346, 5066669.248, 0x00E00000$;

♯False Position 9 - Point 4 on IESSG -not used

Network-Coordinates[9][17] $= 3851173.1033, -80153.7125, 5066647.9356, 0x07000000;$

Network-Coordinates[9][18] $= 3851173.1033, -80153.7125, 5066647.9356, 0x07000000;$

♯False Position 10 - Point 4 on IESSG - not used

Network-Coordinates[10][19] $= 3851173.1033, -80153.7125, 5066647.9356, 0x38000000;$

Network-Coordinates[10][20] $= 3851173.1033, -80153.7125, 5066647.9356, 0x38000000;$

♯♯

♯ Slot mask values:

♯ There are 30 slots total that can be allocated to the LLs. Overlapping

♯ allocations are not advised. Each bit in the slot mask represents a slot.

♯ A value of 1 means the slot is allocated for that LL. A value of 0 means it is

♯ not allocated for that LL. The least significant bit of the slot mask

♯ represents slot 0. The most significant two bits are unused. The slot mask is

♯ given as a hexadecimal value.

♯

♯ Note: When allocating slots to each LL, as a minimum please use contiguous slots

♯ of 3.

♯

♯ Example 1: Example 2:

♯ Network of 5 devices (20

♯ 1. $0x0000003f$, 1. $0x00000007$,

♯ 2. $0x00000fc0$, 2. $0x00000038$,

♯ 3. $0x0003f000$, 3. $0x000001C0$,

♯ 4. $0x00fc0000$, 4. $0x00000E00$,

♯ 5. $0x3f000000$, 5. $0x00007000$,

♯ 6. $0x00038000$,

♯ 7. $0x001C0000$,

♯ 8. $0x00E00000$,

♯ 9. $0x07000000$,

```
# 10. 0x38000000
#

##############################################################################
# Below set the tlsat-params.TXPwrInit, TXPwrL, TxPwrHigh in order
# TXPower-Setting = 0x0100, 0, 0x3fff;
#
TXPower-Setting = 0x0100, 0, 0x3fff;

##############################################################################
# Below set the vga-hi, vga-lo, lna-select in order
# vga-hi and vga-lo ranges from 0 to 13, convert to vga gain settings from −10 to +29
# lna is off when lna-select is 0, vice versa. OxA = +20dBm
#
TXVGA-LNA-Setting = 0x0, 0x0, 1;

##############################################################################
# Specify the initial time and data in the following format:
# Date = YYYY/MM/DD, and
# Time = HH:MM:SS.
#
Date = 2007/03/22;
Time = 11 : 30 : 00;

##############################################################################
# Timeloc threshold in seconds.
# fcode-lock-threshold = 0.000000005;

##############################################################################
# Measurement rate in Hz.
#
# Only the following values are valid:
#
```

♯ 50.0 (for 50 Hz)

♯ 25.0 (for 25 Hz)

♯ 20.0 (for 20 Hz)

♯ 10.0 (for 10 Hz)

♯ 5.0 (for 5 Hz)

♯ 2.5 (for 2.5 Hz)

♯ 2.0 (for 2 Hz)

♯ 1.0 (for 1 Hz)

♯

♯

♯ Note: If no value is specified or the value is invalid the default output

♯ rate of 2.5 Hz for ROVER and MASTER, will be used. SLAVE will always use 50 Hz

♯ measurements and will ignore this field.

♯

♯ Note: Nav will run at same rate as measurement rate unless the rate is

♯ higher than 2.5 Hz. Nav's maximum execution rate is currently 2.5 Hz and it

♯ will be limited to run at this rate if a higher measurement rate is selected.

♯ Measurements will still be computed and output at the higher rate.

♯

Meas-Rate = 2.0;

♯♯

♯ Data output rate in Hz.

♯

♯ Determined by using a multiple of the measurement period. If a rate higher

♯ than the measurement rate is selected, data will be output at the measurement

♯ rate.

♯

♯ At higher rates, the number of channels for which channel data and measurements

♯ are output is restricted to fit the $RS232$ bandwidth. In such cases, only

```
# the first X channels worth of data is output, as specified below.
#
# Only the following values are valid:
#
# 50.0 (for 50 Hz, 5 channel output)
# 25.0 (for 25 Hz, 10 channel output)
# 20.0 (for 20 Hz, 10 channel output)
# 10.0 (for 10 Hz, 15 channel output)
# 5.0 (for 5 Hz, 15 channel output)
# 2.5 (for 2.5 Hz, 20 channel output)
# 2.0 (for 2 Hz, 20 channel output)
# 1.0 (for 1 Hz, 20 channel output)
# 0.50 (for every 2 seconds, 20 channel output)
# 0.10 (for every 10 seconds, 20 channel output)
# 0.03333 (for every 30 seconds, 20 channel output)
# 0.01667 (for every 60 seconds, 20 channel output)
#
#
# Note: If no value is specified or the value is invalid the default output
# rate of 2.5 Hz will be used for the ROVER, SLAVE and MASTER.
#
Data-Output-Rate = 2.0;

# Use smoothed Psudo range or not
Smooth-PR = on;

# Max iterations for navigation solution
Max-Iterations = 5;

##############################################################################
# Hatch Filter Characteristics
#
```

```
♯ Hatch Filter iterations (in measurement counts).
Smooth-Period = 50;
♯
♯ Cycle Slip Detection Threshold (in metres)
Slip-Threshold = 200.0;

##############################################################################
♯ Select the on-board nav solution type.
♯ Only the following values are valid:
♯ 0 WEIRD-MODE (default) same as pseudorange only but with no pseudorange
smoothing
♯ 1 PR-NAV pseudorange only
♯ 2 CP-KPT carrier initialized from known pt
♯ 3 CP-OTF carrier initalized from code solution
♯ Note: If no value is specified or the value is invalid the default
♯ solution type used will be a code solution.
♯
Nav-Solution-Type = 2;

##############################################################################
♯ Tx & Rx antenna offset
♯ Specify any offset (in meters) between the transmit and receive antennas.
♯ Any offset that is not accounted for in this field will result in a range
♯ bias in pseudo-range measurements to this device.
♯
Tx-Rx-Offset = 0.2;

##############################################################################
♯ Tropospheric Correction
♯ (in meters)
♯
Tropo-offset = 0;
```

```
♯Convergence Threshold of the position solutions (carrier and code)
CP-Convergence-Limit = 0.05;
PR-Convergence-Limit = 1.0;

♯ Test Mode
♯ Valid values:
♯ None
♯ Loopback
♯ Simulation
♯ Replay
test-mode = None;
♯
♯ In Replay mode, you also need these two:
♯ replay-file-name = data.txt;
♯ channels-dumped = 20;

♯ The following set the UART ports connection
♯ We define some virtual ports in receiver SW
♯ the defined virtual ports is as below:
♯ gps-receiver, leica box, user, NMEA, debug-dump
♯ each virtual port stand for certain function output
♯ in receiver SW.
♯ two application setting example given here:
♯ If we use as before:
♯ Port2-out = NMEA;
♯ Port1-in = user;
♯ Port1-out = debug-dump;
♯ note: we don't need to define the connection of Port2-in
♯ because we don't use it here.
♯ If we use it to work with Leica:
♯ Port2-in = gps-receiver;
♯ Port2-out = leica-box;
```

♯ Port1-in = user;

♯ Port1-out = NMEA;

Port2-in = gps-receiver;

Port2-out = NMEA;

Port1-in = user;

Port1-out = debug-dump;

♯Enable position logging, set Position-Log to ON, or set Position-Log to OFF

Position-Log = OFF;

♯Enable measurement logging, set Measurement-Log to ON, or set Measurement-Log to OFF

Measurement-Log = ON;

♯Enable incoming message logging, set Message-Log to ON, or set Message-Log to OFF

Message-Log = OFF;

♯Choose to log all message or only the last message

♯option includes: all, last

Msg-log-option = last;

♯below are settings related to Leica message

♯used to determing if the message includes valid position or not

♯Pls refer to the Leica owi message specs

♯Which message GPS receiver output

♯possible types are: POS, TPV, GGA

Input-Msg-type = 4 TPV;

♯possible types are: POS, TPV, NMEA

Output-Msg-type = NMEA;

♯Latency in milliseconds (less than)

♯Ms-Latency = 400;

Msg-Latency = 1000;

♯Initialise Locata Solution from GPS after this many integer seconds
initialise-ambs-after = 10;

♯ >= 99.0%
Confidence = 7;

♯ number of succussful searches completed less than
Num-Searched = 11;

♯ Solution type of Incoming TPV Message considered Valid
Msg-Solution-Type = 254;

♯ Quality of latitude (less than) in meters
♯lat-quality = 0.05;
lat-quality = 0.10;

♯ Quality of longtitude (less than) in meters
♯lon-quality = 0.05;
lon-quality = 0.10;

♯ QUality of height (less than) in meters
♯ height-quality = 0.05;
height-quality = 0.10;

♯ Speed over ground less than in knots
Sog = 0.5;

♯ HDOP less than
HDOP = 5;

♯ TDOP less than
TDOP = 5;

♯ VDOP less than

VDOP = 5;

♯ Number satellites in Pos Computation more than

sats-used = 4;

♯♯♯

♯

♯ Nav configuration

♯

♯♯♯

♯ simplified, or venetia

nav-controller-type = venetia;

♯ none (default), simple-selector, averaged, or weighted.

measurement-combiner-type = averaged;

♯ 3*D* Constraining

NavSolver-MaxPDOP = 20.0;

NavSolver-Max3DVDOP = 1.0;

VerticalWeighting-Mode = fixed; ♯ dynamic (default) or fixed

VerticalWeighting-VDOPThreshold = 50.0; ♯ VDOP at which weighting is applied

VerticalWeighting-FixedModeWeighting = 1.0; ♯ Ignored if mode is dynamic.

♯ Venetia Nav Controller parameters

nav-initialization-timeout = 60;

♯65535;

max-stored-position-divergence = 10.0;

♯Apply either static lever arm correction or dynamic correction

♯LeverArmCorrectionMode could be: static or dynamic

ExternalGps-LeverArmCorrectionMode = static;

♯If LeverArmCorrectionMode is static, correction is in NED format

ExternalGps-StaticLevelArmCorrection = 0.00, 0.00, 0.00;

```
##############################################################################
#
# Measurement configuration
#
##############################################################################

# PLL Scheme
# 0 1ms 2nd order PLL without slip detect
# 1 1ms 3rd order PLL
# 2 2ms 2nd order PLL
# 3 1ms 2nd order PLL with phase extendor with slip detect
# 4 1ms 2nd order PLL with phase extender without slip detect
# 5 1ms 2nd order PLL with SD and BB cycle slip detection
# 6 1ms adaptive 2nd order PLL with SD & BB cycle slip detection (DO NOT USE!)
# 7 1ms 3rd order PLL with SD and BB cycle slip detection (DO NOT USE!)
PLL-Scheme = 4;

# Low correlation power counter threshold used to determine when to count low power
events
# Value is in dB but converted internally to an integer (default is 3.0 dB).
LowCorrelationPowerCounterThreshold = 3.0;

# Absolute low correlation power counter threshold used to determine when to count
absolute
# low power events. Value is in the same units as I and Q. (Default is 50);
AbsoluteLowCorrelationPowerCounterThreshold = 50;

# High phase counter threshold is used to determine when to count high phase events
# Value is in degrees (default is 70.0 degrees).
HighPhaseCounterThreshold = 70.0;

# Metric used in cycle slip detection.
#
```

♯ An instantaneous phase error is compared against the current filtered phase error. If
♯ the difference is greater than the threshold specified in HighPhaseJumpThreshold, a
♯ counter will be incremented.
♯
♯ The cycle slip detection logic will then compare the counter level against the
♯ value specified in CycleSlipDetector-MaxHighPhaseJumpCount.
♯
♯ Value is to be specified in degrees. Default value is 40.0
♯
HighPhaseJumpThreshold = 39.0;

♯ Coefficient used for filtering phase.
♯ The value is used like this:
♯
♯ fphase-error + = iSAR(phase-error − fphase-error + (1 <<(FilteredPhaseCoefficient − 1)), FilteredPhaseCoefficient);
♯
♯ where:
♯ iSAR is the integer shift arithmetic right
♯ phase-error is the current phase error
♯ fphase-error − filtered phase error
♯
♯ Typical values:
♯ ∗8 - default
♯ ∗2 - when used by the high phase jump counter cycle slip metric
♯ ∗10 - when used for the block phase shift auto millisecond dump trigger.
♯
FilteredPhaseCoefficient = 2;

♯ Block phase shift detect threshold

```
♯
♯ Block phase shifts have been observed in low data rate captures. It appears that
the
♯ tracking phase shifts by up to 5-10 degrees for large chunks of time. To see data
♯ at a higher rate, a ms dump will be triggered when the filtered phase error
♯ exceeds this limit.
♯
♯ Specify in degrees. Default is 10.0 degrees.
♯
FilteredPhaseMaxThreshold = 9.0;

♯ Synchronize receiver to network time by slewing the measurement timer. Will
♯ induce a jump in the ICP measurements that is common across all channels
♯ for every timer correction. This will not affect the nav solution.
♯
♯ Select: ON or OFF (default).
♯
SyncToNetworkTime = ON;

♯ AutoDumpTrigger sources
♯
♯ Automatically triggers a 1ms dump when a particular condition is encountered.
♯
♯ Format: Bitmask. Each bit in the range represents a trigger source. A value
♯ of 1 means the trigger source is enabled. A value of 0 means disabled.
♯
♯ Bit 0 (LSB): Filtered ICP difference over the timeloc loss of lock threshold (0.25
cycle)
♯ Bit 1 : High phase push encountered in PLL. When the PLL detects a phase
♯ error greater than the threshold specified in the HighPhaseCounterThreshold
♯ parameter, it increments a counter. When this count value breaches the
♯ threshold specified in the CycleSlipDetector-MaxHighPhaseCount parameter,
```

♯ the $1ms$ dump is triggered.
♯ Bit 2 : Block phase shift. When the filtered phase error gets pushed past the specifed
♯ limit in FilteredPhaseMaxThreshold. The phase error must be filtered heavily
♯ so that phase spikes don't trigger the dump. A FilteredPhaseCoefficient of
♯ 10 is recommended.
♯
♯ Example 1) a value of $AutoDumpTrigger = 0x3$
♯ represents $0b11$ in binary, which means bits 0 and 1 are set. This means both the
♯ Filtered ICP difference and High phase push triggers are enabled.
♯ Example 2) a value of $AutoDumpTrigger = 0x0$
♯ represents 0b00 in binary, which means bits 0 and 1 are clear. This means both the
♯ Filtered ICP difference and High phase push triggers are disabled. (default)
♯
♯ !!!!!WARNING!!!!!
♯ The '0x' infront of the number must be present if specifying the
♯ bitmask in hex, otherwise the parser will interpret the value as a decimal.
♯
$AutoDumpTrigger = 0x0$;

♯ SNR Tweaking Parameters (Temporary Hopefully)
snr-power-filter-coefficient = 1;
snr-noise-filter-coefficient = 12;

Phase-Error-Threshold = 45.0;
Phase-Error-Filter-p1 = 2;
Phase-Error-Filter-p2 = 6;

♯ Carrier Tracking Loop Coasting. If your correlation power is below AbsoluteLow-CorrelationPowerCounterThreshold
♯ there is no value in updating your Carrier Tracking Loop. Set this value to "ON" if you want this
♯ behaviour, "OFF" otherwise.

```
CarrierTrackingLoop-Coasting = ON;

##############################################################################
#
# Signal Quality
#
##############################################################################

SignalQuality-MaxIcpDeltaDiff = 0.3333333333;
SignalQuality-MaxLowPowerCount = 20;
SignalQuality-MaxHighPhaseCount = 501;
SignalQuality-MinSnr = 0.0;
SignalQuality-MaxAbsLowPowerCount = 20;
SignalQuality-MaxPrIcpDeltaDiff = 4.0;
SignalQuality-ReadyToPutIntoSolutionAfter = 3;
```

Appendix D

Additional Information for the Chapter 7

This section is related to the explanations given in Chapter 7.

$22-08-07$	Mid	ROV01	Grass01	Grass02	Tree	Hole
Epochs	750	750	750	750	750	750
VDOP/HDOP	5.23/1.15	5.54/1.42	3.69/0.75	3.46/0.91	4.67/0.91	7.62/2.69
Number of Jumps $[Et\|E\|N\|H]$	[2|2|2|2]	[5|2|3|5]	[5|5|3|5]	[4|3|3|3]	[2|1]|2|2	[3|1|1|3]
μ	0.065	0.396	0.171	0.103	0.142	0.313
StD	0.045	0.230	0.123	0.078	0.150	0.210
μ_E	0.015	0.057	0.051	0.036	0.008	0.062
StD_E	0.010	0.038	0.043	0.025	0.006	0.064
μ_N	0.008	0.008	0.026	0.024	0.005	0.094
StD_N	0.008	0.008	0.029	0.018	0.004	0.083
μ_H	0.061	0.390	0.150	0.086	0.140	0.280
StD_H	0.046	0.230	0.120	0.081	0.151	0.195

Table D.1: Position error in metres of the Rover in Wi-Fi area

WiFi Channels	Before 22/08/2007	After 22/08/07
t2-d2	1	6
t2-b2	1	6
t2-d2	1	11
t2-b4	1	6
Cmb	1	6

Table D.2: Channel number of the WiFi access points.

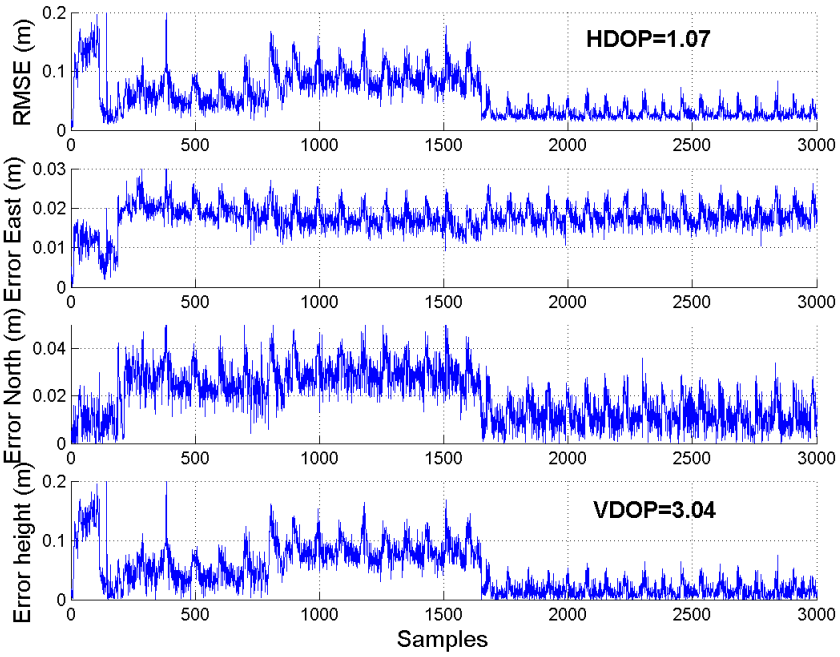


Figure D.1: Wi-Fi interference recorded at Hole [10 – 08 – 07].

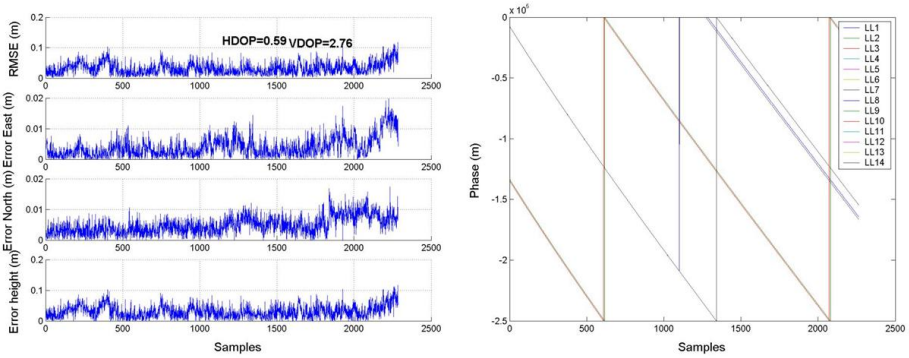


Figure D.2: Comparaison between the accuracy of the rover position and the rollover on the carrier-phase measurements $[15-08-07]$.

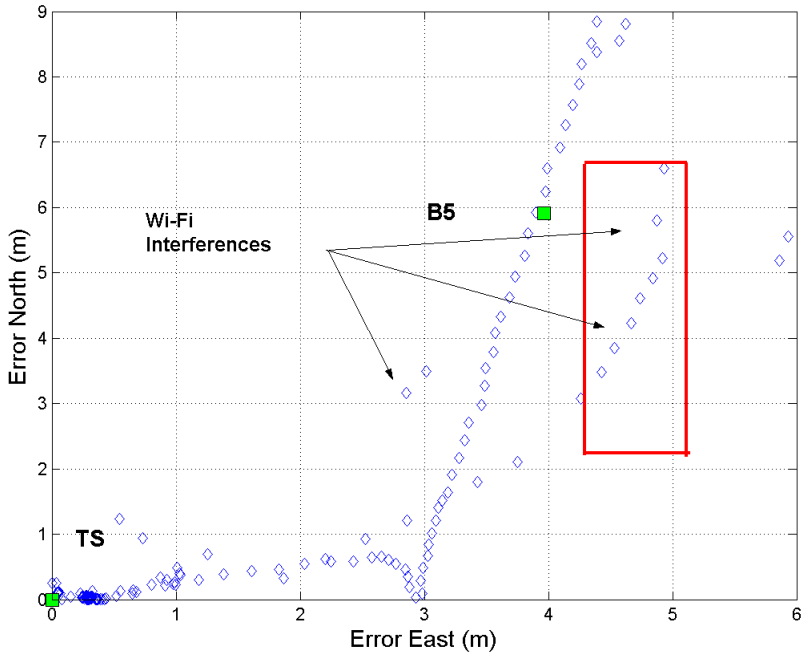


Figure D.3: Wi-Fi interference during kinematic measurements [Australia].

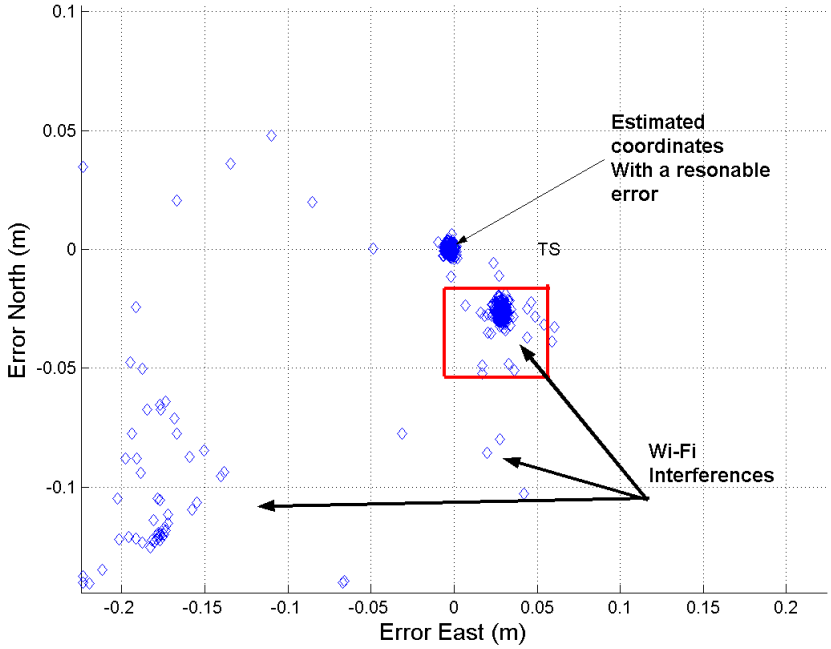


Figure D.4: Wi-Fi interference during kinematics measurements [05 – 04 – 07].

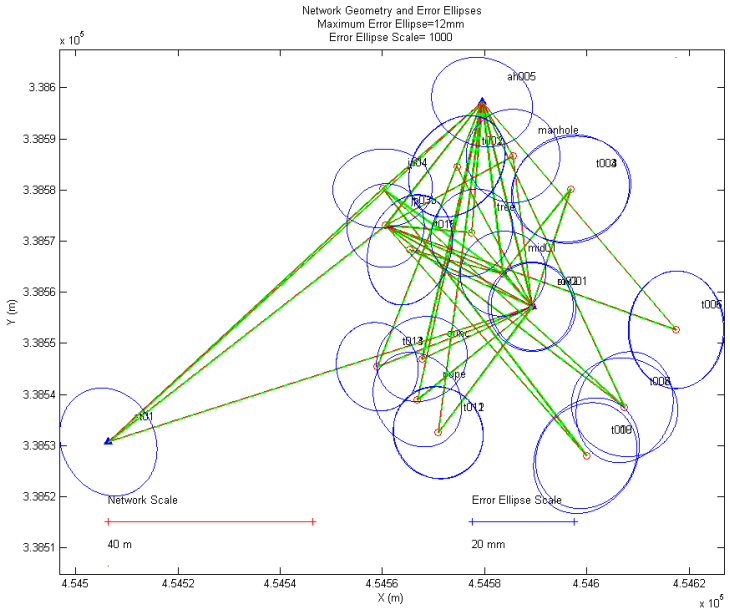


Figure D.5: Network of points measured using the CUPT technique.

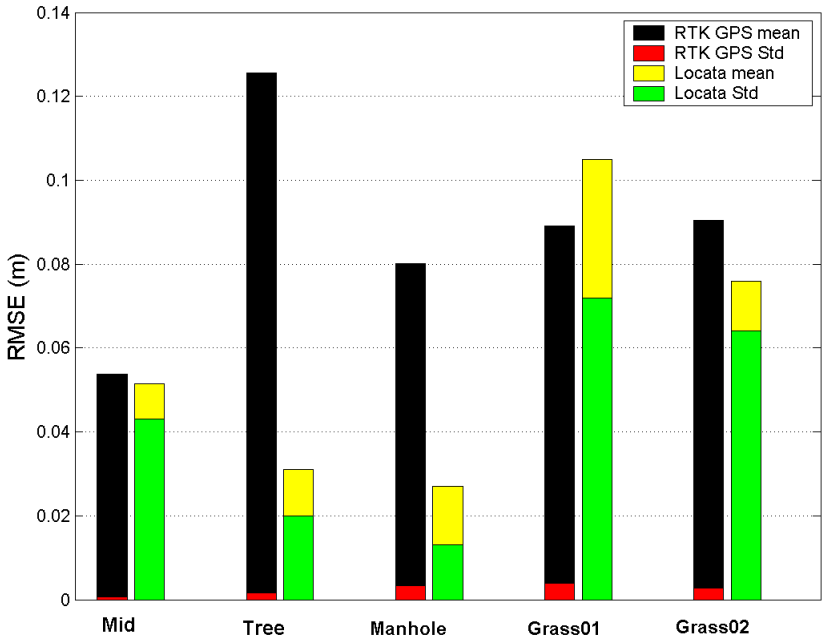


Figure D.6: Comparison of RTK GPS and LOCATA accuracy done the $[01-11-07]$.

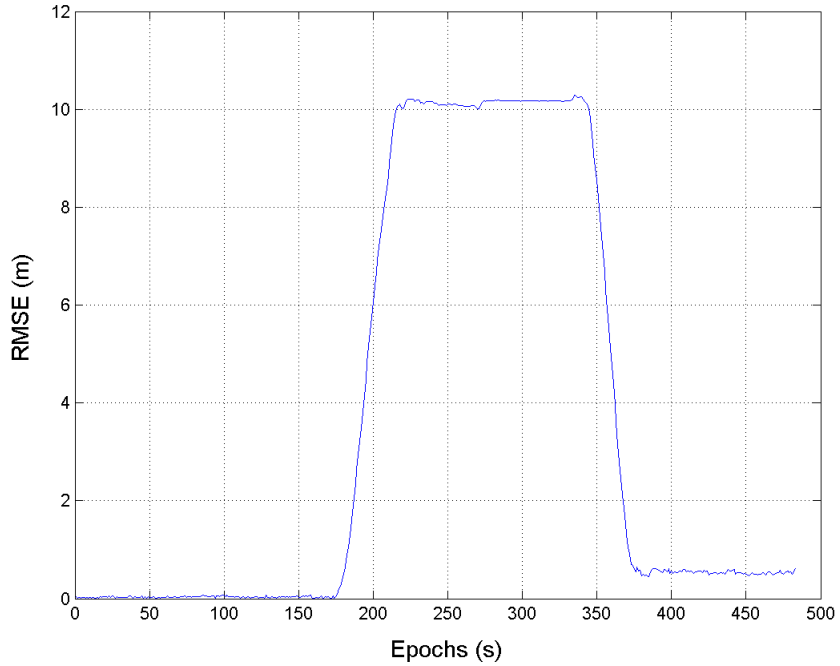


Figure D.7: The track followed by the rover during the experiments $[30-0807]$ starting at *Tree*.

$30-08-07$ Tree	Loc	R. $0.1 < x < 1$	R. $x > 0.3$	$\frac{\delta^2}{dt^2}\phi_i$ or SNR $= 0$	Comments
	1	293	20	88/0	$\rho = 0.66$ — t=[-0.4,0.4]
	2	319	49	30/33	$\rho = 0.68$ — t=[-0.4,0.4]
	3	413	96	25/57	$\rho = 0.81$ — t=[-4,4]
	4	382	69	63/0	$\rho = 0.92$ — t=[-4,4]
	5	**418**	90	42/45	$\rho = 0.73$ — t=[-0.8,0.8]
	6	**402**	68	52/57	$\rho = 0.59$ — t=[-0.5,0.5]
	7	**469**	165	40/45	$\rho = 0.89$ — t=[-2,2]
	8	**473**	177	27/33	$\rho = 0.93$ — t=[-2,2]
	9	**408**	92	30/33	$\rho = 0.71$ — t=[-0.6,0.6]
	10	**452**	124	28/41	$\rho = 0.82$ — t=[-0.8,0.8]
	11	380	70	20/33	$\rho = 0.74$ — t=[-0.4,0.4]
	12	426	118	18/22	$\rho = 0.72$ — t=[-0.4,0.4]
	13	417	90	21/23	$\rho = 0.94$ — t=[-1.5,1.5]
	14	414	92	15/33	$\rho = 0.94$ — t=[-1.5,1.5]
	15	395	97	29/33	$\rho = 0.75$ — t=[-0.6,0.6]
	16	377	56	28/33	$\rho = 0.70$ — t=[-0.5,0.5]

Table D.3: Characteristics of the LOCATA signal [$t = 1355$].

$30-08-07$ Mid	Loc	R. $0.1 < x < 1$	R. $x > 0.3$	$\frac{\delta^2}{dt^2}\phi_i$ SNR $= 0$	Comments
	1	190	9	42/0	$\rho = 0.85$ — t=[-0.4,0.4]
	2	220	29	0/0	$\rho = 0.83$ — t=[-0.4,0.5]
	3	245	44	1/0	$\rho = 0.80$ — t=[-0.5,0.5]
	4	229	27	39/0	$\rho = 0.83$ — t=[-0.6,0.6]
	5	**287**	65	0/3	$\rho = 0.94$ — t=[-1.5,1.5]
	6	**288**	65	1/0	$\rho = 0.93$ — t=[-2,2]
	7	**302**	105	0/0	$\rho = 0.92$ — t=[-1.5,1.5]
	8	**330**	128	2/29	$\rho = 0.88$ — t=[-4,4]
	9	**263**	55	0/1	$\rho = 0.77$ — t=[-0.6,0.6]
	10	**277**	55	2/0	$\rho = 0.80$ — t=[-0.6,0.6]
	11	251	49	2/0	$\rho = 0.80$ — t=[-0.6,0.6]
	12	247	42	1/0	$\rho = 0.80$ — t=[-0.6,0.6]
	13	236	40	0/0	$\rho = 0.81$ — t=[-0.6,0.6]
	14	233	41	1/0	$\rho = 0.78$ — t=[-0.5,0.5]
	15	241	49	0/0	$\rho = 0.76$ — t=[-0.5,0.5]
	16	256	0	0/0	$\rho = 0.84$ — t=[-4,4]

Table D.4: Characteristics of the LOCATA signal [$t = 910$].

Appendix E

Additional Information for the Chapter 8

This section is related to the explanations given in Chapter 8.

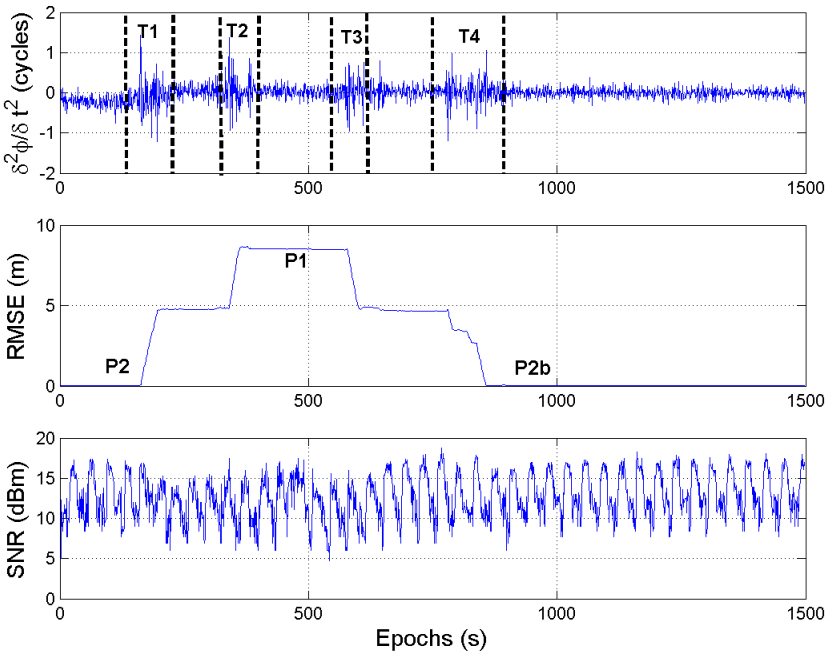


Figure E.1: Double difference of the carrier-phase signal from the LocataLite 6 during the test trial $[14-02-08]$.



Figure E.2: LocataLites during the measurements in the construction site [14 – 02 – 08].

Appendix F

Paper Accepted to the IeCCS Conference

This paper has been published in the International e-Conference of Computer Science (International electronic Conference on Computer Science-IeCCS2007).

Title: **Super – Resolution Algorithm in Cumulative Virtual Blanking** (J-P. Montillet, X. Meng, G.W. Roberts, M.S. Woolfson)

F.0.1 Abstract

The proliferation of mobile devices and the emergence of wireless location-based services have generated consumer demand for precise location. In this paper, the MUSIC super-resolution algorithm is applied to time delay estimation for positioning purposes in cellular networks. The goal is to position a Mobile Station with UMTS technology. The problem of Base-Stations herability is solved using Cumulative Virtual Blanking. A simple simulator is presented using DS-SS signal. The results show that MUSIC algorithm improves the time delay estimation in both the cases whether or not was CVB.

F.0.2 Introduction

In cellular radio system, accurate location estimates widen the range of possible applications. The Location Based Services market is on demand of accurate location of the mobile users. The range of applications starts from the emergency calls location to the governmental users tracking.

Direct Sequences - Spread Spectrum (DS-SS) is a common technique for ranges estimates in cellular networks. In traditional systems, the arriving signal is correlated with the original Pseudo-Noise (PN) sequence to determine the range estimates. This process is also called time delay estimation and is only effective when multipath components are well separated or when only one component is present in the received signal. To overcome this problem the so called super-resolution algorithm may be used.

A number of super-resolution techniques that can separate closely-spaced multipath components have been developed such as root multiple signal classification (MUSIC). It was first developed using Direction-of-Arrival estimation in multiple-emitters location scenario [Schmidt (1986)]. More recently, authors suggest to apply them to multiple transmitters-single receiver cases dividing the received signal in sub vectors via a sliding window. While super-resolution techniques can increase time-domain resolution, it also increases complexity of system implementation [Li and Pahlavan (2004)].

Another problem is the node herability, or in other words, the interferences occurring at a Mobile Station (MS) for listening to several Base Stations (BSs). Cambridge Positioning System has developed a software process called Cumulative Virtual Blanking (CVB) which removes the interferences from the brightest signal. This technique avoids the need of implementing Idle Period Down Link (IP-DL) in the traffic management of the cellular network; and then it avoids all the problems of congestion network [Duffett-Smith and Macnaughtan (2002)].

In this paper the MUSIC super-resolution algorithm is applied to a matched-filter output in the presence of multiple signals received in a multi-users scenario. The performances of the MUSIC algorithm are analysed in terms of error on the time-

delay estimation. The first part explains the CVB. The second part will review the MUSIC algorithm. The third part shows the results given by the simulations; and a conclusion ends the letter.

F.0.3 CVB

The Cumulative Virtual Blanking (CVB) is a technique which removes stronger BSs interferers. The overview of the problem is shown in Figure F.1. It is an alternative

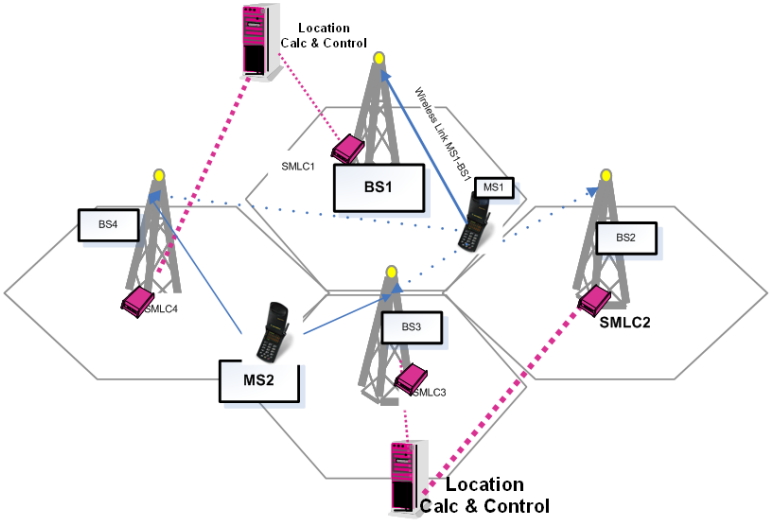


Figure F.1: Localisation Scenario in Cellular Networks

technique of using Idle Period-Down Link (IP-DL) developed by [Duffett-Smith and Macnaughtan (2002)].

The Serving Mobile Location Centers (SMLC) will record the snapshots from each BSs and the MS will send the snapshot of the received signal to the Location and Calculation Servers (*Loc.* & *Calc.*). Then, when the Location and Calculation server has received all the data, it will process the co-incident snapshots from the MS and each relevant BSs by successively cross-correlating the MS snapshot with the BSs snapshots and removing the strongest BS signal from the MS signal by estimation and subtraction. After this pre-processing, the time delay between each BS and the MS is calculated and then the position of the MS can be triangulated.

F.0.4 MUSIC Algorithm

A comprehensive definition of the MUSIC algorithm is given in [Manolakis et al. (2005)]. The MUSIC algorithm is applied at the output of the matched-filter, the output is discretised as $\mathbf{x} = [\mathbf{X}(1)\mathbf{X}(2)...\mathbf{X}(N)]^T$ in the frequency domain at frequency point $f = 1, ..., N$. Then, the vector $\mathbf{x}$ is divided into M smaller vectors.

$$\mathbf{Y}_f = [\mathbf{X}(f)...\mathbf{X}(f+m-1)]^T(m \times 1) \tag{F.1}$$

Where $M = N - m + 1$ and $p < m < N$. Let define the correlation matrix $\mathbf{R_y} = E\{\mathbf{YY}^H\}$ $[(m \times m)]$. H is the Hermitian symmetric. The correlation matrix can also be written in terms of its eigen decomposition

$$\mathbf{R_y} = \sum_{i=1}^{m} \lambda_i \mathbf{q_i} \mathbf{q_i^H} = \mathbf{Q\Lambda Q}^H \tag{F.2}$$

With $\mathbf{q_i}$ the i-th eigenvector associated to the eigenvalue λ_i. According to [Manolakis et al. (2005)], the correlation matrix can be projected on two subspaces, the signal subspace corresponding to the P largest eigenvalues ($P < m$) and the noise subspace. Thus (F.2) can be written as (F.3).

$$\mathbf{R_y} = \mathbf{Q}_s \mathbf{\Lambda}_s {\mathbf{Q}_s}^H + \sigma^2 \mathbf{Q}_w \mathbf{Q}_w^H \tag{F.3}$$

σ^2 is the power spectrum of the noise, $\mathbf{Q}_s$ is a matrix $(m \times P)$ with eigenvectors spanning the signal subspace $\mathbf{Q}_s = [\mathbf{q}_1\mathbf{q}_2...\mathbf{q}_P]$; and $\mathbf{Q}_w$ is reciprocally the matrix of the eigenvectors spanning the noise space $\mathbf{Q}_w = [\mathbf{q}_{P+1}\mathbf{q}_{P+2}...\mathbf{q}_M]$. Since the two subspaces are orthogonal, the multipath delays τ_k,$1 < k < P$ correspond to the values for which the MUSIC pseudospectrum achieves its maxima [Li and Pahlavan (2004)]. The pseudospectrum is given in [F.4].

$$S_{MUSIC}(\tau) = \frac{1}{\sum_{k=P+1}^{M} |\mathbf{q}_k^H \mathbf{e}(\tau)|^2} \tag{F.4}$$

F.0.5 Simulations and Results

A 2-paths signals model is implemented. The simulator simulates 2 transmitters and 1 receiver. The signal transmitted uses the Direct Sequence Spread Spectrum technology (see Figure F.1). In order to simulate the CVB, the first transmitter is

always the closest to the receiver. The signal is first low-pass filtered and then a Fourier transform (FFT) is applied.

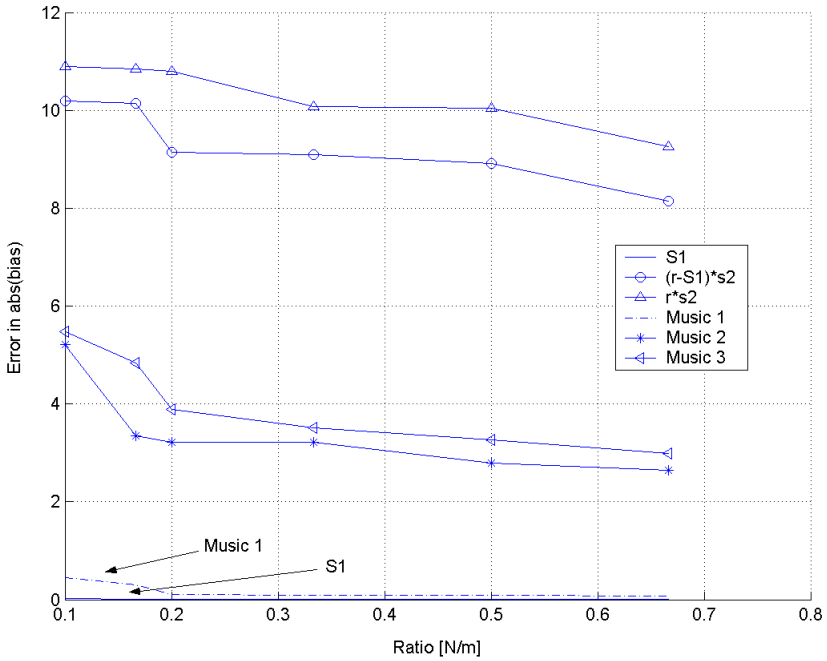


Figure F.2: Bias (in chips) on the time delay estimation Vs the length of the subvector (m)

In the normal case, the received signal $r(t)$ is successively correlated in the frequency domain with a pattern of signals $s_1(t)$ and $s_2(t)$ transmitted by transmitter 1 and 2. When the CVB is used, the received signal is correlated with $s_1(t)$; and then $r(t)-s_1(t)$ is correlated with $s_2(t)$. At the output of the matched-filter either the delay is directly estimated, or MUSIC super-resolution is applied in frequency domain. In both cases, the time delay is chosen as the delay of the highest peak in the time domain.

Moreover, the code used is a Gold code with 64 chips. The code sequence for each transmitter is transmitted twice ($2 \times T_s$), to increase the resolution of the correlation function in frequency domain [Saarnisaari (1997)].

Figures F.2 and F.3 show the results.

In Figure F.2, the Signal-to-Noise-Ratio (SNR) is equal to 16, and its abscisse is the ratio of the length of the subvector (m) over the vector length (N). In Figure F.3, the ratio is equal to 1/3. For each point a Monte Carlo loop is used to average, over

3000 simulations the bias on the error of the time delay estimation. In the legend, S_1 means the received signal r is correlated with the the signal pattern from the first transmitter S_1. $(r - S_1) * s2$ is equal to the received signal is first subtracted to S_1 (signal transmitted by the first transmitter) and then correlated with S_2 the signal transmitted from the second transmitter. $r * s2$ is the correlation of the received signal r with S_2. $MUSIC1$ means the MUSIC algorithm is applied to the output of S_1. In $MUSIC2$, the MUSIC algorithm is applied to $(r - S_1) * s2$; and finally $MUSIC3$, MUSIC is applied to $r * s2$. As we said previously, the MUSIC algorithm performs in the frequency domain of $r * S_1$,$(r - S_1) * S_2$ and $r * S_2$.

From [Li and Pahlavan (2004)] and [Saarnisaari (1997)], two important parameters have been identified: m in (F.1) is the length of the subvector from the output of the matched-filter, and the SNR of the noise.

Through observing both figures, the main result is the MUSIC algorithm does not help to resolve the multipath problem when it is applied on the received signal directly. In other words, it does not improve the delay estimation of the closest transmitter. However, it improves the delay estimation of the second transmitter with or without applying the CVB.

As expected, if the CVB is applied, the time delay estimate is improved compared

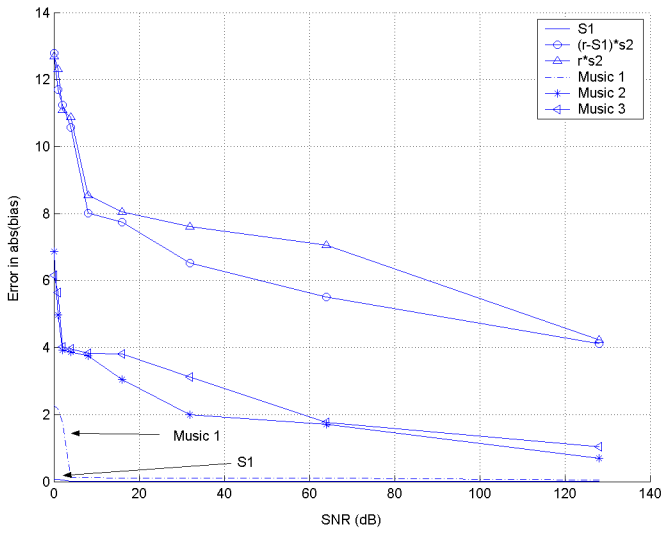


Figure F.3: Bias (in chips) on the time delay estimation Vs the SNR

to the case without CVB. In Figure F.3, the results between the CVB and the direct correlation are close. That can be explained via the only 2-path considered for multipath scenario. It also underlines the general result about the bigger is the SNR, the smaller is the bias on the error of the time delay estimation.
Figure F.2 shows that the bigger m is, the less is the error on time-delay estimation. The subvector are made from the spectrum of the matched-filter via a sliding-window of length m. Thus, the longer are the subvector, the more information they will contain. We have to be careful in choosing M (the number of subvectors) not too small. Otherwise MUSIC may diverge. Figures F.2 and F.3 converge with the result given in [Saarnisaari (1997)].
Moreover, the simulations underline the choice of the P eigenvalues corresponding to the signal subspace in Equation (F.3) is a key point to get MUSIC algorithm converging. As we need to average the results given by MUSIC algorithm on 3000 simulations for each scenario, we decided to use the Rissanen minimum descriptive length criteria (MDL) to select P for each simulation. The criteria is described in [Li and Pahlavan (2004)].

F.0.6 Conclusions

Cumulative Virtual Blanking and MUSIC super-resolution have been explained in this letter and applied to the time delay estimation in multipath environment. In this letter we develop a simple simulator to schematize the problem of estimating the time delay between two BSs and a MS. The results show that super-resolution algorithms like MUSIC can improve the time delay estimation when signals of different transmitters are hidden due to Near-Far effect problems. MUSIC may also be implemented on top of the CVB to get a finer accuracy on time delay estimation.

F.0.7 Acknowledgments

This work is supported by the Visualising integrated Information on buried Assets to reduce Streetworks (VISTA) project funded by the UK DTI. The authors would like to thank Dr. H. Saarnisaari from the university of Oulu (Finland) for his comments

and useful discussions.